Sheffield Hallam University

Measuring Chemotherapy Response in Breast Cancer Using Optical and Ultrasound Spectroscopy

TRAN, William T.

Available from the Sheffield Hallam University Research Archive (SHURA) at:

http://shura.shu.ac.uk/21926/

A Sheffield Hallam University thesis

This thesis is protected by copyright which belongs to the author.

The content must not be changed in any way or sold commercially in any format or medium without the formal permission of the author.

When referring to this work, full bibliographic details including the author, title, awarding institution and date of the thesis must be given.

Please visit http://shura.shu.ac.uk/21926/ and http://shura.shu.ac.uk/information.html for further details about copyright and re-use permissions.

Measuring Chemotherapy Response in Breast Cancer Using Optical and Ultrasound Spectroscopy

William T. Tran

A thesis submitted in partial fulfilment of the requirements of
Sheffield Hallam University
for the degree of Doctor of Philosophy

Faculty of Health and Wellbeing
Sheffield Hallam University

and

Sunnybrook Research Institute
University of Toronto

© William Tran
January 2017

Thesis Overview

Breast cancer is the second leading cause of cancer-related mortality in women and accounts for 33% of all new malignancies. As many as 12% of breast cancer patients present with locally advanced breast cancer (LABC), defined as stage 3 disease, i.e. tumours >5 cm and may involve the skin, chest wall, or lymph nodes. Survival outcomes for LABC are poor; only 50% of patients survive five years after diagnosis. Clinical management involves neoadjuvant (i.e. pre-operative) chemotherapy (NAC) and this is recommended as first-line treatment to downstage tumours before surgery. However, a variable response to treatment has been shown in patients receiving NAC and there is evidence that favourable responses to NAC correlate well with improved survival.

Understanding the likelihood of treatment efficacy at early stages of NAC (i.e. before starting treatment or after one chemotherapy cycle) may inform physicians and patients about the tumour's response; ultimately with the potential to adapt treatments and improve patient outcomes. Standard methods to assess chemotherapy response use clinical palpation or medical imaging, such as magnetic resonance imaging (MRI) to measure the changes in tumour size during treatment. However, the major limitations for current imaging techniques include expensive equipment, need for contrast agents, or poor sensitivity and specificity of gold-standard pathology. Also, it may take many weeks for tumour size to shrink, despite the biological responses that may occur much earlier. With the limitations of current imaging techniques, the motivation for this present study was to investigate quantitative imaging methods to evaluate tumour biology during early phases of treatment as early-response markers for breast tumour response to NAC.

In this thesis, it is proposed that quantitative imaging using diffuse optical spectroscopy (DOS) and quantitative ultrasound (QUS) can be used to address the limitations of conventional imaging in breast cancer. DOS and QUS can measure biological and functional properties in tumours which can subsequently be used to characterize tumour response. Although both DOS and QUS parameters have previously been studied individually, further work is

needed to explore DOS and QUS imaging biomarkers since there remains an opportunity to study the temporal relationships between DOS and QUS parameters. This is because with each modality, one can potentially provide tumour markers for vascularity, cellularity, cell death and tumour oxygenation, which are important hallmarks for tumour progression and tumour killing. In addition, there are further opportunities to investigate DOS imaging before chemotherapy in order to predict the likelihood of tumour response to treatment.

This thesis has four chapters. To establish the groundwork for this study, the first chapter is presented to illustrate the biologically complex breast tumour and to present the treatment and clinical problem associated with locally advanced breast cancer. Additionally, in Chapter 1, a review of the literature was conducted to evaluate the status of breast imaging to measure chemotherapy response in breast tumours. Several clinical imaging modalities were considered, which included magnetic resonance imaging (MRI), computed tomography (CT), positron emission tomography (PET) and technetium 99-m (99m-Tc) scintigraphy. Following this, a systematic review was completed which focused on studies for diffuse optical spectroscopy (DOS) and quantitative ultrasound spectroscopy (QUS).

In Chapter 2, the research methods are presented within the framework of the research questions in this thesis. The study was composed of two major subprojects; in the first subproject, the overarching research question was, "*can DOS and QUS imaging biomarkers be modelled temporally to measure treatment response at early time intervals (i.e. after one or two cycles of chemotherapy)?*". The analysis included clustering DOS and QUS features to test the predictive value (sensitivity and specificity) to NAC response. The results of the first subproject raised questions about using new image analysis techniques (i.e. texture) for DOS. Thus, the aim of subproject 2 was to investigate if DOS imaging before treatment could predict tumour response to chemotherapy. Here, the overarching question of the second subproject was, "*can DOS-texture markers predict chemotherapy response prior to starting treatment?*". In this component, DOS images were analysed using texture features of DOS parametric maps prior to chemotherapy, which were shown to provide an increase in DOS-imaging signatures about the tumour's biological features. Such DOS-texture markers were used in both univariate and multivariate analyses to yield statistical models that correlated DOS-texture

features with pathological response, as measured by Miller-Payne pathological response criteria.

In Chapter 3, the results of the study are presented according to each subproject. For subproject one, the results showed that there was a temporal relationship between DOS and QUS imaging markers during early phases of chemotherapy. Statistical models were developed and showed that both univariate and multivariate DOS and QUS features were correlated to final pathological (Miller-Payne) response with an area under the curve (AUC) of 0.84-1.00 after one week of chemotherapy. For subproject two, it was found that there were significant differences in DOS texture-based features between responsive and non-responsive tumours before NAC. Statistical models using machine learning techniques, found that features of tumour oxygenation and tumour haemoglobin could predict pathological treatment response with an accuracy of 87.8%.

Chapter 4 includes a discussion of the current study's findings and compares to the previous literature as presented in the systematic review. A discussion on the status of DOS and QUS imaging as a clinical decision-making tool are presented in terms of the current translational gaps that DOS and QUS are required to overcome to achieve robust clinical and scientific validation. The thesis concludes with limitations and future directions.

Abstract

Purpose: This study comprises two subprojects. In subproject one, the study purpose was to evaluate response to neoadjuvant chemotherapy (NAC) using quantitative ultrasound (QUS) and diffuse optical spectroscopy imaging (DOS) in locally advanced breast cancer (LABC) *during* chemotherapy. In subproject two, DOS-based functional maps were analysed with texture-based image features to predict breast cancer response *before* the start of NAC.
Patients and Measurements: The institution's ethics review board approved this study. For subproject one, subjects (n=22) gave written consent before participating in the study. Participants underwent non-invasive, DOS and QUS imaging. Data were acquired at weeks 0 (i.e. baseline), 1, 4, 8 and before surgical removal of the tumour (mastectomy and/or lumpectomy); corresponding to chemotherapy schedules. QUS parameters including the mid-band fit (MBF), 0-MHz intercept (SI), and the spectral slope (SS) were determined from tumour ultrasound data using spectral analysis. In the same patients, DOS was used to measure parameters relating to tumour haemoglobin and tissue composition such as %Water and %Lipids. Discriminant analysis and receiver-operating characteristic (ROC) analyses were used to correlate the measured imaging parameters to Miller-Payne pathological response during treatment. Additionally, multivariate analysis was carried out for pairwise DOS and QUS parameter combinations to determine if an increase in the classification accuracy could be obtained using combination DOS and QUS parametric models.

For subproject two, 15 additional patients we recruited after first giving their written informed consent. A pooled analysis was completed for all DOS baseline data (subproject 1 and subproject 2; n=37 patients). LABC patients planned for NAC had functional DOS maps and associated textural features generated. A grey-level co-occurrence matrix (texture) analysis was completed for parameters associated with haemoglobin, tissue composition, and optical properties (deoxy-haemoglobin [Hb], oxy-haemoglobin [HbO_2], total haemoglobin [HbT]), %Lipids, %Water, and scattering power [SP], scattering amplitude [SA]) prior to treatment. Textural features included *contrast (con),*

correlation (cor), energy (ene), and *homogeneity (hom)*. Patients were classified as 'responders' or 'non-responders' using Miller-Payne pathological response criteria after treatment completion. In order to test if baseline univariate texture features could predict treatment response, a receiver operating characteristic (ROC) analysis was performed, and the optimal sensitivity, specificity and area under the curve (AUC) was calculated using Youden's index (Q-point) from the ROC. Multivariate analysis was conducted to test 40 DOS-texture features and all possible bivariate combinations using a naïve Bayes model, and k-nearest neighbour (k-NN) model classifiers were included in the analysis. Using these machine-learning algorithms, the pre-treatment DOS-texture parameters underwent dataset training, testing, and validation and ROC analysis were performed to find the maximum sensitivity and specificity of bivariate DOS-texture features.

Results: For subproject one**,** individual DOS and QUS parameters, including the spectral intercept (SI), oxy-haemoglobin (HbO_2), and total haemoglobin (HbT) were significant markers for response outcome after one week of treatment ($p<0.01$). Multivariate (pairwise) combinations increased the sensitivity, specificity and AUC at this time; the SI+HbO_2 showed a sensitivity/specificity of 100%, and an AUC of 1.0 after one week of treatment.

For subproject two, the results indicated that textural characteristics of pre-treatment DOS parametric maps can differentiate treatment response outcomes. The HbO_2-homogeneity resulted in the highest accuracy amongst univariate parameters in predicting response to chemotherapy: sensitivity (%Sn) and specificity (%Sp) = 86.5 and 89.0%, respectively and an accuracy of 87.8%. The highest predictors using multivariate (binary) combination features were the Hb-Contrast + HbO_2-Homogeneity which resulted in a %Sn = 78.0, a %Sp = 81.0% and an accuracy of 79.5% using the naïve Bayes model.

Conclusion: DOS and QUS demonstrated potential as coincident markers for treatment response and may potentially facilitate response-guided therapies. Also, the results of this study demonstrated that DOS-texture analysis can be used to predict breast cancer response groups prior to starting NAC using baseline DOS measurements.

Candidate's Statement

The purpose of this thesis was to investigate diffuse optical spectroscopy (DOS) and quantitative ultrasound (QUS) imaging methods to obtain: 1) early-response imaging biomarkers and; 2) predictive markers, for Miller-Payne pathological response endpoints to neoadjuvant chemotherapy in locally advanced breast cancer. It is proposed that by using non-invasive imaging modalities such as DOS and QUS, it is possible to characterize the physiological and cellular features of breast tumours into a more complete "biological portrait". The work presented here, builds on previous investigations where DOS and QUS imaging has been studied separately to show biological changes that tumours undergo during chemotherapy. In this study, the aim was to demonstrate the biological inter-relationship of imaging markers as measured by DOS and QUS imaging. Secondly, the study aimed to test if pre-treatment DOS images could be used to predict response before starting chemotherapy.

The research programme is a collaborative doctoral project between Sheffield Hallam University and Sunnybrook Research Institute (affiliated with the University of Toronto). I would like to declare that all work and experiments presented in this thesis were solely collected, analysed, and performed by the author, with the guidance of my supervisory team; Professor Charmaine Childs, Professor Heidi Probst, and Dr. Gregory Czarnota (University of Toronto). All figures including data graphs, histological representations, and schematic figures are the candidate's own, unless otherwise stated.

Acknowledgements

I would like to express my sincere gratitude to my mentor and academic supervisor at the University of Toronto, Dr. Gregory J. Czarnota, M.D., Ph.D. for his guidance, as an expert physician in radiation oncology, and for the rigorous scientific training that he has provided me over the years. I am appreciative of his support, teaching and encouragement over the years. I would also like to extend my gratitude to his laboratory; specifically, to Dr. L. Sannachi, Dr. A. Sadeghi, Dr. M. Gangeh, Dr. Hadi Tadayyon and Dr. A. Al-Mahrouki who had taken countless moments of their personal time to review my manuscripts and research to ensure that I continued to ask the right questions about medicine and science. I would like to thank my supervisory team at Sheffield Hallam University, Professor C. Childs, Ph.D. and Professor H. Probst, Ph.D. who kept me motivated and championed my work. Their guidance has helped shape my learning throughout the course of my doctoral studies. Both Professors Childs, and Probst demonstrate qualities that I strive to embody as a clinician, scientist, and most importantly, as an example of “good people”. Additionally, I thank Ms. Niki Law, Ms. Elyse Watkins, Ms. Rose Lisi, Dr. Ahmed El Kaffas, Dr. Golnaz Farhat, Dr. Calvin Law, and Dr. Eileen Rakovitch for their friendship, support and encouragement during my studies. An important aspect of my progress has been through the support and encouragement of my partner and family, who have been patient and understanding of my focus on my studies and work throughout the years. As refugees from Vietnam, I am reminded by my family constantly that we are obligated to make positive changes and to always give back.

Lastly, I would like to thank the many ladies who participated in these imaging studies. Despite their difficult times, they always remained kind, supportive, and encouraged me; putting the research ahead of themselves even during their challenging treatments. Their selflessness has been inspiring and this was one of the most important lessons for me. Their role in my doctoral studies have been paramount, and I cannot thank those patients enough for their inspirational strength and devotion to helping carry the study to completion. I am forever grateful to them.

Symbols, Units and Abbreviations

(In alphabetical order)

%Acc	Accuracy (percentage)
%Water	Percent Water
%Li	Percent Lipids
%Sn	Sensitivity (percentage)
%Sp	Specificity (percentage)
A.U.	Arbitrary Units
AC-T	Adriamycin, Cyclophosphamide, Paclitaxel
AUC	Area under curve
BIRADS	Breast Imaging Reporting and Data System
BOLD-MRI	blood-oxygen level depending imaging
BRCA-1,2	breast cancer susceptibility gene-1,2
CI	Confidence interval
Con	Contrast (texture feature)
CRUK	Cancer research UK
CT	Computed tomography
CW	Continuous Wave
dB	Decibels
DCE-MRI	dynamic contrast enhancement imaging
DNA	Deoxyribonucleic Acid
DWI-MRI	diffusion-weighted imaging
Ene	Energy (texture feature)
EORTC	European Organization for Research and Treatment of Cancer
ER	Oestrogen receptor
f	frequency
FD	Frequency Doman
FDG	[18F]-fluorodeoxyglucose
FEC-D	Fluorouracil, Epirubicin, Cyclophosphamide, Docetaxel
FNA	Fine needle biopsy
FNF	False negative fraction

FPF	False positive fraction
GLCM	Grey level co-occurrence matrix
GP	General practitioner
H&E	haematoxylin and eosin
Hb	Deoxy-Haemoglobin
HbO_2	Oxy-Haemoglobin
HbT	Total Haemoglobin
HER2	Human epidermal growth factor-2
Hom	Homogeneity (texture feature)
HR	Hazard ratio
HRT	Hormone replacement therapy
IDC	Invasive ductal carcinoma
ILC	Invasive lobular carcinoma
IRB	Institutional review board (ethics)
k-NN	k-nearest neighbour
LABC	Locally advanced breast cancer
LRA	Logistic regression analysis
MBF	Mid-band fit
MP	Miller-Payne Pathological Response Criteria
MRI	Magnetic Resonance Imaging
NCCN	National Comprehensive Cancer Network
NCI	National cancer institute
NICE	National institute for health and clinical excellence (UK)
NIR	Near-infrared (light spectrum)
nm	nanometres
NR	Non-responders (MP1,2)
NSABP	National Surgical Adjuvant Breast and Bowel Protocol
OCM	Optical compensation medium
pCR	Pathological complete response
PET	Positron emission Tomography
PR	Progesterone receptor
QUADAS-2	Quality Assessment for Diagnostic Accuracy Studies tool
QUS	Quantitative Ultrasound Spectroscopy
R	Responders (MP3-5)
RCBI	Residual Cancer Burden Index

RCT	Randomized control trials
RECIST 1.1	Response evaluation criteria in solid tumours Version 1.1
RF	Radiofrequency data (ultrasound)
ROI	Region of interest
SA	Scattering amplitude
SBE	Self-breast exam
SEER	Statistics, Epidemiology, and End-Results Program
SI	Spectral Intercept
SP	Scattering power
SPECT-MRI	MRI spectroscopy
SPL	Spatial pulse length
SS	Spectral Slope
St	Oxygen Desaturation
STARD	Statement for Reporting Studies of Diagnostic Accuracy
StO_2	Oxygen Saturation
TD	Time Domain
TNF	True negative fraction
TOI	Tissue Optical Index
TPF	True positive fraction
TPSF	Time point spread function
US	Ultrasound

List of Figures

Chapter 1

Figure Number	Figure Title
Figure 1.1	Breast cancer arises from the epithelial cells of ducts
Figure 1.2	Breast cancer incidence
Figure 1.3	Breast cancer incidence by age
Figure 1.4	Breast cancer screening and diagnosis guidelines (UK)
Figure 1.5	Treatment (multimodality) decision tree for breast cancer
Figure 1.6	Chemotherapy treatment cycles
Figure 1.7	Aberdeen trial design (Adapted from Heys et al. 2002)
Figure 1.8	Drug pharmacokinetics
Figure 1.9	Drug resistance mechanism: Drug efflux
Figure 1.10	MRI of breast carcinoma (pre-to-post treatment)
Figure 1.11	Systematic search strategy and search results
Figure 1.12	Positron Emission Tomography imaging mechanism
Figure 1.13	Literature review concepts
Figure 1.14	The electromagnetic spectrum
Figure 1.15	Scattering regimes
Figure 1.16	Tissue-light interactions
Figure 1.17	Diffuse optical topography and tomography
Figure 1.18	Wave propagation and transmission in a medium
Figure 1.19	Principles of quantitative ultrasound spectroscopy
Figure 1.20	Ultrasound lateral resolution and beam focal zones
Figure 1.21	Ultrasound axial resolution
Figure 1.22	Apoptosis in cancer cells
Figure 1.23	Vascular organization and regression in tumours
Figure 1.24	Tumour biological composition
Figure 1.25	QUADAS2-Domain (Bias) results

Chapter 2

Figure Number	Figure Title
Figure 2.1	Whole-breast histology mounts
Figure 2.2	Project work-flow and methods summary
Figure 2.3	Schematic of subproject one and subproject two
Figure 2.4	Chemotherapy schedules for patients
Figure 2.5	Quantitative ultrasound spectroscopy breast imaging
Figure 2.6	Diffuse optical spectroscopy breast imaging
Figure 2.7	Representative of QUS power spectrum
Figure 2.8	Calculations of the time-point spread function (TPSF)
Figure 2.9	Absorbance spectra for DOS imaging
Figure 2.10	Scattering spectra for DOS imaging
Figure 2.11	Texture based (GLCM) computations
Figure 2.12	DOS-texture features
Figure 2.13	Ultrasound transducer and beam characteristics
Figure 2.14	Optical phantom construction
Figure 2.15	DOS data verification
Figure 2.16	Inter-user agreement analysis
Figure 2.17	Test distribution to calculate sensitivity and specificity
Figure 2.18	Receiver-operating characteristic (ROC) curve
Figure 2.19	Linear discriminant analysis
Figure 2.20	k-nearest neighbour classification algorithm

Chapter 3

Figure Number	Figure Title
Figure 3.1	DOS haemoglobin parameters (changes over time)
Figure 3.2	DOS tissue parameters measured over time
Figure 3.3	DOS scattering parameters measured over time
Figure 3.4	QUS parameters measured during treatment
Figure 3.5	Representative responder to chemotherapy
Figure 3.6	Representative non-responder to chemotherapy

Figure 3.7 ROC curves for pairwise parameters (week one)
Figure 3.8 ROC curves for pairwise parameters (week four)
Figure 3.9 GLCM texture features for deoxy-haemoglobin features
Figure 3.10 GLCM texture features for oxy-haemoglobin features
Figure 3.11 GLCM texture features for total haemoglobin features
Figure 3.12 GLCM texture features for oxygen desaturation features
Figure 3.13 GLCM texture features for oxygen saturation features
Figure 3.14 Representative DOS and MRI images for a responder
Figure 3.15 Representative DOS and MRI images for a non-responder
Figure 3.16 ROC curves for univariate DOS-texture features
Figure 3.17 ROC curves for multivariate DOS-texture features

Chapter 4

Figure Number	Figure Title
Figure 4.1	Breast cancer treatment pathway

List of Tables

Chapter 1

Table Number	Table Title
Table 1.1	WHO classification of breast cancers
Table 1.2	Breast cancer staging
Table 1.3	Breast tumour subtypes
Table 1.4	Success rates of concomitant cancer treatments
Table 1.5	Chemotherapy drug types and drug regimens
Table 1.6	Comparison of chemotherapy response rates
Table 1.7	Pathologic endpoints (classification systems)
Table 1.8	Nottingham grade system
Table 1.9	Nottingham prognostic index
Table 1.10	Patient survival according to initial tumour size
Table 1.11	Systematic review search strategy
Table 1.12	Breast density grades for mammographic assessment
Table 1.13	Biological measurements according to imaging modality
Table 1.14	Clinical studies characteristics
Table 1.15	Measurement parameters
Table 1.16	DOS imaging techniques
Table 1.17	QUS imaging biomarkers and scatterer properties
Table 1.18	Clinical studies to measure apoptosis in breast cancer
Table 1.19	Physiological measurements by DOS and QUS
Table 1.20	DOS and QUS studies' and parameters
Table 1.21	Detailed summary of DOS and QUS studies
Table 1.22	QUADAS-2 assessment results
Table 1.23	STARD assessment results

Chapter 2

Table Number	Table Title
Table 2.1	Miller-Payne pathologic response classification system
Table 2.2	Trial summaries for the thesis study
Table 2.3	Chemotherapy treatment protocols
Table 2.4	Transducer and beam characteristics
Table 2.5	Optical ROI geometry and quality check
Table 2.6	Optical characteristics from DOS system
Table 2.7	Inter-reader variability testing

Chapter 3

Table Number	Table Title
Table 3.1	Summary of patient characteristics
Table 3.2	Summary of p-values for DOS-haemoglobin parameters
Table 3.3	Summary of p-values for DOS-tissue parameters
Table 3.4	Summary of p-values for DOS-scattering parameters
Table 3.5	Statistical results for QUS parameters
Table 3.6	ROC results for DOS and QUS univariate analyses
Table 3.7	ROC results for DOS and QUS multivariate analyses
Table 3.8	Classification results for univariate DOS features
Table 3.9	Best classification parameters for DOS univariates
Table 3.10	Classification results for multivariate DOS features
Table 3.11	Subgroup analyses and classification results
Table 3.12	Regression co-efficient values for DOS features

Chapter 4

Table Number	Table Title
Table 4.1	Summary of comparisons for DOS studies to thesis
Table 4.2	Summary of comparisons for QUS studies to thesis

Table of Contents

THESIS OVERVIEW ..... **II**

ABSTRACT ..... **V**

CANDIDATE'S STATEMENT ..... **VII**

ACKNOWLEDGEMENTS ..... **VIII**

SYMBOLS, UNITS AND ABBREVIATIONS ..... **IX**

LIST OF FIGURES ..... **XII**

LIST OF TABLES ..... **XV**

CHAPTER 1 ..... **1**

Background and Review of the Literature **1**

1.0 Chapter Overview **1**

1.1 Cancer **2**

1.1.1 Tumourigenesis and Cancer Progression 2

1.2 Breast Cancer **5**

1.2.1 Natural History and Presentation 5

1.2.2 Epidemiology: Incidence and Mortality 8

1.2.3 Risk Factors for Developing Breast Cancer 9

1.2.4 Screening and Diagnosis 13

1.3 Locally Advanced Breast Cancer and Treatment **16**

1.3.1 Multimodality Treatments: Historical Perspective 16

1.4 Study Motivations and Aims 1 ..... **19**

Identifying the Target Study Population **19**

1.5 Breast Cancer Chemotherapy **20**

1.6 Chemotherapy Side Effects **23**

1.6.1 Cardiac Complications 23

1.6.2 Haematopoietic Toxicity 24

1.6.3 Gastrointestinal Toxicity 24

1.6.4 Alopecia 25

1.6.5 Neurotoxicity 25
1.6.6 Anaphylaxis 26
1.7 Mechanisms of Chemotherapy Resistance 27
1.7.1 Pharmacokinetic Influences 27
1.7.2 Chemotherapy Resistance in Molecular Subtypes 29
1.8 Prognostic Factors 32
1.8.1 Pathological Response to Neoadjuvant Chemotherapy 32
1.8.2 Molecular Features 36
1.8.3 Histological Grade (Nottingham Grade) 37
1.8.4 Nottingham Prognostic Index 38
1.8.5 Tumour Size and Lymph Node Invasion 39
1.9 Case Study 41
1.9.1 Reason for Referral and Diagnosis 41
1.9.2 History of Present Illness and Work-Up 41
1.9.3 Past Medical History 42
1.9.4 Family History and Risk Factors 42
1.9.5 Impression and Plan 43
1.9.6 Treatment Interval Assessments 43
1.9.7 Post-Treatment Assessments 44
1.9.8 Case Report Summary 45
1.10 Study Motivations and Aims 2 46
Identifying the Clinical Problem 46
1.11 Systematic Review Question and Search Results 47
1.11.1 Overview and Literature Review Question 47
1.11.2 Systematic Review Strategy 47
1.11.3 Search Strategy Results 50
1.12 Narrative Review of Imaging in Breast Cancer 52
1.12.1 Magnetic Resonance Imaging (MRI) 52
1.12.2 Positron-Emission Tomography (PET) 54
1.12.3 Computed Tomography (CT) 56
1.12.4 X-Ray Mammography 57
1.12.5 Technetium 99m (^{99m}-Tc) scintigraphy 59
1.12.6 Summary of Imaging Studies 59
1.13 Systematic Review of DOS and US Imaging in Breast Cancer 66
1.13.1 Systematic Review Outline 66

1.13.2 Principles of Optical Imaging for Tissue Characterization 67
1.13.3 DOS for Breast Imaging (Concept 1)..... 70
1.13.4 Technical Considerations and Limitations for DOS 72
1.13.5 Principles of Ultrasound Imaging for Tissue Characterization 74
1.13.6 General US Imaging (Concept 2a) and QUS (Concept 2b)..... 75
1.13.7 Technical Considerations and Limitations for US Imaging 79
1.13.8 DOS and QUS Measurements Represent the Tumour's Spatial and Biological Properties..... 84
1.14 Results of DOS and US Systematic Review 92
1.14.1 Patients 92
1.14.2 Quality Assessment Using QUADAS-2 and STARD 98
1.14.3 QUADAS-2 Results 98
1.14.4 STARD Assessment Results..... 103
1.14.5 Summary Findings from Literature Review..... 107
1.14.6 Limitations of Literature Review..... 108

CHAPTER 2 109

Methods..... 109
2.0 Chapter Overview..... 109
2.1 Background 110
2.2 Research Design Summary..... 111
2.2.1 Study Design 111
2.2.2 Aims of the Study 111
2.2.3 Research Questions (Subproject 1 and Subproject 2)..... 112
2.2.4 Endpoints 113
2.2.5 Overview, Research Design Summary..... 116
2.3 Ethics and Regulatory Approval..... 121
2.3.1 Ethics Approval..... 121
2.3.2 Eligibility (Inclusion/Exclusion Criteria) 121
2.3.3 Sample Size Justification..... 123
2.3.4 Access to Patient Electronic Medical Record 126
2.3.5 Research Location..... 127
2.4 Patients and Acquiring Imaging Data..... 128
2.4.1 Chemotherapy Treatment Schedule..... 128

2.4.2 Imaging Schedule Based on Chemotherapy Treatment Schedule . 128
2.4.3 Sequencing DOS and QUS Imaging Per Patient 129
2.4.4 Quantitative Ultrasound Data Acquisition 132
2.4.5 Diffuse Optical Spectroscopy Tomography Data Acquisition 133
2.5 DOS and QUS Image Processing 136
2.5.1 Region of Interest (ROI) Selection 136
2.5.2 QUS: Ultrasound Radiofrequency Spectrum 137
2.5.3 DOS Data Calculations 138
2.5.4 DOS-GLCM (Grey-Level Co-occurrence Matrix) Texture Analysis . 142
2.6 Image Quality Verification 147
2.6.1 Ultrasound Transducer Properties and Beam Characterization 147
2.6.2 Optical Imaging Characterization 148
2.6.3 Inter-Reader Variability Testing 150
2.7 Statistical Analysis and Machine Learning 153
2.7.1 DOS and QUS Data 153
2.7.2 Tests of significance between response groups (R versus NR) 153
2.7.3 Tests of significance Between Time Intervals 153
2.7.4 Selection of Feature Sets for Analysis 154
2.7.5 Receiver Operating Characteristic Curve Analysis 154
2.7.6 Linear Discriminant Analysis 157
2.7.7 Logistic Regression Analysis 158
2.7.8 k-Nearest Neighbour (k-NN) Classifier Statistics 159
2.7.9 Naïve Bayes (Bayesian) Classifier Statistics 160
2.7.10 Training, Test and Validation Sets 161
2.7.11 Subgroup analysis 162
2.7.12 Power Analysis 162

CHAPTER 3 163

Results 163
3.0 Chapter Overview 163
3.1 Patient Characteristics 165
3.1.1 Pre-Chemotherapy and Treatment Characteristics 165
3.1.2 Post-Chemotherapy Characteristics 166
3.2 Results of Subproject One 169

3.2.1 Overview of Results: Subproject One, Research Question 1 169
3.2.2 Results of DOS Measurements- Haematological Parameters..... 170
3.2.3 Results of DOS Measurements- Tissue Parameters..... 174
3.2.4. Results of DOS Measurements- Scattering Parameters 177
3.2.5 Results of QUS Measurements 180
3.2.6 Representative DOS and QUS Changes During Chemotherapy.... 183
3.2.7 Overview of Results: Subproject One, Research Question 2 186
3.2.8 Univariate Analysis of DOS and QUS Parameters 186
3.2.9 Multivariate Analysis of Pairwise DOS-QUS Parameter Combinations 187
3.2.10 Summary of Results and Responses to Research Questions (Subproject One) 192
3.3 Results of Subproject Two 194
3.3.1. Overview and Link to subproject one..... 194
3.3.2 Overview of Results: Subproject Two, Research Question 1 195
3.3.3 Pre-treatment Tumour Haemoglobin-Texture Features Demonstrated Significant Differences Between Miller-Payne Pathologic Response Groups 195
3.3.4 Pre-treatment Tumour Oxygen-Texture Features Demonstrated Significant Differences Between Miller-Payne Pathologic Response Groups 199
3.3.5 Overview of Results: Subproject Two, Research Question 2 205
3.3.6 Classification Results of Univariate DOS-texture features..... 205
3.3.7 Classification Results of Multivariate DOS-texture features 209
3.3.8 Overview of Results of Subproject two, Research Question 3 211
3.3.9 Results of Subgroup Analysis..... 211
3.3.10 Results of Multiple Linear Regression Analysis 212
3.3.11 Summary of Results and Responses to Research Questions (Subproject two) 214

CHAPTER 4 216

Discussion 216
4.0 Chapter Overview..... 216
4.1 Summary of Thesis and Study Motivations 217

4.2 Comparison to Previous DOS and QUS Studies 220
4.2.1 Overview 220
4.2.2 Comparisons to other DOS Studies 221
4.2.3 Analysis of Data Variances in DOS 227
4.2.4 Comparison of QUS studies 234
4.2.5 Analysis of data variances in QUS Studies 237
4.2.6 Modelling DOS and QUS Parameters as Complementary Response Markers 240
4.2.7 Significance of Texture-Analysis of Pre-Treatment DOS parameters 243
4.2.8 Summary of Novel Contributions 244
4.3 DOS and QUS Clinical Translation 247
4.3.1 Current Challenges for DOS and QUS Imaging as a Clinical Tool . 247
4.3.2 Status of DOS and QUS Biomarkers for Breast Cancer Treatment 253
4.4 Potential Impact to Patient Care 259
4.4.1 Using Biomarkers to Make Treatment Decisions for Personalized Medicine 259
4.4.2 Adapting Chemotherapy Dosing Schedules to Optimize Tumour Response and Survival Outcomes 264
4.4.3 Potential Applications for Chemotherapy Drug Trials 265
4.5 Study Limitations 267
4.5.1 Sample Size 267
4.5.2 Sample Heterogeneity 267
4.5.3 Pathologic Endpoints (Ground Truth Labels) 268
4.5.4 Limitations of DOS and QUS Imaging 270
4.6 Future Work 273
4.6.1 Future work for Locally Advanced Breast Cancer 273
4.6.2 Applications to Early Stage Breast Cancer and Other Cancers 274
4.6.3 Other Frameworks for Future Studies 275
4.7 Conclusion 278

APPENDIX 1 280

Supplementary Information to Chapter 1 280
A1.1 Radiological Tumour Response Endpoints 280

A1.1.1 WHO Tumour-response Imaging Guidelines 280
A1.1.2 RECIST 1.1 Guidelines 280
A1.1.3 Limitations of using Radiological Response Endpoints 282

APPENDIX 2 283

Supplementary Information to Chapter 2 283
A2.1 Institutional Ethics Review Board Approval Letters 283
A2.2 Image Processing 285
A2.2.1 Fast Fourier Transform (FFT) (QUS) 285
A2.2.2 Calculation for Sound Intensity (dB) 286
A2.2.3 Calculation for Average Speed of Sound in Soft Tissue 286
A2.2.4 QUS Axial Resolution 286
A2.2.5 QUS Lateral resolution 287

APPENDIX 3 288

Supplementary Information to Chapter 3 288
A3.1. Pathological Assessment 288
A.3.1.1 Pathological responder versus Pathological non-responder 288

APPENDIX 4 289

Supplementary Information to Chapter 4 289
A4.3 Summary of Contributions of Thesis Study 289

APPENDIX 5 290

Academic Output from PhD 290
A5.1 Overview and Summary 290
A5.2 Publications (Primary Author) 290
A5.3 Publications (Contributing Author) 291
A5.4 Conference Presentations and Posters 292
A5.5 Book Chapters 293

BIBLIOGRAPHY 294

Chapter 1

Background and Review of the Literature

1.0 Chapter Overview

This chapter has two major components that begins with background information on breast cancer (**Section 1.1-Section 1.10**), followed by a literature review of imaging biomarkers studied to measure breast cancer response to chemotherapy (**Section 1.11-Section 1.14**).

The first component (i.e. background) describes the biologically complex tumour and the driving factors that initiate tumour growth and progression. This section focuses on the incidence of breast cancer, its natural presentation, risk factors and the current methods used to screen and diagnose breast cancer. Here, a definition of locally advanced breast cancer is presented, which includes the disease presentation, treatment, toxicity (i.e. side effects of treatments) and survival outcomes, which illustrate the clinical problem.

The second major component of this chapter (i.e. review of the literature) begins in **Section 1.11**. Here, the literature review question is presented. The literature review was structured as a narrative review for general imaging such as magnetic resonance imaging, computed tomography, positron emission tomography and 99m-Tc-Scintigraphy. Secondly, a systematic review was completed for previous research, with a focus on diffuse optical spectroscopy and quantitative ultrasound spectroscopy in locally advanced breast cancer. Technical frameworks are presented and a quality assessment of studies was performed using the QUADAS-2 tool (Quality Assessment of Diagnostic Accuracy) and the STARD tool (Standards for Reporting Diagnostic Accuracy). The findings of the literature review were used to provide a framework for the current thesis study and presented at the end of this chapter.

1.1 Cancer

Cancer is a disease characterized by uncontrolled and aberrant cell division (Harrington, 2016). The World Health Organization (WHO) report in 2011 presented data which showed that 8.2 million deaths were caused by cancer globally (Ferlay et al., 2015). In the United States (2014) alone, the annual incidence was 1.7 million cases for all types of cancer (Siegel et al., 2014). Due to an aging population, cancer incidence in the United States is expected to grow to 2.14 million cases by 2030; with breast, prostate and lung cancers projected to account for 747,000 of the newly diagnosed malignancies (Rahib et al., 2014). In the United Kingdom, there were 357,000 new cancer cases in 2014 and cancer incidence rates have grown 12% since the 1990s. (Cancer Research UK, 2017)

Cancer risk factors are correlated to environmental factors, lifestyle habits and genetic causes (Torre et al., 2015). The societal impact of cancer can be measured in terms of its negative effect on population health, quality of life, and is associated with significant costs to the health care system (Campbell and Ramsey, 2009, Will et al., 2000). The growing trends in cancer-related mortality and morbidity have prompted major efforts to improve diagnosis and treatment. Therefore, the examination of the onset, development, progression, and optimal treatment of cancer has become the focus of substantial research.

1.1.1 Tumourigenesis and Cancer Progression

The onset of tumours, known as tumourigenesis is a multistep process that involves transformation of normal cells into cells that exhibit rapid and unstable cell growth (Beckmann et al., 1997). Tumourigenesis is dependent on several factors such as the overexpression of oncogenes, cell signal amplification, and angiogenesis (Luo and Elledge, 2008). These factors are interdependent for tumour growth; for example, oncogenes such as, ras/MAP-kinase have been shown to initiate new blood vessels in tumours, promote tumour growth rate, increase cell signalling activity and enhance the potential for invasion and metastasis. In contrast, other genes play a role in suppressing tumour growth (i.e. tumour suppressor genes) and are also part of the DNA repair process; for example, BRCA1 and BRCA2 genes (Rak et al., 1995,

Carmeliet and Jain, 2000, Atchley et al., 2008, Eerola et al., 2005, Perou et al., 2000).

Hanahan and Weinberg described tumourigenesis and summarized six fundamental and interacting characteristics of cancer (Hanahan and Weinberg, 2011). These include: 1) tumour cell immortality through deregulated cell senescence; 2) resistance factors to cell death; 3) signalling defects that promote tumour cell proliferation; 4) blocking growth suppressors; 5) increase in angiogenesis; and 6) establishing mechanisms for invasion and metastatic spread (Hanahan and Weinberg, 2011). Tumour cell immortality is caused by deregulated cell division and it has been shown that telomeres play an important role in this process and particularly in regulating cell senescence[1] (Kelland, 2005). Tumour cells are genetically programmed to become "immortal" and continue to divide uncontrollably, unlike normal cells that either die or enter into a senescence state. Other mechanisms involve defective cell signalling pathways that inhibit apoptotic cell death (Elmore, 2007). This is regulated by anti-apoptotic proteins, which include survivin, caspase, Bcl-2, and p53 (Elmore, 2007, Lowe and Lin, 2000). For example, mutations in the p53 protein affect cell-cycle checkpoints that are responsible for committing cells into apoptosis; whereas other proteins such as survivin have been shown to supress signalling pathways in the cytoplasm which can lead to cell immortality (Escuin and Rosell, 1999).

An important hallmark of cancer involves angiogenesis and neovascularization (Nishida et al., 2006). Muthukkaruppan et al. (1982) described a critical point, termed the 'angiogenic switch' when neoplasms switch from passive diffusion to vascular perfusion for nutrient supply (Muthukkaruppan et al., 1982). Beyond 2 mm^3 in growth, tumours need a vascular supply to provide nutrients, oxygen and transport blood-borne biochemical signals for survival (Muthukkaruppan et al., 1982, Nishida et al., 2006). The growing vasculature is also driven by tumour cells that release pro-angiogenic factors such as VEG-F (vascular endothelial growth factor), angiogenin, angiostatin, and transforming growth factor. Tumour cells also down-regulate angiogenesis inhibitors such as angiopoietin-2, angiotensin, and

[1] Cell senescence is "cell aging", whereby cells are no longer capable of replicating, but are metabolically active (Campisi, 2013).

angiostatin-2 which lead to uncontrolled vascular growth. The dysfunctional signalling produces vessels that are immature, “leaky”, and poorly formed (Nishida et al., 2006). Tumour blood vessels also increases the risk for malignant cells to spread (i.e. metastasize), as the blood vessels serve as channels for circulating tumour cells (Hanahan and Weinberg, 2011). In summary, tumourigenesis and sustaining the tumour’s lifecycle involves complex oncogene expression, molecular signalling, and angiogenesis. The tumour relies on these processes in parallel to build a microenvironment that promotes cell immortality and tissue invasion. The processes described above are also characteristic of neoplasms of the breast.

1.2 Breast Cancer

1.2.1 Natural History and Presentation

The natural history of breast cancer starts with transformation of epithelial cells of the terminal duct lobules units (TDLU) (Logan et al., 2015). (Santagata et al., 2014, Ellis et al., 2003, Weigelt and Reis-Filho, 2009). At the time of diagnosis, breast cancers may be classified as either non-invasive (i.e. *in situ*) or invasive breast cancer. Non-invasive breast cancer are characterized by tumours that are confined to the lumens of the mammary duct (Burstein et al., 2004). One example of non-invasive breast cancer is ductal carcinoma in situ (DCIS), which accounts for approximately 20% of all newly diagnosed breast cancers; whereas a rarer form termed lobular carcinoma in situ (LCIS) accounts for a smaller portion (0.5-3.9%) of new diagnoses (Logan et al., 2015, Burstein et al., 2004). Both DCIS and LCIS are thought to be precursors to invasive breast cancer and their nomenclature refers to their proximity to the mammary ducts (DCIS), or terminal duct lobular units (LCIS) **(Figure 1.1)** (Hu et al., 2008).

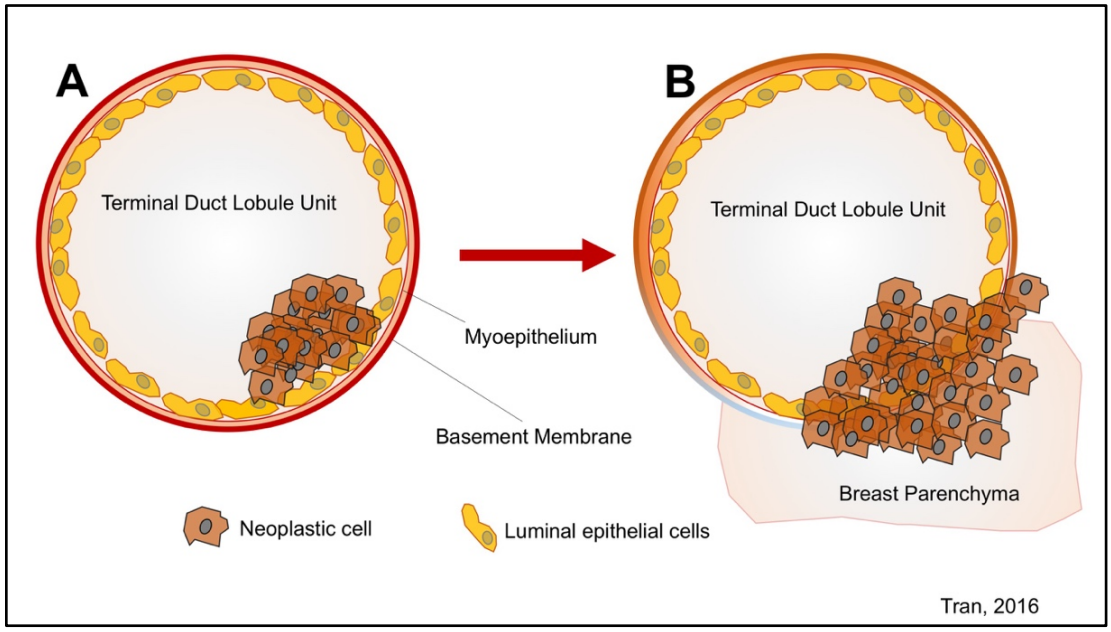

Figure 1.1: Breast cancer arises from the epithelial cells of ducts. A. In situ disease (A) is characterized as lesions contained within the duct itself, such as ductal carcinoma in situ (DCIS). **B.** Invasive carcinomas have features that

show degradation of the basement membrane (myoepithelium) and invasion into the adjacent breast parenchyma.

Tumours that spread beyond the luminal ducts of the breast and travel into the adjacent parenchyma are termed invasive carcinoma. There are as many as 17 invasive breast cancer subtypes, which are characterized by variable histological and molecular features such as hormone receptor status, growth hormone amplification, or tumour cell type (Ellis et al., 2003, Weigelt and Reis-Filho, 2009) **(Table 1.1)**. Additionally, as breast cancer progresses, it is categorized into stages according to the size of the tumour, its spread into lymph nodes and into other parts of the body. Breast tumour staging is outlined in **Table 1.2**.

Histological Classification	**Prevalence (%) (Ellis et al., 2003)**	**ICD-O Code[2]**
Invasive Ductal Carcinoma (NOS)[1]	50-80	8500/3
Invasive Lobular Carcinoma	5-15	8520/3
Medullary Carcinoma	1-7	8510/3
Invasive Cribriform Carcinoma	0.8-3.5	8201/3
Mucinous Carcinoma	2	8480/3
Neuroendocrine Tumours	2-5	8249/3
Invasive Papillary Carcinoma	1-2	8503/3
Apocrine Carcinoma	<4	8401/3
Lipid-rich Carcinoma	1-6	8314/3
Metaplastic Carcinoma	<1	8575/3
Pure Tubular Carcinoma	<2	8211/3
Glycogen-rich Clear-cell Carcinoma	1-3	8315/3
Adenoid Cystic Carcinoma	0.1	8200/3
Secretory Carcinoma	<0.15	8502/3
Acinic-cell Carcinoma	No statistics	8550/3
Sebaceous Carcinoma	No statistics	8410/3

Table 1.1: World Health Organization classification of breast cancers.
[1]NOS: Not otherwise specified; [2]ICD-O Code: International code of diseases-oncology

	Stage	T	N	M	Description
Non-Invasive Breast Cancer (In Situ)					
	0	Tis	N0	M0	Carcinoma in situ
Invasive Breast Cancer					
Early Breast Cancer	**1**	T1	N0	M0	Primary lesion <2 cm
	2A	T0	N1	M0	No primary but axillary lesion
		T1	N1	M0	Primary lesion <2 cm. Involved lymph nodes
		T2	N0	M0	Primary lesion 2 to 5 cm, no node involvement
	2B	T2	N1	M0	Primary lesion >2 to 5 cm Movable axillary lymph nodes
		T3	N0	M0	Primary lesion > 5cm No node involvement
Advanced Breast Cancer	**3A**	T2	N2	M0	Primary lesion >2 to 5 cm Fixed axillary lymph nodes
		T3	N1, N2	M0	Primary lesion > 5cm Movable and/or fixed axillary lymph nodes
	3B	T4	Any N	M0	>5cm, chest wall/skin Movable and/or fixed axillary lymph nodes Internal mammary nodes. Includes inflammatory carcinoma
	3C	Any T	N3	M0	Primary lesion >2 to 5 cm Primary lesions >5 cm Involvement with chest wall/skin Movable and/or fixed axillary lymph nodes May include internal mammary nodes. Includes inflammatory carcinoma
Metastatic Breast Cancer					
	4	Any T	Any N	M1	Distant metastasis

Table 1.2: Clinical presentation and staging for breast cancer, based on TNM classification (primary tumour extent [T], nodal Involvement [N], metastatic spread [M]). Note: Stage 2B disease may be considered inoperable in cases with chest wall and/or skin involvement (Hortobagyi et al., 1988).

Other characteristics of breast cancer include differences in tumour-molecular features such as oestrogen receptor (ER) and progesterone receptor (PR) expression, human epidermal growth factor-2 receptor (HER2), and proliferative rate (Ki67) (Inic et al., 2014). These parameters are used to classify breast cancer subtypes, as outlined by a consensus guideline at the St. Gallen Conference in 2013 (Harbeck et al., 2013, Goldhirsch et al., 2013). The breast tumour subtypes are summarized in **Table 1.3**.

Breast Cancer Subtype	**ER**	**PR**	**HER2**	**Ki67 (Marker for Proliferation)**
Luminal A	+	+	-	Low[1]
Luminal B	+	+/-	+/-	High[1]
Basal-Like	-	-	-	n/a
HER2 Overexpressed	-	-	+	n/a

Table 1.3: Molecular and cell proliferation characteristics of breast cancer according to subtype. [1]High and low Ki67 cut-off values were not indicated in the St. Gallen consensus statement.

Data from 50,571 women in the United States showed that 72.7% of women had luminal A breast cancer; while 12.2% were basal-like. A smaller portion of patients exhibited luminal B breast cancer (10.3%), and only 4.6% of all patients demonstrated HER2 overexpressed (HER2+) breast cancer (Howlader et al., 2014).

1.2.2 Epidemiology: Incidence and Mortality

Breast cancer is the second most diagnosed cancer globally (Ferlay et al., 2015). Incidence rates vary among geographic regions; affecting 27 per 100,000 in Africa and Asia and increasing to 96 per 100,000 in Western Europe and 92 per 100,000 in North America (Ferlay et al., 2015). In terms of mortality rates, breast cancer is listed as the fifth leading cause of cancer-related death in comparison to other malignancies. There are 522,000 deaths caused by breast cancer each year (Ferlay et al., 2015). Mortality is also variable between

developed and developing countries, and this is caused by differences in healthcare infrastructure, ability to access an early diagnosis and treatment.

1.2.3 Risk Factors for Developing Breast Cancer

Race: SEER (Surveillance, Epidemiology, and End Results Program) data between 2004-2011 for American women (n= 373,563) indicated that Non-Hispanic-White and Black women were at highest risk for developing breast cancer (Non-Hispanic White women = 71.9% versus Black women = 10.4%) (Iqbal et al., 2015). Incidentally, Stage 3 breast cancer (i.e. locally advanced) was indicated as highest (16.6%) in Black women amongst all ethnic groups. In comparison, Asian women demonstrated the lowest incidence of breast cancer (range = 0.59%-3.84%) (Newman, 2009, Iqbal et al., 2015) **(Figure 1.2)**.

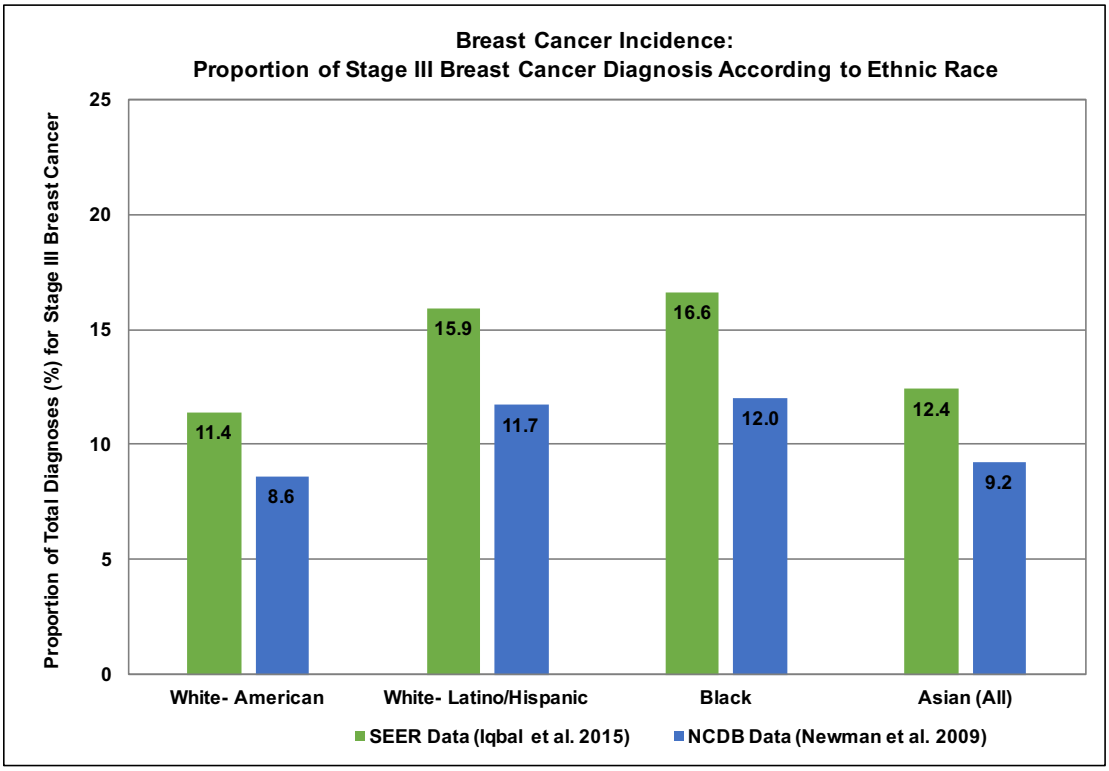

Figure 1.2: Stage 3 breast cancer incidence according to race. [Adapted from: (Iqbal et al., 2015, Newman, 2009)]. Data population: American Women; National Cancer Database [NCDB] (2009, n=178,764), SEER (2015, n=373,563).

Gender: Gender is a significant risk factor for new diagnoses; male breast cancers are very rare and account for only 1% of all breast cancers (Leone et al., 2015). Previous data from 2005 reported 1690 new cases in the

United States and of those cases, the mortality rate showed that 460 men died of the disease (Jemal et al., 2005). After a decade, incidence rates have increased to 2350 diagnoses in 2015 with a stable mortality rate of 440 deaths (18.7%) per year in the United States (Siegel et al., 2015).

Age: The probability of developing breast cancer over a lifetime is 12.3%, however there is an increased risk with an increase in age (Siegel et al., 2015). The median age for developing breast cancer is 60 years old (Iqbal et al., 2015). **Figure 1.3** presents the risk probability in the United States from 2009 to 2011. The peak probability is reported in women above 70 years old. At this age interval, women demonstrate a 6.7% probability of developing breast cancer (i.e., 1 in 15 women) (Siegel et al., 2015).

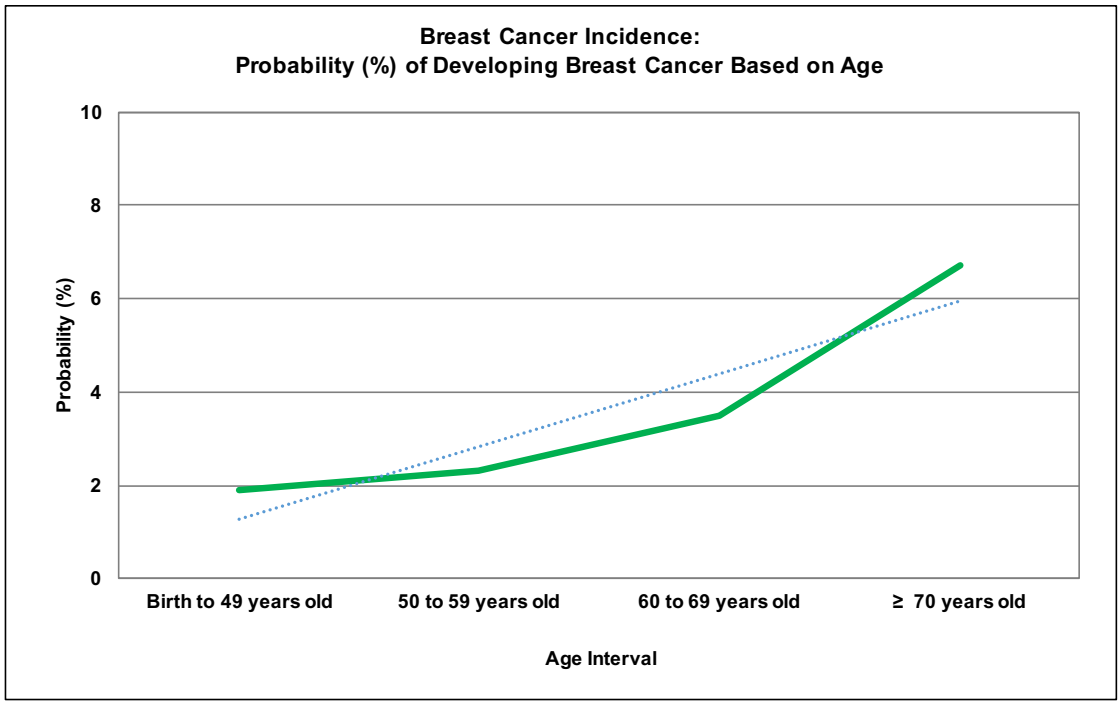

Figure 1.3: Breast cancer incidence related to age (data on women, 2009-2011 in the United States). [Adapted from data obtained by (Siegel et al., 2015)]. The increased incidence of breast cancer is related to older age. Women over the age of 70 show a highest risk of developing breast cancer, with a probability of 6.7%, or 1 in 15 women. The median age for developing breast cancer is 60 years old. *Blue dotted line: Regression line*

Family History and Genetic Conditions: Hereditary factors account for 27% of breast cancer risk; 95% CI [4%, 41%] (Lichtenstein et al., 2000).

The risk ratio for breast cancer in women with one first degree relative who has breast cancer is 1.8; 95% CI [1.70, 1.91], and increases to 2.93; 95% CI [2.37, 3.63], when two first degree relatives have breast cancer. The risk ratio is 3.90; 95% CI [2.03, 7.49], when three or more relatives have breast cancer (Collaborative Group on Hormonal Factors in Breast, 2001). Women with an adoptive parent with breast cancer have not been shown to be at higher risk for breast cancer (Zoller et al., 2014).

In terms of genetic conditions, women who carry mutations in tumour suppressor genes, BRCA-1 (breast cancer susceptibility gene-1) and BRCA-2 demonstrate a higher risk for breast cancer and this is confounded with age, and a family history of breast cancer (King et al., 2003, Antoniou et al., 2003). It should be noted that BRCA mutations are relatively rare in the general population; only 0.11%, and 0.12% of the general population express BRCA-1 and BRCA-2 mutations, respectively. However, approximately 3.0%-3.1% of breast cancer patients under 50 are BRCA-1 and BRCA-2 mutation carriers. BRCA-1 or BRCA-2 mutation carriers develop breast cancer earlier in their lifetime compared to women who are not carriers (i.e. wild type) (King et al., 2003). Each successive year of the carrier's lifetime confers an increased cumulative risk of developing breast cancer. By 70 years of age the cumulative risks are 65% for BRCA-1 mutation carriers and 45% for BRCA-2 mutation carriers (Antoniou et al., 2003).

A family history of breast malignancies elevates breast cancer risk in BRCA mutation carriers. Metcalfe et al. (2010) showed that women with BRCA mutations whose first-degree relatives are diagnosed with breast cancer by age 50 or younger demonstrate a hazard ratio of 1.67; 95% CI [1.04, 2.69] for BRCA-2 carriers. In comparison, BRCA-1 carriers demonstrate a hazard ratio of 1.21; 95% CI [0.94,1.57], indicating that there is a weaker familial association to breast cancer risk within this group (Metcalfe et al., 2010). Other genes have been suggested in increasing the risk of breast cancer such as TP53 (tumour protein-53), ATM (serine/threonine kinase), and CHEK2 (checkpoint kinase-2) (Turnbull and Rahman, 2008). The relative risks associated with gene mutations are >10%, 2-3%, and 2-3%, respectively (Turnbull and Rahman, 2008). However, the carrier frequency of these gene mutations is very low (<0.4%) in the general population (Turnbull and Rahman, 2008).

Gynaecological and obstetric history: Reproductive factors are linked to breast cancer risk and include the age at menarche, age of menopause, and parity. Women who reach menarche earlier during adolescence are at an increased risk of developing breast cancer (McPherson et al., 2000). A meta-analysis which included 117 studies showed that each earlier year at menarche corresponded to an increased risk of 1.050-fold; 95% CI [1.044,1.057] (Collaborative Group on Hormonal Factors in Breast, 2012). In the same study, the later age of menopause was also linked to an increased risk. For every older year of menopause, the risk factor was 1.029; 95% CI [1.025,1.032]. The increased risk may be linked to the lifetime exposure to oestrogens (Yager and Davidson, 2006). Parity has been shown to mitigate breast cancer risk (Collaborative Group on Hormonal Factors in Breast, 2002). The relative risk of developing breast cancer is reduced by 7% with each childbirth (Collaborative Group on Hormonal Factors in Breast, 2002). Also, having children earlier in life reduces the risk; each earlier year reduces the relative risk by 3.0% (Collaborative Group on Hormonal Factors in Breast, 2002). Parity has also been linked to certain types of breast cancer such as hormone-sensitive breast cancer. There is also evidence to suggest that parous women were 25% less likely to develop hormone-sensitive breast cancer. Also, women who had children at an older age were shown to increase their risk by 15% of developing hormone-sensitive breast cancer. Other reproductive-related factors include breastfeeding history, the use of oral contraceptives and hormone replacement therapy (HRT). For every year of breastfeeding, the relative risk of breast cancer is decreased by 4.3%; 95% CI [2.9, 5.8] (Collaborative Group on Hormonal Factors in Breast, 2002). Oral contraceptives account for an increased risk of 1.1%, and post-menopausal HRT is responsible for 3.2% of breast cancer cases in the UK (Parkin, 2011b).

Lifestyle Factors: The patient's lifestyle history can also provide important information for risk factors which include: diet, and weight. Poor diet involving high fat intake, and obesity have been suggested as risk factors for breast cancer; the risk is double for obese patients (McPherson et al., 2000). Finally, alcohol consumption and smoking status have been correlated to increasing the lifetime risk of developing breast cancer. Chen and colleagues (2011) observed 105,986 women between 1980 and 2008 and evaluated the

link between alcohol consumption and breast cancer risk. The study showed that the relative risk (RR) of developing breast cancer was 1.15 when alcohol consumption levels ranged between 5.0-9.9 grams/day, which equates to 3-6 drinks per week (Chen et al., 2011). A British study by Parkin (2011) showed that 6.4% of breast cancer cases between 2000-2001 were attributable to alcohol consumption (Parkin, 2011a). In terms of smoking, a recent study by Gaudet et al. (2013) examined data taken from 73, 388 female participants enrolled in the American Cancer Society's Cancer Prevention Study II (CPS-II) (Gaudet et al., 2013). Breast cancer incidence was higher in current smokers (Hazard Ratio=1.24), and former smokers (Hazard Ratio=1.13), compared to women who never smoked (Gaudet et al., 2013).

1.2.4 Screening and Diagnosis

Screening for breast cancer is completed under two major routes: 1) a self-breast exam (SBE) or; 2) during a routine or urgent referral from the general practitioner (GP). Practicing and educating SBEs have not been shown to improve mortality, although awareness is an important aspect to overall breast care (Thomas et al., 2002, Austoker, 2003). A longitudinal study examined 266,064 Chinese women over 10-11 years. The participants were randomized into two groups that received either SBE instructions (i.e. taught group) or women who did not receive teaching on SBE (non-taught group). The results of the study showed nearly identical death rates related to breast cancer between groups (taught group, n=135 versus non-taught group, n=131) (Thomas et al., 2002).

In the United Kingdom, 51% of women are diagnosed through the "two-week wait" NHS policy; 31% through screening; 9% by way of routine or urgent referrals from general practitioners; and a smaller percentage (4%) are diagnosed in the urgent care unit (Cancer Research UK, 2016d). Quality standards for breast cancer screening and diagnosis in the UK have been developed by the National Institute for Health and Care Excellence (National Institute for Health and Clinical Excellence (NICE), 2009b). NICE guideline standards recommend a "timely diagnosis" where patients are referred to their general practitioner or specialist to carry out a triple-diagnostic assessment (National Institute for Health and Clinical Excellence (NICE), 2009b). Within this

recommendation, a single visit for the patient would include: 1) clinical assessment; 2) mammography and/or ultrasound examination; and 3) a fine-needle aspiration (FNA) or core biopsy for histological analysis (National Institute for Health and Clinical Excellence (NICE), 2009b). Magnetic resonance imaging (MRI) may be recommended for patients when there is poor mammographic quality due to dense breasts, or to assess the tumour's size if breast-conserving surgery is indicated (National Institute for Health and Clinical Excellence (NICE), 2009b). The NICE guideline (algorithm) for screening and diagnosis is presented in **Figure 1.4**.

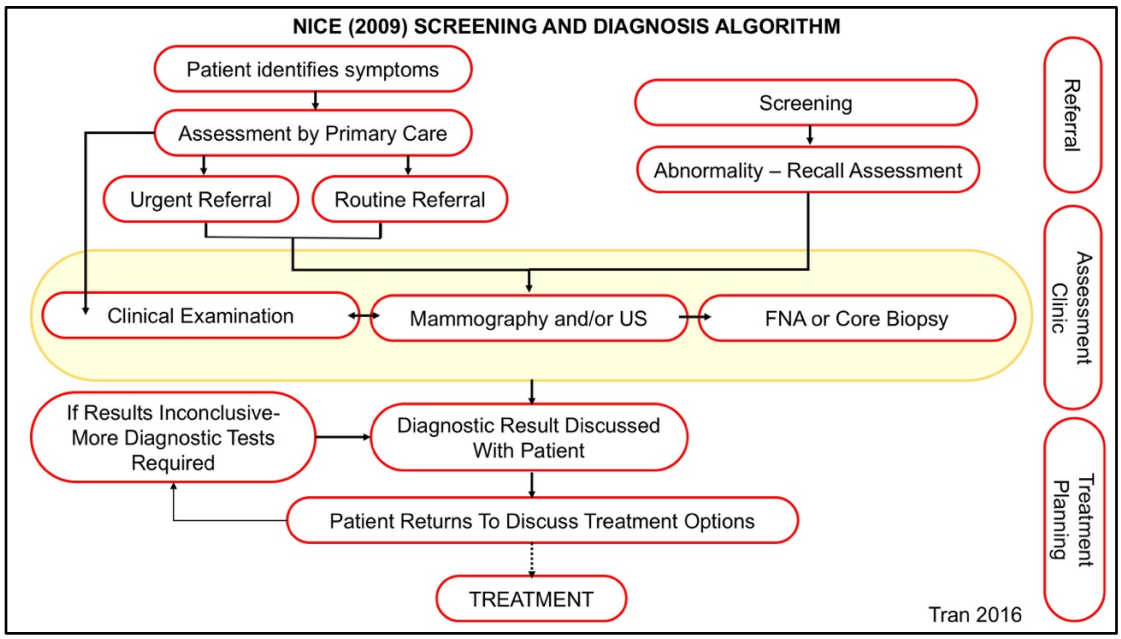

Figure 1.4. Breast cancer screening and diagnosis guidelines were developed by the National Institutes for Health and Care Excellence (2009). The National Institutes for Health and Care Excellence make recommendations for a one-day service where patients undergo a triple-diagnostic assessment that involves clinical assessment (physical palpation), mammography, followed by a fine-needle aspiration or core biopsy to confirm malignancies in the breast (National Institute for Health and Clinical Excellence (NICE), 2009b).

Medical imaging has an important role in the detection of benign and malignant breast masses (Saslow et al., 2007). However, routine mammography has not shown to decrease mortality in women in recent screening trials (Miller et al., 2014). A study by Miller et al. (2014) compared survival data for women (n=89,835) who were randomized into two groups:

annual physical breast examinations (i.e. clinical examination) with mammography versus a control group (no mammography, but clinical examination only). A hazard ratio (HR) of only 1.05 was observed between the two patient groups. The authors concluded that there is no survival benefit when routine mammography is given to women annually (Miller et al., 2014).

A diagnosis of breast cancer is determined from a core biopsy of the primary lesion. Histological features of the cancer cells may also be collected, such as cellularity, grade, molecular and intrinsic features (ER, PR, HER2) to help guide treatments (National Institute for Health and Clinical Excellence (NICE), 2009b). Additionally, current guidelines indicate for a biopsy of axillary lymph nodes as part of the cancer staging work-up (National Institute for Health and Clinical Excellence (NICE), 2009b). An ultrasound-guided fine-needle aspiration is used to confirm for malignancies histologically (National Institute for Health and Clinical Excellence (NICE), 2009b). In cases where there is no evidence of disease in the axilla from biopsy, women with early invasive breast cancer are recommended for sentinel lymph node biopsy at surgery (National Institute for Health and Clinical Excellence (NICE), 2011). Additional investigations include using computed tomography (CT), MRI, or nuclear medicine scans to screen for metastasis in cases where advanced breast cancer is suspected (Murray et al., 2009). These involve examinations of the liver, lungs, brain, and bones (Whitman and Strom, 2009).

Taken together, breast cancer is initiated by environmental, lifestyle, biological, and genetic factors. The development of breast cancer is reliant on physiological processes that form biologically diverse tumours. A diagnosis of breast cancer can be alarming to patients and thus clinical standards have been outlined in the UK to provide rapid screening and diagnosis. Despite the efforts for health agencies such as the NHS (UK) and Health Canada to provide education, rapid screening and diagnosis, a portion of patients may still present with advanced disease, such as locally advanced breast cancer (LABC). LABC carries an especially poor prognosis and the survival for patients is low compared to early stage breast cancer. Since LABC can present itself as a clinical challenge, the details of its presentation, treatment and thus providing the motivation of the thesis is outlined in the next sections.

1.3 Locally Advanced Breast Cancer and Treatment

Locally advanced breast cancer, which is described as stage 3 disease, characteristically is a lesion greater than 5 cm and may involve the lymph node, skin, and chest wall. There is an especially poor prognosis (Newman, 2009, Lee and Newman, 2007); incidence rates of LABC in the United States account for 12.4% of new breast cancer cases in 2015 and 8.5% of cases in the United Kingdom (Iqbal et al., 2015, Cancer Research UK, 2016c). Survival data for patients with LABC in America were reported in 2009 using the *SEER* registry (Statistics, Epidemiology, and End-Results Program) (Newman, 2009, Tryfonidis et al., 2015). Mortality rates for locally advanced breast cancer ranged between 48%- 52% (Newman, 2009). British data showed that between 2002-2006, only 55.1% of women with stage 3 breast cancer survived beyond 5-years (Cancer Research UK, 2016b).

Locally advanced breast cancer requires multimodality treatment to address both local (primary) disease and potential distant microscopic spread. Studies emerged in the 1970s in Europe and the United States, which showed that pre-operative (neoadjuvant) chemotherapy for LABC (stage 3 disease) can have significant practical and clinical advantages (Broadwater et al., 1991, Alvarado-Cabrero et al., 2009). These advantages included down-staging inoperable breast tumours to facilitate resection and allowing clinicians to monitor tumour response during therapy (Cance et al., 2002, Honig et al., 2005). However, there is still some debate about its benefit; specifically since neoadjuvant chemotherapy has not been associated with increasing survival, despite these putative advantages (Lee and Newman, 2007). The following section discusses disease management for locally advanced breast cancer, and specifically focus on chemotherapy treatment in the pre-operative setting (i.e. neoadjuvant chemotherapy).

1.3.1 Multimodality Treatments: Historical Perspective

Treatment for locally advanced breast cancer involves multimodality treatments that are loco-regional (i.e. surgery or radiation), or systemic (i.e. chemotherapy, endocrine therapy, targeted drug therapy) (El Saghir et al., 2008). Multimodality treatments for cancer have only been realized in the past

70 years of medicine (Lee and Newman, 2007). Historically, data from the 1940s reported low rates of survival for patients with stage three breast cancer who received mastectomy alone; only 6% of patients lived beyond five years (Haagensen and Stout, 1943, Lee and Newman, 2007). However, it was during the 1940s, and 1950s that chemical agents that were intended for military warfare were being tested for cancer therapy (DeVita and Chu, 2008). This was initiated from observations that soldiers who were accidentally exposed to mustard sulphurs in World War one, and two demonstrated depleted bone marrow and lymph nodes and thus research began to study its potential treatment for cancer (Krumbhaar and Krumbhaar, 1919, DeVita and Chu, 2008). In the late 1960s multidrug chemotherapy "cocktails" were tested for breast cancer (Bagley et al., 1972, Canellos et al., 1974). Early results in the 1970s using primary chemotherapy-alone, as well as adjuvant chemotherapy (i.e. after mastectomy) showed exciting improvements in survival for patients with advanced breast cancer (Canellos et al., 1974, DeVita and Chu, 2008). The median survival for responders was 13 months compared to 6 months for non-responders (Canellos et al., 1974).

At the same time, trials between 1960-1975 in the United States investigated radiation-alone for locally advanced breast cancer. However early analysis showed high loco-regional failure rates in 37% of patients treated with radiation alone (Bedwinek et al., 1982). Adjuvant radiation improved survival; results indicated a significant reduction of 12% in loco-regional failure rates ($p<0.001$) (Bedwinek et al., 1982). However, distant metastasis remained as a clinical problem despite improved local control using radiation and surgery. **Table 1.4** shows results of that early study (Bedwinek et al., 1982).

(n=183)	**Percent Failure (%)**		
Site	**Radiation-alone**	**Radiation + Surgery**	**p-value**
Local	61	13	0.0001
Regional	37	12	0.0007
Distant Metastasis	65	68	0.7 (NS)

Table 1.4: Radiation and surgery resulted in improved outcomes. "Failure" end-points were defined as disease relapse identified within the site after 5+ years. (NS); Not Significant

In current oncology practice, it has become widely accepted that multimodality therapies that combine surgery, chemotherapy, and radiation

improve overall survival compared to regimens that exclude one or more modalities within the treatment scheme (Cance et al., 2002, Giordano, 2003). Since the 1970s, pre-operative (neoadjuvant) chemotherapy, followed by surgery, then radiation have become standard treatment approaches for locally advanced breast cancer in North America (Valero et al., 1996) **(Figure 1.5)**. Multimodality treatment decisions are dependent on the tumour's response at each phase of the patient's treatment plan.

The focus of the thesis will therefore examine breast cancer neoadjuvant chemotherapy since it is recommended as first-line treatment for LABC in North America, and its effects can influence subsequent surgery and radiation for patients. Neoadjuvant chemotherapy for LABC is described in the subsequent sections.

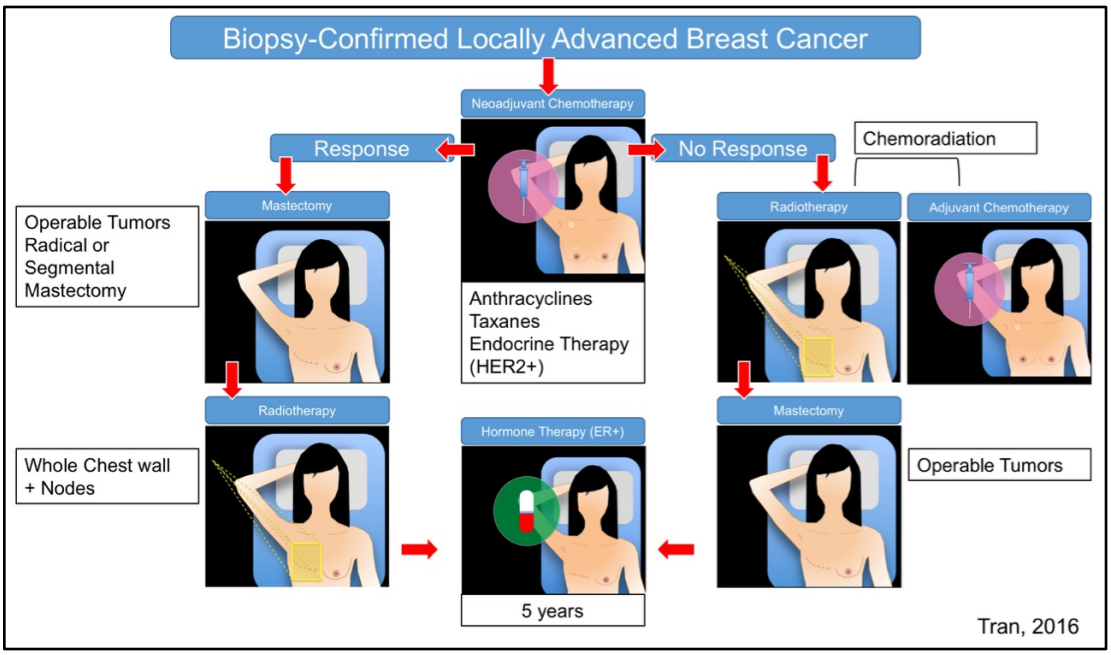

Figure 1.5: Multimodality treatments decision tree. Neoadjuvant chemotherapy is administered to allow tumour surveillance during treatment. Approximately 84% of patients will have sufficient tumour down-staging for mastectomy, then radiation (Cance et al., 2002).

1.4 Study Motivations and Aims 1

Identifying the Target Study Population

The motivation for this thesis is based on studying patients with LABC because:

1) Breast cancer is a global public health problem.
2) Approximately 8.5% (i.e. 4,700 cases) of breast cancer is diagnosed as LABC (i.e. stage 3) in the United Kingdom which accounts for a significant patient population.
3) LABC has a poor 5-year survival rate (55.1%) compared to early stage breast cancer which makes it a clinical problem.

Therefore, the aim of this study will focus on locally advanced breast cancer patients and treatments. Since neoadjuvant chemotherapy is the primary treatment for this patient population, the aim of this thesis is to study locally advanced breast cancer patients treated with neoadjuvant chemotherapy.

1.5 Breast Cancer Chemotherapy

Chemotherapy drugs are among many types of cytotoxic agents used to treat breast cancer. Chemotherapy strategies destroy cancer cells by targeting the cells' ability to replicate and function. In many cases, this is achieved by disrupting the DNA of cancer cells. In contrast to normal cells that are able to repair itself from cytotoxic effects, cancer cells lack repair mechanisms and undergo various forms of cell death such as apoptosis, oncosis or necrosis when exposed to chemotherapy (Okada and Mak, 2004).

Chemotherapy is administered intravenously for breast cancer over a period of several cycles (6-8 cycles, two to three weeks between cycles). Drug strategies also combine several types of drugs simultaneously to target cancer cells **(Table 1.5, Figure 1.6)**. Drug combinations include anthracyclines, taxanes, alkylating agents and antimetabolites (Cancer Research UK, 2016a). Anthracyclines interfere with DNA regulation (Thorn et al., 2011); taxanes disrupt microtubule "building blocks" that are essential for cell replication (Dumontet and Jordan, 2010); alkylating agents interfere with DNA formation (Fu et al., 2012); and antimetabolites interfere with molecules required for DNA synthesis (Parker, 2009). Employing multiple drug combinations were shown to improve survival by the Aberdeen Trial (UK) (Heys et al., 2002). Patients who were randomized for combination drugs demonstrated a 34% rate in pathological complete response (pCR) versus 16% for patients who were randomized to fewer chemotherapies (Heys et al., 2002) **(Figure 1.7)**.

Chemotherapy Drug		Drug Type	Chemotherapy Combination
Cyclophosphamide	[C]	Alkylating Agent	FEC-D or AC-T
Epirubicin	[E]	Anthracycline	FEC-D
Doxorubicin	[A]	Anthracycline	AC-T
Fluorouracil (5FU)	[F]	Antimetabolite	FEC-D
Docetaxel	[D]	Taxane	FEC-D
Paclitaxel	[T]	Taxane	AC-T

Table 1.5: Various chemotherapy drug-types are used to treat breast cancer.

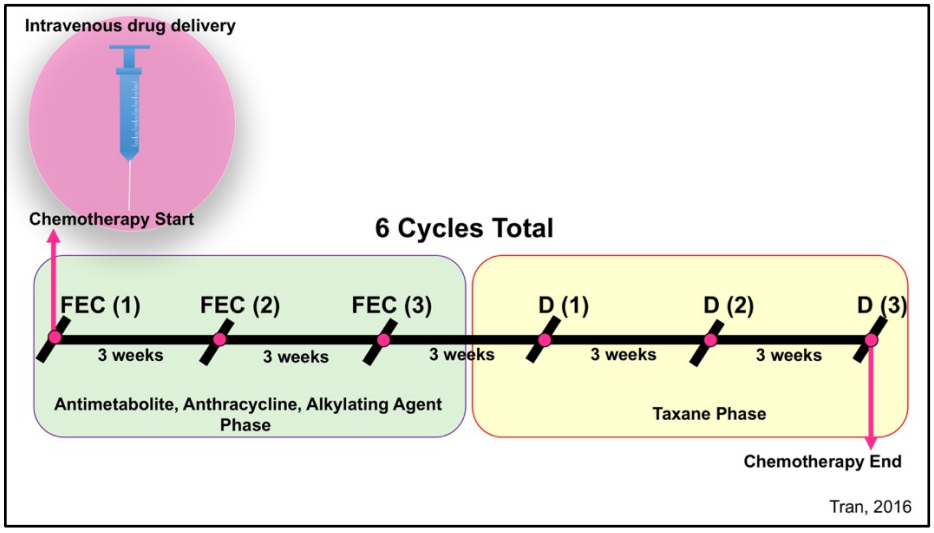

Figure 1.6: Chemotherapy is given in several cycles, over a course of several weeks. In this schematic representation, chemotherapy combinations use Fluorouracil, Epirubicin, Cyclophosphamide in the first three cycles followed by Docetaxel to complete another three cycles (represented in parenthesis). The time intervals are used to allow patients to recover between cycles and to monitor the patient's wellbeing through blood tests and physical examination (Cancer Research UK, 2016a).

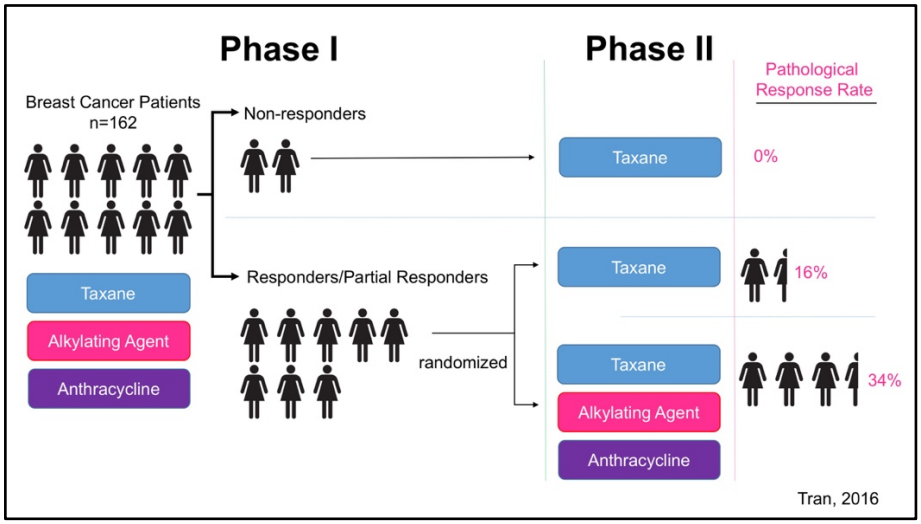

Figure 1.7: [Adapted from (Heys et al., 2002)]. Breast cancer patients (n=162) with large or locally advanced breast cancers were treated with various chemotherapy treatment schemes (Phase I). Responders were randomized into two treatment arms (Phase II), and results indicated that patients who were treated with more combination drugs demonstrated a higher pathological complete response rate (34%) in comparison to patients who received fewer chemotherapy combinations (16%).

Chemotherapy treatment with surgery and radiation have been shown to improve survival for breast cancer; however clinical data collected since the 1980s have shown that there are no significant differences in survival outcomes when chemotherapy is administered pre-operatively (neoadjuvant chemotherapy) versus post-operatively (adjuvant chemotherapy) (Wolmark et al., 2001, Sachelarie et al., 2006). Data from the United Kingdom at the Royal Marsden Hospital reported equivalent survival in both pre-operative and post-operative chemotherapy-treated groups (Powles et al., 1995). Thus, there has been some confusion about the primary role of pre-operative, versus post-operative chemotherapy. Fundamental advantages for pre-operative chemotherapy are mostly pragmatic; which include improving resection from tumour-size reduction, immediate cancer down-staging (i.e. reducing tumour extent), permitting clinical surveillance to gauge tumour behaviour to chemotherapy (i.e. chemosensitivity), and assess metastatic risk (Valero et al., 1996, Cancer Research UK, 2016a). Anecdotal reports also argue that maintaining the tumour intact during chemotherapy may improve drug delivery since the tumour vasculature is left intact before surgery (Giordano, 2003). Disadvantages to neoadjuvant chemotherapy may include delayed loco-regional treatment and it may complicate tumour resection if tumour response is unfavourable. For patients, the major disadvantages of delaying surgery in favour of giving neoadjuvant chemotherapy is the psychological and physical burden of having a tumour in the breast over the course of several months of chemotherapy (Walker et al., 1999).

1.6 Chemotherapy Side Effects

Although chemotherapy strategies are intended to damage tumour cells, treatments also affect normal cells that result in systemic toxicity and side effects. Complications associated with chemotherapy treatment (i.e. treatment morbidity) may present as acute side effects such as nausea, hot flashes, and dry mouth. Chronic (long-term) conditions include cardiac and vascular toxicity (Meinardi et al., 2000). However, morbidities such as cardiac toxicity may also have an early onset but continues into chronic conditions in later life (Yeh and Bickford, 2009). The following section will describe common morbidities associated with chemotherapy treatment.

1.6.1 Cardiac Complications

Cardiac complications include heart failure, myocardial ischemia, hypertension, thromboembolism, and bradycardia, and have been identified during anthracycline use (Yeh and Bickford, 2009, Thorn et al., 2011). The mechanism for cardiac toxicity is poorly understood; although there is evidence to suggest that reactive oxygen species from anthracyclines form metabolites that interfere with cardiac fibrillation by disrupting iron and calcium regulation (Thorn et al., 2011). Another proposed mechanism for causing cardiotoxicity is the disruption of mitochondrial respiration that can initiate apoptosis in cardiac cells (Clementi et al., 2003). Other direct effects on cardiac cells have been linked to 5-fluorouracil, which has been shown to cause cell hypoxia and interfere with metabolic regulation (Meinardi et al., 2000). Targeted therapies such as Trastuzumab have been shown to cause congestive heart failure and compromised left-ventricle ejection fractions (Slamon et al., 2001). Due to these potential hazards, drugs are grouped separately to minimize the additive toxic effects; for example, Trastuzumab is not recommended in combination with anthracycline chemotherapy. A higher incidence of cardiotoxic effects were observed when anthracyclines were given with Trastuzumab (27%) compared to Trastuzumab alone (5%) (Hudis, 2007).

The incidence of heart failure was documented to be as high as 45% of patients who received anthracycline-based drugs (Yeh and Bickford, 2009). Other agents such as antimetabolites can induce myocardial ischemia in up to

68% of patients. Fluorouracil has been associated with cardiotoxicity and present as severe chest pain, and the death rate (mortality) for these episodes is estimated at 13% (Yeh and Bickford, 2009).

1.6.2 Haematopoietic Toxicity

Cytotoxic effects can occur in blood cells and lead to neutropenia, which is a condition associated with severe neutrophil depletion. Neutrophils are a type of white blood cell that are responsible for host immunity to infectious agents. The risk of developing neutropenia increases with age, and its onset is associated with anthracyclines and alkylating chemotherapy treatment (Crawford et al., 2004). Consequences associated with hematopoietic toxicity include susceptibility to bacterial infections from *Escherichia coli, Klebsiella pneumoniae, Staphylococcus, Streptococcus, and Enterococcus,* and are most commonly observed in the digestive tract, lungs and skin (Crawford et al., 2004). Symptoms associated with neutropenia present as fevers and fatigue. Mortality from neutropenia-related infections have been reported around 8% (Crawford et al., 2004).

Other complications include neutropenic sepsis which affect specialized immune-producing cells in the bone marrow. Neutropenic sepsis can be fatal and mortality rates range between 2% - 21% (National Institute for Health and Clinical Excellence (NICE), 2012). Symptoms associated with neutropenic sepsis are similar to neutropenia and involve fever (pyrexia) and susceptibility to infections. Treatments for both conditions involve antibiotic therapy and a temporary suspension of chemotherapy until blood tests indicate a recovery in neutrophils (National Institute for Health and Clinical Excellence (NICE), 2012).

1.6.3 Gastrointestinal Toxicity

Damage to the gastrointestinal (GI) system will present as nausea, diarrhoea, esophagitis, stomatitis, and mucositis and are associated with many chemotherapeutic agents such as taxanes, platinum compounds, anthracyclines, and pyrimidine antimetabolites (Boussios et al., 2012). The gastrointestinal system is especially vulnerable to toxicity from chemotherapeutic agents since normal cells of the GI system divide rapidly

(Boussios et al., 2012). The onset of symptoms is typically acute; for example, cisplatin doses given between 5-120 mg/m^2 trigger vomiting (emesis) within 24 hours after dose administration. Similarly, alkylating agents cause nausea and vomiting as early as 1-2 hours after treatment administration (Boussios et al., 2012). The prevalence of symptoms is dependent on the type of chemotherapy; alkylating agents and platinum based compounds showed the highest incidence of GI toxicity of up to 90% of patients (Boussios et al., 2012).

1.6.4 Alopecia

Chemotherapy-induced alopecia is characterized as hair loss on the scalp and other parts of the body, and is associated with high anxiety and distress in cancer patients (Trueb, 2009). Cells of the hair follicles are rapidly dividing and therefore are prone to injury from cytotoxic therapy (Trueb, 2009). The onset of alopecia often occurs one to three weeks after starting chemotherapy and full hair-loss typically takes place between one to two months (Trueb, 2009). Chemotherapy agents associated with high rates of hair loss include: anthracyclines, alkylating agents, and pyrimidine antimetabolites (Chon et al., 2012). In contrast, platinum-based drugs such as cisplatin rarely cause hair loss (Trueb, 2009).

1.6.5 Neurotoxicity

Neurotoxicity can present in 30-40% of patients as peripheral neuropathy. This condition is described as extremely painful sensations in the toes, fingers, and extremities (Wolf et al., 2008). Peripheral neuropathy can be caused by platinum agents, taxanes, and alkylating agents that damage the neural cells of the peripheral nerves (Wolf et al., 2008). The onset of symptoms may occur spontaneously during treatment, and present as “tingling” in the toes and fingers. Some reports have indicated that full neuropathic recovery is rarely achieved; while others have indicated improvement or resolution within 3-6 months after completing chemotherapy (Kannarkat et al., 2007, Argyriou et al., 2005). Other neurotoxic effects include paclitaxel acute pain syndrome. This condition is characterized as arthralgia and myalgia and is experienced in approximately 58% of patients who have received paclitaxel drugs as part of

their treatment regimen (Wolf et al., 2008). Despite symptoms experienced in the muscle, the suspected mechanism is believed to be caused by hypersensitization of neural fibres of the spinothalamic system (Wolf et al., 2008).

1.6.6 Anaphylaxis

Hypersensitivity to chemotherapy agents can lead to anaphylaxis reactions which involve the rapid activation of inflammatory signals such as histamine, cytokines, and chemokines that result in sudden respiratory contraction, and cardiovascular response (Castells et al., 2012). Taxane-hypersensitivity reactions are common; approximately 30% of patients develop some form of hypersensitivity, however improved pre-treatment protocols such as administering antihistamines and corticosteroids prior to taxane-infusion have reduced the rate to approximately 10% (Castells et al., 2012, Feldweg et al., 2005). The exact mechanism of chemotherapy-induced hypersensitivity is still under investigation, however at extremely high doses of paclitaxel (10-100 times the dose given clinically), human basophil cells were shown to demonstrate elevated histamine production (Essayan et al., 1996).

1.7 Mechanisms of Chemotherapy Resistance

1.7.1 Pharmacokinetic Influences

The variability in tumour response is caused in part by differences in drug pharmacokinetics; i.e., how the body processes the drugs based on biological and physiological mechanisms. These mechanisms are described by how drugs are handled by the body, which include: absorption, distribution, metabolism, and excretion (Garattini, 2007).

Absorption and Distribution

Drug absorption and distribution are important factors, as this represents the delivery of chemotherapeutic agents to the tumour (**Figure 1.8**). The absorption and distribution of chemotherapy in the body affects the chemotherapy concentrations. It has been shown that patients exhibit a two- to ten-fold difference in drug concentrations, which subsequently results in variable drug doses that can reach the tumour (Evans and Relling, 1989, Masson and Zamboni, 1997). The absorption and distribution of drugs are affected by the route of entry into the body. Many chemotherapies are administered through intravenous injection, and therefore the drug's bioavailability is higher when delivered directly into the blood stream, compared to when drugs are given orally. Oral drug administration inhibits optimal absorption and distribution since gastric pH and the intestinal villi can act as barriers (Undevia et al., 2005). By contrast, in the vascular/circulatory system, drugs are bound to serum proteins such as albumin, that facilitates transport and delivery (Garattini, 2007). In the tumour itself, drug distribution may be blocked by tortuous blood vessels that restrict exchange and transport cross the vascular barrier (Goel et al., 2011).

Metabolism and Excretion

Drug metabolism is an important step for activating drugs into molecular forms that are recognizable to tumour cells **(Figure 1.8)**. For example, the alkylating agent, cyclophosphamide is biologically active in the liver, which

metabolizes cyclophosphamide into intermediate biochemical products that are readily transported into the tumour cell (Garattini, 2007). Metabolic activation relies on enzymes such as Cytochrome P450, CYP2B10, CYP2C29, CYP2C19 and CYP3A, which is responsible for 45-60% of drug activation (Garattini, 2007, Undevia et al., 2005). For patients who are enzyme-deficient, chemotherapies are not activated therefore the drugs remain inactive and ineffective in the system (Undevia et al., 2005). Other metabolic defects are caused by dysfunctional drug uptake into the cell itself, which are caused by drug efflux mechanisms that pump out the drugs across the cell's plasma membrane **(Figure 1.9)** (Coley, 2008).

Excretion can influence drug clearance and is handled by the kidney, and biliary tract. Renal and hepatic dysfunction may affect drug concentrations in the blood by rapidly excreting drugs (Undevia et al., 2005).

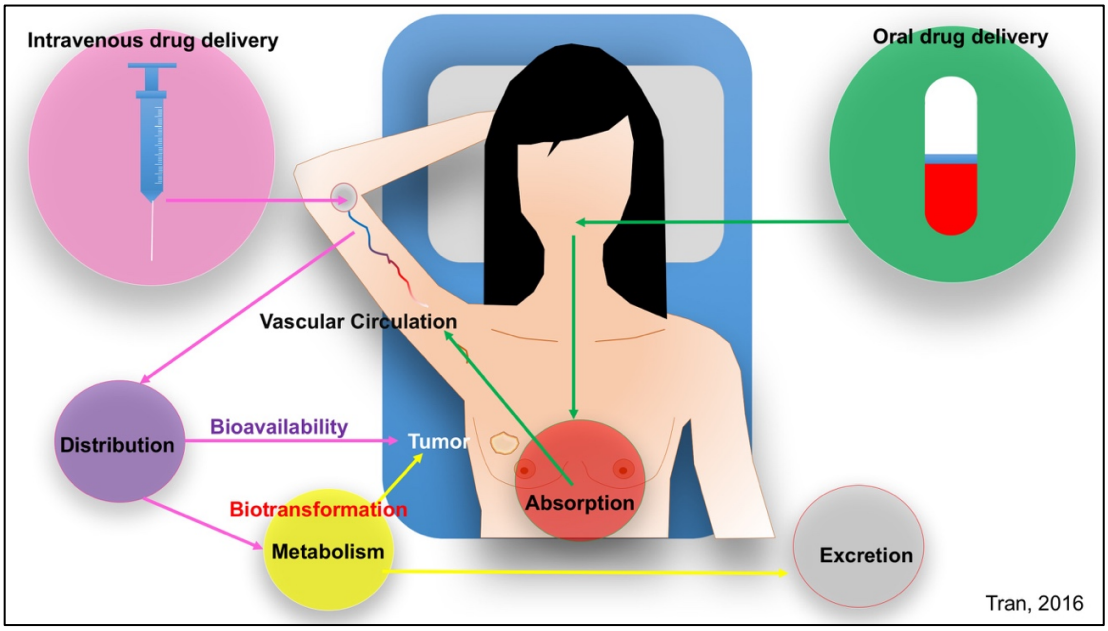

Figure 1.8: Drug pharmacokinetics can influence drug resistance. Pharmacokinetics are defined by the drug's interaction with the body through absorption, distribution, metabolism and excretion. The efficacy of a drug can be reliant on its bioavailability and biotransformation that activates the mechanism of action on the tumour cells.

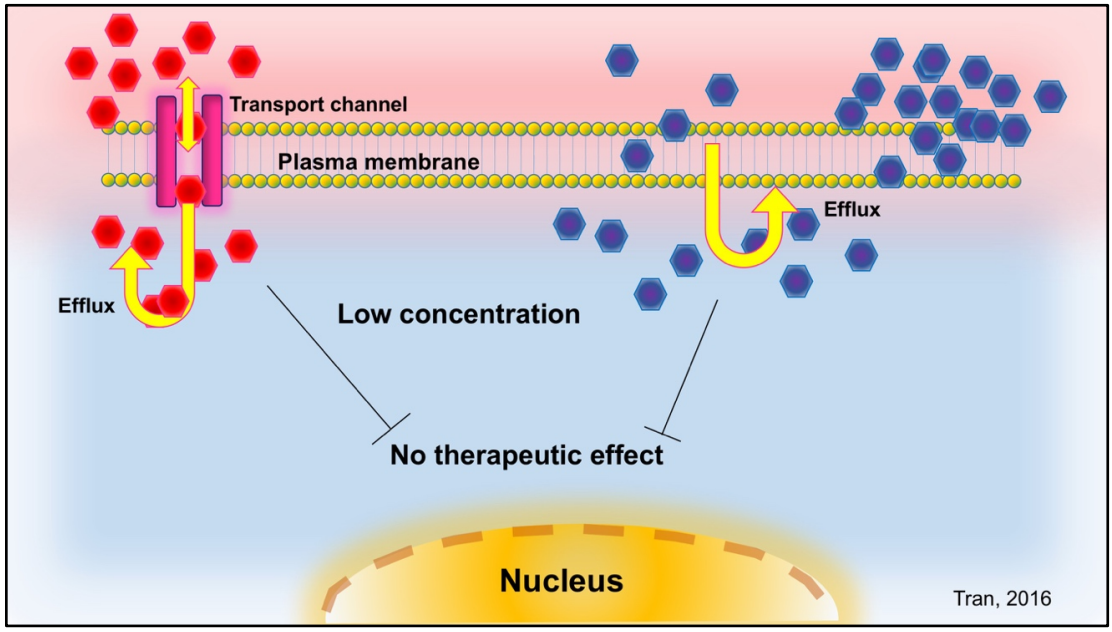

Figure 1.9: Chemotherapies are transported into the cell by either active transport or passive diffusion across the plasma membrane. Ineffective chemotherapy can occur when drug efflux occurs that result in low drug concentrations in the cytoplasm. This results in inadequate delivery of drugs into cell targets, such as the nucleus.

1.7.2 Chemotherapy Resistance in Molecular Subtypes

Breast cancer molecular subtypes, as described earlier as having different ER, PR and HER2 status, demonstrate variable response to neoadjuvant chemotherapy (von Minckwitz et al., 2012, Carey et al., 2007, Rouzier et al., 2005). Reports of over 6,000 patients have showed that basal-type, and HER2+ breast cancers have the highest rate of pathological complete response (pCR) to anthracycline- and taxane-based chemotherapies **(Table 1.6)**. In contrast, luminal A and luminal B breast cancers (i.e. ER+, PR+) are highly resistant to chemotherapy. There is evidence in rodent models that luminal breast cancer cells exhibit stem-cell-like behaviours that are genetically driven and cause tumour cell immortality, higher rates of differentiation, and rapid proliferation (Sims et al., 2007). Some studies have also suggested that basal-type tumours have dysfunctional cell-repair mechanisms in comparison to luminal A and luminal B tumours that make it more susceptible to chemotherapy-induced DNA damage (Desmedt et al., 2008). **Table 1.6**

summarizes tumour response rates based on breast cancer molecular subtypes.

Reference	n	Neoadjuvant Chemotherapy	pCR Rate by Molecular Subtype
(Babyshkina et al., 2014)	198	5-FU[1] Doxorubicin Cyclophosphamide Capecitabine Taxotere Methotrexate	Luminal A+B: 2.1% Basal-Type: 10.7% HER2 +: 0.0%
(Carey et al., 2007)	107	Doxorubicin Cyclophosphamide Taxotere	Luminal A+B: 15.0% Basal-Type: 27.0% HER2 +: 36.0%
(Chang et al., 2010)	74	Docetaxel Carboplatin	Luminal A+B: No Data Basal-Type: 55.0% HER2 +: NS
(Goldstein et al., 2007)	68	5-FU Doxorubicin Cyclophosphamide Epirubicin Taxotere	Luminal A+B: 19.4% Basal-Type: 57.1% HER2 +: 62.5%
(Kim et al., 2010)	257	Doxorubicin Docetaxel	Luminal A+B: 8.9% Basal-Type: 21.1% HER2 +: 21.1%
(Liedtke et al., 2008)	1118	5-FU Doxorubicin Cyclophosphamide Epirubicin Paclitaxel	Luminal A+B: No data Basal-Type: 22.0% HER2 +: No data
(Rouzier et al., 2005)	82	5-FU Doxorubicin Cyclophosphamide Paclitaxel	Luminal A+B: 7.0% Basal-Type: 45.0% HER2 +: 45.0%

(Sanchez-Munoz et al., 2008)	127	Doxorubicin Cyclophosphamide Gemcitabine Epirubicin	Luminal A+B: 5.4% Basal-Type: 58.3% HER2 +: 39.5%
(von Minckwitz et al., 2012)	4193	Anthracyclines[2] Taxanes[2]	Luminal A+B: 13.9% Basal-Type: 35.8% HER2 +: 43.0%

Table 1.6: Comparison of chemotherapy response according to breast cancer molecular subtypes. All values within the 95% confidence interval. [1]5-Fluorouracil; [2]Anthracycline and Taxane type drugs not specified. NS: Not significant; pCR: Pathological complete response. Luminal A = ER+, PR+. HER2-. Luminal B = ER+, PR+, HER2+. Basal-Type= “Triple negative” (ER-, PR-, HER2-).

1.8 Prognostic Factors

1.8.1 Pathological Response to Neoadjuvant Chemotherapy

Pathological complete response (pCR) is a prognostic indicator and is defined as demonstrating no residual disease following chemotherapy (Ogston et al., 2003). There are several methods previously proposed to measure pathological response after neoadjuvant chemotherapy as a treatment endpoint that include the following classification systems: Chevalier, Sataloff, Residual Cancer Burden Index (RCBI), Miller-Payne, and the National Surgical Adjuvant Breast and Bowel Protocol B-18 (NSABP B-18), and Residual Disease in Breast and Nodes (RDBN) (Marchio and Sapino, 2011) **(Table 1.7)**. However, there is still no consensus on defining or classifying pathologic response in terms of pathological complete response and partial response (Corben et al., 2013).

Resected breast specimens are analysed microscopically to measure residual disease, assess cellularity, and examine if any cancer remains in the lymph nodes. The agreement on pathological complete response remains undetermined; for example, residual disease from ductal carcinoma in situ is still defined as pathological complete response for RCBI and Miller-Payne classification. On the other hand, Chevalier classification define pCR as complete disappearance of microscopic cells. This has led to varying practices between clinics and has also posed a challenge in research for correlating diagnostic tests to final pathologic endpoints (Symmans et al., 2007).

Pathological complete response is an important prognostic factor. There is an association between pCR and longer survival; a meta-analysis on 3,182 locally advanced breast cancer patients demonstrated a better survival time for patients who achieved pCR after neoadjuvant chemotherapy (odds ratio: 3.44 [95% CI: 2.45,4.84]; overall survival=2.3-7.6 years) (Kong et al., 2011). Another study by Chollet et al. (2002) followed 396 locally advanced breast cancer patients for 15 years, following neoadjuvant chemotherapy treatment. A significant difference in the disease-free survival (*P=0.039*) and overall survival (*P=0.047*) was reported in favour of pCR patients compared to partial responders (Chollet et al., 2002). In another study, 87% of patients who achieved pCR survived after 5 years (Kuerer et al., 1999). The rate of pathological complete response ranges between 15.2%-17.4% (Kong et al.,

2011, Chollet et al., 2002). Although pCR is the desired treatment outcome, patients achieving partial response (defined below in **Table 1.7**) may still benefit from therapy and live beyond five years. The German Breast Group reported that smaller residual tumours after chemotherapy were associated with better survival (HR range: 1.53-7.97, *p<0.001)*) (von Minckwitz et al., 2012). Also, a study by Huang et al. (2015) showed that the 5-year overall survival rate for partial responders was 68.5% (Huang et al., 2015). Poor prognosis and low survival rates in this response group are attributed mainly to local recurrence and distant metastasis (Huang et al., 2015).

System	Characteristics	Reference
Chevalier	**System Classification Type: Categorical** **Grade 1:** Disappearance of all tumour either on macroscopic or microscopic assessment. **Grade 2:** Presence of in situ carcinoma in the breast, no invasive tumour and no tumour found in the lymph nodes. **Grade 3:** Presence of invasive carcinoma with stromal alteration, such as sclerosis or fibrosis. **Grade 4:** No or few modifications of the appearance of the tumour.	(Chevallier et al., 1993)
Miller-Payne[2]	**System Classification Type: Categorical** **Grade 1:** No change or some alteration to individual malignant cells but no reduction in overall cellularity.	(Ogston et al., 2003)

[2] Miller-Payne pathological grading system is used in this study and described later in **Chapter 2 (Methods)** and **Chapter 3 (Results)**.

	Grade 2: A minor loss of tumour cells but overall cellularity still high; up to 30% loss. **Grade 3:** Between an estimated 30% and 90% reduction in tumour cells. **Grade 4:** A marked disappearance of tumour cells such that only small clusters or widely dispersed individual cells remain; more than 90% loss of tumour cells. **Grade 5:** No malignant cells identifiable in sections from the site of the tumour; only vascular fibroelastotic stroma remains often containing macrophages. However, ductal carcinoma in situ (DCIS) may be present. No assessment of lymph nodes.	
NSABP B-18	**System Classification Type: Categorical** **Pathological Complete Response (pCR):** No presence or recognizable presence of invasive tumour cells present. **Pathological Partial Responder (pPR):** Presence of scattered individual or small clusters of tumour cells in a desmoplastic or hyaline stroma. **No Pathologic Response (pNR):** Tumours not exhibiting any of the changes and characteristics as listed for pCR, and pPR. No assessment of lymph nodes.	(Fisher et al., 1998) (Marchio and Sapino, 2011)

RCB Index	**System Classification Type: Continuous** Parameters used to calculate the RCB index: *Primary Tumour Bed:* 1) Primary tumour bed area (mm) 2) Overall cancer cellularity (%) 3) Cancer that is in situ disease (%) *Lymph Nodes:* 1) Number of positive lymph nodes (n) 2) Diameter of largest metastasis (mm) A Cox-regression model is calculated. RCBI indices were classified as: **RCBI0:** Pathological complete response **RCBI1:** Moderate response **RCBI2:** Moderate response (relative score) **RCBI3:** Extensive residual disease **RCBI4**: Extensive residual disease (relative score)	(Symmans et al., 2007)
Sataloff	**System Classification Type: Categorical** *Tumour Characteristics Scoring (T)* **T-A:** Total or near total therapeutic effect. **T-B:** Subjectively >50% therapeutic effect, but less than total, or near total therapeutic effect. **T-C:** <50% therapeutic effect. **T-D:** No therapeutic effect evident. *Lymph Node Status (N):* **N-A:** Evidence of therapeutic effect, no metastatic disease.	(Sataloff et al., 1995) (Marchio and Sapino, 2011)

	N-B: No nodal metastasis; no therapeutic effect. **N-C**: Nodal metastasis; therapeutic effect. **N-D:** Nodal metastasis: no therapeutic effect.

Table 1.7: Pathological response classification systems use variables such as primary tumour dimensions, cellularity, and lymph node status to calculate the overall pathological scoring. Some scores are categorical data versus continuous data. The score/index indicates the relative therapeutic effect.

1.8.2 Molecular Features

Molecular subtypes in breast cancer are associated with variable prognosis and survival outcomes (Smid et al., 2008). A study examining 3,726 patients showed that the 10-year overall survival rate was 70% in patients with luminal A tumours, 54.4% in luminal B tumours, and 52.6% in basal-like tumours. HER2-overexpressed tumours were associated with 48.1% overall survival (Kennecke et al., 2010). A significant decrease in overall survival was indicated when distant metastasis was involved; luminal A tumours were associated with a median survival of 2.2 years, while patients with luminal B, and basal-like tumours had a median survival of 1.6 and 0.5 years, respectively. HER2-positive tumours resulted in a survival duration of 0.7 to 1.3 years (Kennecke et al., 2010). Women with HER2-overexpressed (i.e. HER2+) tumours also presented with the highest relapse rates in the liver and lung (Kennecke et al., 2010, Smid et al., 2008). Additionally, previous work from the German Breast Group (GBG) reported improved disease-free survival for Luminal B/HER2-, HER2+ (non-luminal), and triple negative (ER-/PR-/HER2-) breast cancers that achieve pCR (von Minckwitz et al., 2012).

At first glance, there seems to be conflicting data between survival outcomes of cancer subtypes and the rate of pathological complete response. For example, HER2-overexpressed tumours demonstrate high pCR but also have poor prognosis. This is explained as a proportion of HER2-overexpressed tumours demonstrate high relapse rates, and therefore patient deaths are caused mainly by metastasis to distant organs (Huber et al., 2009). Despite the

generally favourable response rates in HER2-overexpressed tumours; a large majority of HER2+ breast tumours do not achieve pathological complete response.

1.8.3 Histological Grade (Nottingham Grade)

According to the American Pathologists Consensus Statement, histologic grade is included as a prognostic indicator (Fitzgibbons et al., 2000). The "Bloom-Richardson-Nottingham" grade is calculated from histological features such as tubule formation, nuclear pleomorphism, and mitotic count of tumour cells (Elston and Ellis, 1991). The tubule formation describes the morphological characteristics of the cell; nuclear pleomorphism denotes the shape, size and structure of the cell's nuclei; whereas mitotic count represents the number of cell divisions that are present within the specimen. Clinicians interpret the Nottingham grade as the degree of cellular abnormalities present in the tumour and represents the tumour's "aggressiveness" (Elston and Ellis, 1991). **Table 1.8** outlines the scoring algorithm of individual features **(Table 1.8A)** and the resulting Nottingham tumour grade **(Table 1.8B)**. The Nottingham grade has been shown to be reproducible with a low relative disagreement rate (RDR) of 0.10 (95% confidence interval 0.05-0.19) and kappa [κ] statistic of 0.77 (95% confidence interval: 0.66-0.88) (Harvey et al., 1995).

Histological Features Measured	Score
Tubule Formation (TF)	
Majority of tumour (>75%)	1
Moderate degree (10-75%)	2
Little or none (<10%)	3
Nuclear Pleomorphism (NP)	
Small, regular uniform	1
Moderate increase in size and variability	2
Marked variation	3
Mitotic Counts (MC)[1,2]	
0-9	1
10-19	2
>20	3

Table 1.8A: Histological grade as measured by the Nottingham grade system. [1]Mitotic counts are counted per ten fields; [2]Mitotic counts are based on Leitz Ortholux microscope with an objective of 25x, field diameter of 0.59 mm, and field area of 0.274 mm^2. (Elston and Ellis, 1991).

Nottingham Grade (Modified Bloom-Richardson):	Grade
3-5 points: well differentiated (low)	1
6-7: moderately differentiated (intermediate)	2
8-9: poorly differentiated (high)	3

Table 1.8B: The Nottingham grade is calculated based on the sum of each feature score, and represents the potential aggressiveness of the tumour.

Previous work by Elston and Ellis (1991) showed that the Nottingham grade is associated with recurrence-free intervals and disease-free survival (Elston and Ellis, 1991). In this previous study, 1,830 patients were followed for up to 16 years after a mastectomy or local excision and radiotherapy (Elston and Ellis, 1991). The patient cohort comprised of 19% of patients who were Nottingham grade one, 34% were Nottingham grade two, and 47% were Nottingham grade three. A 16-year follow-up demonstrated that grade one patients were significantly correlated to a longer recurrence-free interval compared to grade two and three patients (χ^2=133.70 d/f; *p<0.0001*). Also, a greater survival rate was significantly correlated to grade one tumours, compared to grade two and three tumours (χ^2=198.06 d/f; *p<0.0001*).

1.8.4 Nottingham Prognostic Index

The Nottingham prognostic index (NPI) is modelled from a multivariate Cox regression based on an initial analysis of 387 breast cancer patients. The regression model includes multiple prognostic variables (age, menopausal status, tumour size, lymph node stage, tumour grade, cell reaction, sinus histiocytosis, oestrogen receptor status, adjuvant chemotherapy) to prognosticate patient outcomes (Haybittle et al., 1982, Blamey, 2002). The NPI is described as:

NPI = Grade [1-3] + LN Stage [1-3] + 0.2(Size) [cm] (**Equation 1.1)**

The NPI categorizes patients into potential prognostic risk groups based on the final index **(Table 1.9).**

Prognostic Group	NPI range[1]
Excellent	2.08-2.40
Good	2.42-3.40
Moderate I	3.42-4.40
Moderate II	4.42-5.40
Poor	5.42-6.40
Very Poor	6.50-6.80

Table 1.9: The Nottingham Prognostic Index was developed using a Cox regression analysis. The NPI classifies the patient's prognostic risk into categories that range from "Excellent" to "Very Poor". [1]Note the cut-off points between categories is based on the mathematical properties of the regression model.

Survival data was collected between 1990-1999 for 2,238 patients at Nottingham City Hospital. Researchers found a significant difference in the 10-year survival between "Excellent" NPI patients compared to other risk categories ($p<0.001$); for example, the 10-year survival for "Excellent" patients was 96%, compared to only 38% in patients who were classified as "Very Poor" (Blamey, 2002). Experimental work has also emerged in recent studies using a modified Nottingham prognostic indicator "plus" system (NPI+), which includes up to ten biomarkers in the Cox regression model: 1) Oestrogen receptor; 2) Progesterone receptor; 3) Cytokeratin 5/6 expression; 4) Cytokeratin 7/8; 5) Epidermal growth factor receptor, 6) HER2; 7) HER3; 8) HER4; 9) p53; and 10) Mucin 1 (Green et al., 2016, Rakha et al., 2014). In those studies, patient groups were stratified based on the tumour's molecular profiles. The modified NPI+ tool could differentiate significant differences in survival outcomes ($p<0.0001$) within the following subgroups: oestrogen receptor+, HER2+, and triple-negative breast tumours (Rakha et al., 2014, Green et al., 2016).

1.8.5 Tumour Size and Lymph Node Invasion

The initial tumour size and lymph node invasion before and after neoadjuvant chemotherapy is a prognostic factor (Huber et al., 2009, Honkoop et al., 1998, Cianfrocca and Goldstein, 2004). Data on 2310 Canadian women have shown that 15-year overall survival was improved when nodal status was negative at diagnosis (survival range 78.5%-91.8%) (Narod, 2012). Also, larger

tumours were associated with a lower survival rate in comparison to smaller tumours and this was independent of nodal status **(Table 1.10).**

Tumour Size Group (cm)	Survival after 15 years (%)	
	Node +	Node -
0.1-1.0	80.4	91.8
1.1-2.0	70.1	89.3
2.1-5.0	47.1	78.5

Table 1.10: [Adapted from (Narod, 2012)]. 15-year survival data on Canadian women (n=2310). Data demonstrates a negative correlation between survival, tumour size, and nodal status.

1.9 Case Study

The purpose of the following section describes the “breast cancer patient experience”. In so doing, the patient experience, provides an aid to conceptualize Section 1.1 to Section 1.8 where the diagnostic and treatment pathway for a typical breast cancer patient, (screening, diagnosis, tumour characteristics and treatment frameworks) are relevant to this thesis. To this end, a case study is presented for a 45-year old woman who was diagnosed with locally advanced breast cancer, and received treatment at the host healthcare institution.

1.9.1 Reason for Referral and Diagnosis

A 45-year-old, pre-menopausal, woman presented with a left sided mass in the upper outer quadrant of the breast, diagnosed as locally advanced breast cancer in July 2015.

1.9.2 History of Present Illness and Work-Up

The patient first discovered a lump in her left breast, during a breast self-examination in May 2015. She sought medical attention from her family physician who referred her to the Rapid Diagnostic Unit (RDU) at the host healthcare institution (Toronto Canada) for further examination. She underwent bilateral mammograms and bilateral breast ultrasound which revealed a benign sub-areolar cyst in her right breast, and a hypoechoic mass in her left breast. Further investigation included a bilateral ultrasound-guided biopsy, which confirmed a cystic lesion measuring 12 x 7 x 11 mm in her right breast. Results of the biopsy indicated malignant cells in the left breast at 2:00 o’clock radian position, and histological analysis confirmed invasive ductal carcinoma, which was ER/PR positive, and HER2/Neu positive. A fine needle aspiration biopsy of the left axillary lymph node was positive for metastatic lymphadenopathy. A follow-up MRI confirmed malignancy in the left lateral breast; measuring 59 x 27 x 62 mm and involved both the upper and lower quadrants. Radiological

grading was BIRADS 6[3]. From the MRI, prominent and thickened left axillary lymph nodes, consistent with previous ultrasound findings for lymphadenopathy in the left axilla was noted. At the time of diagnosis, the patient did not present with any skin changes, erythema, or nipple discharge that would otherwise indicate inflammatory breast cancer.

Two months later, the patient underwent staging and metastatic work-up; CT of the chest, abdomen, and pelvis. CT of the chest revealed several dense nodules measuring 1-3 mm, in the superior segment of the left lower lobe, and the right middle lobe. The nodules were reported as post-pulmonary infection fibrosis, and findings did not indicate metastatic disease to the lungs. CT of the abdomen and pelvis did not show any evidence of osseous metastatic disease, or otherwise distant metastasis in the soft tissue. A bone scan was also performed, and revealed no abnormalities. A multi-gated acquisition (MUGA) scan was also performed, which revealed a normal cardiac ejection fraction of 65%.

1.9.3 Past Medical History

The patient was previously diagnosed with Coeliac disease. The patient reported taking no other medications. There were no known drug allergies.

1.9.4 Family History and Risk Factors

The patient's maternal grandmother was diagnosed with breast cancer. There was otherwise no history of breast cancer or ovarian cancer in her family. Her gynaecological and obstetric history was *gravida* 4, *parity* 3, and *abortus* 0; with her first child at 34 years old. She had reached menarche at 13 years old and was pre-menopausal at the time of consultation. She was a non-smoker, and did not consume alcohol regularly.

---

[3] Scale 1-6: BIRADS 0 (Incomplete, need for additional imaging); BIRADS 3 (Benign lesion); BIRADS 6 (Histologically proven malignancy) (Balleyguier et al., 2007).

1.9.5 Impression and Plan

The patient was scheduled to receive 6 courses of FEC-D neoadjuvant chemotherapy, and Herceptin due to her HER2/Neu status. Following chemotherapy, the patient underwent a total mastectomy approximately 6 weeks after chemotherapy completion. Recovery of the chest wall persisted for another 6 weeks, in which the patient underwent radiotherapy of the chest wall, and supraclavicular nodes for 5 weeks (25 fractions, 50 Gy)[4].

1.9.6 Treatment Interval Assessments

The patient presented with shortness of breath approximately after two cycles of chemotherapy. A CT angiogram was ordered to rule out any pulmonary embolus, and was negative. At mid-treatment, she presented with mucositis of the mouth, and was referred to a head and neck physician for management. She was prescribed mouthwash (Lidocaine and Nystatin), and advised to take over-the-counter Tylenol, which helped resolve the symptoms. The patient has also complained of persistent back pain during treatment. Given her risk of neutropenia, the patient underwent several blood tests, and all blood work was within normal range (haemoglobin, white blood cell count, platelet count, and neutrophil count). Additionally, due to her persistent difficulty in breathing, and complaints of chest pain, an echocardiogram was ordered and did not reveal any cardiac abnormalities. After the first (FEC) treatment cycle, the patient experienced frequent episodes of diarrhoea, however this could have been a result of her Coeliac disease. Her pain increased during treatment; specifically, symptoms of neuropathy and swelling were present and the patient was prescribed Tylenol 3 to alleviate pain. The patient presented with low white blood cell count on routine blood work and was prescribed Neupogen (i.e. to recover white blood cells). Due to higher risk of infection, the patient was monitored carefully to assess for any signs of respiratory distress, or otherwise signs of infection.

---

[4] Canadian practice guidelines use NCCN (USA), NINV-1 V.2.2016 (National Comprehensive Cancer Network, 2016). In the UK, breast radiotherapy guidelines indicate 40 Gy/15 fractions (Haviland et al., 2013).

1.9.7 Post-Treatment Assessments

The post-treatment MRI scan indicated that the patient was responsive to treatment and was classified by RECIST[5] criteria as having at least a 30% decrease in the sum of diameters of the target lesion. Under pathological examination, there was a significant reduction in tumour cellularity, with significant fibroadenomas, and fibrosis present within the tumour bed, and the patient was determined as a "responder" to chemotherapy treatment. **Figure 1.10** demonstrates the pre- and post-MRI.

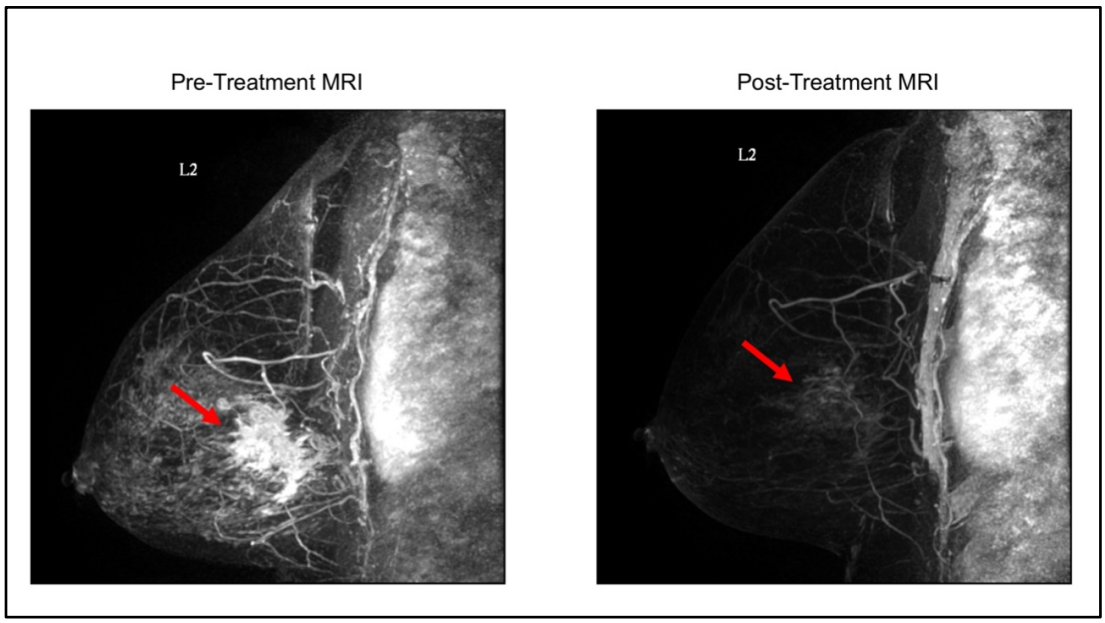

Figure 1.10: Left breast carcinoma prior to treatment (left image) and after neoadjuvant chemotherapy (right image). A significant reduction in the mass was observed in the patient, with remaining fibrosis within the tumour bed. The patient mastectomy samples revealed that she responded to treatment. *Red arrows indicate the tumour area.*

---

[5] RECIST is the *Response Evaluation Criteria In Solid Tumours* and is a system used to evaluate tumour size changes from CT and/or MR images. Response categories are based on the overall percent-changes in size: Complete Response (Disappearance of lesion); Partial Response (At least 30% reduction in lesion size); Progressive Disease (At least 20% increase in lesion size); Stable Disease (Insufficient shrinkage or no overall change) (Eisenhauer et al. 2009).

1.9.8 Case Report Summary

The case report demonstrates that in this patient:

1) Chemotherapy causes severe toxicity (i.e. side effects) and this can affect the patient's quality of life and wellbeing in this patient only.
2) The unknown pathological response during treatment is a real clinical problem because clinicians cannot modify or adapt treatment based on tumour response to therapy.

In this patient, it was important for this particular patient to know if treatments were working or if she was a good candidate for the chemotherapy treatment.

1.10 Study Motivations and Aims 2

Identifying the Clinical Problem

The clinical challenges for managing LABC patients include:

1) A significant proportion of patients (i.e. 80%) will respond only partially (i.e. tumours do not demonstrate a significant reduction in size according to the current methods, i.e. RECIST). This can make resecting the tumour during surgery more difficult.
2) The proportion of partial responders will be at higher risk for recurrent disease, which will affect long-term survival.
3) Ineffective and suboptimal chemotherapy exposes patients to many months of unnecessary chemotherapy toxicity.
4) Pathologic evaluation of treatment response is completed at the end of chemotherapy when it is too late to modify treatments.

To address these challenges, clinicians have traditionally used clinical palpation or conventional medical imaging to measure the changes in the tumour size during treatment. However clinical palpation is unreliable because the estimated size may be confounded with fibrosis, collagen, fatty tissue and oedema of the breast. Additionally, palpation only estimates the size at the surface of the breast and therefore the deep tumour margins cannot be appropriately evaluated. Conventional medical imaging is also limited since the tumour size changes may take several weeks before detectable. Hence, the aim for this research was to identify imaging-based markers that could be used in the future as a predictor of outcome should the parameters under test correlate with the selected endpoint. The final pathologic endpoints would be determined by a standard and systematic technique such as Miller-Payne pathological response criteria. Thus, in the next section, a review of the status of existing imaging techniques was completed to identify the gaps, challenges and areas for which research could be focused for addressing the current clinical problem.

1.11 Systematic Review Question and Search Results

1.11.1 Overview and Literature Review Question

This systematic review of the literature is presented as three major sections. In the first section, the literature review strategy and search results are presented, as indicated in the following literature search question:

Which previous imaging biomarker analysis and modalities have been studied to measure tumour response in locally advanced breast cancer patients treated with neoadjuvant chemotherapy? Are there gaps and limitations of using such imaging techniques?

The second section presents literature of studies on the following imaging modalities as a narrative literature review: 1) Magnetic Resonance Imaging (MRI), Positron Emission Tomography (PET), Computed Tomography (CT), X-Ray Mammography and 99-Technetium Scintigraphy Imaging (99-Tc).

In the third section, a systematic review was completed which focussed on DOS and QUS imaging only. This section provides a framework to support the research questions of the thesis, which are presented in the subsequent chapters (**Chapter 3 Methods**, and **Chapter 4 Results**).

1.11.2 Systematic Review Strategy

A literature review was conducted to find previous studies between 1975-2016 that used medical imaging to evaluate neoadjuvant chemotherapy response in locally advanced breast cancer. The search dates were selected based on the dates that neoadjuvant chemotherapy for breast cancer was first introduced as a treatment. The literature review had two components: 1) a narrative literature review of all previous imaging modalities such as MRI, PET, CT, X-Ray Mammography, and 99-Tc to evaluate NAC treatment response in locally advanced breast cancer; and 2) a systematic review that focused on imaging modalities studied in this thesis; specifically, diffused optical

spectroscopy (concept 1), ultrasound imaging (concept 2a) and quantitative ultrasound spectroscopy (concept 2b).

A summary of the search strategy such as databases used, and MESH words are outlined in **Table 1.11**. For the systematic review, the PRISMA Statement (Preferred Reporting Items for Systematic reviews and Meta-Analyses) was used as a reporting guideline (Moher et al., 2009). The systematic review also evaluated the quality of DOS, US, and QUS studies using the following standardized tools: 1) Statement for Reporting Studies of Diagnostic Accuracy [*STARD*] (Bossuyt et al., 2003); and 2) Quality Assessment for Diagnostic Accuracy Studies tool (*QUADAS-2*) (Whiting et al., 2011). The literature review search results are indicated in **Figure 1.11**.

The literature review did not include imaging studies specifically targeted at tumour-size changes as markers for treatment response since the focus of this thesis was to study functional imaging for treatment response evaluation. A description of radiological tumour response endpoints and its limitations are outlined in **Appendix 1** for reference. To highlight the limitations of size-based measurements, previous studies that have used changes in the tumour's size as an indicator for treatment response have reported the following limitations: 1) objective measurements are not always attainable due to multiple imaging planes from MRI and CT (i.e. tumour localization can vary depending on the volumetric view); 2) reproducibility (i.e. inter-user variability); 3) and repeatability of obtaining the same image quality between imaging series during treatment; (Kang et al., 2012, Eisenhauer et al., 2009, Park et al., 2003).

CRITERIA	DESCRIPTION	REFERENCE
Search Databases	Medline PubMed EMBASE Cochrane library Science Direct (secondary database after initial search) Database search from 1974- 1 April 2017	Scally and Brealey, 2010 in Medical Imaging and Radiotherapy Research, (Ramlaul, 2010) Date entries based on the years that NAC have been used.
MeSH Headings	Locally advanced breast cancer imaging Imaging biomarkers Neoadjuvant chemotherapy Breast cancer response imaging markers, neoadjuvant chemotherapy Headings were combined with the following key words: Sensitivity and specificity "Related articles" were searched	 STARD guideline (Bossuyt et al., 2003)
Inclusion/Exclusion Criteria		
Number of subjects	Minimum number of 10 subjects Case studies also excluded	Studies with less than 10 participants could not make statistically significant conclusions. (Leff *et al*., 2008). Case studies were excluded from this analysis since it is the lowest level of evidence and are limited in its generalizability (Scally and Brealey, 2010 in Medical Imaging and

		Radiotherapy Research, (Ramlaul, 2010).
Types of studies	Human studies included only Phantom and pre-clinical (animal) work excluded	Animal and phantom systems were used for foundational and background information
Anatomic site	Breast only	Imaging of other anatomic sites uses variations in imaging system settings, such as ultrasound frequency, and limitations in imaging depth from modalities such as DOS.
Publication Dates	Studies published between 1974-2016 were included. These dates were chosen based on the approximate date in which NAC was introduced clinically.	Only recent studies within the last 10 years were analysed to keep the review relevant to the improvements in computing and image processing systems.
Quantitative and semi-quantitative imaging studies only.	Tumour size changes were not included in search strategy.	Size and volume measurements do not fall under the definition of biomarkers. These are classified as radiological response criteria.

Table 1.11. Systematic review search strategy. A systematic review of breast cancer imaging studies was conducted to extract relevant studies that were related to neoadjuvant chemotherapy monitoring.

1.11.3 Search Strategy Results

The literature search resulted in 194 articles related to imaging biomarkers after screening for subject relevance and applying the inclusion and exclusion criteria. There were 158 duplicate studies in the search results and 2804 studies were excluded because the reports were animal and phantom experiments, case reports or proceedings, studies on other tumour types, trials

that involved experimental or unconventional drugs and therapies, or trials that did not examine biologically-based imaging markers. Of the eligible studies, magnetic resonance imaging studies yielded the largest number of studies (n=113) for measuring LABC response to NAC. The results demonstrated several imaging modalities used to measure chemotherapy response in breast cancer from imaging biomarkers such as positron emission tomography (PET; n=42), computed tomography (CT, n=1), X-ray mammography (n=1), 99m-Technium (99-Tc, n=6), diffuse optical tomography (DOS, n=16), and ultrasound (US, n=15). The systematic search strategy and results is presented in **Figure 1.11**. Results of the literature search showed that medical imaging was used to measure biological features such, morphology, blood flow, metabolism, cell death, and tissue composition as markers for chemotherapy response in breast cancer. Studies that used tumour volume or size changes to measure chemotherapy response did not meet inclusion/exclusion criteria.

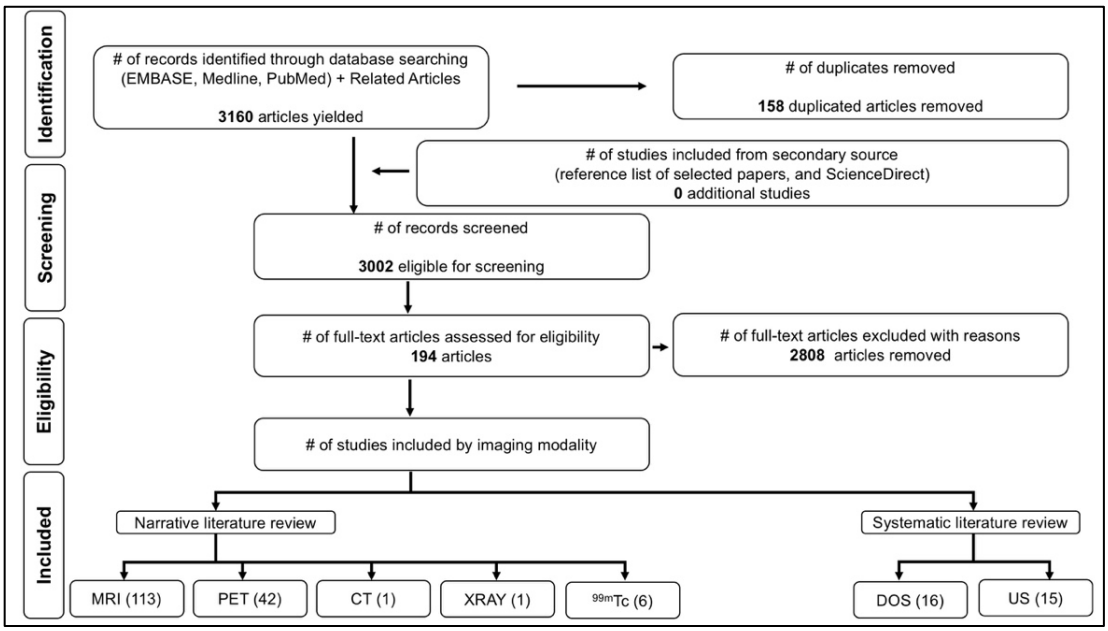

Figure 1.11: Systematic search strategy and search results. A systematic literature search was completed for imaging studies conducted between 1974-2016. The search strategy was based on identifying imaging systems that were used to measure chemotherapy response in breast cancer. The results of the literature search yielded studies that involved MRI, PET, CT, XRAY and 99m-Technitium, DOS and QUS imaging biomarkers. The literature review was divided into a narrative literature review for MRI, PET, CT, XRAY and 99m-Technitium. A systematic review was conducted for DOS and US studies.

1.12 Narrative Review of Imaging in Breast Cancer

The results of the narrative review showed that more than 12,000 locally breast cancer patients have been included into imaging studies with the aim of measuring tumour response to chemotherapy. The imaging modalities included: MRI, PET, CT, XRAY and 99m-Technitium. In the proceeding sections, these imaging modalities are described and the corresponding studies and results are reviewed.

1.12.1 Magnetic Resonance Imaging (MRI)

MRI-based imaging includes diffusion-weighted imaging (DWI-MRI), dynamic contrast enhancement imaging (DCE-MRI), blood-oxygen level depending imaging (BOLD-MRI) and MRI-spectroscopy (MRI-SPEC). These techniques are capable of mapping tumour oxygenation, vascularization, metabolism and the extracellular matrix as response markers to neoadjuvant chemotherapy in breast cancer. Diffusion-weighted MR measure the diffusion of water molecules (i.e. Brownian motion) in tissue (O'Flynn and DeSouza, 2011, Belli et al., 2011). Tissue contrast can be displayed in DW-MRI imaging based on areas of high and low water diffusion; where areas of low water motion (i.e. tumours) demonstrate an enhanced signal. Previous studies have demonstrated that areas with low water motion are associated with malignant tissue due to densely arranged cells which limit the motion of water in the extracellular space (Belli et al., 2011).

Extrinsic contrast imaging techniques include dynamic contrast enhancement imaging (DCE-MRI) which detects the concentration of an injected contrast agent (gadolinium chelate) in the intravascular and extravascular space using primarily T1-weighted signals (O'Flynn and DeSouza, 2011). DCE-MRI images provide information on tumour vascularity and blood flow and measures the gadolinium “wash-in” and “wash-out”. Tumours preferentially accumulate gadolinium from an increased vascular supply compared to normal tissue, and therefore demonstrate an enhanced signal in MRI (Craciunescu et al., 2009). Blood-oxygen level dependent (BOLD-MRI) imaging is also used to measure the tumour vascularity, and tumour oxygenation. This is accomplished by detecting deoxyhaemoglobin,

which is paramagnetic and therefore results in signal loss in T2-weighted images (Jiang et al., 2013).

Other techniques include MR spectroscopy imaging (MRI-SPECT) which detects the activity of atoms with unpaired protons such as Hydrogen (^{1}H), Phosphorus (^{31}P), Sodium (^{23}Na) and Fluorine (^{19}F) within a magnetic field (O'Flynn and DeSouza, 2011). Biochemical compounds such as Choline and N-acetyl aspartate (NAA) demonstrate high 1H atomic energy shifts in magnetic fields and provide spectral signatures in cancer. For example, MRI-SPECT has been used to distinguish between normal and malignant lesions as well as identifying areas of necrosis within tumours (Horska and Barker, 2010). Malignancies contain variations in spectral frequencies and peaks within the measured signal compared to normal tissue (O'Flynn and DeSouza, 2011).

MRI has been used to measure chemotherapy response in breast cancer. The literature search results yielded studies that showed variations in the chemotherapy drugs and schedules administered to patients, imaging time-points measured during chemotherapy, contrast-injection protocols, and data analyses used to obtain the sensitivity, specificity and accuracy of imaging tests against gold-standard endpoints. There were variations in the chemotherapy drugs and schedules between institutions. Ah-See et al. (2008) did not study patient response to taxane-based drugs which are commonly used in breast cancer treatment (Ah-See et al., 2008); whereas Cao et al. (2012) used only four cycles of chemotherapy compared to conventional 6-8 cycles (Cao et al., 2012a). A report by Chang et al. (2002) studied 13 patients using DCE-MRI who received variable chemotherapy drugs within their study sample: three patients in this study received anthracycline drugs; three patients were given taxanes; six patients received weekly taxanes combined with antimetabolites and one patient underwent plant-alkaloid chemotherapy as primary treatment (Chang et al., 2004). A Japanese study used 12 cycles of chemotherapy which is not traditionally implemented in North America and Europe (Michishita et al., 2015). Because of these variations in chemotherapy drug schedules, different research groups measured chemotherapy response at different times. There were also variable measured time intervals between patients, within the same study, for example, Yu et al. (2010) imaged their patients at variable chemotherapy times, i.e. between their second and fourth cycle of

chemotherapy (Yu et al., 2010); yet, the results were pooled together. This may have affected the results since chemotherapy response is time-dependent.

There were also variations in the MR imaging protocols used to obtain quantitative data across studies. Gadolinium chelate contrast agents used for DWI-MRI, DCE-MRI, BOLD-MRI imaging employed a standard injection dose of 0.1 mmol/kg however the MRI machines used to collect data varied in magnet field-strengths that were between 1.5 T-3.0 T. Experiments by Abramson et al. (2013), Ahmed et al. (2013), Ko et al. (2013), and O'Flynn et al. (2011) used 3.0 T imaging units which can provide greater image resolution, higher signal-to-noise ratio and thus provide overall better image quality compared to 1.5 T systems (Ko et al., 2013, Ahmed et al., 2013, O'Flynn and DeSouza, 2011, Abramson et al., 2013, Tanenbaum, 2006).

Data processing and analysis techniques included variations in selecting the tumour regions of interest (ROIs). ROIs were selected in either single-frame or multi-frame slices of the MRI images, and the distance and slice thickness varied between studies which can affect study outcomes. Also, ROIs were selected manually by observers (Wu et al., 2016, O'Flynn and DeSouza, 2011, Yu et al., 2010, Pickles et al., 2005) or by using a semi-automated approach which used an intensity-map histogram after an initial contour by the observer (Teruel et al., 2014, Minarikova et al., 2016). In select studies, radiologists were not involved in MRI analysis to define tumour ROIs which can affect the quality of the study and analysis (Atuegwu et al., 2013, Aghaei et al., 2016, Teruel et al., 2014, Mani et al., 2013, De Los Santos et al., 2013). Other studies also didn't report on using blinded-analysis which could potentially cause bias from knowing pathologic and radiologic response.

1.12.2 Positron-Emission Tomography (PET)

PET imaging can be used to measure the metabolic activity by tracking the cellular uptake of a glucose analogue, [^{18}F]-fluorodeoxyglucose (FDG). FDG is injected intravenously, and transported into cells like glucose and is labelled with a radioactive tracer that undergoes radioactive decay; permitting PET imaging to map metabolic activity in tissue. Increase FDG-uptake is shown in tumours since tumour metabolism is greater compared to normal tissue. PET imaging can therefore serve to identify the extent of malignancies

(Andrade et al., 2013). PET imaging is achieved with the release of a pair of annihilation photons and is detected by a photon-detection device during radioactive decay; this is known as positron-electron annihilation **(Figure 1.12)**. Another radiotracer used in PET includes the radionuclide ^{15}O-H_2O, which permits tumour blood flow measurements; where the distribution of water can be equated to blood activity in blood vessels (Lodge et al., 2000).

PET imaging has been studied to measure glycolytic metabolism and vascular alterations in breast tumours (Garcia Vicente et al., 2014, Lodge et al., 2000). However, there are significant limitations to using PET clinically and studies demonstrate data variations based on image processing techniques used between studies. One major limitation includes not being able to use PET imaging for patients who are diabetic (Burcombe et al., 2002). PET imaging depends on glycolytic activity and therefore patients with diabetes mellitus (DM) who exhibit altered sugar metabolism are excluded for this reason. Other limitations include undetectable signals for smaller tumours. A study by Park et al. (2011) studied 50 patients and reported that 50% of the tumours that were not detectable by PET were less than 1 cm in size (Park et al., 2011). However, Kolesnikov-Gauthier et al. (2012) did not find a correlation between tumour size and the standard uptake value but all tumours in their study were greater than 2 cm (Kolesnikov-Gauthier et al., 2012).

Imaging protocols were compared between studies and showed differences in approaches to acquire PET data. In terms of preparing patients before imaging, patients are required to fast, however the fasting period ranged between 4-6 hours between studies (Duch et al., 2009, Martoni et al., 2010) (Hatt et al., 2013, Keam et al., 2011, Andrade et al., 2013, Burcombe et al., 2002). This can affect the glycaemic index and alter the uptake of the FDG into the tumour (Berriolo-Riedinger et al., 2007). Also, the radiotracer-injection doses differed between studies; with some studies adjusting the dose according to the subject's body mass (Ogino et al., 2014); while others gave standard doses to all patients (Buchbender et al., 2012). Imaging protocols across studies showed differences in the time to measure the SUV after FDG injection. Andrade et al. (2013) measured the tracer signal after 90 minutes from injecting; while another study by Berriolo-Reidlinger et al. (2007) quantified tracer-uptake after 60 minutes (Andrade et al., 2013, Berriolo-Riedinger et al., 2007). The elapsed time between tracer injection to its detection can affect the

measured signal intensity. This is due to the tracer's radioactive decay and its time-dependent uptake and clearance from the tumour.

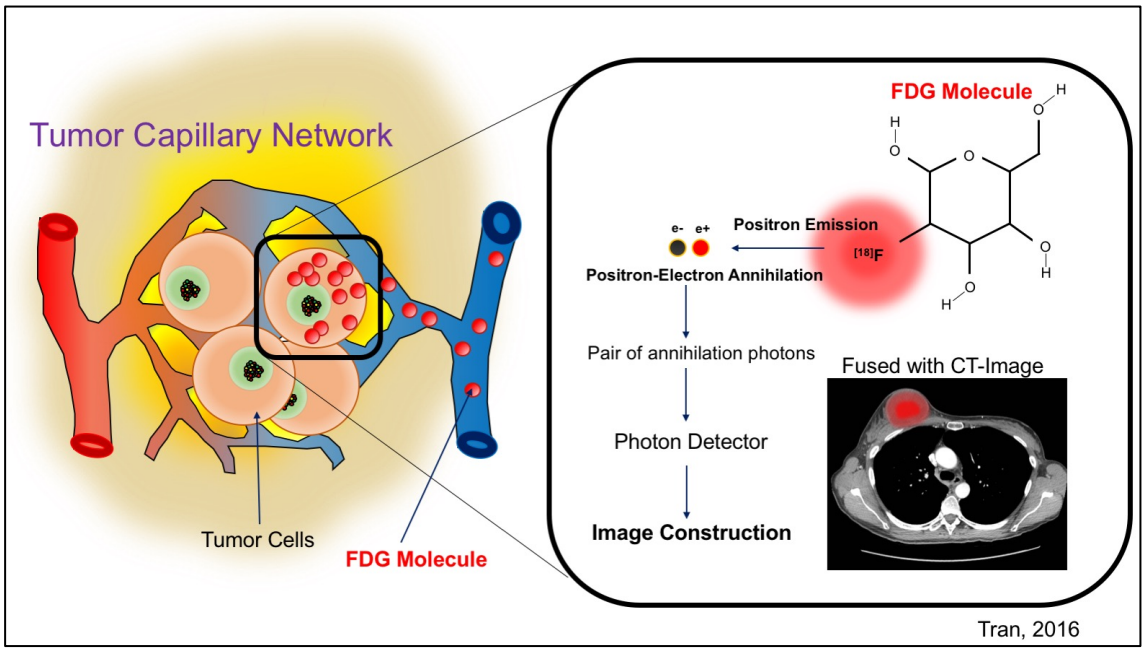

Figure 1.12: PET Imaging. Tumour cells exhibit high metabolism which require energy from glucose. PET imaging uses radiolabelled FDG molecules which are glucose analogues and tracks its uptake in tissue. FDG molecules release a positron and annihilate with an electron to create a pair of annihilation photons. A photon detector collects the radioactive signal and constructs the image based on the signal intensity.

1.12.3 Computed Tomography (CT)

CT imaging uses an X-ray source and detector to construct volumetric images based on differences in photon attenuation. CT helical perfusion imaging, which exploits dynamic contrast-enhanced computed tomography captures physiological information such as regional tumour blood flow and blood volume (Li et al., 2012). The image resolution is high and data is acquired from both the unenhanced anatomical CT-images and images obtained from iodinated contrast agents to produce vascular maps (Eastwood et al., 2003). Imaging data is generated from an arterial time-attenuation curve that output blood-parameters: blood flow (ml/min/100ml), blood volume (ml/100 ml), and the flow extraction product (ml/min/100 ml) (Li et al., 2012).

Conventional applications for CT imaging measure the tumour's size during treatment or as an anatomical reference to PET imaging. However, one study by Li et al. (2012) has used quantitative perfusion CT to investigate vascular parameters in breast tumours treated with neoadjuvant chemotherapy (Li et al., 2012). These parameters included the regional blood flow (BF), blood volume (BV), and the flow extraction product (FE). The study examined 20 patients and the results indicated that there was a significant difference in the BF, and FE between patients who achieved pathological complete response compared to non-responders (P=0.032) and this corresponded to an AUC of 0.87 (Li et al., 2012). Although these studies demonstrated promising results, the study population was small and no power calculation was included. Additionally, CT imaging employed a slice collimation of 5 mm and therefore limits this technology from detecting microscopic disease below this size. Additionally, the study used a single-observer to analyse the ROI which may cause additional bias to the study results. CT imaging is not advantageous because it exposes patients to ionising radiation and therefore limits the number of repeated scans that can occur during the patient's chemotherapy treatment. This study also involved variable treatments for patients; one patient received an anti-angiogenic drug which can affect the results since blood volume and perfusion are measured. Also, two patients in this study did not undergo surgery but were classified as non-responders. Therefore, not all patients underwent standard ground-truth classification and this can affect the results of the receiver operating characteristic (ROC) curve.

1.12.4 X-Ray Mammography

X-Ray mammography for monitoring NAC response uses radiographic breast density (BD) to correlate to pathologic response (Elsamany et al., 2015). The mammographic BD is defined as the ratio between radio-dense areas to normal breast and represents the stromal, epithelial cells, collagen, fibroglandular and adipose tissue (McCormack and dos Santos Silva, 2006). It is hypothesized that dense breasts carry an increased risk of aggressive breast cancer since dense breasts demonstrate rapidly dividing epithelial cells (McCormack and dos Santos Silva, 2006). Radiographic breast density is classified by methods established by Wolfe et al. (1976) into a 4-point scale

based on the radiologist's visual assessment (Wolfe, 1976, Saftlas et al., 1991) **(Table 1.12).**

X-Ray mammography has not been studied to monitor chemotherapy response in breast cancer; rather the BD from diagnostic x-ray mammograms have been previously used as a predictive marker (i.e. before treatment has started). Elsamany et al. (2015) previously showed that patients with a low BD on mammographic assessment at diagnosis were more likely to achieve a pathological complete response to NAC compared to those patients who had dense breasts (p=0.056) (Elsamany et al., 2015). However, the BD demonstrated a relatively poor area under the curve of only 0.59 which suggests that the BD is a poor parameter for predicting response in patients. There are significant limitations for using mammographic breast density to predict treatment response. One limitation involves the potentially variable assessment from the radiologist's visual assessment of breast density and thus can lead to inter-observer variability (Spayne et al., 2012). This has also been observed in both digital and analogue breast images (Spayne et al., 2012). **Table 1.12** presents the criteria used by radiologists to assess breast density based on visual inspection.

BD Category	Description
N1	Non-dense breasts, composed of fat and few fibrous connective tissues.
P1	Beaded linear patterns denoting prominent ducts. Up to 25% of the breast presented as nodular densities.
P2	Prominent duct patterns in radiograph. Over 25% of the breast demonstrates nodular and mammographic densities.
DY	Highly dense parenchyma pattern in radiograph. Homogenous dense areas which appear like sheet-like regions.

Table 1.12: Breast Density (BD) grades for mammographic assessment.

1.12.5 Technetium 99m (^{99m}-Tc) scintigraphy

Previous studies have shown that increased drug efflux in tumour cells is mediated by P-glycoproteins (PgP) that can lead to chemotherapy resistance (Mechetner and Roninson, 1992). ^{99m}-Tc scintigraphy is a molecular imaging technique that measures PgP activity with a radiolabelled tracer, ^{99m}-Tc-Sestamibi (Ciarmiello et al., 1998). An increase in ^{99m}-Tc-Sestamibi efflux through PgP was previously correlated to increased PgP activity in taxane- and anthracycline-based chemoresistant breast tumours (Mittal et al., 2012, Ciarmiello et al., 1998). More recent ^{99m}-Tc scintigraphy techniques include ^{99m}-Tc-3PRGD$_2$ SPECT to evaluate the vascular status of tumours undergoing treatment (Ji et al., 2015). A radiotracer ^{99m}-Tc-3PRGD$_2$ is used to detect biomolecules responsible for vascular and tumour cell growth. A study by Ji et al. (2015) recently reported that ^{99m}-Tc-3PRGD$_2$ SPECT can predict breast tumour response to NAC with a sensitivity and specificity of 86.7% and 85.7%, respectively (Ji et al., 2015).

The major limitation to ^{99m}-Tc scintigraphy is the repeated radiation exposure to patients. ^{99m}-Tc scintigraphy is also dependent on the uptake and metabolism of radiotracers which can vary between patients (Ji et al., 2015). Additionally, patients must be excluded from ^{99m}-Tc scintigraphy on the basis of renal and liver dysfunction (Mittal et al., 2012). Studies also showed variations in the tracer's radioactivity (range: 500-925 MBq) which can potentially alter the measured signal intensity if not normalised (Ji et al., 2015, Ciarmiello et al., 1998, Spanu et al., 2008, Wilczek et al., 2003, Zaman et al., 2009). In one study by Spanu et al. (2008), the analysis included patients who received a range of treatment types that included chemotherapy or hormonal therapy only (Spanu et al., 2008, Travaini et al., 2007). A study by Ciarmiello et al. (1998) showed that tumour region-of-interest (ROI) selection varied between 3-7% which can affect the measurements and outcomes (Ciarmiello et al., 1998).

1.12.6 Summary of Imaging Studies

A summary of imaging studies (MRI, PET, CT, 99m-Tc Scintigraphy) is outlined in **Table 1.13, Table 1.14,** and **Table 1.15**. DOS and QUS imaging descriptions are outlined in the subsequent section (i.e. systematic literature

review). **Table 1.13** describes the biological measurements associated with each imaging modality. **Table 1.14** presents the clinical study characteristics and **Table 1.15** shows the measured performance outcomes (i.e. the best measurements) of each imaging test.

Modality/Technique	Biological Measurements	Reference
Magnetic Resonance Imaging		
DWI-MRI	Extracellular water motion Tumour-cell density Tissue micro-structure Cell membrane integrity Cell membrane permeability	(Belli et al., 2011) (O'Flynn and DeSouza, 2011)
DCE-MRI	Vascular permeability Dynamic blood flow Tumour oxygenation	(O'Flynn and DeSouza, 2011) (Martincich et al., 2011)
BOLD	Tumour vascularity Angiogenesis Blood Volume Blood Flow	(Fan et al., 2011) (Jiang et al., 2013) (Padhani, 2002)
SPECT	Reduction in mitotic count Tumour cellularity Cell membrane integrity Tumour metabolism Tissue composition (lipid)	(Baek et al., 2009) (Tozaki et al., 2010)
Positron-Emission Tomography		
^{18}F-FDG	Tumour metabolism	(Mankoff et al., 2002)
^{15}O-H_2O	Tumour blood flow	(Lodge et al., 2000) (Mankoff et al., 2002)
Computed Tomography Imaging		
DCE-CT	Tumour metabolism	(Li et al., 2012)

	Blood flow per unit volume in tissue (BF) Proportion of tissue with blood flow (BV) Rate of transfer of contrast agent from intra- to extravascular space (FE).	
X-Ray Mammography		
X-Ray	Stromal cell density Epithelial cell density Collagen Fibroglandular tissue Fatty (adipose) tissue	(McCormack and dos Santos Silva, 2006)
^{99m}Tc Scintigraphy		
^{99m}Tc scintigraphy	P-glycoprotein (P-gP): Cell pumps that export chemotherapy out of tumour cells (drug resistance mechanism).	(Takamura et al., 2001)
$^{99m\text{-}Tc}$3PRGD$_2$-SPECT	Integrin proteins in tumour vasculature; measuring tumour vasculature	(Ji et al., 2015)

Table 1.13 Biological measurements according to imaging modalities. Imaging studies included measurements of several biological features that included cellularity, tissue composition, cell structure and tumour cell activity.

Imaging Modality	Patients (n)	Drug Treatments	Chemotherapy Cycles	Response Measurements
MRI	8446	Anthracyclines Taxanes Trastuzumab	3-12 cycles	Mandard RECIST 1.1 RCBI Score Miller-Payne No clinical convention followed (pathologist evaluation)
PET	3138	Anthracyclines Taxanes Alkylating Agents Antimetabolites Trastuzumab Bevacizumab	3-6 cycles	RCBI Score Miller-Payne Sataloff NCI-EORTC Collaborative (1977) PERCIST
CT	20	Anthracyclines Taxanes Alkylating Agents Antimetabolites Trastuzumab Bevacizumab	6 cycles	RECIST 1.1 No clinical convention followed (pathologist evaluation)
X-RAY	241	Anthracyclines Taxanes Alkylating Agents Antimetabolites Trastuzumab	4-8 cycles	No clinical convention followed (pathologist evaluation)
99m-Tc	255	Anthracyclines Taxanes Alkylating Agents Antimetabolites Trastuzumab	3-8 cycles	RCBI Score No clinical convention followed (pathologist evaluation) Radiologically Assessed (no convention) WHO criteria (radiographic)

Abbreviations and Legend

Response Measurements:

RECIST 1.1 (Response Criteria in Solid Tumours 1.1)

RCBI (Residual Cancer Burden)

NCI-EORTC (National Cancer Institute-European Organization for Research on Treatment of Cancer)

WHO (World Health Organization)

PERCIST (PET Response Criteria in Solid Tumours)

Table 1.14 Clinical Study Characteristics. Clinical study characteristics included the number of patients included in all studies combined. Studies were focused on breast cancer patients treated with anthracycline and taxane based chemotherapies. The response criteria (endpoints) varied between studies.

Modality	Chemo Cycle Measured	Measurement Techniques	Imaging Markers	Maximum Outcome, (Time Interval)
MRI	B, M1, M2, M3, M4, P	Diffusion-Weighted (DW) Dynamic-contrast Enhanced (DCE) Spectroscopy Blood-oxygen level dependent (BOLD)	ADC MPTS Texture ∆SI MD VC VO ECU Cho L-Trans Kep R2 T2R RBV RBF Wash-in Wash-out EF	AUC=0.96, (B)
PET	B, M1, M2, M3, M6, P	^{18}FDG ^{15}O-H_2O	SUV MTV TLG	AUC=0.85, (M4)
CT	B	Dynamic contrast-enhanced (DCE)	BF BV FE	AUC=0.87 (B)
X-RAY	B	Mammographic Density	BD	AUC=0.59 (B)
99m-Tc	B, M1, M2, M3, P	^{99m}Tc Scintigraphy ^{99m}Tc- SPECT	^{99m}Tc-D SPECT	Acc=89% (B) (AUC not reported)

Abbreviations and Legend

Imaging Timeline Measures:

B (Baseline)

M (Mid-treatment, chemotherapy cycle)

P (Post-chemo)

Maximum Outcome Measures:

Acc (Accuracy %)

AUC (Area Under Curve)

Biomarkers

MRI:

ADC (Apparent Diffusion Coefficient)

MD (Mean Diffusivity)

MPTS (Morpho-Physiological Tumour Score)

VC (Vascular Count)

VO (Vascular Oxygenation)

∆**SI** (Change in Signal Intensity)

ECU (Early Enhancement Ratio)

EF (Enhancement Fraction)

Cho (Normalized Choline Signal)

k-Trans (Transfer Constant)

Kep (Rate Constant)

R2 (Transverse Relaxation Rate)

T2R (T2-weighted Relaxivity)

RBV (Relative Blood Volume)

RBF (Relative Blood Flow)

PET:

SUV (Standardized Uptake Value)

MTV (Metabolic Tumour Volume)

TLG (Total Lesion Glycolysis)

CT:

BF (Regional Blood Flow)

BV (Blood Volume)

FE (Flow Extraction Product)

X-Ray:

BD (Breast Density)

99m-Tc:

^{99}Tc-D (^{99m}Tc-sestamibi Decay [Half-life])

RI (Retention Index)

SPECT (Single Photon Emission Computed Tomography Signal)

Table 1.15 Measurement parameters. Imaging modalities were used to measure chemotherapy response at various time intervals (indicated as chemo cycle measured in table). Imaging biomarkers varied between imaging studies and modalities. The best performance time intervals are indicated in the table. The results show that MRI imaging biomarkers were the best features to measure tumour response.

1.13 Systematic Review of DOS and US Imaging in Breast Cancer

1.13.1 Systematic Review Outline

In this section, a review of diffuse optical spectroscopy and ultrasound imaging are reviewed in terms of their technical framework, their use for characterizing tissue and the technical limitations associated with each imaging modality. The descriptions are divided into two major concepts: 1**)** *Concept 1*: DOS Imaging and; 2) *Concept 2*: Ultrasound Imaging. Since ultrasound imaging is a broad domain, the proceeding sections will describe ultrasound imaging as two subcategories: 1) General ultrasound imaging which include power Doppler ultrasound, elastography and contrast enhanced ultrasound (*Concept 2a*) and; *Concept 2b*, quantitative ultrasound spectroscopy (**Figure 1.13**).

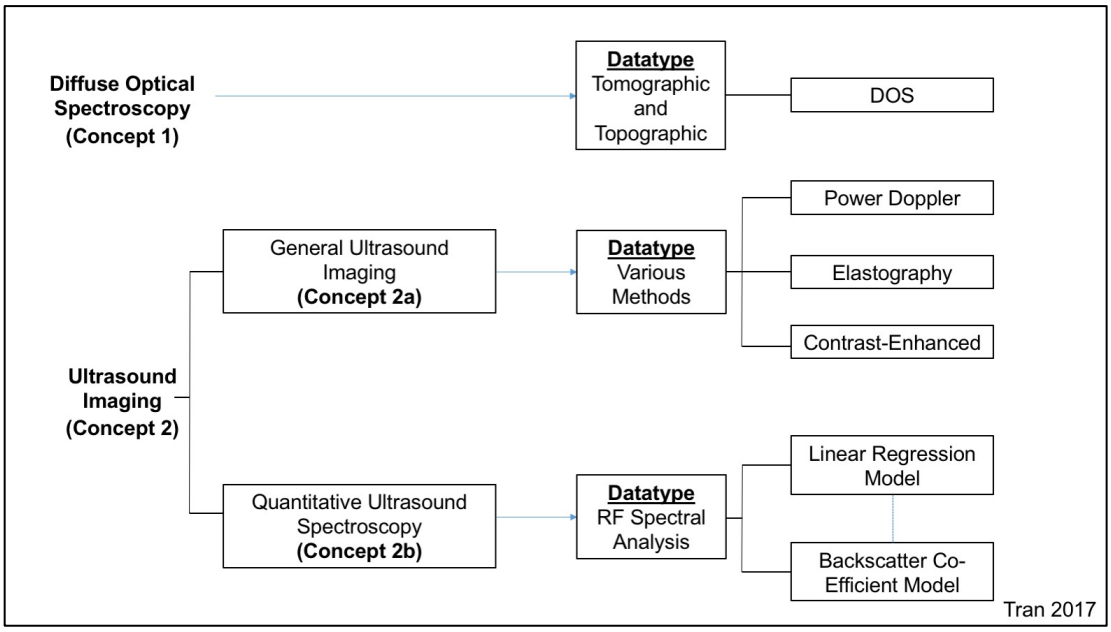

Figure 1.13 The literature review was divided into two major concepts for the purpose of describing the various DOS and QUS imaging techniques. **Diffuse Optical Spectroscopy:** Concept 1 included studies that used both topographic and tomographic DOS. **Ultrasound Imaging:** Concept 2a (general ultrasound imaging) included power Doppler ultrasound, elastography and contrast-enhanced ultrasound imaging. Concept 2b includes two QUS-based techniques.

1.13.2 Principles of Optical Imaging for Tissue Characterization

Light can be described using wave theory where it is characterised as an electromagnetic wave or using particle theory to describe photon migration in a medium (Welch and Gemert, 2010). Both theories describe the nature of light propagation within two common parameters, in which light is dependent on: 1) frequency and; 2) wavelength (Welch and Gemert, 2010). Both light theories (i.e. electromagnetic wave and particle theory) are used to describe attributes of light; for example, the wave's frequency and wavelength are proportional to a photon's energy. The energy, frequency and wavelength of light is represented by an electromagnetic spectrum whereby the optical wavelength is inversely proportional to the photon's energy (**Figure 1.14**). The light energy is an important parameter since it determines the dominant light interactions in tissue, such as absorption and scattering. Optical absorption and scattering in tissue are the basis of understanding DOS-based measurements in tissue.

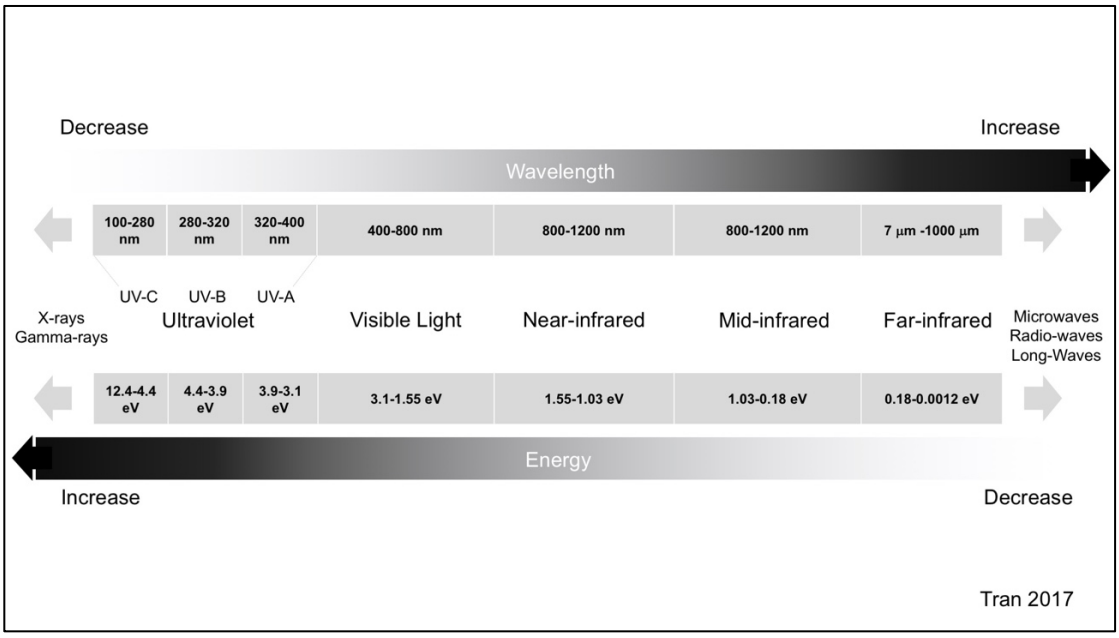

Figure 1.14: The electromagnetic spectrum. The electromagnetic spectrum demonstrates the various bands of light such as ultraviolet light, visible light and near-infrared light. The various bands are defined by a range of wavelengths that are inversely proportional to the energy of light. This is represented by the following equation: $E = h\upsilon$; where E is the energy (units; eV) and h is Plank's constant and υ is the frequency (units; Hz) (Welch and Gemert, 2010).

For near-infrared light interactions in tissue, scattering dominates over absorption; here, absorption is referred to as the decrease in the light intensity as a function of increasing path length in tissue (Jacques, 2013). Also, light scattering in tissue is defined as a deflection (change in direction) from the incident light path after the photon interacts with a particle (Liu, 2011). The near infrared (NIR) optical scattering in tissue is described predominantly by either Mie scattering theory or Raleigh scattering theory[6], which is a function of the size of the scatterer (particle), relative to the optical wavelength (**Figure 1.15**) (Xu and Povoski, 2007).

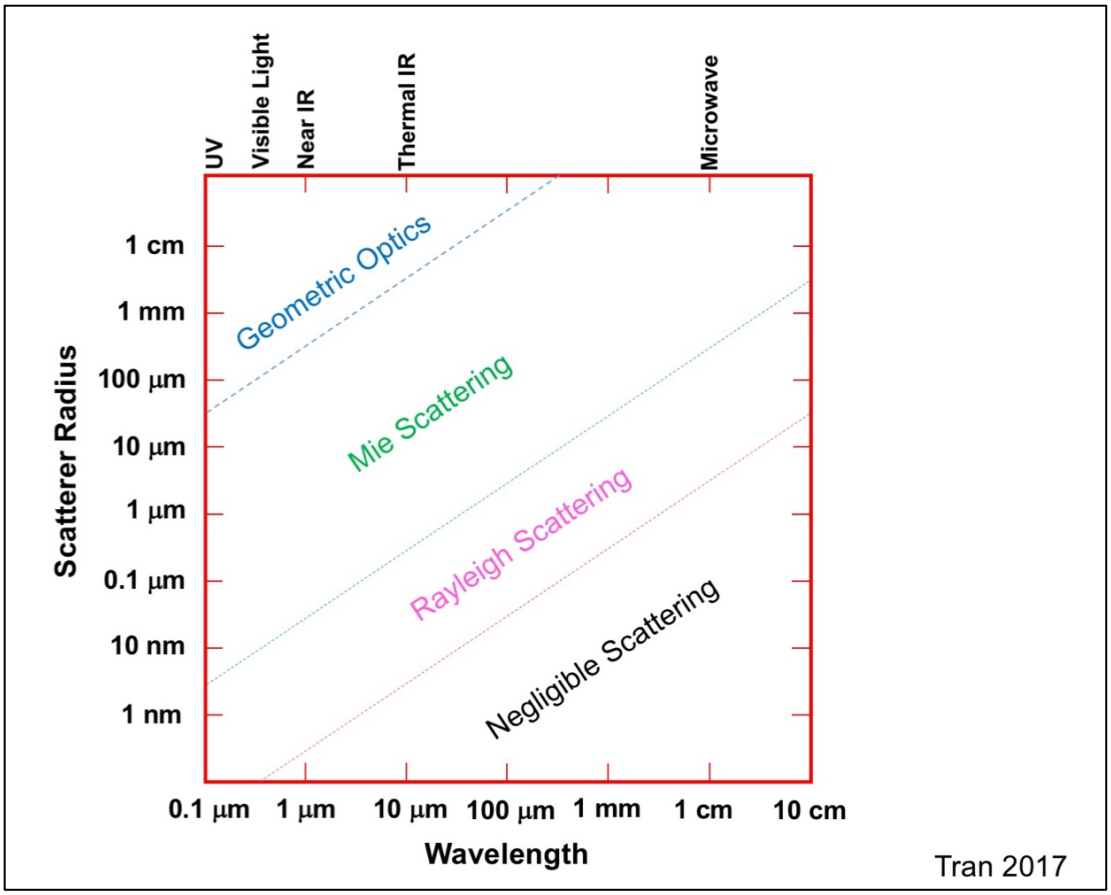

Figure 1.15. Scattering regimes based on wavelength and scatterer size. Adapted from (Petty, 2006). The scattering is based on the relationship between the size of the scatterer and the wavelength of the photon.

---

[6] Mie scattering theory describes the phenomenon when the incident photon is scattered by particles approximately of the same size of the photon wavelength. This causes anisotropic and forward scattering. Raleigh scattering (also referred to as elastic scattering) describes the phenomenon when the size of the particle is much smaller than the photon wavelength, thus causing no change in the incident wavelength, thus resulting in predominantly isotropic scattering.

Diffuse optical spectroscopy measures the near-infrared light interactions in tissue that result from optical absorption and scattering from intrinsic chromophores such as water, lipid, and haemoglobin (Cerussi et al., 2001). Light transmission from one medium to another medium (e.g. tissue) depends on the refractive index, n, and is expressed as the ratio of the speed of light in a vacuum (c) to the phase velocity ($\bar{v}$) in tissue. The refractive index is dependent on tissue density and early works by Barer et al. (1957) reported that tissue constituents such as cells, cell proteins and water were significantly involved in light refraction in tissue (Barer, 1957). Using Snell's law, the refractive index can provide information on the directional change of the propagating light wave between the incident light and the transmitted light travelling across two mediums. The direction of the light in tissue is an important consideration since DOS mammography detects light transmission (or reflection) across the breast tissue (**Figure 1.16**).

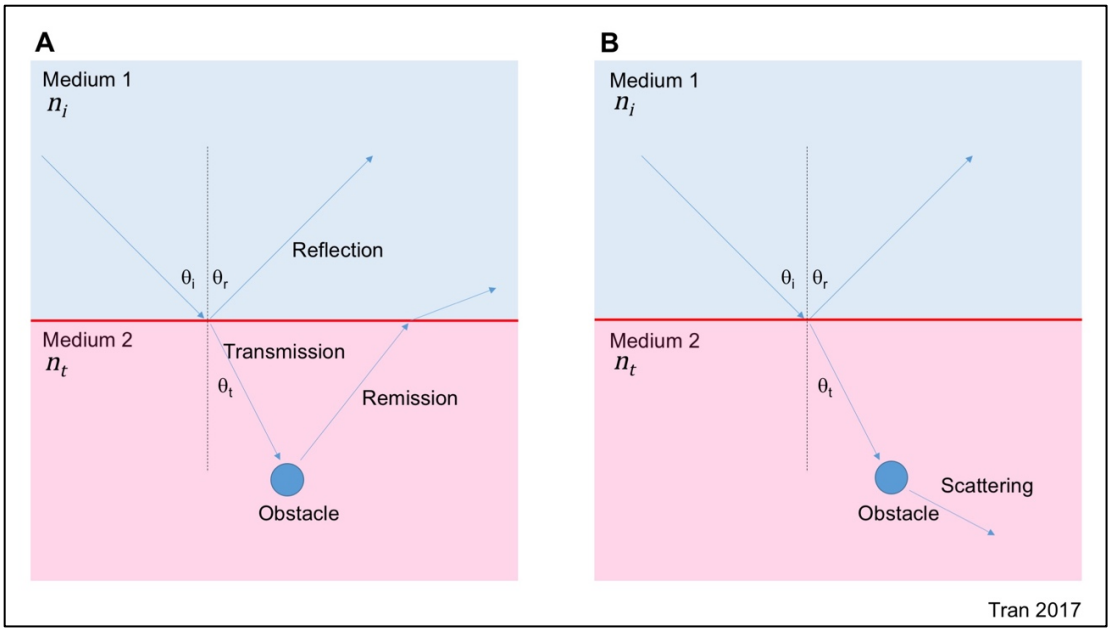

Figure 1.16: Tissue-Light interaction. **A**. Light can be absorbed at the tissue interface. The light that is transmitted may also result in remission. **B.** Light that is transmitted may alternatively undergo elastic scattering whereby the incident light and the scattered light has the same wavelength. Transmission of light is represented by Snell's law: $n_i \sin(\theta_i) = n_t \sin(\theta_t)$.

Tissue measurements using diffuse optical spectroscopy are based on optical absorption and scattering principles in the near-infrared spectrum (wavelengths=600nm-1100 nm). In breast tissue, light scattering is significantly greater (100-fold) than light absorption, and hence the term "diffuse" in DOS refers to a diffusion regime that is caused by multiple scattering events across the gradient (Cerussi et al., 2001, Dehghani et al., 2009, Tromberg et al., 2005). Although chromophore measurements are based on the absorption co-efficient (haemoglobin, water, lipids, oxygen saturation), measuring the scattering in tissue can give important insight to tissue substructures such as the scattering that can occur from tumour cell nuclei or mitochondria. Raleigh scatterers such as mitochondria, nuclei, and collagen fibres can be measured from DOS; thus, measuring the scattering coefficient can also indicate substructural constituents (and its state from cell death and cytotoxic stress) in the breast and tumours that arise in the breast (Cerussi et al., 2006, Liu, 2011).

1.13.3 DOS for Breast Imaging (Concept 1)

Diffuse optical spectroscopy (DOS) imaging can measure tumour response to chemotherapy by detecting changes in haemoglobin content, tissue composition and light scattering features (Roblyer et al., 2011, Cerussi et al., 2007, Jiang et al., 2014). Maps of tumour physiological features, such as haemoglobin are computed from tissue-optical properties that are based on near-infrared optical scattering and absorption within the near-infrared spectrum (600-1100 nm) (Cerussi et al., 2006). For breast tissue, significant optical absorbers include oxy-haemoglobin (HbO_2), deoxy-haemoglobin (Hb), water (H_2O) and lipids (Li) (Cerussi et al., 2006). Chromophore concentrations can be estimated by measuring the absorption co-efficient [μ_a] and using Beer's law equation (Cerussi et al., 2011). Also, tissue optical parameters such as the reduced scattering co-efficient [μ'_s] can provide additional information on tissue microstructure (~0.2 μm); corresponding to optical scattering effects from mitochondria and the cell nucleus (Mourant et al., 2000, Cerussi et al., 2006) (methods for calculating chromophore concentration is further described in **Chapter 2, Methods**).

DOS systems can be built as topographic devices (usually handheld and obtain 2D images), or larger tomographic systems that are referred to as diffuse optical tomography (DOT) devices that construct three-dimensional images of the breast **(Figure 1.17)**. Both systems have their respective advantages, such as broad optical bandwidth and tissue penetrance. For example, advantages for DOT include the capability of imaging deeper tumours, and major technical advancements have increased the performance of DOT systems to separate the specific contributions of light absorption and scattering in tissue for improved tissue contrast.

Three types of DOS techniques, such as frequency domain (FD), time domain (TD) or continuous wave (CW) have been used to measure photon migration in tissue. Continuous wave systems emit light with constant amplitude and measure the attenuation (Xu and Povoski, 2007); whereas frequency domain DOS employ light emission that is sinusoidally modulated at high frequencies. FD systems measure the attenuation and phase shift of the light to measure the optical absorption and scattering. The major advantage to FD systems is a relatively higher signal-to-noise ratio, and it is generally portable, which makes it potentially desirable as a “bedside” tool. In a TD system, used in the thesis study, short pulses of light are emitted and the times of flight are measured. The major advantage is the tissue-depth penetrance and improved resolution, compared to other DOS systems. However, TD systems are often large due to the requirement for several subcomponents used in signal detection and processing.

Continuous wave, frequency domain and time domain systems utilize the absorption co-efficient to calculate the biochemical composition of tissue. Using the Beer-Lambert law, with the known molar extinction co-efficient, one can calculate the concentrations of haemoglobin, oxy-haemoglobin, water, and lipids. It is important to note that breast tissue demonstrates significantly higher scattering than absorption, and this is due to the tissue’s composition, and cellular structure. Other DOS parameters such as the scatter power and scatter amplitude, calculated by using the power-law function, are representative of the tissue’s substructure, which is related to cellularity, cell arrangement and light-scatterer spatial distributions (Fantini and Sassaroli, 2012). As a result, DOS can demonstrate a good sensitivity to the biochemical characteristics of tissue. A summary of DOS imaging is described in **Table 1.16**.

DOS Imaging Technique	Description	Reference
Frequency Domain (FD)	Emits light that is sinusoidally modulated at high frequencies. FD detection systems measure the attenuation and phase shift of the light to report the absorption and scattering. Portable Relatively higher signal-to-noise ratio	(Soliman et al., 2010) (Durduran et al., 2010) (Gibson et al., 2005)
Time Domain (TD)	Uses short pulses of light and measure the times of flight of the transmitted light. The major advantage is the tissue-depth penetrance and improved resolution, compared to other DOS systems. Large system due to many subcomponents in detection and computing system.	(Soliman et al., 2010) (Fantini and Sassaroli, 2012) (Gibson et al., 2005)
Continuous Wave (CW)	Continuous wave systems emit light with constant amplitude and measure the attenuation.	(Xu and Povoski, 2007)

Table 1.16. DOS imaging can be approached using several systems that employ frequency domain, time domain and continuous wave techniques

1.13.4 Technical Considerations and Limitations for DOS

In terms of technologies used, DOS clinical studies showed variations in the use of frequency domain, time domain or continuous wave systems. Imaging devices were built as laboratory (i.e. research devices) or commercially manufactured systems. The systems were either topographic systems that acquired 2-dimensional images or tomographic systems that were capable of constructing 3-dimensional breast images (**Figure 1.17**). Hand-held topographic devices were capable of only measuring fixed-sized areas of up to

20 cm, while bulkier tomographic devices were capable of probing the whole breast volume. All the devices used near-infrared light (600-1100 nm) and this corresponded to the spectral window of known chromophores such as haemoglobin, lipids and water. It is important to note the distinction between DOS topography and DOS tomography systems used in previous studies. Although both systems use similar light scattering and absorption measurements, DOS tomography enables volumetric image reconstruction compared to DOS topography, and can penetrate at greater depths. Hand-held topography DOS systems, such as those used by Cerussi et al. (2011) may be limited by its optical penetrance due to the geometry of the detectors and the probe's construction. Therefore, hand-held DOS devices are often restricted to tumours situated 10-20 mm below the skin surface (Cerussi *et al.*, 2011). Also, tumours with deep posterior margins beyond this distance are poorly measured by DOS topography, and are better measured using DOS-tomography.

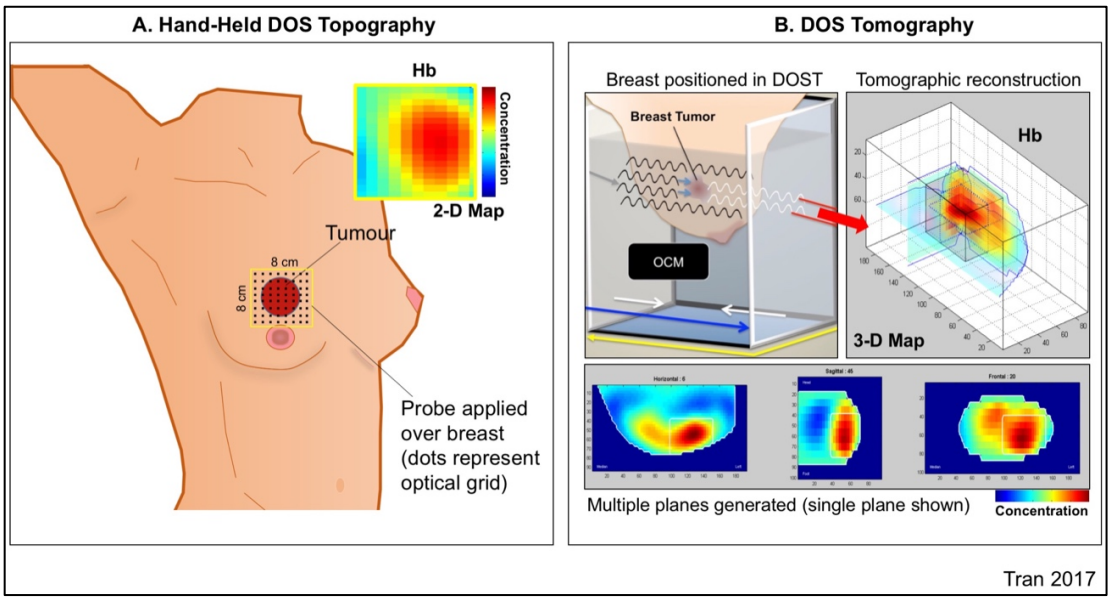

Figure 1.17. Differences between hand-held reflectance-type topography probes (left) and DOS tomography systems (right). **A.** Hand-held devices are placed over the breast and 2-D chromophore maps are constructed. **B.** Tomography devices (as used in this study) involve whole-breast imaging and are coupled with optical compensation medium (OCM). 3-D maps are constructed with multiple scan planes that report the concentration of the chromophore of interest, for example deoxy-haemoglobin (Hb).

1.13.5 Principles of Ultrasound Imaging for Tissue Characterization

The ultrasonic signal represents the tissue composition and microstructure. Tumour structures such as cells and the vasculature are susceptible mediums for ultrasound scattering. Ultrasound is a propagating pressure wave that has frequencies greater than the audible range in humans, which is approximately 20 KHz (Shung and Thieme, 1993). Medical applications exploit ultrasound waves that carry energy and demonstrate predominantly longitudinal wave properties; thus, causing particle displacements that are parallel to the direction of the propagating wave (Shung and Thieme, 1993).

Ultrasound waves that travel from one medium to another medium undergo refraction or reflection which causes a change in the wave's direction at the interface. For refraction, the directional change can be calculated using Snell's law, where the angle and velocity of the incident wave is proportional to the angle and velocity of the reflected or refracted wave. In biological tissue (i.e. tumours), the transmitted wave encounters a highly inhomogeneous medium and the acoustic energy is lost as a function of distance; this is caused by acoustic absorption and scattering. The absorbed energy produces heat while the scattered energy results in either forward- or backscattering. Thus, acoustic scattering is defined as the redistribution in the acoustical energy in a non-uniform medium; where there is a change in the amplitude, frequency, phase velocity, or direction of the acoustical wave (Chivers, 1977) (**Figure 1.18**).

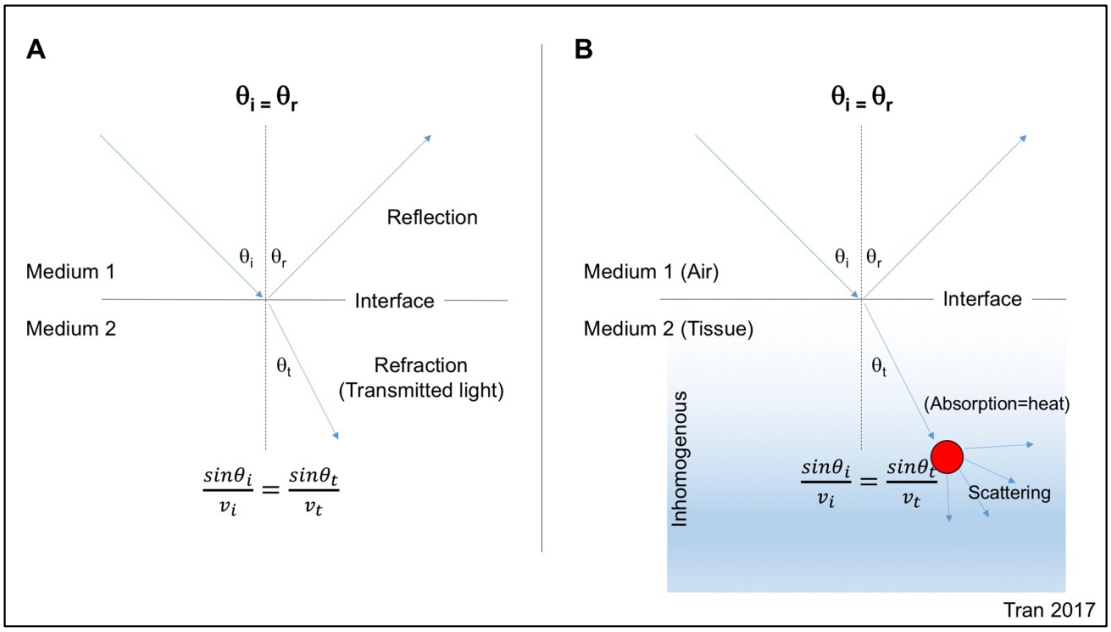

Figure 1.18: Wave propagation and transmission. **A.** Ultrasound waves that travel between interfaces demonstrate reflection and refraction. For reflection, the incident angle (θ_i) is equal to the reflected angle (θ_r). For refraction, the incident angle and the refraction (transmitted) angle (θ_t) is dependent on the speed of sound between interfaces (Snell's law). **B.** Wave propagation in biological tissue encounter a highly inhomogeneous medium and therefore the refracted wave loses energy as a function of distance. The loss in energy is a result of absorption (producing heat) and scattering.

1.13.6 General US Imaging (Concept 2a) and QUS (Concept 2b)

General Ultrasound Imaging (Concept 2a)

Conventional breast ultrasound uses acoustic frequencies between 9-15 MHz to obtain good contrast and axial (depth) resolution in breast tissue (Athanasiou et al., 2009). Breast sonography techniques include mechanical imaging such as elastography or functional imaging such as contrast-enhanced imaging, power-Doppler ultrasound and quantitative ultrasound spectroscopy. Ultrasound elastography measures the tissue's stiffness and therefore characterizes the tissue's biomechanical properties. Tumours are "harder" than the surrounding normal parenchyma because it is comprised of densely populated and rapidly dividing cells, increased vasculature and fibroglandular components that alter its mechanical properties (Schrader et al., 2011, Wells

and Liang, 2011, Hayashi et al., 2012). Tissue stiffness can be measured in terms of tissue stress and strain (units; pascals [Pa]) using shear-wave elastography or compression-based elastography. These imaging techniques compute the alterations in sound wave propagation in soft and hard tissue (Wells and Liang, 2011).

Functional ultrasound imaging, such as contrast-enhanced imaging (CEUS) and power Doppler measures tumour blood flow; while quantitative ultrasound techniques have been used to measure morphologic features of the whole-cell and subcellular structures such as the nucleus (Czarnota et al., 2002, Cao et al., 2012b, Shia et al., 2015). Contrast-enhanced ultrasound (CEUS) uses a contrast medium, such as microbubbles for improved visualization of the blood vessels. Microbubbles are small lipid, protein or biopolymer microspheres that encapsulate a gas. Under varying acoustic pressure, microbubbles oscillate due to their echogenicity which result in increased echoes that are detected by the ultrasound system (Blomley et al., 2001). For power Doppler imaging, the vasculature is assessed by detecting the frequency shift and amplitude (power) of the ultrasound backscatter signal caused by scatterers in the blood vessels (Martinoli et al., 1998).

Quantitative Ultrasound Spectroscopy (QUS) (Concept 2b)

Quantitative ultrasound spectroscopy for tissue characterization has many medical applications such as detecting cardiac ischemia, characterising liver histology and renal imaging (Lizzi et al., 1997b). In oncology, QUS aims to provide acoustic data about tumour microstructure (cells and cell nuclei) that can be used for diagnosis and treatment-response evaluation (Sannachi et al., 2015). The major advantage of analysing the radiofrequency data in comparison to conventional B-Mode “grey-scale” ultrasound is the added information about tissue properties such as attenuation, integrated backscatter, scatterer size and concentration (Kolios et al., 2002). Additionally, a significant advantage to using QUS data to characterize tumours is to mitigate operator dependent variations associated with conventional grey-scale imaging such as time-gain compensations and image contrast adjustments.

Quantitative ultrasound spectroscopy (QUS) uses the spectral information of radiofrequency (RF) backscatter signals that are typically

discarded in conventional grey-scale sonography; thus, it is unique from other types of sonography since the information collected is based on the frequency-dependent power spectrum. QUS can employ either low or high (>20MHz) frequency ultrasound for tissue characterization based on the desired acoustic resolution, and required depth for imaging (Feleppa et al., 2011). QUS parameters using spectral analysis, such as the mid-band fit (MBF), 0-MHz intercept (SI) and spectral slope (SS) are determined by applying a linear regression function within a discrete frequency bandwidth of the computed power spectrum (Czarnota et al., 1999, Kolios et al., 2002, Lizzi et al., 1997b, Feleppa et al., 2011) (methods for calculating QUS parameters are described in **Chapter 2, Methods**). In early studies by Lizzi et al. (1997), QUS parameters were studied for therapy response monitoring in hyperthermia-treated ocular tumours (Lizzi et al., 1997b). The results of their study showed an increase in the SI in responsive lesions, in comparison to the surrounding normal tissue (*p=0.003*). This increase in the backscatter intensity was explained as corresponding to changes in tissue microstructure caused by focal areas of increased cell death (Lizzi et al., 1997b). It was hypothesized that changes in the scattering surfaces at subcellular levels from cell death, such as fragmented nuclear structures, may modulate acoustic scattering in tissue. Later reports by Czarnota and colleagues applied Lizzi *et al*.'s theoretical framework to study the effects of apoptotic cell death and QUS in acute myeloid leukaemia (AML) cells treated with chemotherapy *in vitro* (Czarnota et al., 1999). That work used QUS methods as markers for apoptotic cell death. Chemotherapy-treated AML cells demonstrated a 2.92-fold to 5.83-fold increase in backscatter intensity compared to non-treated cells, and histological data revealed morphological changes resulting from cellular pyknosis, karyorrhexis and apoptotic cell death (Czarnota et al., 1999). In another study, Kolios *et al*. demonstrated an increase in the MBF (+13 dB) after treating AML cells to chemotherapy *in vitro*, and linked these findings to morphological changes from chromatin condensation (Kolios et al., 2002). These studies demonstrated the link between changes in tissue features, nuclear morphology and the resulting acoustic scattering in tissue (Sannachi et al., 2015) **(Figure 1.19)**. Theoretical frameworks in these early QUS studies for cancer imaging have driven efforts to study chemotherapy response in breast cancer *in vivo* (Sadeghi-Naini et al., 2013b, Tadayyon et al., 2014). To date, QUS has been used to monitor

treatment response in photodynamic therapy, chemotherapy, and radiation therapy; both in animal and human studies (Lee et al., 2012, Czarnota et al., 1999, Banihashemi et al., 2008, Sadeghi-Naini et al., 2013a, Sadeghi-Naini et al., 2013b, Tadayyon et al., 2014).

The sensitivity of QUS to measure the biomechanical features of tumours is dependent on two main factors: 1) Tissue-dependent features (i.e. scatterer size, distribution, organization) and; 2) the ultrasound (wave) properties (Lizzi et al., 1997a, Lizzi et al., 1997b, Insana and Hall, 1990). In this section, important principles of ultrasound imaging are discussed since the experimental QUS parameters used in this study should be interpreted in terms of its relationship to the tumour response and biology. The important factors discussed here include image resolution, image reconstruction and system corrections that have a critical role in the QUS data that represents the tumour's biological characteristics.

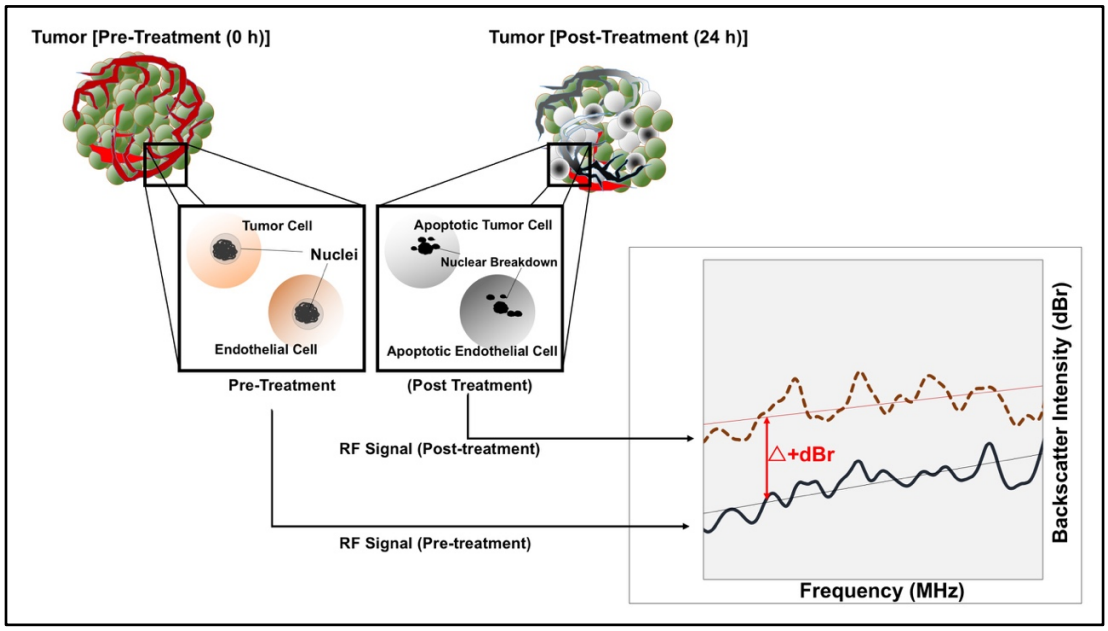

Figure 1.19: Quantitative ultrasound using spectral analysis can be used to estimate morphological changes in cells. Increased nuclear fragmentation caused by treatments can affect the intensity of the spectral form. The backscatter is measured in terms of the normalized intensity (power) in decibels (dBr).

1.13.7 Technical Considerations and Limitations for US Imaging

Ultrasound image quality is affected by the characteristics of the ultrasound system itself, such as the quality of the display monitor and its display settings (Sehgal et al., 2006). The system's hardware include transducer types that use variable frequencies, bandwidths, focal distances and aperture that can change the output display of the ultrasound image (Sehgal et al., 2006).

Ultrasonic Parameters for Optimal QUS Imaging

QUS data is based on the digitized radiofrequency signal from tissue backscatter. The practical challenges of optimal QUS imaging arises in terms of achieving a desirable resolution in both the lateral and axial direction of the ultrasound image and this is dependent on the ultrasound parameters used for imaging. In order to attain useful QUS data and information, QUS imaging parameters must be capable of resolving cellular and subcellular structures. For this, the optimal lateral and axial resolution are dependent on the following parameters: wavelength (λ), f number (f_{number}), acoustic frequency bandwidth (B), and the speed of sound (c). These parameters are described below in terms of its relationship to achieving the desired lateral and axial resolution in an ultrasound image for useful QUS analysis.

The lateral resolution is spatially perpendicular to the beam axis (O'Brien, 2007) and permits imaging objects that are positioned side-by-side. The lateral resolution is defined as the minimum resolvable distance to differentiate or contrast two adjacent reflectors or structures (O'Brien, 2007). The lateral resolution is high when the beam width is at its narrowest due to a small distance between acoustic scan lines. The lateral resolution is dependent on the frequency (and thus wavelength, λ) and the geometric characteristic of the acoustic focus, such as the diameter of the transducer (D) and the focal depth (F). The optimal parameters for optimal imaging include the following parameters:

i. Shorter wavelength (λ);
ii. High frequency (f)
iii. Large diameter (D)

At distances beyond the focal zone (i.e. the far zone), the lateral resolution deteriorates as the beam width diverges (i.e. wider) beyond this point. Thus, optimal lateral-resolution is achieved within the near zone and up to the focal zone (**Figure 1.20**).

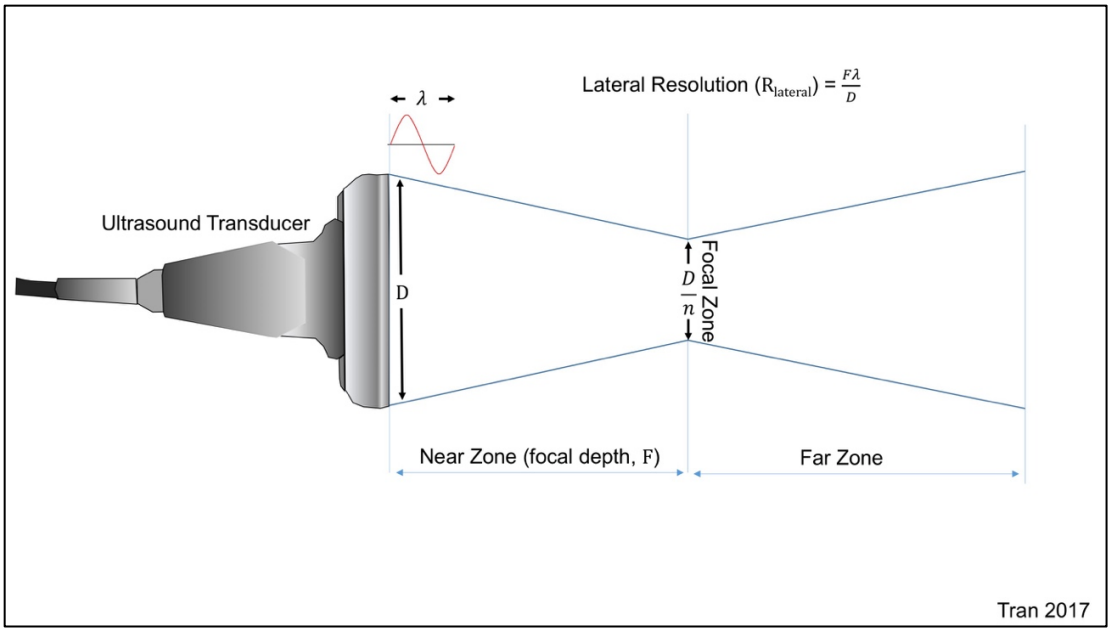

Figure 1.20: Lateral resolution is best when the beam width is narrow; allowing for distinguishing side-by-side structures. The lateral resolution is highest within the focal zone at the focal point ($\frac{D}{n}$); where the beam converges, and is narrowest.

The lateral and axial resolution are important in imaging locally advanced breast cancer tumours due to the size of the tumour which can span several cm across the breast (>5 cm). The axial resolution is defined as the distance of one wavelength (λ) along the axis of the ultrasound beam. Thus, an object can be resolved that is equal to the distance occupied from one cycle or pulse of ultrasound (O'Brien, 2007). In practical US imaging, single wavelengths are not used rather, pulses of ultrasound are employed that contain *N* wavelengths per pulse; this is termed the spatial pulse length (SPL). The SPL can be used to calculate the axial resolution based on the frequency bandwidth (**Figure 1.21**).

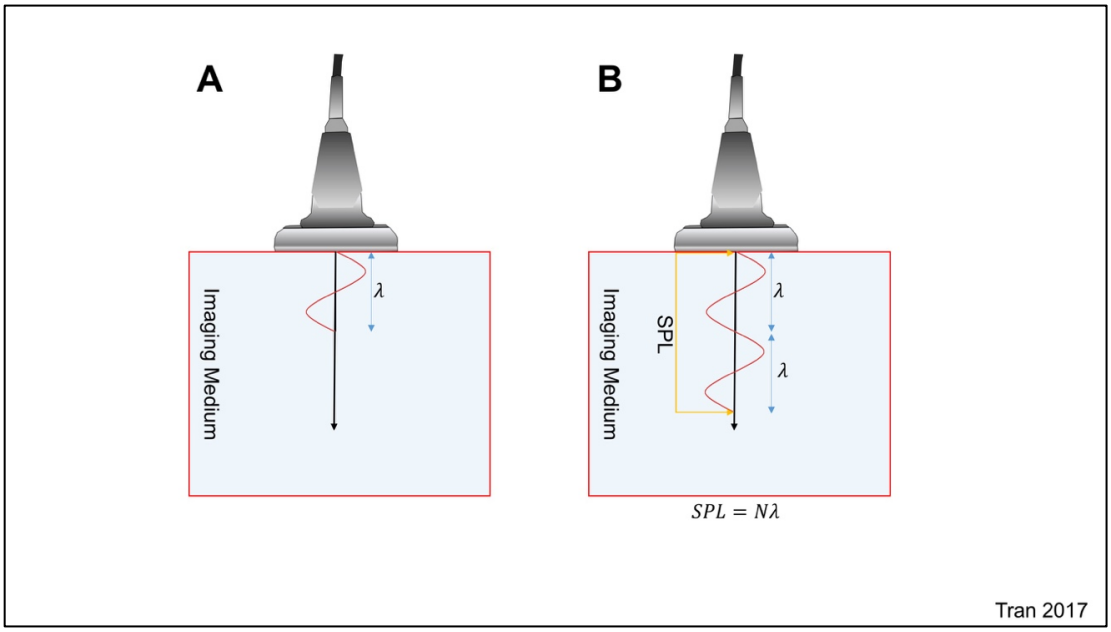

Figure 1.21: Axial resolution for ultrasound imaging. The axial resolution is determined by the wavelength of an ultrasound pulse (**A**). However, in practical ultrasound imaging, a pulse of ultrasound will contain several wavelengths as it propagates through the imaging medium (e.g. tissue). The spatial pulse length (SPL) is defined as the number of wavelengths in a repeated pulse waveform. For practical ultrasound imaging, the SPL is used to determine the optimal (best) axial resolution. In this example in (**B**), the SPL is equal to 2λ.

For QUS quantification of biological tissue which can contain several scatterers, a Born approximation is assumed; that is, the backscattered field is the sum of the individual scatterers within that acoustic field (Chivers, 1977). Thus, QUS measurements in breast tumours represent the net change in scatterers (i.e. dying cells). It is also important to mention that in QUS modelling, the backscatter intensity calculations assume that the tumour is a low-density medium and that scatterers within the tumour microenvironment are randomly distributed (Oelze et al., 2002). Previous experiments have developed a framework to show the relationship between QUS parameters and scatterer properties (outlined below in **Table 1.17**) (Lizzi et al., 1997b, Insana and Hall, 1990, Kolios et al., 2002, Feleppa et al., 1986).

Scatterer Property	QUS Parameters	Findings	Reference
Size	Spectral Intercept	A two-fold increase in the scatterer diameter showed an 18 dB increase in the Spectral Intercept.	(Feleppa et al., 1986)
Size	Spectral slope	The size of the scatterer of less than ~20 μm has insignificant effects on the spectral slope (i.e. slope remains constant).	(Feleppa et al., 1986)
Size	Mid-band Fit	The mid-band fit increases from an increase in the scatterer diameter for effective diameters of up to ~60 μm	(Feleppa et al., 1986). (Lizzi et al., 1997b)
Number of scatterers	Spectral Intercept	An increase in the number of scatterers increases the spectral intercept due to an increase in the number of scattering surfaces	(Lizzi et al., 1997b)
Concentration of scatterers	Spectral Slope	An increase in the concentration of the scatterers decreases the spectral slope	(Lizzi et al., 1997b)

Table 1.17: QUS dependence on scatterer properties. Scatterer properties such as the size, number and distribution have been shown previously to change the acoustic scattering in tissue

In general, the quality of US imaging is reliant on angle dependence, aliasing (indeterminate ultrasound signals) and a poor signal-to-noise ratio that can result from user error (Hamper et al., 1997). Other technical considerations for US include breast density and breast-tissue composition (connective tissue, lactiferous ducts) that can affect image quality since it can alter the speed-of-sound in tissue, cause speckle, and scattering; these factors may result in image artefacts (Sehgal et al., 2006). For elastography, tissue composition can affect the elasticity reading between patients that demonstrate higher fatty-tissue content and fibrosis, as these features can change the biomechanical properties of the breast and alter the strain measurements (Butcher et al., 2009, Wells and Liang, 2011). US imaging can also be limited by penetrance, also known as the acoustic impedance. This is because US imaging is dependent on the wavelength and frequency of the acoustic wave. Variations in the ultrasound frequency may limit the quality of images if tumours are situated deeper into the breast tissue (Athanasiou et al., 2009). Conventional breast sonography uses frequencies between 9-12 MHz, and this allows imaging axial distances of up to 5 cm (Athanasiou et al., 2009). As a rule, higher frequency (>20 MHz) ultrasound can improve resolution but due to high scattering in tissue, these frequencies are better suited for superficial lesions. Conversely, lower frequency ultrasound (2-5 MHz) can penetrate greater tissue depths, but resolution is compromised (Athanasiou et al., 2009). Previous US clinical studies have employed transducers that operated at between 5-13 MHz (Gangeh et al., 2016, Sadeghi-Naini et al., 2013b, Sannachi et al., 2015, Tadayyon et al., 2016, Tadayyon et al., 2017, Amioka et al., 2016, Shia et al., 2015). These frequencies are consistent with clinical breast sonography but the variations in acoustic parameters (i.e. frequency, time-gain compensation, pulse repetition frequency and focal depth) limit the comparisons that can be made between studies since the experimental conditions (i.e. technology, biological measurements, image processing techniques) were different.

Functional imaging techniques such as contrast-based ultrasound (CEUS) also have limitations. For CEUS, invasive injections are required and there are potential adverse reactions from using contrast agents (Stewart and Sidhu, 2006). Also, the contrast agents' lifetime in blood vessels are short and therefore multiple injections are needed for optimal image acquisition (Heijblom et al., 2011).

1.13.8 DOS and QUS Measurements Represent the Tumour's Spatial and Biological Properties

The Tumour's Biological Architecture

One mechanism by which chemotherapy agents exert their therapeutic effect is by committing tumour cells to apoptosis (**Figure 1.22**) (Bold et al., 1997, Mizutani et al., 2005). In comparison to other forms of cell death such as necrosis, apoptotic cell death is energy dependent, genetically controlled and morphologically distinct, i.e., developing apoptotic bodies, cell shrinking and nuclear condensation (Majno and Joris, 1995). Under microscopy apoptosis is identified as cell shrinking, membrane blebbing, forming apoptotic bodies and having nuclear restructuring. Nuclear reorganization undergoes karyolysis (nuclear breakdown), pyknosis (nuclear condensation), and finally karyorrhexis (nuclear fragmentation) (Majno and Joris, 1995). Fragmented cellular and nuclear debris are engulfed by phagocytes. Apoptosis has been identified in primary breast tumours treated with neoadjuvant chemotherapy *in situ.* Studies by Chang et al. (2000) and Ellis et al. (1997) demonstrated that there was an increase in apoptosis in responsive tumours and detected as early as 24 hours after the administration of chemotherapy using immunohistochemistry analysis (Chang et al., 2000, Ellis et al., 1997). Chang et al. (2000) showed that increased apoptosis, as assessed by serial biopsies, was linked to pathological complete response where there was no residual or palpable disease after therapy (Chang et al., 2000). Buchholz et al. (2003) also measured the apoptotic activity in breast tumours after 48 hours of chemotherapy using breast tumour biospecimen analyses. Patients who had a 25% increase in the apoptotic actively, as assessed by immunohistochemistry, had gone on to achieve pCR. The apoptotic activity was significantly different to patients who did not achieve pCR ($p<0.015$) (Buchholz et al., 2003). These previous clinical experimental results suggest that apoptosis is a major biological response mechanism to chemotherapy response in tumours (Simstein et al., 2003, Bold et al., 1997, Okada and Mak, 2004). In contrast, chemoresistant tumours show defects in the apoptotic pathway and have evolved to evade programmed cell death (Simstein et al., 2003). A summary of previous studies that have evaluated apoptosis using serial biopsies is presented in **Table 1.18**.

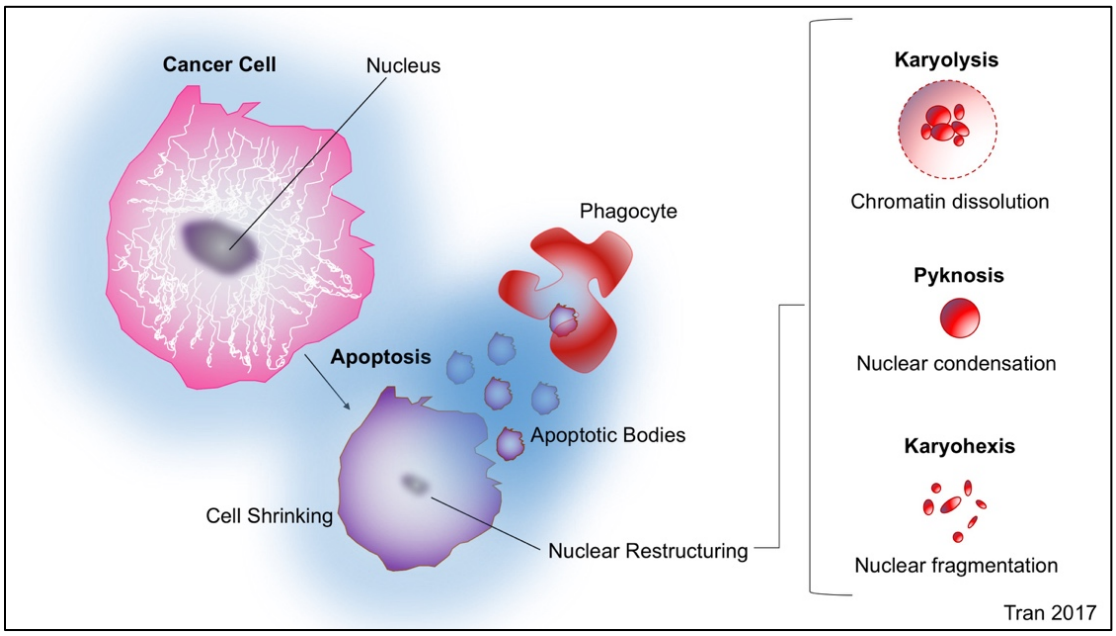

Figure 1.22: Apoptosis in cancer cells. Apoptosis is characterised as an energy dependent mechanism where cells undergo programmed morphological changes. Chemotherapies drive apoptosis in tumour cells and this results in cell shrinking and nuclear restructuring such as karyolysis, pyknosis and karyorrhexis. These morphological changes are the basis of detection methods in quantitative ultrasound.

	Reference	n	Cx	Time	Findings/Notes/Limitations
1	(Arpino et al., 2005)	33	• A	• D_0 • 24h • D_7 • D_s	• Results did not demonstrate a significant difference between responders and non-responders at all time points. However, the trends for responders and non-responders demonstrated a higher apoptotic index in responders compared to non-responders (p=0.1). • **Limitations:** Small sample size and data from study did not demonstrate statistical significance which contrasted other studies.
2	(Buchholz et al., 2003)	25	• A • T	• D_0 • 24h • D_2	• There was a 25% difference in the apoptotic index between responders and non-responders at 48 hours (p=0.015). • **Limitations:** Data based on 16 breast tumours only (small sample size).
3	(Chang et al., 2000)	28	• M	• D_0 • 24h • D_7 • D_{21}	• Median change of 3.4% in responders versus -0.1% in non-responders (p=0.03) after 24 hours. • **Limitations:** Variable tumour types were included in the study sample. • **Limitations:** Mixed areas of necrosis and apoptosis identified in all tumours (risk of overestimated findings).
4	(Symmans et al., 2000)	11	• T	• D_0 • 24h • D_3 • D_4	• All patients were pooled for analysis. There was a 3.0-6.0-fold increase in the apoptotic activity at 4 days after one treatment. • **Limitations:** No statistical tests were performed to compare between responders and non-responders and this was due to the small sample size.
5	(Ellis et al., 1997)	27	• A • AL • M	• D_0 • 24h	• Responders showed >50% increase in the apoptotic index. • Non-responders showed no significant changes in apoptosis after 24 hours (p=0.22). • **Limitations:** small sample size and unequal responder/non-responder ratio.

Cx (Chemotherapy): A=Anthracycline; T=Taxane; M=Antimetabolite; AL=Alkylating Agent. **Time (Measured relative to chemo-cycle 1):** D_0=Baseline (prior to chemotherapy starting), 24h (hours), D_2=2 days (48 hours); D_3=Day 3; D_4=Day 4; D_7=Day 7, D_{21}=Day 21; D_s=Surgical Specimen.

Table 1.18: Clinical studies that used serial biopsies to measure apoptosis in breast tumours. The results indicate that apoptotic tumour response may be initiated as early as 24 hours after giving chemotherapy.

Additionally, tumour cells exhibit genetic modifications that enable proliferation, despite unstable environments caused by hypoxia, overpopulation and inefficient vascularization (Jain, 2005). Tumours have abnormal vascular architecture which contributes to a spatially heterogeneous environment (Jain, 2005). The vascular morphology and organization have been well studied; blood vessels are disorganized, distributed unevenly, immature and leaky, which also affects the tumour's response to treatment (Dvorak et al., 1988). The tortuous vessel formations have been shown previously to inhibit drug efficacy by secreting factors that block chemotherapy effects (Gilbert and Hemann, 2010, Junttila and de Sauvage, 2013) . Additionally, abnormal morphologies such as variable vessel diameters and weak junctions in the vessel walls have been shown to inhibit efficacious drug delivery since leaky vessels reduce drug concentrations in tumours (Hashizume et al., 2000, Damia and Garattini, 2014). Additionally, the uneven vascular scaffold creates areas with variable and high interstitial fluid pressure, which resists the transport of cytotoxic agents into the stroma (Rofstad et al., 2014, Junttila and de Sauvage, 2013, Minchinton and Tannock, 2006). Solid tumours that respond to chemotherapy exhibit characteristic patterns in their vessel reorganization (Jain, 2005). Jain et al. (2005) described these patterns as vascular "normalization" by which the vascular architecture is reconfigured to eliminate inefficient, saccular, leaky and immature vessel formations (Jain, 2005). This results in improved oxygen delivery and cytotoxic efficacy. In highly responsive tumours, the vasculature eventually regresses and limits the nutrient supply to tumour cells (Jain, 2013). Taken together, the important hallmarks in tumour response to chemotherapy include vascular normalization and regression, cell death and changes in the tissue composition and are observed explicitly under microscopy (**Figure 1.23**). These biological changes result in spatial and structural reorganization in tumours which can be detected by ultrasound and optical imaging techniques.

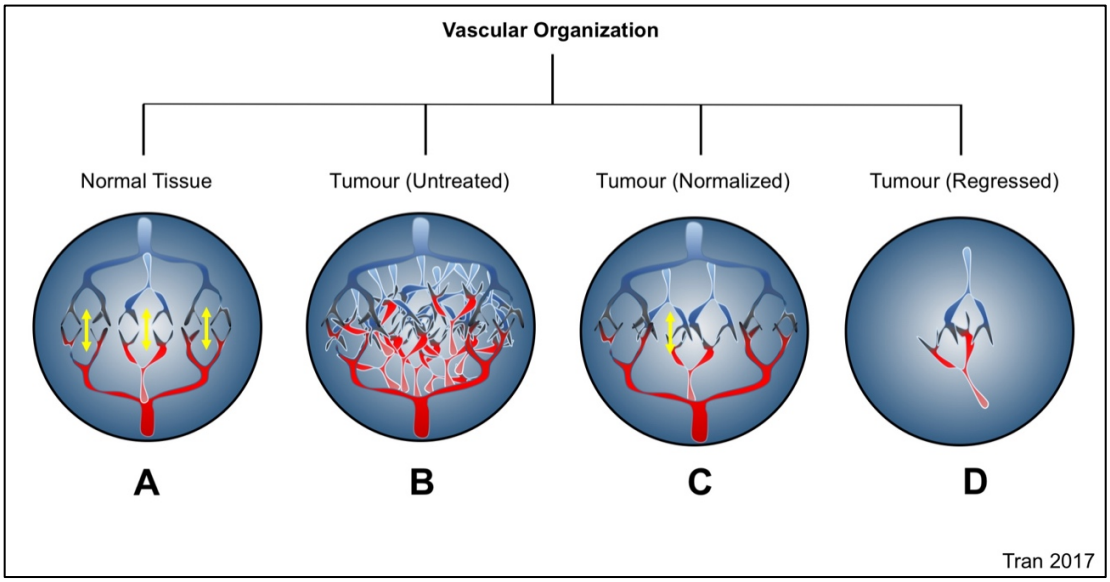

Figure 1.23: A comparison of the vascular organization. **A.** Normal tissue exhibits normal sized and well-organized vasculature, which permit exchange of biomolecules and gas (arrows). **B.** Untreated tumours show high density vasculature and do not permit free exchange of biomolecules and gasses. **C.** Normalized tumours demonstrate greater organization closer to that of normal tissue. **D.** In regressed tumours, the vasculature may be absent, or minimal.

Detecting the Tumour's Biology and Characterizing its Structure using DOS and QUS

Ultrasonic and optical wave interactions in tissue are a function of the tumour's biologic properties. The tumour's biological components, i.e. tumour cells, normal cells, fragmented apoptotic bodies, stromal features, vasculature and substructures such as mitochondria and cell nuclei can scatter light and sound. Thus, these components are often termed "scatterers" in the context of optical and acoustic imaging. As tumours respond to chemotherapy, alterations occur with respect to scatterer spacing, organization, density and concentration, which can affect the DOS and QUS signals that are measured.

The current understanding of a solid tumour's biological matrix illustrates a microenvironment that is made from densely arranged cells, tortuous vasculature, and high interstitial fluid at its onset and progression (Nishida et al., 2006). Tumours that respond to chemotherapy show opposite characteristics such as sparse tumour cells, low vascularity and low interstitial

fluid and this is the basis of optical and acoustic parameters to measure tumour response to chemotherapy.

Here it is important to illustrate the biological “landscape” in solid tumours at initial diagnosis. Before treatments are administered to kill the tumour, it has been shown that there is a high interdependency between cellularity and vascularity; i.e., tumour cells trigger the growth of blood vessels, and blood vessels support tumour cell growth by supplying vital nutrients. Previous work by Muthukkarruppan et al. (1982) showed that tumours that grow beyond 2 mm^3 initiate an “angiogenic switch” to drive neovascularization (Bergers and Benjamin, 2003, Muthukkaruppan et al., 1982). Growing blood vessels infiltrate the tumour into a woven matrix that enables oxygen exchange and trafficking of proteins for cell signalling. The irregular vascular distribution and variable tumour cell phenotypes also contribute to intratumoural heterogeneity (Polyak, 2011). Cancer cells may transform into more aggressive tumour cells with each replication cycle and this can result in morphological heterogeneity such as condensed and irregular nuclear bodies and enlarged or shrunken cell sizes (Swanton, 2012). Thus, even within short distances within the tumour’s subregions, tumour cells may demonstrate variable rates of cell proliferation and cell cycling. Other physiological conditions that lead to spatial variances within the tumour stroma include fluctuating interstitial fluid, variable vascular perfusion and circulating biomolecules (O'Connor et al., 2015). To compound the spatial complexity, the tumour stroma is also constructed from a variety of cell-types such as fibroblasts, immune cells, adipocytes and normal breast epithelial cells (**Figure 1.24**) (Polyak, 2011, Pietras and Ostman, 2010). Taken together, tumours are composed of disorganized and aberrant cells, and circulating biomolecules that are “woven” into a turbulent vascular scaffold and environment. These aberrations are the cause of inter- and intra-tumour heterogeneity and result in significant treatment challenges in breast cancer (Rofstad et al., 2014).

Tissue-dependent Factors in Ultrasonic Backscattering

QUS is a measure of the ultrasonic backscatter intensity in tissue. Scatterers in tissue include fibroblasts, collagen, tumour cells, blood-related cells, collagen, normal cells and their subcellular structures such as the nucleus

and proteins. Spatial heterogeneities of those structures cause changes in ultrasonic scattering in tissue. The backscatter is measured in terms of intensity (power) in decibels (dB) (Chivers, 1977). The average speed of sound (c) in soft tissue is 1540 m/s and this is dependent on the tissue's elastic properties (compressibility, κ) and density (ρ).

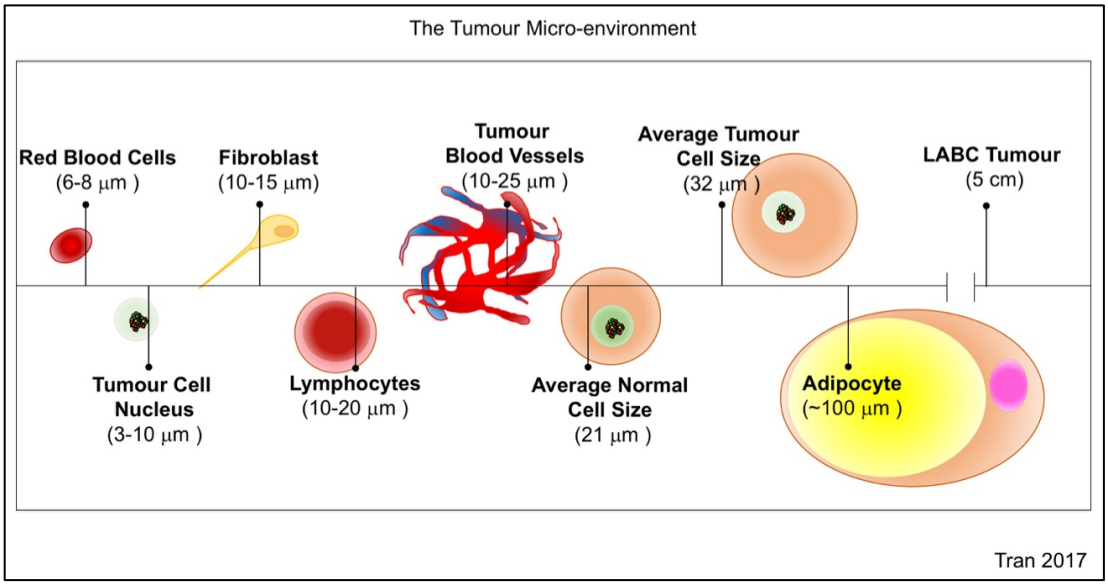

Figure 1.24: Tumour composition. The tumour is a complex system which is composed of several cell types and subcomponents which contribute to its spatial heterogeneity.

Thus, variations in ultrasonic scattering is dependent on tissue biophysical properties such as its density and compressibility that are regulated by cells, vasculature, fluid and biomolecules. In this study, it is hypothesized that changes in the tumour's biophysical properties are a result of the spatial heterogeneities that can be detected by ultrasound and subsequently used to measure tumour response during chemotherapy. This hypothesis is based on previous studies by Czarnota et al. (1999) and Kolios et al. (2002), in which the results showed that there was a relationship between cell structural changes from apoptosis that were detected from ultrasonic backscatter signals (Czarnota et al., 1999, Kolios et al., 2002). In those studies, a time-course analysis (0h-48h) under microscopy showed changes in size, number and concentration of the scatterers (cells and cell nuclei). The conclusions of these previous studies indicated that the backscattered signal was correlated to condensed nuclei (pyknosis), fragmented DNA (karyorrhexis) and membrane blebbing from apoptotic cell death (Czarnota et al., 1999). A summary of the biological

correlates associated with DOS and US imaging biomarkers, as indicated from previous studies, is outlined in **Table 1.19**.

Technique	Biological Measurements	Reference
Diffuse Optical Spectroscopy		
DOS	Metabolism	
	Cell activity	
	Vascular Density	(Cerussi et al., 2006)
	Oedema	(Cerussi et al., 2001)
	Breast tissue composition	(Cerussi et al., 2011)
	Cellularity	(Intes, 2005)
	Cell distribution	(Fantini and Sassaroli, 2012)
	Cell death	(Cerussi et al., 2006)
	Tissue contrast	(Fantini and Sassaroli, 2012)
	Hypoxia	(Fantini and Sassaroli, 2012)
	Nuclear fragmentation	
General Ultrasound Imaging and Quantitative Ultrasound Spectroscopy		
Elastography	Tumour progression	(Hayashi et al., 2012)
	Extracellular matrix	(Schrader et al., 2011)
	Collagen crosslinking	(Evans et al., 2013)
	Tissue composition (fibrosis)	
CEUS	Vascular blood flow	(Cao et al., 2012b)
Power Doppler	Vascular blood flow	
	Blood perfusion	(Shia et al., 2015)
	Vascularity	
QUS	Cell Death (Apoptosis)	(Lizzi et al., 1997a)
	Scatterer size	(Lizzi et al., 1997a)
	Scatterer distribution	(Hunt *et al*., 2002)
	Scatterer concentration	

Table 1.19. **Physiological measurements by DOS and US.** Scatterers for QUS include tumour cells and subcellular organelles and other cell and tissue types**.**

1.14 Results of DOS and US Systematic Review

1.14.1 Patients

Between 1975-2017, DOS (n=394 patients), US (n=294 patients) and QUS (n=244 patients) have been studied in 932 patients with locally advanced breast cancer to measure neoadjuvant chemotherapy response **(Table 1.20)**. Patients from these studies exhibited breast tumours that were histologically and molecularly heterogeneous (ER +/-, PR+/-, HER2+/-), and were treated with taxane- and anthracycline-based chemotherapies **(Table 1.20)**. However, two DOS studies included a subset of patients (n=23) who were treated with bevacizumab, which is an anti-angiogenic agent (Cerussi et al., 2011, Roblyer et al., 2011). Since DOS, CEUS, and power Doppler ultrasound measures blood perfusion and vascular density; it is unclear if this affected the comparative haematological measurements between patients treated +/- bevacizumab.

Imaging Modality	Patients (n)	Drug Treatments	Chemotherapy Cycles	Response Measurements
DOS	394	Anthracyclines Taxanes Alkylating Agents Trastuzumab Bevacizumab	3-12 cycles	No clinical convention followed (pathologist evaluation) Radiologically Assessed (no convention) RECIST 1.1 Miller-Payne
General US and QUS	538	Anthracyclines Taxanes Alkylating Agents Antimetabolites Trastuzumab	3-8 cycles	No clinical convention followed (pathologist evaluation) Radiologically Assessed (no convention) RECIST 1.1

	Miller-Payne RCBI Score

Abbreviations and Legend

Response Measurements:

RECIST 1.1 (Response Criteria in Solid Tumours 1.1)

RCBI (Residual Cancer Burden)

NCI-EORTC (National Cancer Institute-European Organization for Research on Treatment of Cancer)

WHO (World Health Organization)

PERCIST (PET Response Criteria in Solid Tumours)

Table 1.20: Patients, treatment and endpoints in DOS and QUS imaging studies.

A summary of each study identified from the systematic literature search is presented in **Table 1.21**, which outlines the number of study participants, the chemotherapies used within each study and study results.

	Reference	N	Cx	Tumour Histology	Time points (weeks)[§]	Imaging	Markers	Study Results
Concept 1: Diffuse Optical Spectroscopy Imaging								
1.	(Cerussi et al., 2007)	11	A, T, +	1, 2, 3	B, W3, W6, W9, F	DOS, FD	Hb, HbO_2, H_2O, Li, SP	1
2.	(Zhu et al., 2008)	11	A, T, +	1, 2, 3, 4	B, W3, W6, W15, F	DOST	HbT	1,2
3.	(Jiang et al., 2009)	7	A, T, +	1, 3, 4	B, W1, W3, W4, F	DOST, FD	Hb, HbO_2, H_2O, SP, SA, St, StO_2	1,2
4.	(Soliman et al., 2010)	10	A, T, +	1, 2, 3, 4	B, W1, W4, W8, F	DOST, TD	Hb, HbO_2, H_20, Li, TOI	1,2
5.	(Cerussi et al., 2011)	34 (36)[a]	A, T, + B	N/A	B, W8, W9, F	DOS, FD	Hb, HbO_2, H_2O, Li, TOI	1,2
6.	(Pakalniskis et al., 2011)	11	A, T, + B	1, 2, 3, 4	B, W (N/A)[b], F	DOST, FD	HbT	1,2
7.	(Roblyer et al., 2011)	23 (24)[a]	A, T, +	1, 2, 3, 4	B, D1-7	DOS, FD	Hb, HbO_2, H_2O, Li	2
8.	(Falou et al., 2012)	15	A, T, +	1, 2, 3, 4	B, W1, W4, W8, F	DOST, TD	Hb, HbO_2, HbT, St, StO_2, SP, SA, H_2O, Li, TOI	1,2
9.	(Ueda et al., 2012)	41	A, T, +	1, 2, 3, 4	B	DOS, FD	Hb, HbO_2, HbT, StO_2, TOI	3

10.	(Zhu et al., 2013)	32	A, T, + B	1, 2, 3, 4	B, W3, W6, W9, W12, W15, F	DOST	Hb, HbO_2, HbT	2,3
11.	(O'Sullivan et al., 2013)	28	A, T, +	N/A	B, W4, F	DOS, FD	Hb, HbO_2, HbT, StO_2, H_2O, Li, TOI	1
12.	(Jiang et al., 2014)	19	A, T, +	1, 2	B, W1, W2, W3, W8	DOST, FD	HbT, StO_2, H_2O	1,2,3
13.	(Schaafsma et al., 2015)	22	A, T, +	1, 2, 3	B, W3, W6, W9	DOST, TD	Hb, HbO_2	2
14.	(Sadeghi-Naini et al., 2015)	12	A, T, +	1,2,3	B, W1, W4, W8, F	DOST, TD	Hb, HbO_2, HbT, H_2O, TOI + Texture	1,2
15.	(Tromberg et al., 2016) (ACRIN 6691 Trial)	34	N/A B	1,2,3	B, W1, W (N/A)[b], F	DOS, FD	Hb, HbO_2, HbT, StO_2, TOI	1,2,3
16.	(Ueda et al., 2016)	84	A, T, + B	1,2,3	B, W3, W6	DOS, FD	Hb, HbO_2, HbT, StO_2	1,2

Concept 2a: General Ultrasound Imaging

1.	(Singh et al., 2005)	25	A, +	1	B, F	CFUS, CD	V_{max}, PI, RI	1
2.	(Huber et al., 2009)	17	+	1,2,5	B, F	CFUS, CD	CPD	1
3.	(Hayashi et al., 2012)	55	A, T, +	1, 3, 4, 5	B	CFUS, EL	EG	3
4.	(Cao et al., 2012b)	31	A, T	1	B, F	CFUS, CEUS	MTT, PI(C), RT, TTP, WIS	1

5.	(Evans et al., 2013)	40	A, T, +	1	B	CFUS, EL	ME	3
6.	(Falou et al., 2013)	15	A, T, +	1, 2, 3, 4	B, W1, W4, W8, F	CFUS, EL	SD, SR	1,2
7.	(Shia et al., 2015)	29	A, T, +	1, 3, 4, 5	B, W3, W6	CFUS, PD	VI, FI, VFI	2,3
8.	(Amioka et al., 2016)	63	A, T, + B	1, 3, 4	F	CFUS, CEUS	PI(C), TTP, AS	1
9.	(Saracco et al., 2017)	19	A, T, B	1,2,5	B, W2, W5	CFUS, CEUS	MTT, PI(C), C_{max}, TTP, WIS	2

Concept 2b: Quantitative Ultrasound Spectroscopy

10.	(Sadeghi-Naini et al., 2013b)	24	A, T, +	1, 2, 3, 4	B, W1, W4, W8, F	CFUS, QUS	MBF, SI, SS	1,2
11.	(Sadeghi-Naini et al., 2014)	20	A, T, +	1, 2, 3, 4	B, W1, W4, W8, F	CFUS, QUS	MBF, SI, SS, Texture	1,2
12.	(Sannachi et al., 2015)	30	A, T, +	1, 2, 3, 4	B, W1, W4, W8, F	CFUS, QUS	IBC, ASD, AAC	1,2,3
13.	(Gangeh et al., 2016)	56	A, T, +	1, 2, 3, 4	B, W1, W4, W8, F	CFUS, QUS	MBF, SI, SS	1,2
14.	(Tadayyon et al., 2016)	58	A, T, +	1, 2, 3, 4	B, W1, W4, W8, F	CFUS, QUS	MBF, SS, SI, SAS, ACE, ASD, AAC	1,2
15.	(Tadayyon et al., 2017)	56	A, T, +	1, 2, 3, 4	B	CFUS, QUS	MBF, SI, SS,	3

ACE,
ASD,
AAC,
Texture

Patients Enrolled: [a]Number of tumours studied (patients with bilateral disease, or multifocal disease)
Chemotherapy Strategy (**Cx**): A=Anthracycline-based chemotherapies; T=Taxane-based Chemotherapies; +=Other chemotherapies; B=Bevacizumab (Avastin).

Tumour Histology: 1=Invasive Ductal Carcinoma, 2=Invasive Lobular Carcinoma, 3=Oestrogen/Progesterone Receptor Positive, 4=Growth Hormone Amplification (HER2), 5=Other Types

Measured Timelines: B=Baseline (Pre-Chemotherapy); D=Number of Days; W=Number of Weeks; F=Finish of Chemotherapy; [b]Authors indicate "during treatment" but no times specified. Study authors report the cycle, and this has been converted to weeks relative to start of chemotherapy.

Imaging: DOS=Diffuse Optical Spectroscopy Imaging (Topographic 2D); DOST=Diffuse Optical Tomography. FD= Frequency Domain. TD= Time Domain. All optical imaging uses NIR light (600 nm-1000 nm). CFUS=Conventional Frequency Ultrasound. QUS=Quantitative Ultrasound Spectroscopy. EL=Elastography. CEUS= Contrast Enhanced Ultrasound. PD= Power Doppler Ultrasound. CD=Colour Doppler Imaging (Velocity Doppler).

Parameters Measured Per Study: Hb=Deoxy-haemoglobin; HbO_2=Oxyhaemoglobin; HbT=Total Haemoglobin; St=Oxygen Desaturation; StO_2=Oxygen Desaturation; SP=Scatter Power; SA=Scatter Amplitude; H_2O=%Water; Li=%Lipid; TOI=Tissue Optical Index; MBF=Mid-band Fit, SI= Spectral Intercept (0-MHz Intercept); SS=Spectral Slope; SAS=Spacing Among Scatterers; ESD=Effective Scatterer Diameter; EAC=Effective Acoustic Concentration; IBC=Integrated Backscatter Coefficient; ASD=Average Scatterer Diameter; AAC=Average Acoustic

Concentration, ACE=Attenuation Coefficient Estimate. Vmax=Maximum Flow Velocity. PI=Pulsatility Index. RI=Resistivity Index. CPD=Percentage of Colour Pixels (Colour Doppler). SR=Strain Ratio. SD=Strain Difference. EG=Tsukuba Elasticity Score. MTT=Mean Transit Time. PI(C)=Peak Intensity. RT=Rising Time. TTP=Time To Peak. WIS=Wash-in Slope. AS=Ascending Slope. ME=Mean Elasticity. VI=Vascularization Index. FI=Flow Index. VFI=Vascularization-flow Index. C_{max}=Curve Maximum

Study Results: 1=Significant parameter changes for Responders but not Non-Responders after NAC (95% CI, α=0.05); 2=Significant parameter changes for Responders but not Non-Responders during NAC (intra-treatment monitoring) (95% CI, α=0.05); 3=Significant difference in parameters between Responders and Non-Responders at baseline (prior to NAC) (95% CI, α=0.05)

Table 1.21: Summary of research for DOS and US in breast cancer chemotherapy response.

1.14.2 Quality Assessment Using QUADAS-2 and STARD

For this review, 31 observational trials were identified. Due to the recent use of DOS and QUS for chemotherapy response monitoring for breast cancer compared to other modalities, no trials were identified as randomized controlled trials (RCTs) and there were no RCTs for other US-based imaging. Thus, it should be noted that these limitations affect the generalizability of this literature review. Further, it should be noted that a single evaluator performed the quality assessments only (William Tran), thus limiting the objectivity of the results of this review. Nevertheless, the results of the review identified areas of high risk for bias.

1.14.3 QUADAS-2 Results

A risk for bias for patient selection was identified in 26% of all studies and this was higher in DOS studies (5/16, 31%) compared to US and QUS studies (3/15, 20%). The major weaknesses were found in signalling questions

surrounding case-control designs and related to the index test (48% of all studies), where there was a higher risk in DOS studies (11/16, 69%) compared to US studies (4/15, 27%). A higher risk of bias could be due to analysis performed with prior knowledge of pathological response to NAC, and when studies were performed retrospectively. One study demonstrated an unclear risk with respect to the reference standard because pathologic outcomes were not described clearly with current clinical standards (Huber et al., 2000). In all applicability concern categories, the reference standard was reported as high risk for US studies (6/9, 67%). This is due to the variabilities in which the tests and measurements were completed during chemotherapy (i.e. various measurement timelines) and technical concerns about the parameters used to acquire and measure the ultrasound signals. For example, ultrasound studies did not indicate the ultrasound frequency (MHz) used to acquire images and image optimization methods were missing from the materials and methods section. Additionally, DOS and US studies that measured chemotherapy response demonstrated variable chemotherapy regimens which could have affected the results of the studies as the heterogeneity of tumours (i.e. intrinsic molecular features) could be responsive to one treatment over another. In some studies, an antivascular drug (Bevacizumab; tradename, Avastin®) was transiently used in some patient populations and studies and this could have affected the results for tests that measured haemoglobin, blood flow and vascularity (Ueda et al., 2012, Zhu et al., 2013, Tromberg et al., 2016, Pakalniskis et al., 2011, Cerussi et al., 2011, Amioka et al., 2016, Saracco et al., 2017). A summary of the QUADAS-2 results is presented in **Table 1.22** and **Figure 1.25**.

QUADAS-2 References (Study)		RISK OF BIAS				APPLICABILITY CONCERNS		
		Patient Selection	Index Test	Reference Standard	Timing & Flow	Patient Selection	Index Test	Reference Standard
Concept 1: Diffuse Optical Spectroscopy Imaging								
1	(Cerussi et al., 2007)	☹	☹	☺	☹	☹	☹	☺
2	(Zhu *et al.*, 2008)	☺	☹	☺	☺	☺	☺	☺
3	(Jiang et al., 2009)	☹	☹	☺	☺	☹	☺	☺
4	(Soliman *et al.*, 2010)	☺	☹	☺	☺	☺	☺	☺
5	(Cerussi et al., 2011)	☹	☹	☺	☺	☺	☺	☺
6	(Pakalniskis *et al.*, 2011)	☹	☺	☺	☹	☹	☺	☺
7	(Roblyer *et al.*, 2011)	☺	☹	☺	☺	☺	☺	☺
8	(Falou *et al.*, 2012)	☺	☺	☺	☺	☺	☺	☺
9	(Ueda *et al.*, 2012)	☺	☹	☺	☺	☺	☺	☺
10	(Zhu *et al.*, 2013)	☺	☹	☺	☺	☺	☺	☺
11	(O'Sullivan et al., 2013)	☹	☹	☹	☺	☹	☺	☹
12	(Jiang et al., 2014)	☺	☹	☺	☺	☺	☺	☺
13	(Schaafsma *et al.*, 2015)	☺	☹	☺	☺	☺	☺	☺
14	(Sadeghi-Naini et al., 2015)	☺	☺	☺	☺	☺	☺	☺
15	(Tromberg et al., 2016)	☺	☺	☺	☺	☺	☺	☺
16	(Ueda et al., 2016)	☺	☺	☺	☺	☺	☺	☺
Concept 2a: General Ultrasound Imaging								
1	(Singh et al., 2005)	☺	☺	☺	☺	☺	☺	☺
2	(Huber et al., 2009)	☹	☹	?	☺	?	?	☹
3	(Hayashi et al., 2012)	☺	☹	☹	☺	☺	☹	☹
4	(Cao et al., 2012b)	☺	☺	☹	☺	☺	☺	☹
5	(Evans et al., 2013)	☹	☹	☺	☺	☹	☹	☺
6	(Falou et al., 2013)	☺	☺	☺	☺	☺	☺	☺
7	(Shia et al., 2015)	☹	☺	☹	☺	☹	☺	☹
8	(Amioka et al., 2016)	☺	☺	☹	☺	☺	☺	☹
9	(Saracco et al., 2017)	☺	☹	☹	☺	☺	☹	☹

Concept 2b: Quantitative Ultrasound Spectroscopy

10	(Sadeghi-Naini et al., 2013b)	☺	☺	☺	☺	☺	☺	☺
11	(Sadeghi-Naini *et al*., 2014)	☺	☺	☺	☺	☺	☺	☺
12	(Sannachi *et al*., 2015)	☺	☺	☺	☺	☺	☺	☺
13	(Gangeh et al., 2016)	☺	☺	☺	☺	☺	☺	☺
14	(Tadayyon et al., 2016)	☺	☺	☺	☺	☺	☺	☺
15	(Tadayyon et al., 2017)	☺	☺	☺	☺	☺	☺	☺

Risk of Bias and Applicability Concerns scale:

☺ Low	☹ High Risk	? Unclear Risk

Table 1.22. QUADAS-2 was used to study the diagnostic accuracy of previous studies. The QUADAS-2 evaluation tool was adapted from (Whiting et al., 2011).

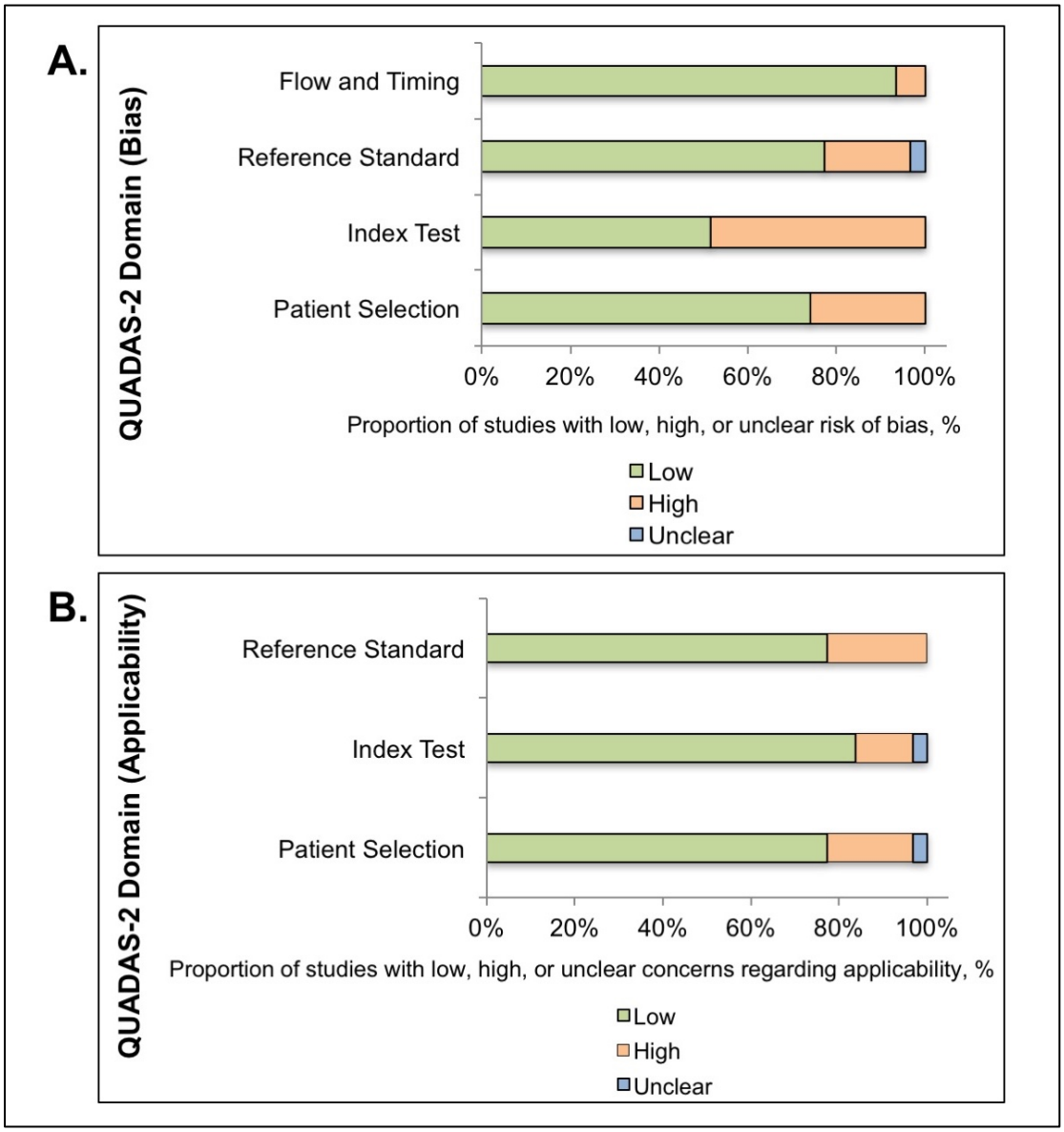

Figure 1.25. A. QUADAS-2 Domain (Bias); **B.** QUADAS-2 Domain (Applicability)**.** Proportion of studies with low, high, or unclear concerns regarding bias and applicability, % for DOS, US, and QUS studies.

1.14.4 STARD Assessment Results

For STARD results, 4/25 items scored less than 50% across all studies. These scores corresponded with items no. 10, 11, 20 and 24 of the STARD assessment. Of the studies yielded in this literature review, test methods demonstrated lower reporting on the number, training and expertise of readers who did the imaging analysis (STARD, no. 10). (Bossuyt et al., 2003). This was particularly high in QUS studies. There was a risk of data variance which could have resulted from differences in tumour volume analysis, 2D versus 3D image acquisition and determining tumour ROIs for analysis. Schaafsma et al. (2015) reported that a 5-mm displacement of DOS ROIs could affect the results of up to 8% depending on the size of the tumour (Schaafsma et al., 2015). Additionally, 45% of the studies did not report blinding readers from the reference standard (STARD, no.11) and these limitations are consistent with the QUADAS-2 assessment results. For adverse events reporting (STARD, no.20), it would be expected to observe a low reporting rate for this category because QUS and optical imaging does not involve any contrast agents, and the risk for adverse effects to contrast-based ultrasound is relatively low (Stewart and Sidhu, 2006). Finally, another area of concern involves the reproducibility of results which include inter- and intra-user variance (STARD, no. 24). Only 42% of all studies reported a kappa-statistic or inter-user validation and analysis. This was particularly low in QUS studies that reported no such methods. Results of the STARD assessment are presented in **Table 1.23.**

STARD CHECKLIST RESULTS SECTION AND TOPIC		Imaging Technique DOS n (%)	 US n (%)	 QUS n (%)	 ALL n (%)
	TITLE/ABSTRACT/KEYWORDS				
	1. Identify the article as a study of diagnostic accuracy (recommended MeSH heading 'sensitivity and specificity').	15 94	9 100	6 100	30 97
	INTRODUCTION				
	2. State the research questions or study aims, such as estimating diagnostic accuracy or comparing accuracy between tests or across participant groups.	16 100	9 100	6 100	31 100
	METHODS				
Participants	**3.** Describe the study population: The inclusion and exclusion criteria, setting and locations where the data were collected.	15 94	9 100	6 100	30 97
	4. Describe participant recruitment: Was recruitment based on presenting symptoms, results from previous tests, or the fact that the participants had received the index tests or the reference standard?	15 94	9 100	6 100	30 97
	5. Describe participant sampling: Was the study population a consecutive series of participants defined by the selection criteria in items 3 and 4? If not, specify how participants were further selected.	16 100	9 100	6 100	31 100
	6. Describe data collection: Was data collection planned before the index test and reference standard were performed (prospective study) or after (retrospective study)?	13 81	9 100	6 100	28 90
Test methods	**7.** Describe the reference standard and its rationale.	15 94	8 89	6 100	29 94

	8. Describe technical specifications of material and methods involved including how and when measurements were taken, and/or cite references for index tests and reference standard.	16 100	9 100	6 100	31 100
	9. Describe definition of and rationale for the units, cut-offs and/or categories of the results of the index tests and the reference standard.	15 94	8 89	6 100	29 94
	10. Describe the number, training and expertise of the persons executing and reading the index tests and the reference standard.	9 56	6 67	0 0	15 48
	11. Describe whether or not the readers of the index tests and reference standard were blind (masked) to the results of the other test and describe any other clinical information available to the readers.	4 25	5 56	5 83	14 45
Statistical methods	**12.** Describe methods for calculating or comparing measures of diagnostic accuracy, and the statistical methods used to quantify uncertainty (e.g. 95% confidence intervals).	16 100	9 100	6 100	31 100
	13. Describe methods for calculating test reproducibility, if done.	16 100	9 100	6 100	31 100
	RESULTS				
Participants	**14.** Report when study was done, including beginning and ending dates of recruitment.	9 56	8 89	1 17	18 58
	15. Report clinical and demographic characteristics of the study population (e.g. age, sex, spectrum of presenting symptoms, comorbidity, current treatments, recruitment centres.	16 100	9 100	6 100	31 100
	16. Report the number of participants satisfying the criteria for inclusion that did	15	9	6	30

	or did not undergo the index tests and/or the reference standard; describe why participants failed to receive either test (a flow diagram is strongly recommended).	94	100	100	97
Test results	**17.** Report time interval from the index tests to the reference standard, and any treatment administered between.	15 94	9 100	6 100	30 97
	18. Report distribution of severity of disease (define criteria) in those with the target condition; other diagnoses in participants without the target condition.	15 94	8 89	6 100	29 94
	19. Report a cross tabulation of the results of the index tests (including indeterminate and missing results) by the results of the reference standard; for continuous results, the distribution of the test results by the results of the reference standard.	16 100	8 89	6 100	30 97
	20. Report any adverse events from performing the index tests or the reference standard.	0 0	0 0	0 0	0 0
Estimates	**21.** Report estimates of diagnostic accuracy and measures of statistical uncertainty (e.g. 95% confidence intervals).	16 100	9 100	6 100	31 100
	22. Report how indeterminate results, missing responses and outliers of the index tests were handled.	14 88	9 100	6 100	29 94
	23. Report estimates of variability of diagnostic accuracy between subgroups of participants, readers or centres, if done.	16 100	9 100	6 100	31 100
	24. Report estimates of test reproducibility, if done.	9 56	4 44	0 0	13 42

DISCUSSION				
25. Discuss the clinical applicability of the study findings.	16 100	9 100	6 100	31 100

STARD checklist for quality assessment of studies. Studies were stratified into their respective imaging domains and overall score (all studies combined).

Stratified data: DOS; n=16, Ultrasound Imaging; n=9, QUS; n=6.

All pooled studies; n=31.

Areas with scores of less than 50% are highlighted in orange.

Table 1.23: STARD assessment results. The STARD assessment tool was adapted from (Bossuyt et al., 2003).

1.14.5 Summary Findings from Literature Review

The results of the literature review showed that MRI studies were most frequently reported for measuring chemotherapy response in locally advanced breast cancer. MRI technique included: DCE-MRI, DWI-MRI, BOLD-MRI and SPECT-MRI. MRI imaging biomarkers were used to measure tumour vascular perfusion, tumour cellularity and tumour cell features (i.e. cell membrane integrity associated with cell death). The major limitations for using MRI included needing contrast agents (i.e. variable contrast injection techniques caused variability in data) and variable image quality (i.e. using 1.5T and 3.0T MRI systems produced images with variable signal-to-noise ratios). Other imaging studies for PET, CT, X-Ray and 99m-Tc Scintigraphy showed promising results that reached a classification accuracy of up to 89%; however, the major limitations included small sample sizes that may have caused overestimated results, variable definitions of tumour response endpoints (i.e. radiological versus pathological endpoints) and imaging results were dependent on the adequate uptake of contrast agents in tumours.

For DOS and QUS, QUADAS-2 and STARD tools were used to systematically identify the quality of previous imaging studies. QUADAS-2 and STARD assessment results demonstrated that more work is required to optimize the index test and reference standards of future studies in DOS and QUS. Based on analysis of previous studies, the experimental design of future

DOS and QUS studies should involve the following to optimize the quality of studies due to the limitations identified from previous work:

a. **Blinded analysis**. There should be no prior knowledge of the disease outcome or reference standard for tumour analysis.
b. **Reference standards**. Ground-truth labels (i.e. tumour response endpoints) should follow standard pathologic classification from established and accepted clinical guidelines.
c. **Expertise and Experience of Analysts**. Clinical breast images using DOS and QUS should be verified with expert radiologists to confirm correct analysis of the tumour volume;
d. **Reproducibility.** Reproducibility should be verified by using the same technical frameworks with DOS and QUS systems that are comparable. There should also be a comparative analysis of tumour ROI analysis (i.e. kappa statistic) should be completed.
e. **Index Tests**. Patients should demonstrate the most homogenous chemotherapy treatments.

1.14.6 Limitations of Literature Review

Limitations to this systematic review include the small number of studies available for analysis. Additionally, this review was conducted by one observer with experience in QUS analysis which could result in a bias in assessing QUS experiments. Taken together, since the research question was to test if DOS and QUS markers could be used to measure NAC response in breast cancer, it is acknowledged that this focused research area may limit the search results from the literature.

Chapter 2

Methods

2.0 Chapter Overview

The first section of this chapter will highlight the background and clinical problem, as described previously from Chapter 1. In section two, the research questions to the study are presented, which will also introduce the primary and secondary aims of the study. Section three outlines the ethical and regulatory approval, which will lead to describing the inclusion and exclusion criteria of patients that were enrolled in the study. In section four, the chemotherapy treatment protocol and imaging schedule pertaining to the aims of the study are presented. In section five, the DOS and QUS imaging methods, in terms of experimental analysis to the research study are outlined. These sections cover DOS and QUS imaging instrumentation, data handling and the computations involved in DOS and QUS biomarker extraction. In section six, the quality assurance methods are presented, and the chapter ends with section seven, which describes the statistical frameworks used to model DOS and QUS parameters as indicators (markers) for chemotherapy response in locally advance breast cancer.

2.1 Background

Treatment for locally advanced breast cancer (LABC) involves neoadjuvant chemotherapy (NAC) to reduce tumour size before surgery. However, tumour response to NAC is variable and only 45% of patients achieve sufficient down-staging prior to surgery (Cance et al., 2002) . Measuring tumour response during NAC may help guide treatments and help both patients and physicians make the best treatment choices for improved outcomes.

Currently, tumour response during NAC is measured by routine physical examination, or sometimes conventional imaging to measure the tumour size (Therasse et al., 2000). However, conventional imaging using MRI, CT or FDG-PET are associated with high equipment costs and these procedures require contrast agents for image optimization (Eisenhauer et al., 2009). Due to these limitations, major efforts have been made to explore alternative imaging techniques to evaluate both pre-treatment and intratreatment indicators for tumour response to therapy. However clinical adoption of past and newly developed quantitative imaging techniques to guide chemotherapy have not surpassed the experimental setting (Eccles et al., 2013).

Recent priorities for breast cancer treatment and research were outlined by a UK-based working group (Eccles et al., 2013). The group made recommendations for advancing biomarker discovery and integrating imaging biomarkers into the clinical workflow to guide therapies. The endpoints were precision medicine and individualization (personalization) of treatments. The recommendations were made to address the current treatment practices which delivers a “one-size-fits-all” chemotherapy approach. This is problematic as this approach often leads to variable tumour response to treatment and have been shown to demonstrate higher mortality (von Minckwitz et al., 2013).

Taken together, the potential benefits of exploring imaging biomarkers to help guide treatments is enticing and can potentially improve patient care. The overall benefit will be to advance treatment outcomes (i.e. improve patient survival) and optimize healthcare economics by saving money on unnecessary and ineffective treatments (Eccles et al., 2013).

2.2 Research Design Summary

2.2.1 Study Design

This project was an exploratory, observational (cross sectional) study in human subjects. The study was approved by the institutional ethics review board (IRB)[7]. The research was performed to study quantitative ultrasound and diffuse optical spectroscopy imaging in breast tumours treated with neoadjuvant chemotherapy. The results were used to examine the utility of DOS and QUS imaging parameters (biomarkers) as potential surrogate markers for pathological tumour response to chemotherapy, as assessed by Miller-Payne pathologic response criteria. The project was divided into two subprojects (described below).

2.2.2 Aims of the Study

Subproject one Aims

- To measure the biological changes in breast tumours during chemotherapy using quantitative ultrasound spectroscopy (QUS) and diffuse optical spectroscopy (DOS). The intratreatment measurements were aimed at the following times, which corresponded to the chemotherapy schedule: pre-treatment, week one, week four, week eight, and preoperatively.

- To test the relationship between multivariate QUS+DOS statistical models with the final pathologic tumour response as assessed by Miller-Payne pathologic response scale (defined in **Table 2.1**).

[7] The IRB approval forms are found in **Appendix 2**: Supplemental Information to Chapter 2 (Methods).

- To evaluate the earliest time points when DOS and QUS measurements demonstrate significant differences between Miller-Payne pathologic response classes (i.e. responders versus non-responders).

Subproject Two Aim

- To identify pre-treatment DOS imaging biomarkers for significant differences between response classes (responders versus non-responders), as measured by Miller-Payne pathological response criteria.

- To test the utility of DOS-texture analysis for predicting chemotherapy responders from non-responders before treatment starts.

- To investigate the accuracy of pre-treatment DOS-texture features in multivariate models for predicting chemotherapy response.

- To evaluate the relationship between DOS imaging biomarkers and the tumour's biological characteristics and treatment types.

2.2.3 Research Questions (Subproject 1 and Subproject 2)

- Do DOS and QUS imaging biomarkers demonstrate statistically significant changes over the course of chemotherapy?

- Can DOS and QUS imaging biomarkers be modelled using univariate and multivariate parameters to measure treatment response at early time intervals (i.e. after one or two cycles of chemotherapy)?

- Do breast tumours demonstrate significant differences in DOS-texture parameters between responders and non-responders, as measured before chemotherapy?

- Can DOS markers predict chemotherapy response prior to starting chemotherapy?

- ❖ Are there differences in DOS-texture prediction models for breast cancer subtypes (i.e., ER+ and triple negative) and chemotherapy treatments (i.e. FEC-D and AC-T)?

2.2.4 Endpoints

Primary Endpoints

- ❖ The primary endpoint of subproject one was accuracy in measuring chemotherapy response, in terms of its association to Miller-Payne pathologic response criteria, using intratreatment DOS and QUS imaging biomarkers.

- ❖ The primary endpoint of subproject two was accuracy of predicting chemotherapy response, in terms of its association to Miller-Payne pathologic response criteria, using the pre-treatment DOS-texture parameters.

Accuracy of Measuring Chemotherapy Response

Within the patient's standard of care, all mastectomy specimens were evaluated with high-magnification light microscopy by board-certified breast pathologists at the host institution. Mastectomy specimens were prepared in paraffin blocks and 5-micron-thick microtome specimens and whole-mounted for histological staining. The samples were stained using standard haematoxylin and eosin (H&E) techniques (**Figure 2.1**). Pathologic outcome measures were assessed using Miller-Payne response criteria by a breast pathologist. The tumour response to treatment was reported in the patient's electronic treatment record based on Miller-Payne assessment criteria, described further below.

Standardized Tumour Response Endpoints (Pathologic Response Definition)

For this study, Miller-Payne Pathologic Response Criteria (MP) was used to define "pathologic response" outcomes in the sample population

(Ogston et al., 2003). As there is no current consensus on defining "pathologic response" in breast cancer chemotherapy, the MP scale was chosen among other clinically-accepted standards, since it systematically defines the changes in cellularity within the primary lesion only. This is important since defining the change in the primary lesion corresponds to the imaging measurements of the tumour only in this study. In comparison to other pathologic response scales, such as the residual cancer burden index (RCBI), those scales use multiple variables such as lymph node status and tumour size reduction as part of the criteria for pathologic response (von Minckwitz et al., 2012, Symmans et al., 2007).

Thus, in this study, "pathologic response" were defined systematically using Miller-Payne (MP) pathologic response criteria (Ogston et al., 2003). A cut-off score was chosen within the MP scale for binary classification, based on the recommendation of a breast pathologist. Tumours that were graded as MP1 or MP2 were classified as non-responders [NR]. Tumours graded as MP grade 3, 4, or 5 were classified as responders [R]. The classification decision-tree is outlined in **Table 2.1**.

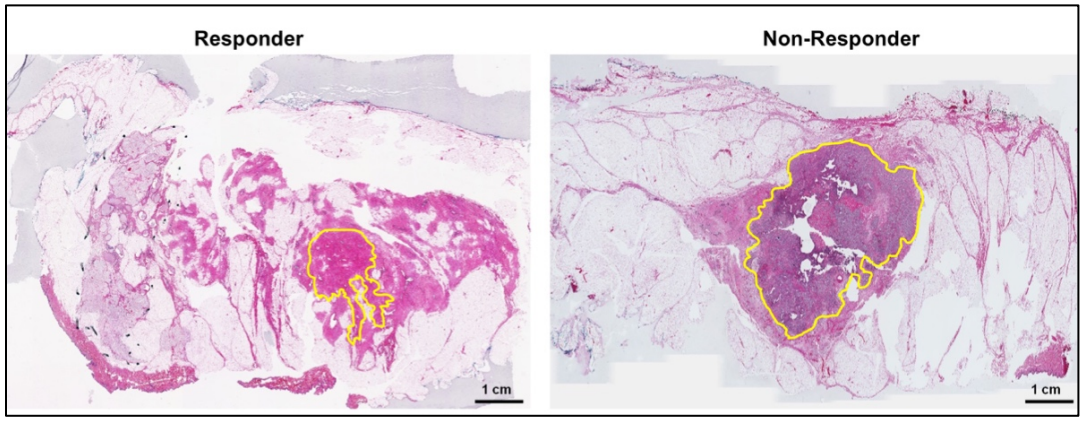

Figure 2.1: H&E-stained whole breast mounts for a representative responder and non-responder. The pathologists used H&E to measure tumour response after neoadjuvant chemotherapy. The cellularity of the tumour bed was quantified and reported using a graded score (Miller-Payne criteria). On the left slide (yellow contour), a responder demonstrated a significant reduction in the size and cellularity under microscopy. In contrast on the right specimen, a patient who did not respond to chemotherapy demonstrated a large, bulky residual tumour (yellow contour) with high cellularity.

Grade	Pathologic Description	Binary Classification
Grade 1	No change to overall tumour cellularity	Non-Responders [NR]
Grade 2	Minor loss; up to 30% loss	
Grade 3	Between 30%-90% loss in tumour cells	Responders [R]
Grade 4	Greater than 90% loss of tumour cells	
Grade 5	No remaining tumour cells.	

Table 2.1: The MP classification method is based on a comparison of the cellularity before and after treatment. A binary classification was used to classify patients into responders (R) or non-responders (NR) based on a chosen cut-off point that was recommended by the breast pathologist.

In addition, other histological assays were completed outside of the patient's usual standard of care for this study and were approved by the institution's IRB. This included cluster of differentiation staining (CD-31), which was used to quantify the number of blood vessels within the tumour bed after chemotherapy (JC07 clone, Leica Biosystems, Concord, Ontario Canada). Quantification for CD-31 stained vessels were performed on the whole-mount specimens after staining (TissueScope, Huron Digital Pathology, Waterloo, Canada). Stained vessels were counted for each specimen (counts/field) and the vessel counts were averaged across all respective normal or tumour regions.

Radiologic Endpoints

Radiologic endpoints were collected from the patient's medical record to compare the treatment size before, and after chemotherapy only as to report the patient's clinical characteristics.

As part of the patient's standard of care at the host institution, all patients who completed chemotherapy with operable tumours underwent a surgical planning MRI. The surgical-planning MRI was used to compare the tumour size changes from before and after chemotherapy. Radiologic endpoints were evaluated using standard RECIST 1.1 criteria (Eisenhauer et al., 2009). Pre- and post-chemotherapy tumour size measurements were recorded as part of the patient's clinical data.

2.2.5 Overview, Research Design Summary

The research design summary is outlined in **Table 2.2** and also presented schematically in **Figure 2.2**.

Title	**Thesis Title:** Measuring Chemotherapy Response in Breast Cancer Using Optical and Ultrasound Spectroscopy. **Subproject one:** Multiparametric Monitoring of Chemotherapy Treatment Response in Locally Advanced Breast Cancer using Quantitative Ultrasound and Diffuse Optical Spectroscopy **Subproject two:** Predicting Breast Cancer Response to Neoadjuvant Chemotherapy Using Pre-treatment Diffuse Optical Spectroscopic-Texture Analysis
Aim	**Subproject one Aims:** The purpose of this observational study was to measure breast tumour response to chemotherapy using DOS and QUS imaging. The aims were: 1. To measure the biological changes in breast tumours during chemotherapy using imaging biomarkers from quantitative ultrasound spectroscopy (QUS) and diffuse optical spectroscopy (DOS). The intratreatment measurements were aimed at the following times, which corresponded to the chemotherapy schedule: pre-treatment, week one, week four, week eight, and preoperatively. 2. To test the relationship between multivariate QUS+DOS statistical models with the final pathologic tumour response.

3. To evaluate the earliest time points when DOS and QUS measurements demonstrate significant differences between response classes (i.e. responders versus non-responders).

Subproject two Aims:

The purpose of this study was to evaluate texture features of pre-treatment DOS functional maps for predicting LABC response to NAC. The aims were:

1. To identify pre-treatment DOS imaging biomarkers for significant differences between response classes (responders versus non-responders).

2. To test the utility of DOS-texture analysis for predicting chemotherapy responders from non-responders before treatment starts.

3. To investigate the accuracy of pre-treatment DOS-texture features into multivariate models for predicting chemotherapy response.

4. To evaluate the relationship between DOS imaging biomarkers and the tumour's biological characteristics and chemotherapy type.

Eligibility Criteria	All the following criteria were met for entry to the study. • Both men and women were eligible. • Histologically confirmed locally advanced breast carcinoma. • All tumour molecular subtypes were eligible. • Patients who had **not** been treated with any other first-line therapy. • Treatment with anthracycline or taxane based neoadjuvant chemotherapy. • The patients must have had measurable disease $\geq$ 10 mm in the breast. This minimal size was needed to visualize the tumour upon DOS and QUS imaging.

	• Scheduled for mastectomy or lumpectomy after neoadjuvant chemotherapy with pathologic assessment. • Life expectancy of at least 6 months. • Patients had the ability to understand and the willingness to sign a written consent form document in English. **Exclusion Criteria** • History of allergic reactions attributed to compounds of similar chemical or biologic composition to ultrasound gel or optical compensation medium. • Any condition that is unstable or could jeopardize the safety of the patient and their compliance in the study during imaging. • Inability to position arm above the head for ultrasound scanning or lay supine for QUS imaging. • Inability to position in the prone position for optical scanning. • Tumours deeper than 4 cm in the posterior direction of the breast, or tumours that were larger than 6 cm across the lateral distance. • A maximum cranio-caudal breast separation (thickness) of 80 mm.
Study Design	This study is an observational (cross sectional) study in human subjects.
Endpoints	**Primary Endpoints for Observational Study** • The primary endpoint of subproject one was accuracy in measuring chemotherapy response, in terms of its association to Miller-Payne pathologic response criteria, using intratreatment DOS and QUS imaging biomarkers • The primary endpoints of subproject two was accuracy of predicting chemotherapy response, in terms of its association to Miller-Payne pathologic response criteria, using the pre-treatment DOS-texture parameters. **Primary Efficacy Endpoint** • Accuracy in discriminating pathologic response classes is calculated using statistical measures within the 95%

	confidence interval. It is expected that DOS and QUS imaging biomarkers can be used as surrogate endpoints towards standardized pathologic response criteria.
Sample Size Calculation	A sample size calculation was completed based on the following: **<u>DOS</u>** Z=1.96 (Confidence interval of 95%) Margin of Error (ME): 20% (based on literature) Standard Deviation (SD): 43% (based on literature) **<u>QUS</u>** Z=1.96 (Confidence interval of 95%) Margin of Error (ME): 30% (based on literature) Standard Deviation (SD): 65% (based on literature) Thus, the calculation for the sample size in this study, given an expected attrition of 20% is: Sample size required: **22 patients**
Outcomes	**Outcome 1 (Subproject one)** • Significant differences in the mean DOS and QUS parameters between responders and non-responders during chemotherapy, as measured at week one, 4, 8 and pre-operatively. • Correlation to pathologic response, as defined by Miller-Payne response criteria. **Outcome 2 (Subproject two)** • Pre-treatment DOS-texture parameters demonstrate significant differences between response classes before treatment begins. • Discrimination of responders and non-responders are determined prior to treatment. • Correlation to pathologic response, as defined by Miller-Payne response criteria.

Table 2.2: Trial summaries for the study.

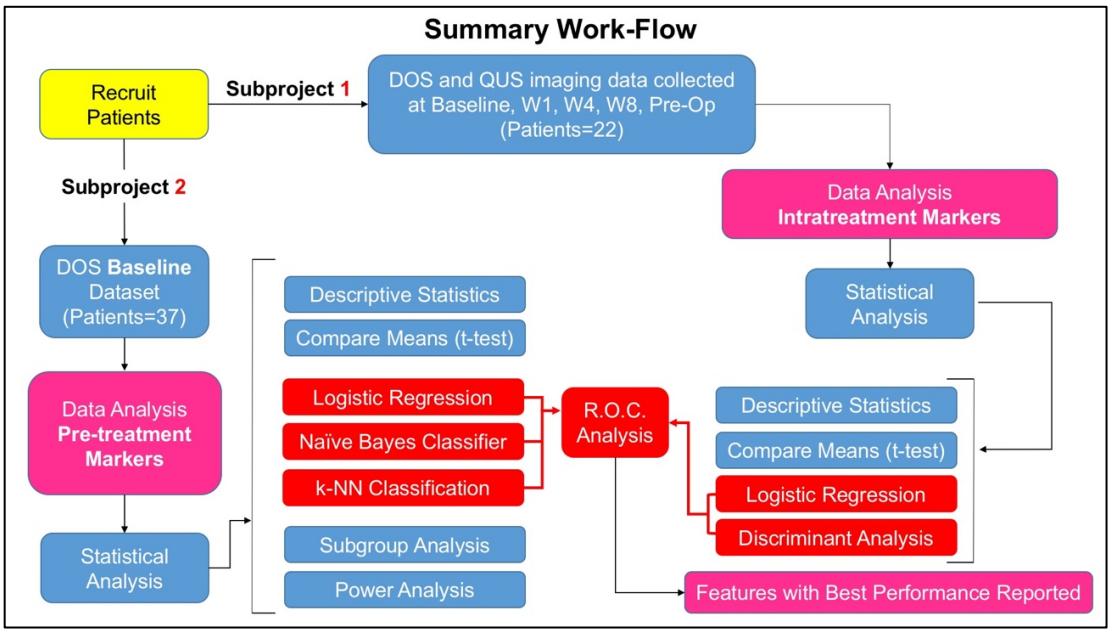

Figure 2.2: Work-flow and methods summary. The study entailed two subprojects. The objective of subproject one was to demonstrate the utility of intratreatment DOS and QUS imaging biomarkers to discriminate pathologic response, as defined by Miller-Payne pathologic grading; while subproject two used pre-treatment DOS imaging biomarkers to classify pathologic response (Miller-Payne) before the start of chemotherapy. Novel classification approaches included multiparametric DOS-QUS modelling, machine learning algorithms and textural analysis of DOS parameters.

2.3 Ethics and Regulatory Approval

2.3.1 Ethics Approval

All research was conducted at the host institution (Toronto, Canada). DOS and QUS imaging studies were approved by the institutional ethics review board (IRB) prior to data collection and analysis (IRB # 186-2006 and IRB# 185-2006, documentation presented in **Appendix 2**). All patients enrolled in this study signed a written consent form to participate in DOS and QUS studies prior to any data collection. No patients were within the investigator's circle of care at the time of recruitment.

2.3.2 Eligibility (Inclusion/Exclusion Criteria)

Patients were approached to participate in the study based on a biopsy-proven diagnosis of locally advanced breast cancer during their initial visit to the medical oncologist. Patients were referred for participation in the clinical study by the medical oncologists involved in the patients' care. Patients were identified using the hospital's electronic medical appointment system. Both men and women between 18-65 years of age were eligible for this study; however, since men accounted for <1% of the institution's patient population for breast cancer, no men were eligible during the study recruitment phase and therefore no male enrolments were made. A detailed summary of the inclusion and exclusion criteria are outlined below:

Inclusion Criteria:

- Both men and women were eligible to participate in the study
- Participants of all races were eligible to the trial.
- Histologically confirmed locally advanced breast carcinoma (Stage IIB/III disease, invasive breast cancer with all histological types eligible).
- All molecular subtypes were included: ER +/-, PR +/-, HER2-Neu +/-.

- Patients who had **not** been treated with any other first-line therapy (hormone therapy, other chemotherapy, surgery, radiation, or experimental anticancer drugs).
- Treatment with neoadjuvant chemotherapy: fluorouracil, epirubicin, cyclophosphamide, docetaxel (FEC-D); or Adriamycin (doxorubicin), cyclophosphamide, paclitaxel (AC-T). Patients with HER2-Neu amplified tumours who were scheduled for Trastuzumab were eligible to participate.
- The patients must have had measurable disease $\geq$ 10 mm in the breast and for imaging using DOS and QUS (this size is needed in order to visualize the tumours for analysis). Patients' tumours were thus radiologically defined by MRI or CT, or mammogram or ultrasound, prior to neoadjuvant chemotherapy and participation in the trial.
- Scheduled for mastectomy or lumpectomy after neoadjuvant chemotherapy with pathologic assessment for response to treatment or eligible for surgical consultation.
- Eastern Co-operative Oncology Group (ECOG) Performance Status of 0 or 1.
- Life expectancy of at least 6 months
- Patients had the ability to understand and the willingness to sign a written consent form document, or in the cases where English was not the primary language, the patient were accompanied by a translator or a substitute decision maker at the time of consent. Signed informed consent was obtained prior to any study specific procedures.

Exclusion Criteria

Patients were not eligible for inclusion in the study in the event of the following criteria:

- Past or recent history of allergic reactions attributed to compounds of similar chemical or biologic composition to ultrasound gel.
- Uncontrolled or unmanaged other illnesses or medical conditions including, but not limited to ongoing or active infection, symptomatic congestive heart failure, unstable angina pectoris, and cardiac

arrhythmia or psychiatric disorders that could jeopardize the safety of the patient during the study.

- An inability to position the arm above the head for ultrasound scanning or unable to lay in supine position.
- An inability to position in the prone position for optical scanning.
- Due to the optical absorption caused by melanin in the skin, patients with dark skin or freckled skin were excluded from this study.

2.3.3 Sample Size Justification

A sample size was calculated for each imaging modality. The justification for the sample size proposed is presented below. Separate calculations were performed for DOS and QUS imaging, since each imaging modality had separate reference data that was needed within the following statistical frameworks:

1. A desired 95% confidence interval (with corresponding Z score)
2. Margin of error (ME) permitted (based on previous works)
3. Standard deviation of the outcome of interest.

Sample size calculation (DOS imaging)

The sample size for DOS imaging was determined from the following calculation:

One sample, continuous outcome (based on oxy-haemoglobin, Cerussi et al. 2011).
The concentration of oxy-haemoglobin was previously reported in the literature as 15.3 μM $\pm$ 1.1 (STE) (Cerussi et al., 2011)[8].

[8] The concentration of oxy-haemoglobin represents the value obtained in breast tumours, as measured at the end of chemotherapy. The time interval corresponded with the desired time interval measured in the thesis study.

The standard deviation was calculated based on the reported population size in that study of n=24; therefore:

$$Standard\ deviation\ (SD) = STE\ \times \sqrt{n}$$
$$SD = 1.1\ \times \sqrt{36}$$
$$SD = \mathbf{6.6}$$

To calculate the margin of error (ME), a value of 20% was used based on observations of the literature; therefore:

$$Margin\ of\ Error\ (ME) = 20\%\ \ (15.3\ \mu\text{M}\ ) = \mathbf{3.06}$$

Therefore, the sample size calculation would be (**Eq. 2.1**):

$$n = \left(\frac{Z \cdot (SD)}{ME}\right)^2$$
$$n = \left(\frac{1.96 \cdot (6.6)}{3.06}\right)^2$$
$$n = 17.87 \cong 18\ patients$$

Based on the sample calculation, a total of 18 patients were required as the minimum sample size for DOS imaging. However, an attrition rate of 20% was estimated; therefore the study was aimed to recruit 22 patients for DOS imaging.

Sample size calculation (QUS imaging)

The sample size was determined for QUS imaging using the following calculation:
One sample, continuous outcome (based on MBF, Sadeghi-Naini et al. 2013). The MBF was reported as 9.1 dBr ± 1.2 (STE) (Sadeghi-Naini et al., 2013b). The standard deviation was calculated based on the reported population size in that study of n=24; therefore:

$$Standard\ deviation\ (SD) = STE\ \times \sqrt{n}$$
$$SD = 1.2\ \times \sqrt{24}$$

$$SD = \mathbf{5.8}$$

To calculate the margin of error, we use a value of 30% based on observations of the literature; therefore:

$$Margin\ of\ Error\ (ME) = 30\%\ \ (9.1\ ) = 2.7$$

Therefore, the sample size calculation would be (**Eq. 2.2**):

$$n = \left(\frac{Z \cdot (SD)}{ME}\right)^2$$
$$n = \left(\frac{1.96 \cdot (5.8)}{2.73}\right)^2$$
$$n = 17.33 \cong 18\ patients$$

Based on the sample size calculation, a minimum of 18 patients were calculated for imaging with QUS. However, an attrition rate of 20% was estimated; therefore the study was aimed to recruit 22 patients for DOS imaging. All patients were presented with the option to participate in either QUS and/or DOS imaging for the study.

Taken together, the sample calculation indicated a minimum of 22 patients required to obtain a significant result within the 95% confidence interval for either QUS or DOS imaging. Subproject one involved DOS and QUS imaging; therefore, 22 subject data-points (i.e. samples) were targeted. Subproject two involved DOS imaging only, and therefore, the objective was to recruit 22 subjects. The recruitment results of this study were:

1) *Subproject one;* 22 patients were recruited and imaged using DOS and QUS.
2) *Subproject two;* 15 patients were recruited for pre-treatment DOS imaging. The baseline DOS images from subproject one (n=22 patients) were included into a pooled analysis of the pre-treatment

DOS images. Therefore, 37 samples were included for analysis in this subproject[9].

As previously mentioned, patients were recruited into the study by way of referral from the medical oncologists involved in the patients' care. A summary of the recruitment scheme is outlined in **Figure 2.3**.

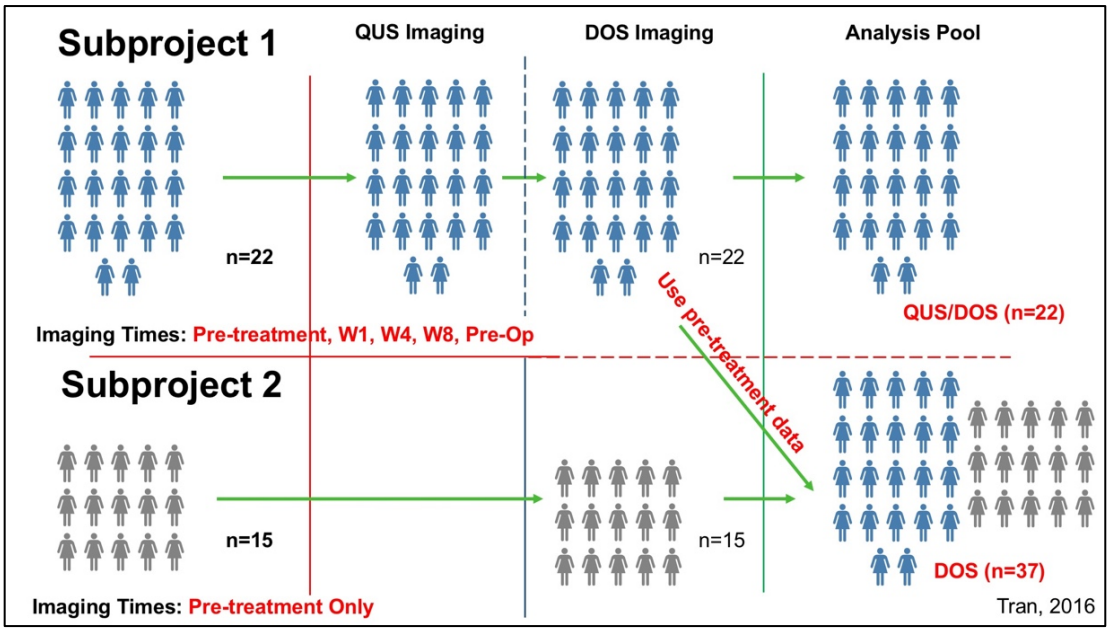

Figure 2.3: Schematic representation of Subproject one and Subproject two. The aim of the study was to recruit 22 subjects, which was based on the sample size calculation. However, this study (subprojects one and two) recruited a total of 37 patients. Subproject one included 22 samples in the dataset; while subproject two had 37 samples within the dataset, that was pooled from the baseline DOS data from subproject one.

2.3.4 Access to Patient Electronic Medical Record

Patient demographics and medical information was recorded from the electronic medical record and included the following descriptors: age, sex, tumour/breast laterality, clinically and radiologically measured tumour size before and after treatment, tumour histological features, chemotherapies,

[9] The institution's IRB approved a sample size of 100 patients; thus, permitting the inclusion of 37 patients in subproject two.

pathologic response criteria (MP), radiologic endpoints (RECIST 1.1 data) and physician notes were recorded to monitor the patient's eligibility during the study and for subsequent statistical analysis (described further below).

2.3.5 Research Location

Data reading and analysis was carried out on specifically designed image-processing workstations (Dell Dimension 2400 work stations) in a locked examination/analysis room for data security. The electronic DOS and QUS data was copied for the purposes of handling and stored electronically in a password protected server and a secondary copy was made for security purposes separately in a secured facility at the host institution. All patient case-report forms (CRFs) were stored in paper-form and locked in a cabinet, inside a locked storage area as per institutional regulations. All electronic imaging data for analysis were anonymized (de-identified) for patient confidentiality. The data key was encoded only to the investigator and the investigator's supervisor to ensure patient confidentiality.

2.4 Patients and Acquiring Imaging Data

2.4.1 Chemotherapy Treatment Schedule

Patients enrolled into the study received the institution's chemotherapy treatment protocol which was in accordance with NCCN guidelines (National Comprehensive Cancer Network, 2016). There were two chemotherapy treatment protocols at the host institution and the treatment course was determined by the medical oncologist responsible for the patient's care. Each protocol contained an anthracycline-drug for the first phase of treatment (phase 1), followed by a taxane-drug in the second phase (phase 2). Other concomitant drugs were given according to the treatment protocol and are listed in **Table 2.3.** The chemotherapy dose and schedule are outlined in **Table 2.3A, B**.

2.4.2 Imaging Schedule Based on Chemotherapy Treatment Schedule

DOS and QUS imaging was completed according to the specific aims of each subproject. Subproject one involved imaging patients with DOS and QUS (n=22) during chemotherapy (1 pre-treatment scan and 5 intratreatment scan points) **(Figure 2.4)**. The imaging timelines were: (Scan 1) baseline (prior to treatment), (Scan 2) week one, (Scan 3) week four, (Scan 4) week eight, (Scan 5) preoperatively and these corresponded with the patients' chemotherapy schedule **(Figure 2.4, Table 2.3)**. For subproject two, an additional 15 patients were recruited and those patients underwent only 1 scan time, which was the pre-treatment DOS imaging only. A schematic summary of the imaging times in correspondence to the chemotherapy protocols is outlined in **Figure 2.4**.

A. Chemotherapy Treatment Protocol 1 (AC-T)			
Phase	**Drug Name [Abbreviation]**	**Drug Class**	**Schedule**
1	Adriamycin [A]	Anthracycline	• 4 cycles • Every 2 weeks
	Cyclophosphamide [C]	Alkylating Agent	
2	Paclitaxel [T]	Taxane	• 4 cycles • Every 2 weeks
	Trastuzumab [H][10]	Monoclonal Antibody	• Every 3 weeks

B. Chemotherapy Treatment Protocol 2 (FEC-D)			
Phase	**Drug Name [Abbreviation]**	**Drug Class**	**Schedule**
1	Fluorouracil [F]	Antimetabolite	• 3 cycles • Every 3 weeks
	Epirubicin [E]	Anthracycline	
	Cyclophosphamide [C]	Alkylating Agent	
2	Docetaxel [D]	Taxane	• 3 cycles • Every 3 weeks
	Trastuzumab [H][2]	Monoclonal Antibody	• Every 3 weeks

Table 2.3: Chemotherapy treatment protocols. **A.** Protocol 1 included AC-T chemotherapy. **B.** Protocol 2 included FEC-D chemotherapy. Chemotherapy treatments were given in two phases. Trastuzumab was given to patients who were HER2 positive in phase 2 (this was due to potential cardiac toxicity if given with anthracycline drugs during phase 1).

2.4.3 Sequencing DOS and QUS Imaging Per Patient

Subproject one (DOS + QUS serial imaging)

DOS and QUS scans were completed sequentially within the same appointment session. Patients were imaged with QUS first, then immediately following the imaging procedure, the patient was transferred onto a DOS imaging device for scanning.

[10] Trastuzumab was given to patients who were HER2 positive only.

Subproject two (baseline DOS imaging (i.e. pre-treatment) only)

Patients recruited into subproject two participated in one DOS scan which included the baseline (pre-treatment) scan only. No QUS acquisition was acquired for this patient group (patients declined participation into parallel DOS and QUS studies).

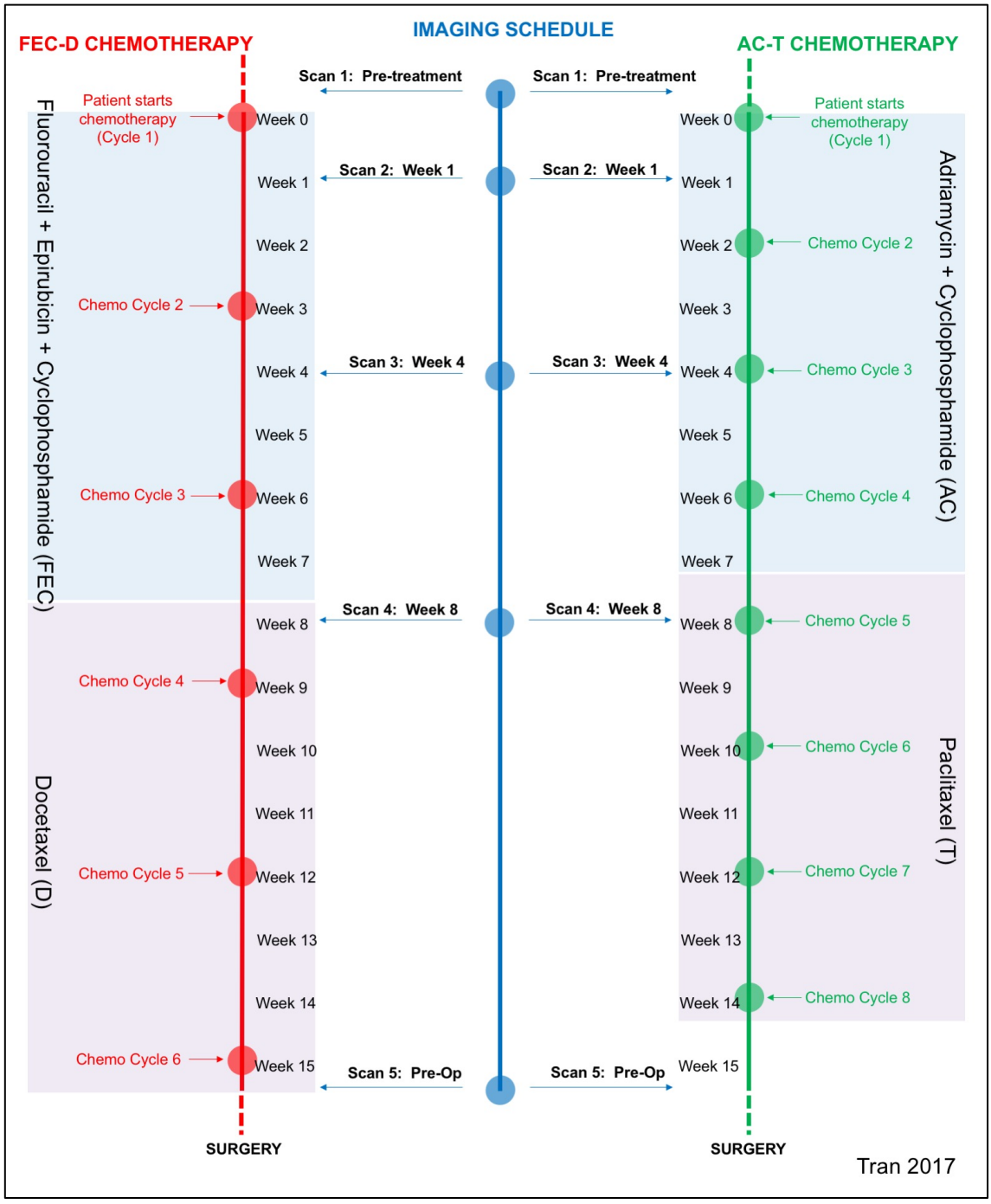

Figure 2.4: LABC patients received either FEC-D (red dots) chemotherapy or AC-T chemotherapy (green dots), which required two dosing schedules. The types of chemotherapy drugs given are indicated as blocks in the figure. For subproject one, the intratreatment imaging scans (QUS+DOS, yellow dots) were scheduled based on an early assessment aim of after 1 cycle of chemotherapy and 2 cycles of chemotherapy for both chemotherapy regimens. For subproject two, patients only attended for the pre-treatment DOS scan.

2.4.4 Quantitative Ultrasound Data Acquisition

For this imaging modality, patients were positioned supine with the ipsilateral arm positioned over the head (**Figure 2.5**). The total duration of the ultrasound scans were approximately 20 minutes.

Data was collected in both normal breast tissue and within the whole tumour volume by employing a continuous panoramic scan across the breast (**Figure 2.5**). To acquire the data, a Sonix RP system (Ultrasonix, Vancouver, Canada) operating with a 128-element, 60 mm- linear array transducer was used (L14-5/60, Ultrasonix, Vancouver Canada). The ultrasound transducer frequency was 10 MHz, corresponding to conventional breast imaging. The centre frequency was ~7 MHz, 40 MHz 8-bit dynamic range radiofrequency digitization frequency and data collected included 512 axial radiofrequency scanlines. The lateral scan distance was 6 cm and the axial depth was 4 cm. Also, the focal depth was placed to correspond to tumour position. The focal depth remained constant throughout the ultrasound imaging series for each patient. The axial resolution was 0.154 mm and the lateral resolution at the focus was 0.21 mm[11] based on the central frequency (i.e. ~7 MHz) used during scans.

The ultrasound data collected included conventional b-mode (greyscale) images and the radiofrequency (RF) data. The data was stored within the system and subsequently downloaded for image processing on a separate computer workstation.

[11] Calculations for the axial and lateral resolution can be found in **Appendix 2**.

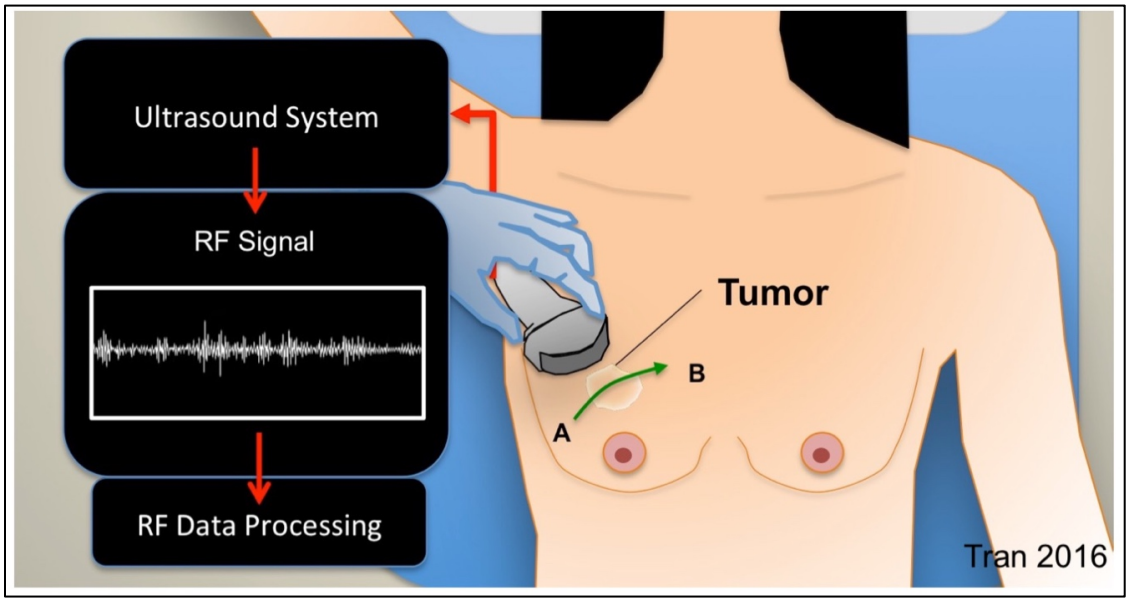

Figure 2.5: QUS breast imaging. Radiofrequency (RF) data and grey-scale images were acquired over the entire volume of the tumour and included normal breast tissue (point A-B).

2.4.5 Diffuse Optical Spectroscopy Tomography Data Acquisition

Patients were scanned with a commercially available diffuse optical tomography system to acquire DOS images (SoftScan, Advanced Research Technologies, Montreal, Canada). The pre-treatment DOS data was collected in 37 patients (22 patients from subproject one, and 15 during subproject two).

The patient was positioned prone and the breast was placed into an enclosed imaging aperture (aquarium) and stabilized by opposing plexiglass plates with soft compression in the cranio-caudal direction **(Figure 2.6)**. The distance (thickness) between plates was recorded at baseline (average thickness = 73.3 ± 10.3 mm [STD]) and this distance was maintained during the imaging series for each individual patient. The optical compensation medium (OCM) was warmed to 23°C and then added to the imaging aperture (aquarium) and filled to cover the entire breast surface **(Figure 2.6)**. The OCM was used to improve light transmission between surfaces and was formulated as an emulsion of lipids, water, and dye to mimic optical properties of breast tissue. The optical absorbance (μ_a) and scattering (μ_s) of the OCM was characterized prior to experimentation (μ_a=0.05 cm^{-1} and μ_s =11 cm^{1}, (λ)=780 nm) (Schaafsma et al., 2015, Intes, 2005).

Optical mammography employed a time-resolved system using four individual semiconductor diode lasers (LDH-P, PicoQuant, Berlin, Germany) that operated at 687, 734, 782, 834 nm. The optical wavelengths were chosen to correspond to the optimal absorbance spectra of breast tissue chromophores such as haemoglobin, water, and lipids (Intes, 2005, Cerussi et al., 2001). The pulse duration at the full width half maximum was less than 150 ps, driven at 20 MHz. For the optical detection system, the light was collected using a photomultiplier (H7422P-50, Hamamatsu Photonics, Shizuoka, Japan), which was opposite to the light source **(Figure 2.6)**. The optical detection array was a mobile platform that was constructed with five lens multi-mode fibres and arranged in an X-constellation (Intes, 2005, Falou et al., 2012). Temporal point spread functions (TPSF) were collected with a resolution of 10 ps within a 4s-delay window (Intes, 2005). The TPSF was used to calculate the optical absorption and scattering. The absorbance and scattering calculations are found in subsequent section (**Section 2.5**).

DOS images were reconstructed into tomographic and parametric maps of the optical parameters (deoxyhaemoglobin, oxy-haemoglobin, total haemoglobin, %water, %lipids, scattering amplitude, scattering power, tissue optical index). The calculation of these parameters is described later in **Section 2.5**. Each voxel size of the parametric image was 3 mm x 3 mm x 7 $mm^{3.}$ The DOS image planes used for analysis were dependent the size of the breast which determined the volume reconstruction. The total duration of the optical mammography scan was approximately 30-40 minutes. DOS imaging data was stored into the system's permanent memory drive and extracted for imaging analysis.

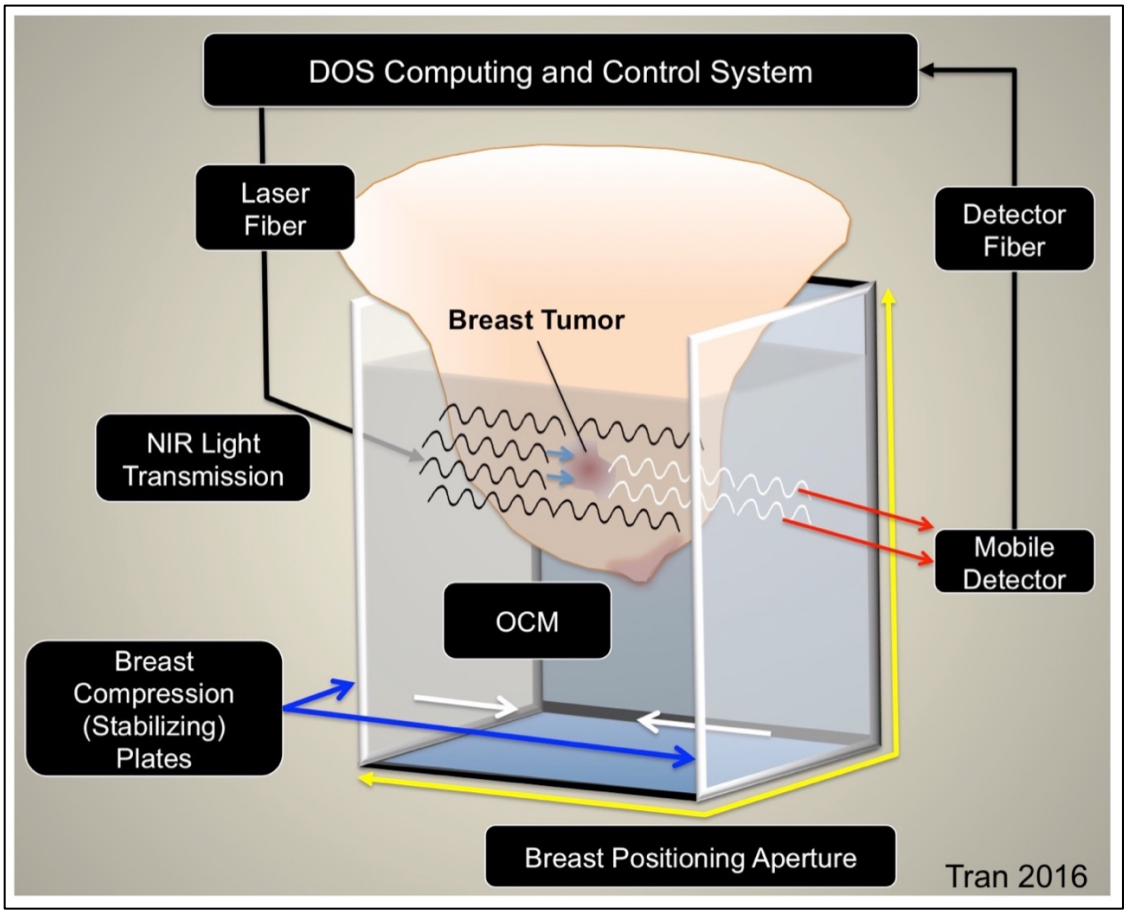

Figure 2.6: DOS tomography imaging involved whole-breast (volumetric) data acquisition. For DOS imaging, the whole breast is immersed into an aqua-tank which is filled with optical compensation medium (OCM). The OCM is used to enhance the light transmission between surfaces. The breast is compressed to allow for better light transmission. The light is transmitted through the breast and detected on the opposite side by a mobile detector. The detector fibre transmits the DOS data to a computing system for data storage. The data is later extracted, processed and analysed on a separate workstation.

2.5 DOS and QUS Image Processing

2.5.1 Region of Interest (ROI) Selection

The ROIs were selected under the guidance of a breast radiologist with more than 15 years of breast imaging experience. For QUS, conventional B-Mode images (grey-scale) were used to guide analysis and ROI selection. For DOS, the patients' diagnostic MRI images were used to determine the location and extent of tumours in the breast. The ROI contours were chosen in-plane for each of the volumetric DOS and QUS image datasets before knowing the ground-truth labels[12].

QUS ROI selection

QUS imaging was completed in subproject one only. The ROIs were selected on 10-14 equally spaced scan planes for QUS. For QUS, 22 patients were analysed over five scheduled time intervals (baseline, week one, week four, week eight, pre-operatively). The total number of ROIs contoured for QUS was 1210.

DOS ROI selection

For subproject one, 22 patients had DOS imaging over the entire course of chemotherapy. There were 5-8 equally spaced scan planes for each patient; thus, 862 ROIs were selected.

In subproject two, the 22 patients from subproject one were included in a pooled analysis. The additional 15 patients who were recruited for subproject two underwent pre-treatment DOS imaging, which included an additional 120 ROI contours that were completed for this component of the study.

[12] Ground truth labels are a statistical term for the pathological classification groups used in the study. In this study, it refers to responders versus non-responders, as assessed by Miller-Payne pathologic response criteria.

2.5.2 QUS: Ultrasound Radiofrequency Spectrum

For the calculation of QUS parameters, spectral analysis of the acoustic backscatter signal was done using the radiofrequency signal within a fixed-size analysis window. The ROIs were kept constant for the duration of the imaging series and determined from the baseline scan. Radiofrequency data was analysed across 10-14 equally spaced ultrasound scan planes. Spectral analysis of the ultrasound radiofrequency spectrum was previously described by Lizzi *et al.* (Lizzi et al., 1997a), and adapted for this study. These studies demonstrated that the acoustic backscatter signal was correlated to tissue microstructure. All spectrum analyses were performed using a MATLAB-based software (Matlab, MathWorks, Natick MA, USA) developed by Oelze *et al.* from the University of Illinois and based on previous work by Insana et al. (Insana and Hall, 1990).

Calculation of the parameters of power spectrum is undertaken by applying a fast Fourier transform (FFT) of a gated radiofrequency data line segment to obtain the amplitude line spectrum (complete calculations can be found in **Appendix 2**). To reduce spectral-noise artefacts, a sliding window algorithm was used with the settings of a Hamming window function for gating, where there was an 80% overlap between adjacent windows in the axial direction. A reference phantom technique was used to remove system transfer effects from the data using a tissue-mimicking agar-embedded glass-bead phantom with known acoustic properties (Tadayyon et al., 2014). To normalize the tissue sample signal to the reference phantom, the amplitude line spectrum was calculated in the same manner; where the fast Fourier transform (FFT) of the gated radiofrequency signal was processed from the ROIs of the reference phantom. The log power spectrum is computed by the average of the squared magnitudes of the amplitude line spectra by lateral windowing. The depth-dependent acoustic attenuation was employed for calculating the power spectrum (the normalized power spectrum calculation can be found in **Appendix 2**) (Insana and Hall, 1990).

A linear regression line using the least squares of the normalized power spectrum was applied across the frequency spectrum. Previous work from Lizzi et al (1983) demonstrated that the frequency bandwidth over the -6 dB

range from the peak amplitude were capable of characterizing tissue microstructure. From the regression line of the spectral form, the mid-band fit (MBF), 0-MHz intercept (SI) and the spectral slope (SS) QUS parameters were calculated (Lizzi et al., 1983). The MBF denotes the spectral intensity of the mid-point of the best-fit line; the SS is the slope of the line; and the SI is the interpolated line to the Y-axis (**Figure 2.7**).

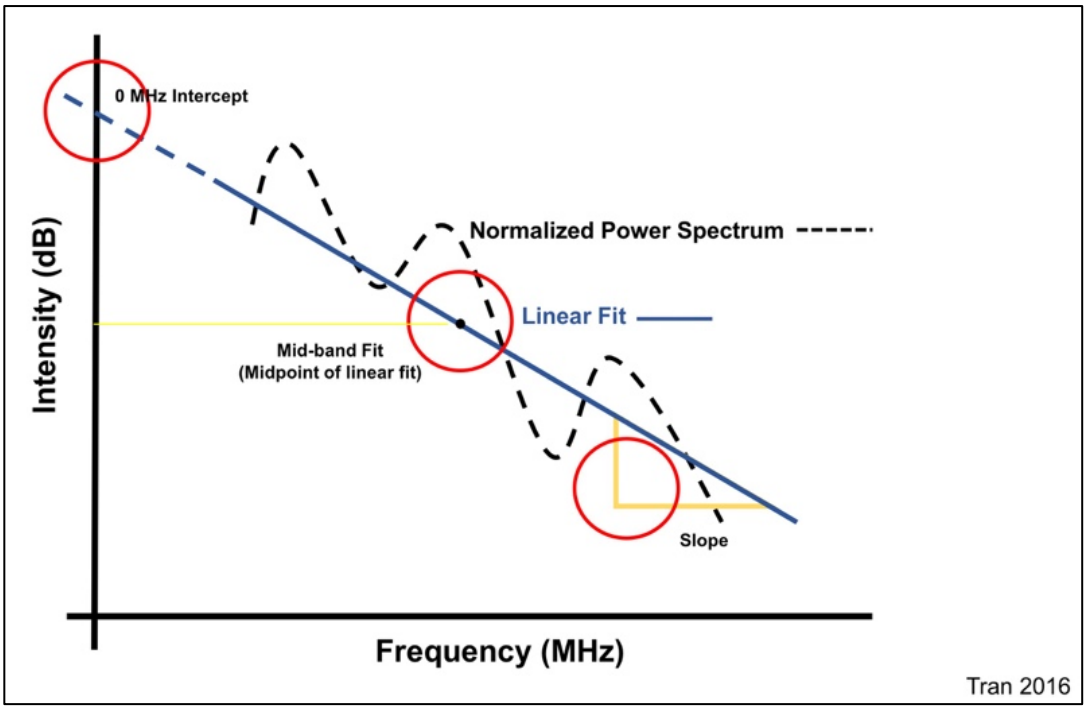

Figure 2.7: Representative power spectrum. QUS parameters were obtained by applying a regression line to the spectral form, within the -6 dB[13] window. The red circles indicate the parameters obtained by analysing the regression line: 1) The 0-MHz intercept (spectral intercept, SI) is the interpolated line to the Y-axis; 2) the midband fit is the midpoint of the regression line; 3) the last parameter is the slope of the regression line (spectral slope, SS).

2.5.3 DOS Data Calculations

The optical tomography device used a time-resolved system to determine the absorbance and scattering properties of the sample. These measurements were used to calculate the concentration of tissue

[13] dB refers to *decibels*. The dB is a logarithmic unit of measurement for sound intensity.

chromophores. The system employed short pulses of light and measured the photons' arrival time and was plotted as the time-point spread function (TPSF) (Enfield et al., 2009) (**Figure 2.8A, B**).

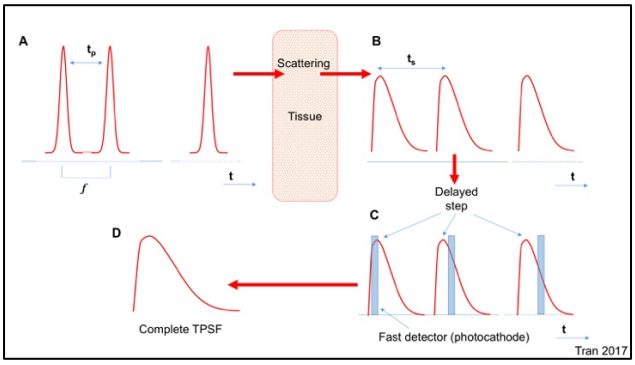

Figure 2.8.A: Calculating the TPSF in tissue. Pulses of light are emitted within a discrete time (**t**) and frequency (*f*) **(A).** The light pulses are attenuated through tissue and causes a delay and broadening of the light pulse profile **(B)**. A photocathode is used to measure the delay of the transmitted light pulse **(C)** and used to plot a complete (integrated) TPSF **(D)**. Adapted from *Handbook of Biomedical Optics* (Boas et al., 2011).

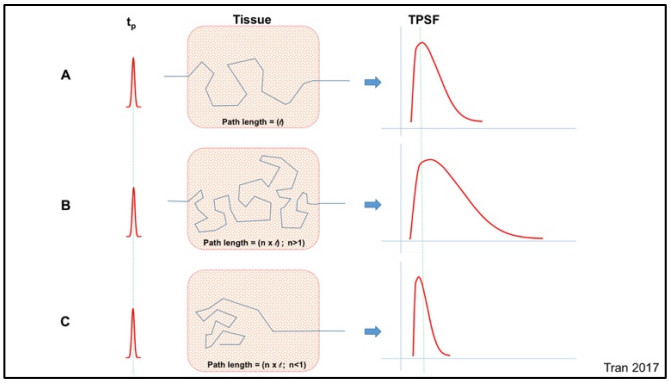

Figure 2.8.B: **(A)** The tissue properties (i.e. composition and biologic layout) can affect the TPSF and dictated by scattering and absorption. **(B)** A highly scattering medium will cause the TPSF to broaden since the path length is longer. **(C)** In highly absorbing mediums, the TPSF will narrow since many photons will be attenuated within the medium. Adapted from (Enfield et al., 2009)

The experimental TPSF from the tissue sample was fitted against a model of light propagation by curve fitting and this was previously reported by Patterson et al. (Sato et al., 2013, Patterson et al., 1989) . For the DOS system, the attenuation coefficient (μ_a) was calculated from a time domain diffusion equation that used a Rytov approximation to characterize light

propagation in a medium (Intes, 2005, Intes et al., 2002). The concentration of dominant DOS chromophores in breast was estimated and included oxy-haemoglobin [HbO_2], and deoxy-haemoglobin [Hb] (Cerussi et al., 2006). Their concentrations [*C*] were calculated using the Beer-Lambert law, with the known molar extinction coefficients [ε] (**Eq. 2.3**):

$$\mu_a = \varepsilon \times C \quad \textbf{(Eq. 2.3)}$$

Other DOS parameters, such as [%Water], [%Lipid], scattering power [b], and scattering amplitude [A] were measured using the power-law fit of the scattering spectra within a given wavelength bandwidth (λ) (**Eq. 2.4**). This relationship was based on a Mie scattering approximation (Tromberg et al., 2005):

$$\mu_s(\lambda) = A \times \lambda^{-b} \quad \textbf{(Eq. 2.4)}$$

Additionally, other optical parameters such as oxygen saturation [StO_2], oxygen desaturation [St], total haemoglobin [HbT] and the tissue optical index [TOI] were calculated from the [Hb], [HbO_2], [%Water], and [%Lipid], and these calculations are described as (Cerussi et al., 2011, Intes, 2005):

Total Haemoglobin;

$$HbT = Hb + HbO_2 \quad \textbf{(Eq.2.5)}$$

Oxygen Saturation;

$$StO_2\ (\%) = \frac{HbO_2}{HbT} \times 100 \quad \textbf{(Eq. 2.6)}$$

Oxygen Desaturation;

$$St\ (\%) = \frac{Hb}{HbT} \times 100 \quad \textbf{(Eq. 2.7)}$$

Tissue Optical Index;

$$TOI = \frac{Hb \times \%Water}{\%Lipids} \quad \textbf{(Eq. 2.8)}$$

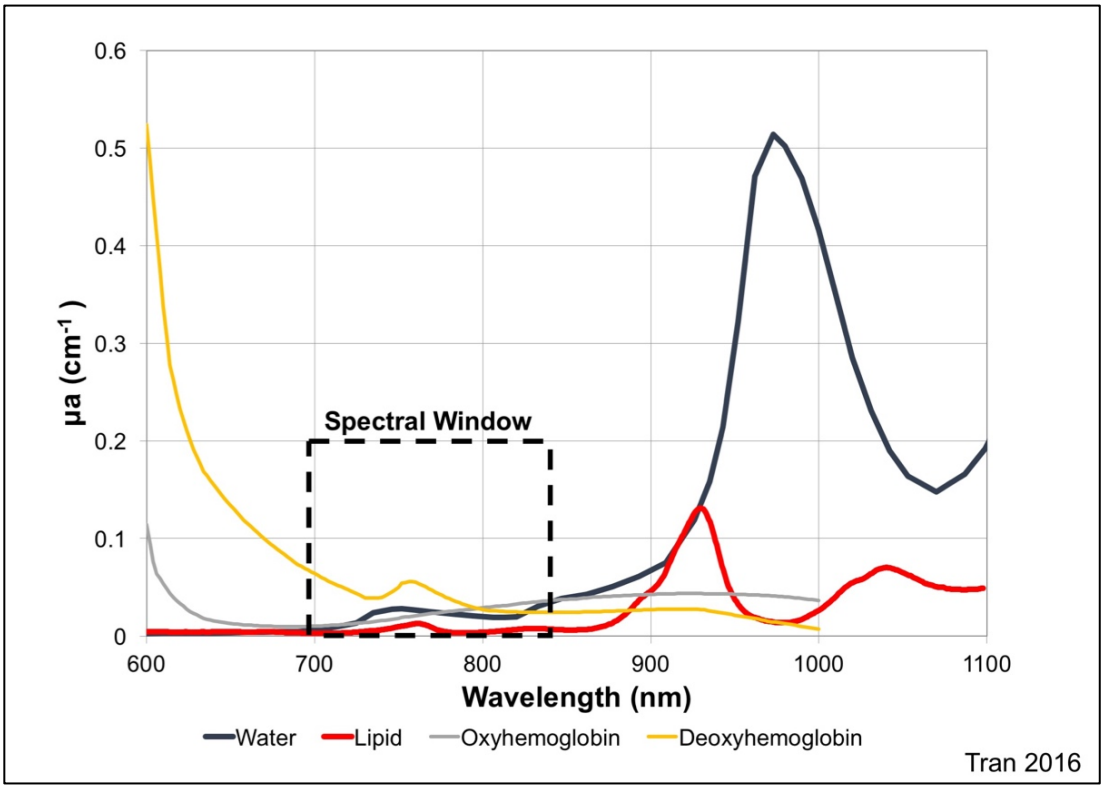

Figure 2.9: Absorbance spectra. Significant optical chromophores in breast tissue include water, lipid and oxy- and deoxy-haemoglobin. The absorption of light in physiological chromophores is dependent on the optical wavelength. Optical imaging systems operate within a fixed optical bandwidth, denoted as the spectral window (dotted box in figure). The spectral window permits the investigation of multiple chromophores within the medium. The μ_a (cm-1) indicates the optical absorbance in a medium.

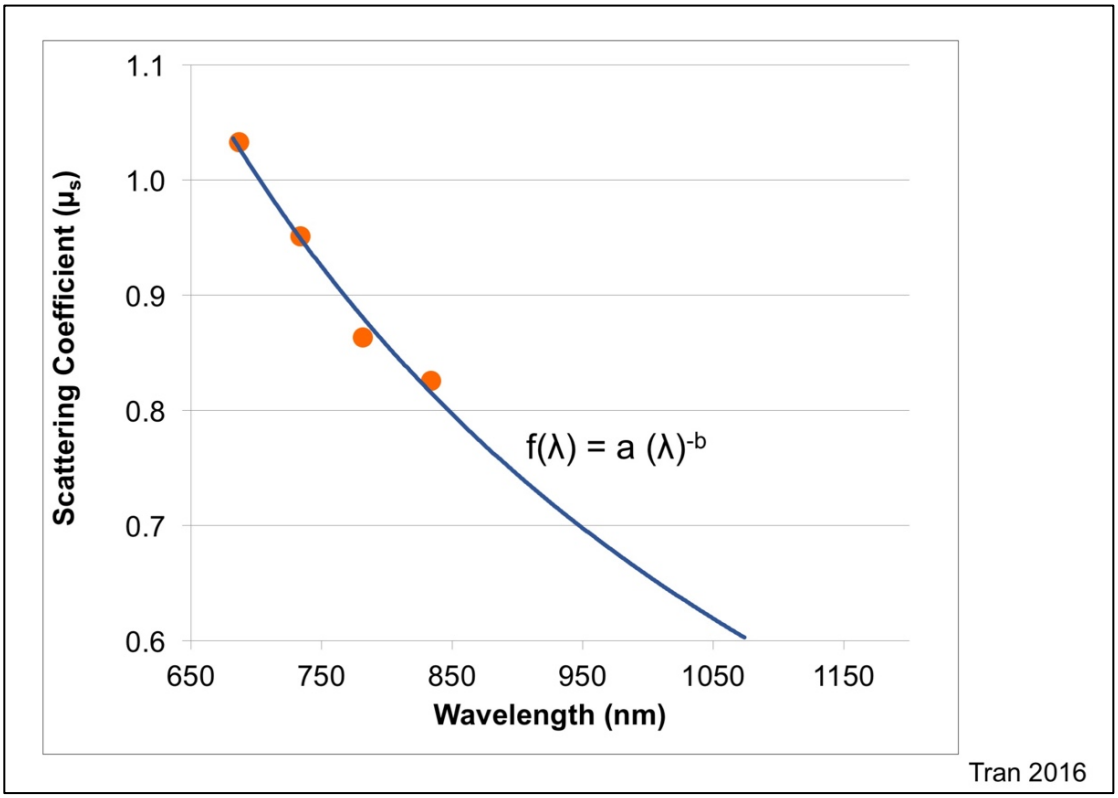

Figure 2.10: Scattering spectra. A power-law fit[14] is applied to the scattering spectra to obtain other DOS parameters such as the scattering power (b) and scattering amplitude (A).

2.5.4 DOS-GLCM (Grey-Level Co-occurrence Matrix) Texture Analysis

Texture feature-extraction methods using a grey-level co-occurrence matrix (GLCM) can be applied to compute the probabilities of relative pixel intensities of images from the spatial distribution of their voxels (Haralick et al., 1973). This work has previously been demonstrated to provide deeper information about the image's spatial and textural features in breast cancer using other modalities such as MRI (Chen et al., 2007). The texture features of an image can quantify the heterogeneity of the tumour image and provide meaningful statistical frameworks that are correlated to tumour and histopathological characteristics (Yang et al., 2012, Davnall et al., 2012). In other studies, GLCM analysis has been able to classify benign and malignant lesions using planar (2D) and volumetric (3D) MRI images (Chen et al., 2007, Gibbs and Turnbull, 2003). For X-ray mammography, GLCM analysis has been

[14] The power-law is a mathematical expression of a power function.

used to segment lesion borders of stellate (malignant) breast masses (Gupta and Undrill, 1995). It was also recently reported that texture-based features from quantitative ultrasound (QUS) imaging can be used to classify responders and non-responders early during NAC treatment (Sadeghi-Naini et al., 2014). These previous findings suggested that textural features may detect the acute, heterogeneous microstructural features carried in the parametric layout (Sadeghi-Naini et al., 2014).

In this study, a GLCM-texture analyses were applied to whole-breast tomographic DOS parametric maps (**Figure 2.11**). DOS images were constructed with an in-plane resolution of 3 × 3 mm^2 and slice thickness of 7.5 mm. The GLCM-texture analysis was applied to the entire tumour volume and averaged over multiple frames of the DOS parametric maps. The image's properties are first defined by shades of grey levels (N_g) within a finite scale and the texture of the image describes the intensity of one pixel within a neighbourhood of image pixels. A bilinear interpolation was applied to compensate for differences in the spatial resolutions, thus obtaining volumetric images with isotropic voxels (3 × 3 × 3 mm^3) (Sadeghi-Naini et al., 2015). For the GLCM, grey-tone intensities (N_g) were quantized into 16 grey-levels from the DOS parametric maps. A symmetric GLCM was constructed based on the spatial relationship of each voxel's neighbours using a displacement vector; the magnitude of the displacement vector was one to four voxel distances.

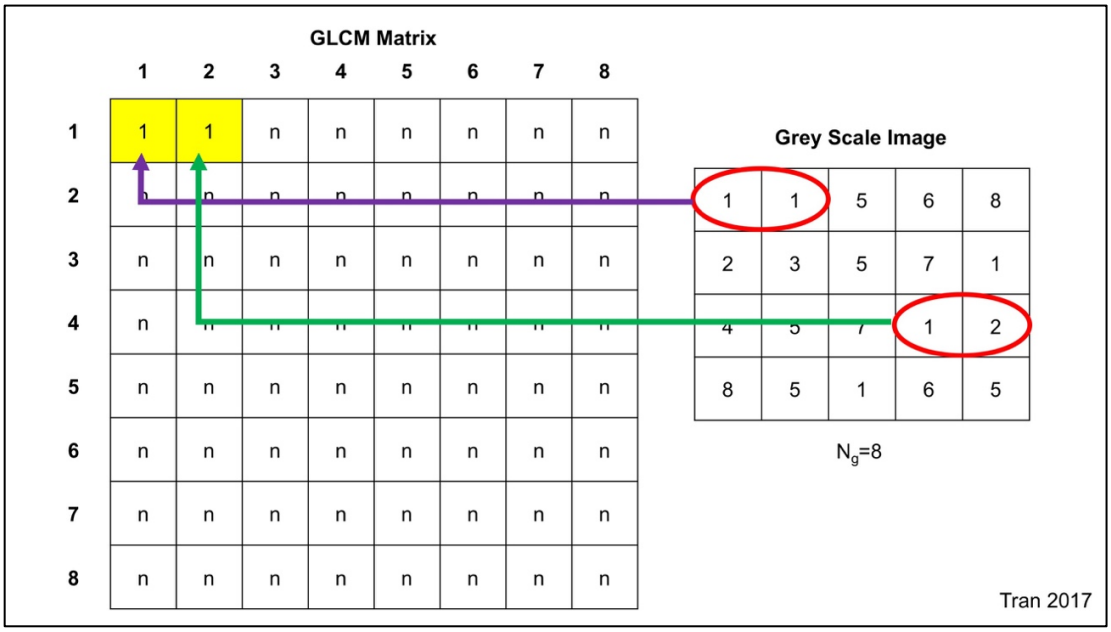

Figure 2.11: GLCM computation. This matrix is a representation of an ROI region with pixels. Each box represents one pixel that is spatially arranged next to the other. The right matrix is a representation of an image with quantized grey-scale values. There are eight grey-scale levels and this is represented by, N_g=8 (i.e. eight grey-levels, 3-bit data). The left is the GLCM matrix corresponding to the pixel relationships of the grey-scale image or within a region of interest. Here, the displacement vector is used to compute the matrix, where its magnitude is equal to one voxel distance at an angle of 0° (highlighted yellow with the adjacent pixels).

A cumulative GLCM was calculated in 13 directions (45° rotations in each adjacent direction) relative to the central voxel (Chen et al., 2007). The resulting co-occurrence features included: Energy, Homogeneity, Contrast, and Correlation. These were previously defined as (Haralick et al., 1973, Haralick, 1979):

Energy;

$$(\text{Ene}) = \sum_{i=1}^{N_g} \sum_{j=1}^{N_g} p(i,j)^2 \quad \textbf{(Eq. 2.9)}$$

where the energy (angular second moment) describes the textural uniformity of the image, 0 ≤ Ene ≤ 1. The function *p(i,j)* is the probability of having two neighbour voxels with a grey-tone intensity (*i* and *j*) in the matrix;

Homogeneity;

$$(\text{Hom}) = \sum_{i=1}^{N_g} \sum_{j=1}^{N_g} \frac{p(i,j)}{1+|i-j|} \quad \textbf{(Eq. 2.10)}$$

where the homogeneity (inverse difference moment) measures the diagonal elements within the displacement vector of the GLCM and relates the similarities in grey-tones between voxels;

Contrast;

$$(\text{Con}) = \sum_{|i-j|=0}^{N_g-1} |i-j|^2 \times \left(\sum_{i=1}^{N_g} \sum_{j=1}^{N_g} p(i,j) \right) \quad \textbf{(Eq. 2.11)}$$

where the contrast measures the differences between the lowest and highest voxels' grey-tones and lastly;

Correlation;

$$(\text{Cor}) = \frac{\sum_{i=1}^{N_g} \sum_{j=1}^{N_g} (i)(j) p(i,j) - \mu_i \mu_j}{\sigma_i \sigma_j} \quad \textbf{(Eq. 2.12)}$$

where the correlation measures the linear dependency on neighbouring grey-tone intensities; and σ_i, σ_j are the standard deviations, and μ_i, μ_j are the means of the probability matrix. Therefore, a total of 40 DOS-texture features was included for analysis; there were 10 DOS parameters comprised of 4 GLCM features for each parameter **(Figure 2.12).** DOS-texture features were calculated using MatLab R2011b (The MathWorks Inc., Natick, MA, USA). The GLCM-texture functions used in MatLab were obtained from an online tool by The Mathworks Inc (Uppuluri, 2008). The function codes were adapted for DOS image analysis at the University of Toronto by Sadeghi et al. (2015).

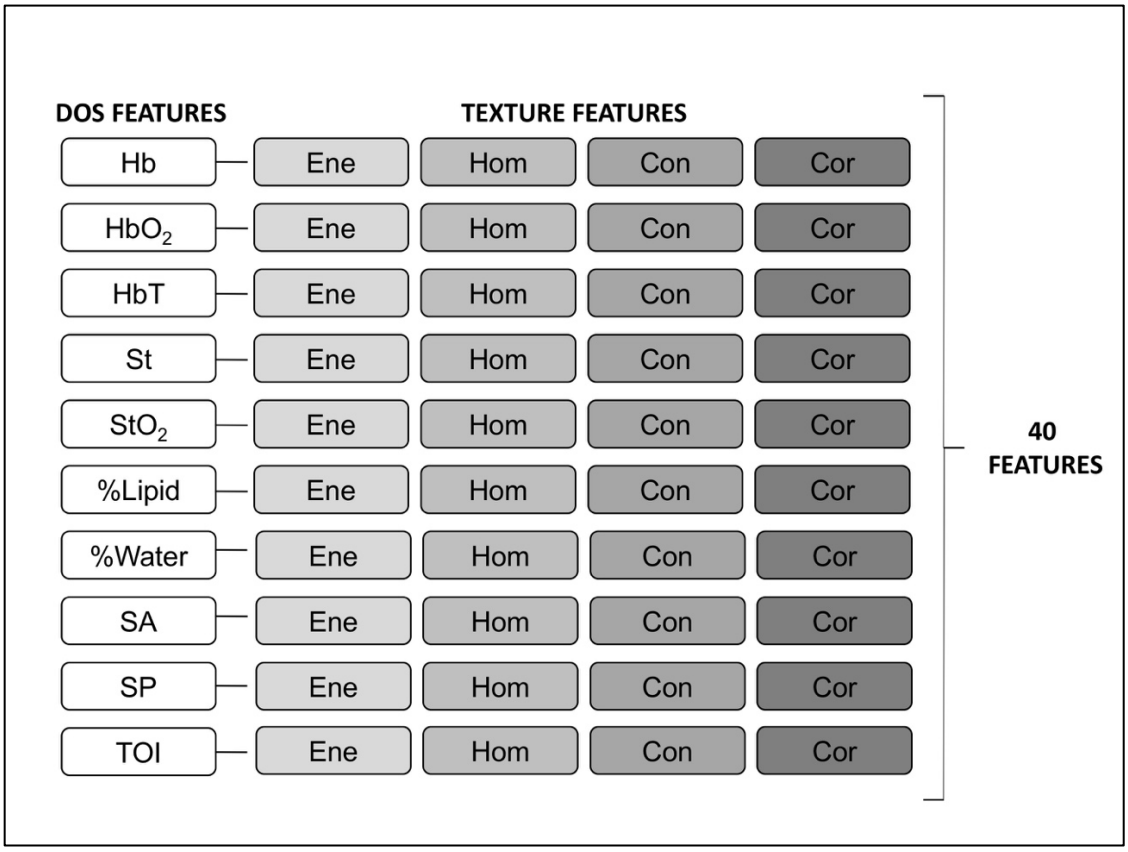

Figure 2.12 DOS-Texture Features. Parametric maps were generated for each of the pre-treatment DOS features. In order to obtain the texture features, a GLCM function was used on the parametric maps to obtain the following texture features: *Energy (ene), Homogeneity (hom), Contrast (con), and Correlation (cor)*. A total of 40 features were extracted from texture analysis of the DOS parametric maps (i.e. 10 DOS features x 4 texture features = 40 total features).

2.6 Image Quality Verification

Quality verification was completed on imaging devices to ensure data consistency and quality throughout the imaging scans. A description of the various quality procedures is described in the subsequent sections.

2.6.1 Ultrasound Transducer Properties and Beam Characterization

The ultrasound beam was characterised from the Ultrasonix L5-14/60 transducer used in this study. Beam characterisation was completed using an open-access MATLAB-based software platform (Field II, Biomedical Engineering Group, Lyngby Denmark, (Jensen, 2017)). The point-spread function was computed based on measurements obtained from several locations of an acoustic phantom. The phantom had an echogenic surface and was constructed of plexiglass with known acoustic properties. Beam characteristics obtained included the axial depth, the focal depth, centre frequency, frequency bandwidth, and FFT-frequency response along the axial waveform. The frequency-response curve was obtained and corresponded with the 0-mm lateral distance. The data presented in **Table 2.4** were taken within the -6dB window, referenced at 0 mm lateral distance. The characterization features are listed below with the beam profiles (**Figure 2.13, Table 2.4**).

Transducer Properties	**Measurements**
Number of elements (n)	128
Kerf (distance between elements) [μm]	25
Element width [mm]	0.48
Element length (elevation) [mm]	4
Elevation focus [mm]	14
Beam Characteristics	**Measurements**
Focus position [mm]	13.8
Centre frequency [MHz]	~7
Frequency bandwidth range [MHz]	3-8
Depth of focus [mm]	6.9
Elevation beam resolution [mm]	0.77
Lateral beam width at focus [mm]	0.21

Table 2.4: Transducer and Beam Characteristics. The above characteristics were measured and compared to references (outlined by the manufacturer) for quality assurance.

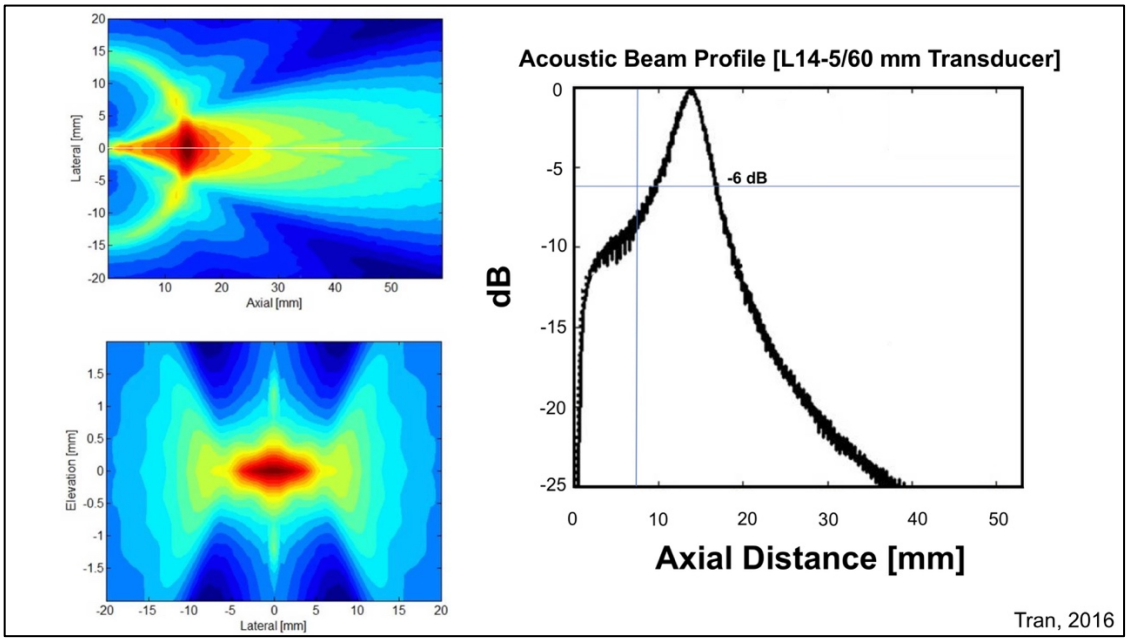

Figure 2.13: Transducer Beam Characteristics. The ultrasound beam characteristics evaluated using a MATLAB-based software platform. Feature profiles are outlined in **Table 2.4**. The colour maps represent the relative signal intensity (red; high intensity and blue; low intensity)

2.6.2 Optical Imaging Characterization

The diffuse optical spectroscopy tomography device was tested for data stability using an end-user phantom from the manufacturer (Advanced Research Technologies, Montreal, Canada). The phantom was constructed of a polyurethane phantom suspended from a monofilament within a metal frame **(Figure 2.14)**. The phantom mimicked tissue optical properties within the near-infrared spectrum.

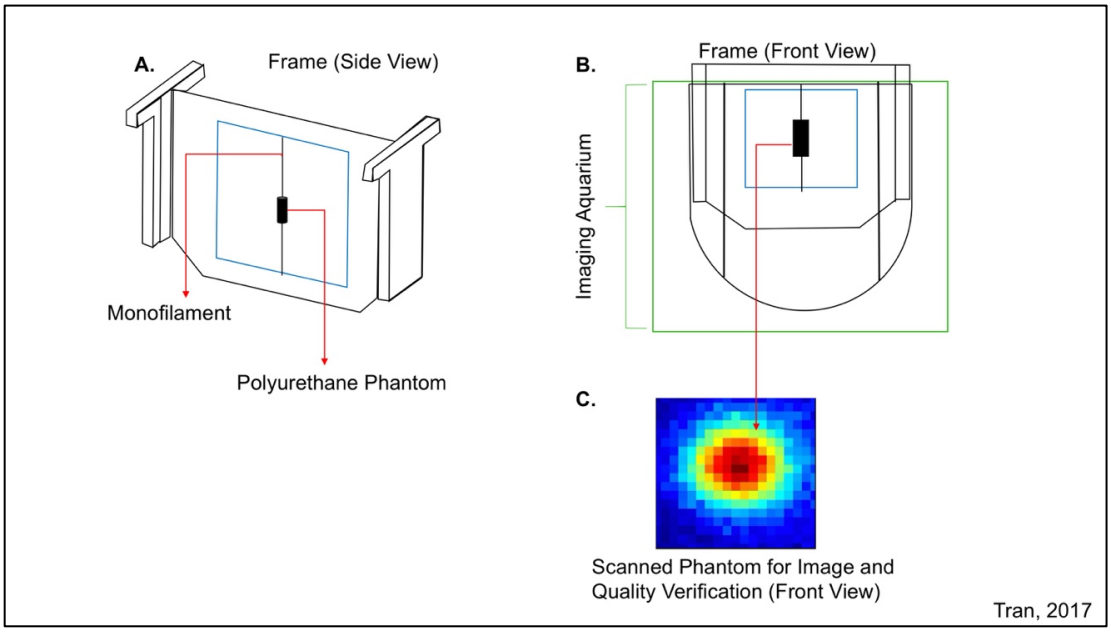

Figure 2.14: Optical Phantom Construction. The phantom was constructed from a frame with a polyurethane cylinder material that was optically compatible. The phantom permitted verification of the imaging geometry, and tested the quality of the light transmission of the device. The colour maps represent the relative signal intensity (red; high intensity and blue; low intensity)

To verify the imaging and data, the phantom was inserted into the DOS device for imaging. A predefined ROI was selected with the following geometry for imaging to obtain the quality-check parameters (**Table 2.5**):

Adjustment Scan Area	
Setting	**Measurement (mm)**
Phantom Width	54.0
Phantom Offset	58.0
Phantom Height	54.0
Top Offset	25.0

Table 2.5: Optical ROI Geometry for Quality Check.

Optical scanning was completed using the same scanning protocol indicated for patients. The data output was analysed on a separate workstation (ART Review Workstation, V. 1.07.01, Montreal Canada) (**Figure 2.15, Table 2.6**).

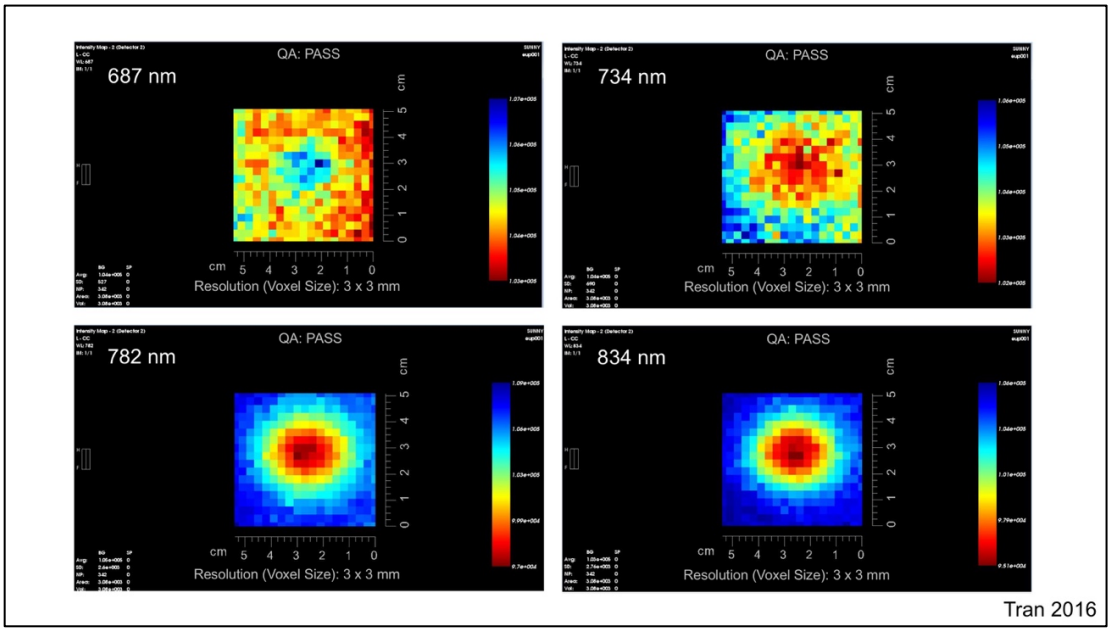

Figure 2.15: DOS Data Verification. Data verification included testing each transmission wavelength. The test performance was based on verifying the image's geometry and to test the transmission patterns. The transmission patterns are compared to a reference image for verification.

Analysis of the DOS data are outlined below in **Table 2.6**.

DOS Imaging Characteristics	Measurements
Complete Scanning Area (mm) (W x H)	170 x 185
Optical Wavelength Verification (nm)	687, 734, 782, 834
Pixel dimension (in-plane) [mm]	3 x 3
Contrast scale range [a.u.]	3-20

Table 2.6: Optical characteristics. The DOS imaging characteristics are outlined with the corresponding measurements from the quality management process.

2.6.3 Inter-Reader Variability Testing

Inter-user variability was tested on 25 DOS and 25 QUS datasets. The ROI contour and volume were tested for pairwise agreement between two users. Thus, each dataset had two readers analyse an ROI contour on the same DOS image and a QUS image (**Figure 2.16**). A Cohen's κ used to

compare ROI placement and this was based on the reader's interpretation of whether the ROIs delineated between the "inside" and "outside" region of the tumour. These methods were previously used in a simulation-based study for PET imaging (Rucker et al., 2012). To analyse if readers selected similar ROI volumes, an independent t-test was used. A significance level of 0.05 was used to determine significant results.

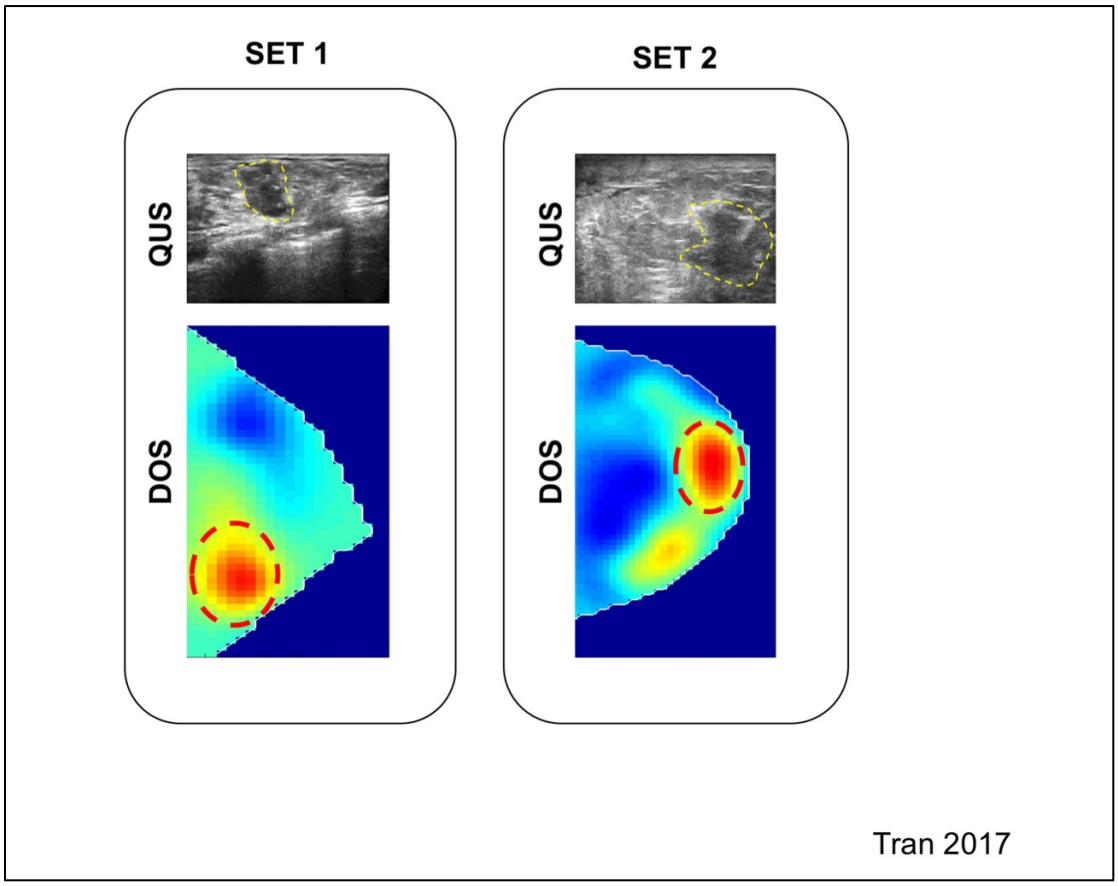

Figure 2.16. Inter-user agreement analysis. For inter-user variability testing, the placement of the ROI was analysed by two readers for agreement statistics (κ).

Cohen's κ is expressed as:

$$\kappa = \frac{\Pr(a) - \Pr(e)}{1 - \Pr(e)} \quad \textbf{(Eq. 2.13)}$$

where; $\Pr(a)$ denotes the observed agreement and $\Pr(e)$ represents the chance agreement (Rucker et al., 2012) and $0 \leq \kappa \leq 1$.

The value and range of κ represent the level of agreement; where 0-0.2 demonstrate only a small probability of agreement; 0.21-0.40 is considered fair;

0.41-0.60 is moderate; 0.61-0.80 denotes a substantial agreement; and 0.81-1.00 is an ideal agreement range between readers (McHugh, 2012). A summary of tests and statistical measures are outlined in **Table 2.7**.

Test	**Value**	
n=25	**DOS**	**QUS**
(ROI Placement) [Cohen's κ]	0.779, *p<0.001*	0.740, *p<0.001*
Volume Comparison (t-test) [p-value]	NS *(p=0.993)*	NS *(p=0.839)*

Table 2.7: Tests of comparisons (Inter-reader variability). A Cohen's κ was calculated ROI placement. Tumour ROI volumes were also compared for significant differences in chosen volumes between users.

2.7 Statistical Analysis and Machine Learning

All statistical tests were performed using SPSS 20 (IBM Inc., Armonk New York, USA) and MatLab R2011b (The Mathworks Inc., Natick, MA, USA). A summary of the study workflow is outlined below.

2.7.1 DOS and QUS Data

Descriptive statistics were used on both DOS and QUS parameters. Mean value with standard deviation was calculated for each imaging dataset taken at each time interval when data was collected. For QUS the change [Δ] in QUS parameters was calculated by subtracting the measurements at each time interval from the value measured at baseline. DOS measurements were expressed in percent changes from the baseline [% Change].

2.7.2 Tests of significance between response groups (R versus NR)

A comparison of each parameter mean values, using the DOS and QUS data were tested for significant differences between responders and non-responders at each time interval. First, a normality violation was tested for each parameter using a Shapiro-Wilk test (W). For normally distributed parameter changes, an independent t-test was used (unpaired, two-sided, 95% confidence interval). Otherwise, an unpaired, Mann-Whitney U-test within the 95% confidence level was utilized (SPSS Inc., Chicago IL, USA) for parametric changes that were not normally distributed. The Mann-Whitney U-test is based on a calculation of the U-statistic for each group (Mann and Whitney, 1947). The U-statistic is then compared against a known distribution for which the null hypothesis is either accepted or rejected (Nachar, 2008).

2.7.3 Tests of significance Between Time Intervals

Significant changes over time were tested for each DOS and QUS parameter to compare its difference to baseline values using a one-way with repeated-measures ANOVA (analysis of variance). For this, a Dunnett's test

was used. The statistical measures were considered significant at an alpha level of 0.05 or less.

2.7.4 Selection of Feature Sets for Analysis

Both univariate and multivariate analyses tested the performance of individual and combined DOS and QUS parameters against final pathologic endpoints, as measured by Miller-Payne response criteria. All imaging parameters calculated from DOS and QUS were considered for univariate analysis. For multivariate features and models, a maximum of two combined (binary) parameters were used and all binary forward combinations were considered for analysis. The maximum feature set (multivariate model) were constrained by the number of data samples in this study. Using a binary feature model would mitigate the “curse of dimensionality” based on a maximum of 1/10 of the data sample (Jain et al., 2000). In subproject one, a total of 22 patients were analysed (maximum 2 feature sets in the multivariate model). In subproject two, a maximum of 2 features was permitted within a multivariate model given the mathematical constraints of the prediction models used in the machine learning algorithm.

2.7.5 Receiver Operating Characteristic Curve Analysis

A receiver-operating characteristic curve (ROC) analysis was completed. The ROC provides the diagnostic accuracy of DOS and QUS parameters to discriminate between pathologic responders and pathologic non-responders (Metz, 2006). The ROC is based on a distribution of the true positive fraction (TPF) and the false positive fraction (FPF) (**Figure 2.17, Table 2.8**).

Test	Disease				
	Present	**n**	**Absent**	**n**	**Total**
Positive	True Positive Fraction **(TPF)**	a	False Positive Fraction **(FPF)**	c	a+c
Negative	False Negative Fraction **(FNF)**	b	True Negative Fraction **(TNF)**	d	b+d
Total		a+b		c+d	

Table 2.8: Measures of Diagnostic Test Accuracy. Table corresponds to **Figure 2.17.** The TPF, FNF, FPF and TNF are used to calculate the test accuracy.

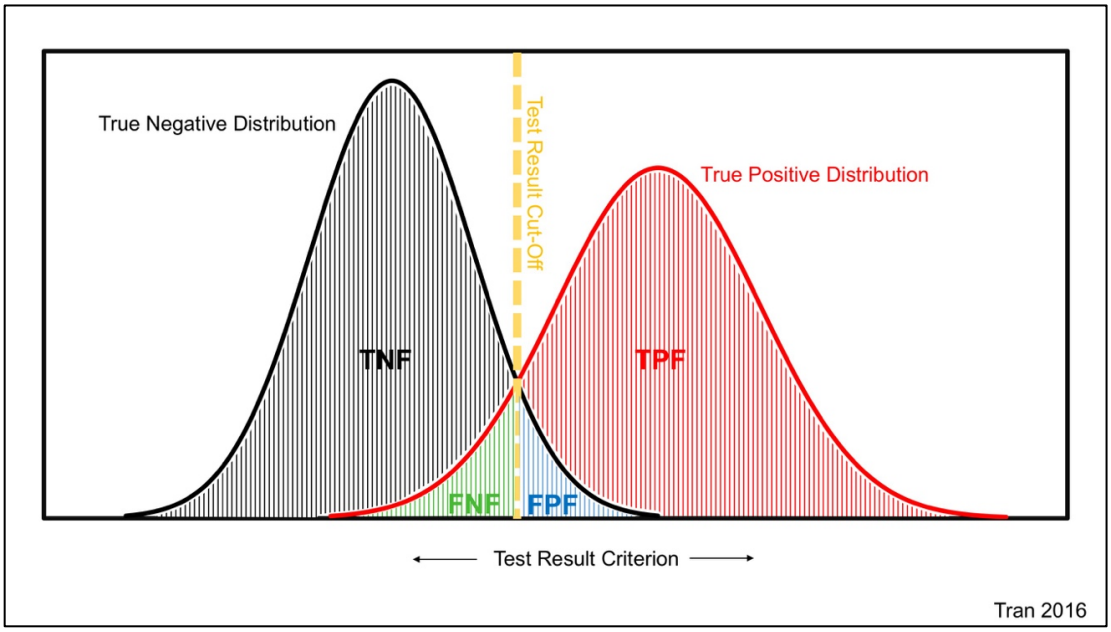

Figure 2.17: Test Distribution. The sensitivity, specificity and accuracy of a diagnostic test can be calculated based on the true negative distribution and the true positive distribution. The sensitivity and specificity points are employed to compute the ROC curve.

Using the true positive distribution and the true negative distribution, predictive values can be expressed (using the notations in **Table 2.8**) as;

Sensitivity;

$$\%Sn = \frac{a}{(a+b)} \times 100 \quad \textbf{(Eq. 2.14)}$$

where the %Sn represents the probability that the test result is positive when there is disease present;

Specificity;

$$\%Sp = \frac{d}{(c+d)} \times 100 \quad \textbf{(Eq. 2.15)}$$

where the %Sp represents the probability that the test result is negative when the disease is not present;

Accuracy;

$$\%Acc = \frac{(a+d)}{(a+b+c+d)} \times 100 \quad \textbf{(Eq. 2.16)}$$

where the %Acc represents the number of true assessments.

To plot the ROC curve, the sensitivity and specificity was used as coordinates within the curve axes **(Figure 2.18)**. To determine the best cut-off point, Youden's index (Q-point) was used. The area under the curve (AUC) was determined by calculating the integral of the ROC.

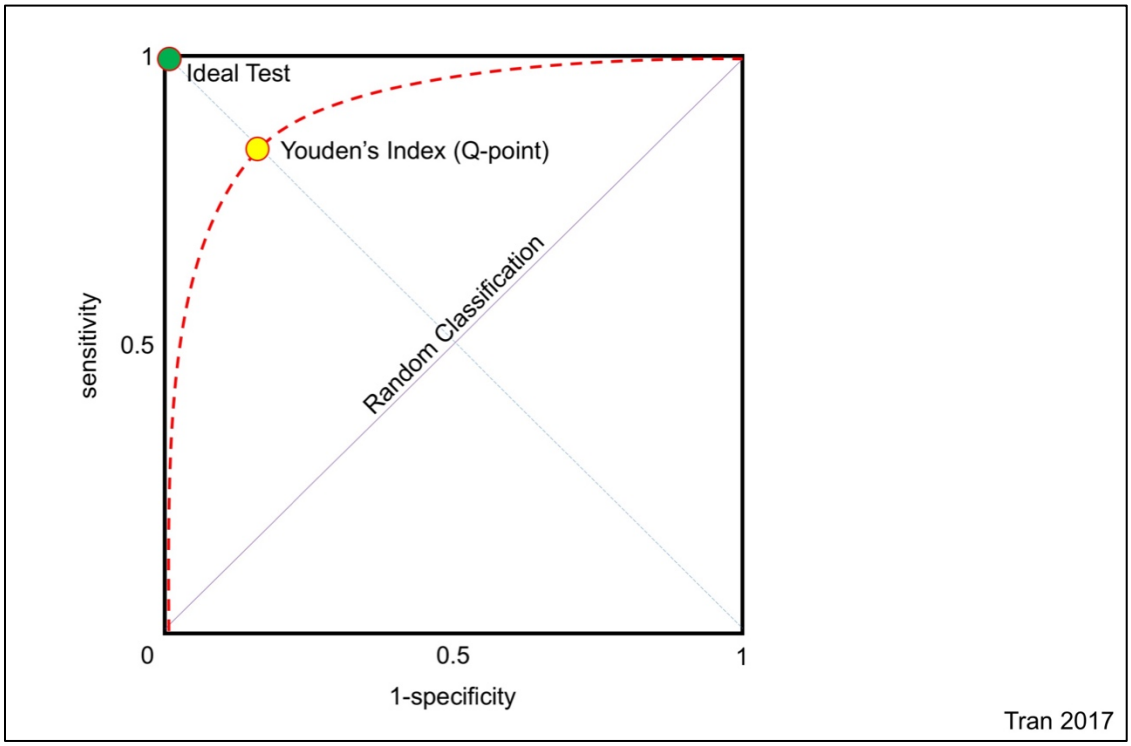

Figure 2.18: Receiver-Operating Characteristic Curve. The ROC is plotted based on the sensitivity and the specificity of the test. A random classification is determined at 0.5; while an ideal diagnostic test is depicted where the sensitivity and specificity is equal to 1 (top left corner of ROC). Youden's index at the Q-point (Q-Index) denotes where the sensitivity and specificity are equal (optimal test).

In this study, multiple statistical models were used to calculate the sensitivity, specificity, accuracy and AUC of DOS and QUS imaging biomarkers. The following sections will describe classifier models used to discriminate DOS and QUS imaging parameters between pathologic response groups to obtain the sensitivity, specificity, area under the curve and accuracy.

2.7.6 Linear Discriminant Analysis (LDA)

For subproject one, a LDA was used to classify responders and non-responders based on their univariate DOS and QUS parameters. The linear function was used as the cut-off point to determine the sensitivity, specificity and accuracy of the individual DOS and QUS variables.

Linear discriminant analysis is based on Fisher's linear discriminant model where a linear function is used to separate binary classes; given a set of

variables, [x_1, x_2,…. x_n]. The linear classifier thus separates two “species” based on its feature space; whereby the goal is to determine the optimal ratio of the means and standard deviations that would discriminate the classes within the feature space (dimension) (Fisher, 1936). The discriminant linear function is also referred to as the “decision boundary” (**Figure 2.19**).

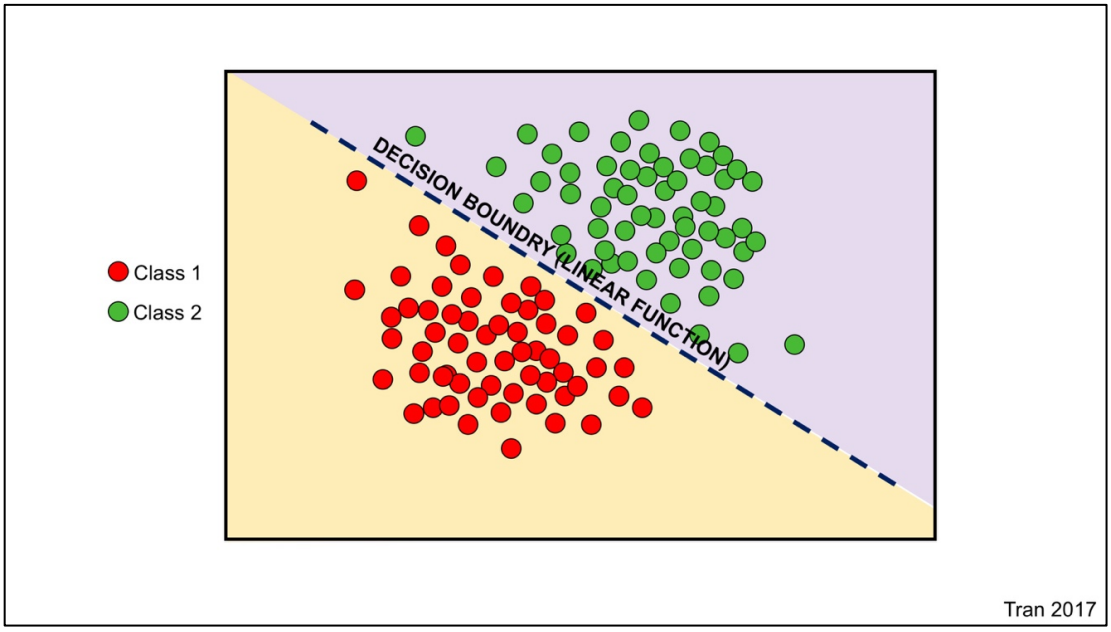

Figure 2.19: Linear Discriminant Analysis. The LDA is used to calculate the linear function which is used to discriminate between two species (Class 1 and Class 2, for example responders versus non-responders).

2.7.7 Logistic Regression Analysis (LRA)

Following methods by Xu et al. (2015), a logistic regression analysis (LRA) was used to compute the probability of multivariate combinations for DOS and QUS imaging markers to a dichotomous response variable (Y, Y_1=Responder; Y_2=Non-Responder) (Xu et al., 2015). The predictive performance of the models was evaluated by using the LRA model within the training set and then a test set to measure the classification error.

2.7.8 k-Nearest Neighbour (k-NN) Classifier Statistics

The k-NN classification is a non-parametric algorithm used for classification. It was chosen since it is one of the least computationally-demanding algorithms for supervised machine-learning (as this present study is exploratory). The k-NN algorithm makes no assumptions about the form of the data (e.g. Gaussian distribution) and therefore it is ideal for exploratory studies where there is no prior knowledge about the attributes and distribution of the data. (Dudani, 1976). The k-NN classification uses a weighting function that varies in value based on the distance between a sample and its neighbour; seeking out patterns in the distribution of the data within a sample set (Dudani, 1976). The data samples (known as "instances") are treated in groups or "bags" with a defined label (Wang and Summers, 2012). The bags are analysed in terms of their attributes or features. In this study, the bags were labelled as either pathologic responders or non-responders and the attributes were all baseline DOS features **(Figure 2.20)**.

The k-NN algorithm first organizes the bags into a feature space based on the values of the attributes and this is used for the training set. The test set is assigned a label according to a majority vote that is dependent on the nearest neighbour as determined by the Euclidean distance calculation (**Eq. 2.17**, **Figure 2.20**). For baseline DOS features, the training and test set used a k value of k=3 (three nearest neighbours).

A Euclidean distance is defined as;

Euclidean distance

$$\sqrt{\left(a_1^{(1)} - a_1^{(2)}\right)^2 + \left(a_2^{(1)} - a_2^{(2)}\right)^2 + \cdots . \left(a_k^{(1)} - a_k^{(2)}\right)^2} \quad \textbf{(Eq.2.17)}$$

where; ($a_k^{(n)}$) represents the number of attributes for each instance. Since different attributes may have varying scales or units of measure; they are all normalized between 0 and 1 for analysis within the k-NN feature space.

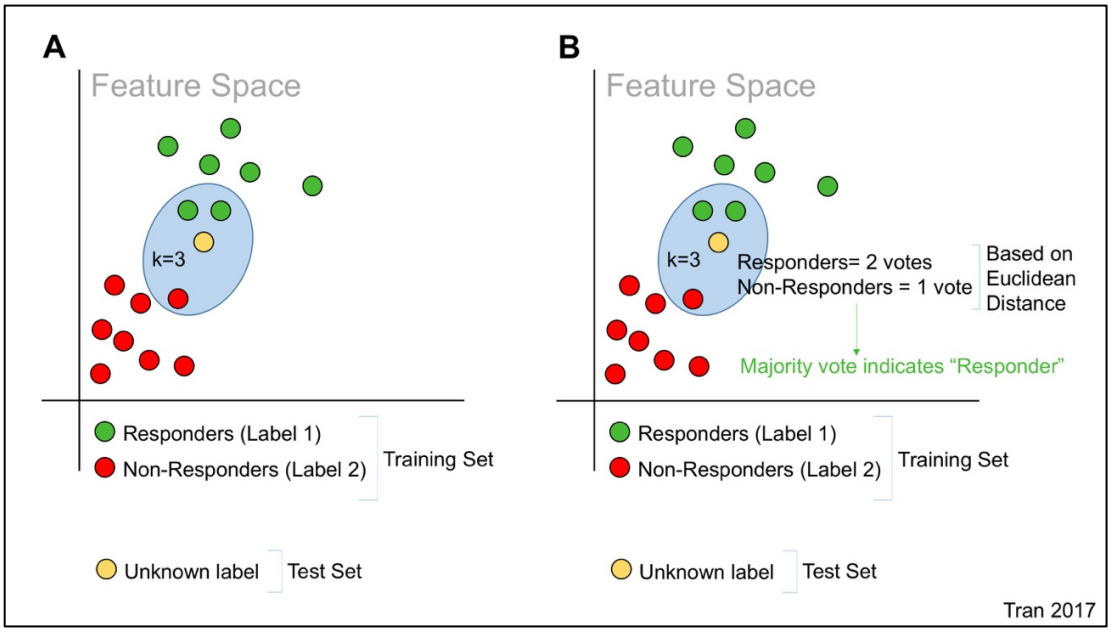

Figure 2.20: k-NN Classifiers. The k^{th} nearest neighbour is three in this representation. The bags are labelled as responders (green) or non-responders (red) in the training set (**A**). A test sample is used to compute the three nearest neighbours using a Euclidean distance calculation. Depending on the labels of the nearest neighbours, a vote is tabulated and the majority vote determines how the test sample is labelled (**B**).

2.7.9 Naïve Bayes (Bayesian) Classifier Statistics

Naïve Bayes classification can be used to predict the probability of a binary class membership (i.e. chemotherapy responder versus chemotherapy non-responder). The algorithm uses the probabilities of the class label and its attributes to compute a probability prediction of a sample. An important assumption for naïve Bayes classification algorithms is that the individual attributes $(a_1, a_2, \ldots a_n)$ of a class are independent to each other (conditional independence) (Han and Kamber, 2006). The naïve Bayes classifier function is expressed as (**Eq. 2.18**):

Naïve Bayes Classifier

$$P(X|C_i) = \prod_{k=1}^{n} P(x_\kappa|C_i) \quad \textbf{(Eq. 2.18)}$$

where; $P(X|C_i)$ is the probability of sample (X) labelled into a class (C_i); and x_κ represents the value of A_κ attributes for sample X (Han and Kamber, 2006). For this study, (C_i) is the response class (responder versus non-responder; i = 1, 2) and A_κ corresponds to all the baseline DOS-texture features.

2.7.10 Training, Test and Validation Sets

Prior to training and test validation, the data set was randomly subsampled into 20 subsets with replacement. Each subset had equal numbers of responders and non-responders; this method was used to account for the data imbalance between the two response groups. Since each patient was represented using 40 DOS-GLCM features, and due to a limited sample size, in order to prevent the "curse of dimensionality" (Jain et al., 2000), a feature selection based on sequential forward selection (SFS) algorithm in a wrapper framework (Duda et al., 2001) was performed to find the best (in the univariate case), or at most two (in the multivariate case) features. In order to prevent the peaking phenomenon due to the curse of dimensionality (Jain et al., 2000), the number of features should be at most 1/10th of the number of data samples, and since in the balanced data, there were only 20 data samples, a maximum of two features were selected for multivariate analysis using the SFS algorithm. The classifiers were evaluated using a leave-one-out cross validation at subject level. At each fold, the test set (one patient) remained unseen during the feature selection, tuning, and training of a classifier. Furthermore, at each fold, a leave-one-out cross validation was performed on the training set for the purpose of feature selection and tuning a classifier parameter (such as *k* in *k*-NN). Thus, at each fold, the training set was further divided into train and validation sets. The most discriminative feature(s) and the optimal classifier parameter were selected on the training set at each fold without involving the left-out test sample. Subsequently at each fold, the classifier was trained on the whole training set using the optimal classifier parameter and selected features, and tested on the test sample. This process was repeated on all samples (in the leave-one-out process) to evaluate the performance of the classifier.

2.7.11 Subgroup analysis

To test if there was a correlation between DOS-GLCM features and tumour biology and clinical features, a multiple linear regression analysis was completed using methods previously reported for imaging biomarker analysis (Evans et al., 2013). The following clinical variables were considered in the model: Patient's age, ER/PR status, HER2 status, tumour size, and pathologic response. The regression coefficient (r) was calculated between the clinical variables and DOS-GLCM features. A statistical test of significance was also performed using an ANOVA test with an alpha of 0.05.

2.7.12 Power Analysis

The statistical test of significance was performed with a relatively small sample size in each responding group and handling small datasets have been previously described (Siegel and Castellan, 1988, de Winter, 2013). In order to evaluate the reliability of the performed tests, the statistical power was calculated using PASS[14] where the label with the highest sample size was fixed for analysis. A power threshold of 0.70-0.80 was used (NCSS, LLC. Kaysville, Utah, USA).

Chapter 3

Results

3.0 Chapter Overview

In this chapter, the results of subproject one and subproject two of this study are presented. The structure of this chapter is presented in three sections: 1) patients' clinical and demographic characteristics; 2) measurements of DOS and QUS in breast tumours during chemotherapy (i.e. subproject one) and; 3) measurements of pre-treatment DOS in breast tumours before chemotherapy (i.e., subproject two). Section one presents data on patient demographics (i.e. age) and the clinical presentations before chemotherapy (i.e. tumour size, tumour subtype, chemotherapy regimens) and after chemotherapy (i.e. Miller-Payne graded pathology response outcome and tumour size reduction). The demographic and clinical characteristics were analysed in terms of its representation of cross-sectional breast cancer data (i.e. prevalence to cancer subtypes, age, tumour size at diagnosis).

In section two of this chapter, the results from subproject one are presented within the framework of the following research questions:

(Subproject one)

1. **Research Question 1**: Do DOS and QUS imaging biomarkers demonstrate statistically significant changes over the course of chemotherapy?

2. **Research Question 2**: Can DOS and QUS imaging biomarkers be modelled together to measure treatment response at early time intervals (i.e. after one or two cycles of chemotherapy)?

Here, parallel imaging time intervals using DOS and QUS are presented and statistical analyses are given in terms of their correlation to final pathologic endpoints (i.e. Miller-Payne score).

In section three, the results from subproject two are presented in terms of addressing the following research questions:

(Subproject two)

1. **Research Question 1**: Do breast tumours demonstrate significant differences in DOS-texture parameters between responders and non-responders, as measured before chemotherapy?

2. **Research Question 2**: Can DOS markers predict chemotherapy response prior to starting chemotherapy?

3. **Research Question 3**: Are there differences in DOS-texture prediction models for breast cancer subtypes (i.e., ER+ and triple negative) and chemotherapy treatments (i.e. FEC-D and AC-T)?

In this section pre-treatment DOS texture results are presented and analysed for statistical differences between responders and non-responders using a total sample set of 37 patients. To address the second and third research questions from subproject two, machine learning statistics and discrimination analyses results are presented from the 37 patients, and then subgroup analysis with ER+ tumours (subgroup of 27 patients), triple negative tumours (subgroup of 7 patients), FEC-D chemotherapy-treated patients (subgroup of 16 patients) and finally AC-T chemotherapy-treated patients only (subgroup of 21 patients).

3.1 Patient Characteristics

There were 37 patients recruited into the overall study. For subproject one, there were 22 patients who enrolled and completed all DOS and QUS imaging scan times (i.e. baseline, week one, week four, week eight, pre-operative). For subproject two, an additional 15 patients were recruited who completed one DOS imaging session before starting their chemotherapy (i.e. pre-treatment). All patients who signed the consent form completed their baseline scan for subproject two. In the entire study, there were no study deviations and no attrition. Patients were recruited consecutively. Participants did not report any side-effects related to the study procedure. A medical chart-review showed that all participants completed their chemotherapy as scheduled. A summary of patient characteristics is outlined in **Table 3.1** and described below.

3.1.1 Pre-Chemotherapy and Treatment Characteristics

The mean age was 50 years. Tumour characteristics were recorded at the time of diagnosis. In terms of histological type, lobular carcinoma accounted for 3% of patients (1 case) and the majority (97%, n=36) of cases were invasive ductal carcinoma in this study. Previous studies have indicated that invasive lobular carcinomas account for 7.6-10% of breast cancer cases; while invasive ductal carcinomas were the most prominent histological type; accounting or 72.8% of histological types (Dossus and Benusiglio, 2015, Li et al., 2003).

The search results from the patients' electronic medical record indicated that 27 patients had oestrogen receptor (ER) positive tumours; while seven were "triple-negative" breast tumours and 12 patients had tumours that were HER2-positive. Participants' clinical characteristics in this study were comparable to cross-sectional breast cancer data by the National Cancer Institute (NCI). The NCI database includes information on the prevalence of breast cancer subtypes such as, ER-expression and triple negative tumours; their data indicated that among 50,571 women, 72.7% of breast cancers were ER+, 12.2% were triple negative and 4.6-10.3% were HER2+. (Howlader et al.,

2014). In this study, 73% of patients were ER+, 19% were triple negative and 32% had HER2+ breast tumours. With the exception of the proportion of HER2+ cancers there was an otherwise good correspondence to NCI cross-sectional data.

In this study, 21 patients were given AC-T based chemotherapy and 16 patients were given FEC-D chemotherapy. The chemotherapy regimen was consistent with treatment guidelines for advanced breast cancer, as recommended by the National Comprehensive Cancer Network (USA) and the National Institute for Health and Care Excellence (UK) (National Comprehensive Cancer Network, 2016, National Institute for Health and Care Excellence, 2017). All patients completed their chemotherapy treatments. A chart-review was performed and no additional or other chemotherapy drugs were administered to patients. However, in 12 patients who were HER2+, Trastuzumab[15] was given during their taxane phase chemotherapy, as this was also consistent with guidelines from the NCCN and NICE (National Comprehensive Cancer Network, 2016, National Institute for Health and Care Excellence, 2017).

3.1.2 Post-Chemotherapy Characteristics

A review of the patients' medical records indicated that there were 27 patients that were classified as responders, which corresponded to Miller-Payne scores 3-5 (MP3= 15 patients; MP4=7 patients; MP5=5); thus, there were 5 pathological complete responders, i.e. categorized as Miller-Payne score 5[16]. There were 10 patients that were non-responders as these patients had a Miller-Payne score of 1 or 2 (MP1=4 patients, MP2=6 patients). For responders, the mean tumour size reduction from pre- to post-chemotherapy, as measured by MRI was 4.8 cm; 95% CI [3.8, 5.8], $p<0.0001$, paired t-test); while for non-responders, tumours shrunk by a mean value of 0.9 cm; 95% CI [0.4, 1.4], $p=0.0029$, paired t-test). Thus, both responders and non-responders

[15] Trastuzumab is a monoclonal antibody (targeted therapy) used for breast tumours that are HER2-positive.

[16] Representative pathological specimens of a responder and non-responder are presented in **Appendix 3**.

had a statistically significant reduction in the tumour size between the pre- and post-treatment times as measured by MRI.

Summary of Patient and Tumour Characteristics

Patient Demographic Information	**Number of patients =37 (All Subjects)**
Patients' Age	
	Years (Range)
Mean Age	50 (29-79)
Pre-Treatment Clinical Characteristics	
Breast Tumour Size	
	cm (Range)
Mean Tumour Size at Diagnosis (MRI)	5.9 (2.1-12.8)
Molecular and Histological Features	
	Number of patients n, (%)
Oestrogen Receptor (ER)+	27, (73)
Triple Negative/Basal-Like	7 (19)
HER2+	12 (32)
Invasive Ductal Carcinoma	36 (97)
Invasive Lobular Carcinoma	1 (3)
Chemotherapy and Targeted Therapies	
	Number of patients n, (%)
AC-T	21 (57)
FEC-D	16 (43)
Trastuzumab[1]	12 (32)

Post-Treatment Clinical Characteristics	
Post-Treatment Response Classification (Miller-Payne Pathologic Endpoints)[2]	
	Number of patients n, (%)
Responders (MP 3-5)	27 (73)
Non-Responders (MP 1-2)	10 (27)
Mean Tumour Size Change from Pre- to Post-Chemotherapy (Largest Dimension of Tumour as Measured by MRI)[3]	
	Change cm, (%)
Responders (MP 3-5)	-4.8, (-88)
Non-Responders (MP 1-2)	-0.9, (-13)

Table 3.1. Summary of Patient Characteristics. Pre- and Post-chemotherapy characteristics were recorded. [1] Trastuzumab was given to HER2+ patients in the second phase of treatment (i.e. during the patient's docetaxel (D) or paclitaxel (T) treatment). [2] Miller-Payne (MP) Pathologic Response Criteria was defined as: MP1-No reduction in overall cellularity, MP2-Up to 30% loss in tumour cells, MP3-30-90% loss in tumour cells, MP4-more than 90% loss, MP5-Complete disappearance of tumour cells. [3]MRI measurements were obtained from the patients' electronic medical record.

3.2 Results of Subproject One

3.2.1 Overview of Results: Subproject One, Research Question 1

In this section, the results to the following research question are presented: *Do DOS and QUS imaging biomarkers demonstrate statistically significant changes during chemotherapy in responders and non-responders?* This research question was approached using two statistical methods, as described below.

The first statistical approach was an independent sample t-test to compare the mean differences between responders and non-responders during early and late time intervals. Early time intervals were defined as corresponding to one to two cycles of chemotherapy, i.e. week one and week four of the imaging timelines of this study. Late time intervals were defined as corresponding to the third cycle of chemotherapy and up to the end chemotherapy, i.e. week eight and the pre-operative time interval. In the second statistical approach, a repeated measures ANOVA (i.e. within-subjects ANOVA) was calculated for responders, and for non-responders. The repeated measures ANOVA was used to test if the changes in DOS and QUS parameters were significant over the entire treatment course for each response group (responders and non-responders). All statistical tests were considered significant at a significance level of less than 0.05.

The following section presents the results of the independent sample t-test and repeated measures ANOVA in the following format: 1) DOS data and; 2) QUS data. Lastly, representative case studies of responders and non-responders are presented to compare the coincident changes in DOS and QUS parameters at early and late time intervals. DOS data is shown as *a relative change from baseline*, which was calculated for each time interval and defined as the percent comparison between the mean DOS parameter at each time interval to the mean DOS parameter measured at baseline. QUS data is presented as the change in magnitude (increase/decrease) for each of the QUS parameters (i.e., ΔMBF, ΔSI, ΔSS).

3.2.2 Results of DOS Measurements- Haematological Parameters

Early Time Intervals (week one and week four)

Haematological parameters included the deoxy-haemoglobin (Hb), oxy-haemoglobin (HbO_2) and the total haemoglobin (HbT). After one week of treatment, there were significant differences in the HbO_2 and HbT between responders and non-responders (*p<0.01*). The HbO_2 concentration increased to 110.7% ± 5.4% (SD[17]) for non-responders, compared to responders whose tumours had a reduction in the HbO_2 concentration to 73.7% ± 2.0%. Similarly, the HbT concentration increased 103.2% ± 5.5% for non-responders; while responders showed a reduction in the HbT concentration to 78.2% ± 3.2%. During the fourth week of treatment, all haematological parameters (Hb, HbO_2, HbT) were very statistically different between responders and non-responders (*p<0.01*) (**Table 3.2**). The Hb parameter showed a greater reduction in responders; the change in Hb concentration was reduced to 29.9% ± 6.32% and non-responders had a smaller reduction to 68.7% ± 7.9%. These trends in which there was a greater haematological reduction in responders compared to non-responders, was observed in the HbO_2 and HbT parameters (**Figure 3.1**) at the same time interval. A summary of the statistical differences for each parameter are presented in **Table 3.2**.

Late Time Intervals (week eight and pre-operative time interval)

All haematological parameters (Hb, HbO_2, HbT) were very statistically different between responders and non-responders at late time intervals, as measured at week eight and pre-operatively (*p<0.001*). After eight weeks of treatment, the Hb parameter showed a decrease in concentration to 21.0% ± 2.9% for responders and non-responders had tumours with higher Hb concentration (81.9% ± 9.4%, relative to baseline). The reduction in the HbO_2 and HbT parameters were greater for responders compared to non-responders; the HbO_2 and HbT corresponded to a reduction to 10.2% ± 2.3% and 12.7% ±

[17] SD; standard deviation

2.2%, respectively for responders. The pre-operative measurements showed a further reduction in haematological parameters for responders; the Hb concentration reduced to 25.4% ± 4.5%, the HbO_2 reduced to 10.5% ± 2.8% and the HbT concentration reduced to 12.7% ± 2.1% from the baseline value. Non-responders at this time interval showed a lesser change in tumour haemoglobin; the Hb reduced to 82.9% ± 7.9%, the HbO_2 reduced to 84.9% ± 7.6% and the HbT reduced to 84.4% ± 6.8% from the baseline value. A summary of changes is presented in **Figure 3.1**.

Tests of Significance Over the Treatment Time Course

The ANOVA tested if there were significant changes in haemoglobin parameters over the entire treatment course (i.e. from the pre-treatment time interval to the pre-operative scan) for responders and for non-responders. The results indicated that responders and non-responders had a significant change in all haemoglobin parameters (**Table 3.2**). Thus, both responders and non-responders demonstrated haematological changes from chemotherapy.

	Comparison between responders (R) and non-responders (NR) (Independent samples t-test)[1]				Within-subjects comparison (ANOVA)[2]	
	Early Time Intervals		Late Time Intervals		All Time Intervals	
	Week 1	Week 4	Week 8	Pre-Op	R	NR
Haematological Parameters						
	p-value	p-value	p-value	p-value	p-value	p-value
Hb	0.375	**0.002**	**0.000**	**0.000**	**0.000**	**0.005**
HbO_2	**0.000**	**0.001**	**0.000**	**0.000**	**0.000**	**0.015**
HbT	**0.004**	**0.000**	**0.000**	**0.000**	**0.000**	**0.003**

Table 3.2: Summary of measured *p* values for DOS-haemoglobin parameters. [1]DOS parameters were also tested for significant differences between responders and non-responders using an independent t-test within the 95% confidence level following a test for normality. Otherwise, a Mann-Whitney test was performed. [2]A repeated-measures ANOVA was used to test for significant changes over time (i.e. repeated measures between time intervals) for DOS parameters. ***Bold and blue fonts indicate statistically significant results; p<0.05= statistically significant; p<0.01 very statistically significant.***

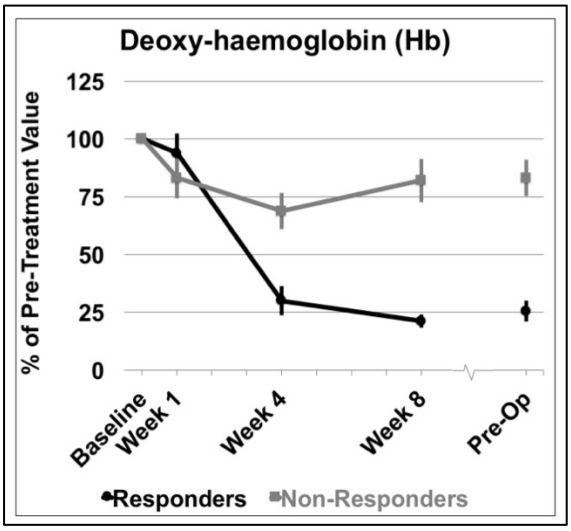

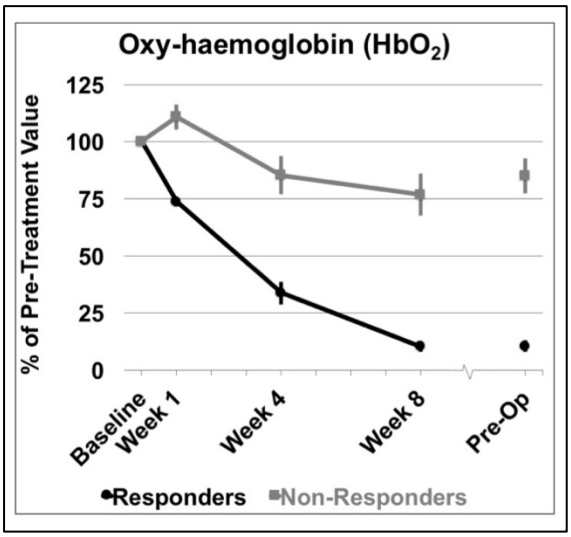

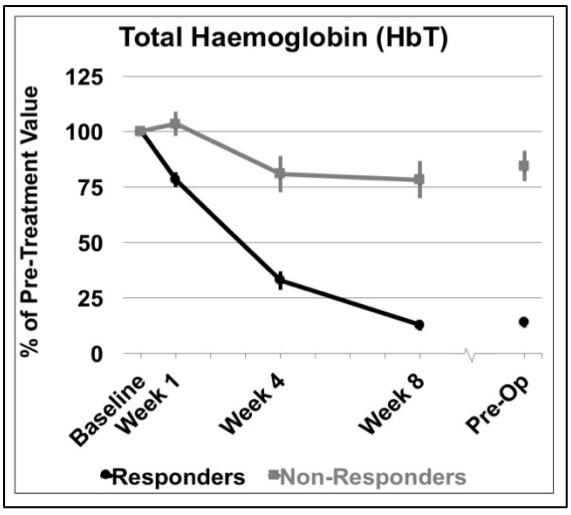

Figure 3.1: DOS haemoglobin parameters. Changes in haemoglobin parameters, measured as relative percent changes from baseline values. Error bars = Standard deviation, n = 14 responders and n = 8 non-responders. Significant differences between responders and non-responders were tested at each time interval and parametric changes over time were tested for responders and non-responders (**Table 3.2**).

3.2.3 Results of DOS Measurements- Tissue Parameters

Early Time Intervals (week one and week four)

Tissue parameters included the %Water, %Lipids and the tissue optical index (TOI). There were no significant differences between responders and non-responders after one week of treatment ($p>0.05$). However, after four weeks of treatment, the %Water, %Lipids and TOI parameters were very statistically different between response groups ($p<0.001$). The %Water reduced to 53.9% $\pm$ 3.3%, %Lipids increased to 166.4% $\pm$ 1.7%, and TOI reduced to 8.1% $\pm$ 2.9% for responders; whereas non-responder tumours had a smaller reduction to 86.9% $\pm$ 10.9% for the %Water, 121.1% $\pm$ 5.6% for %Lipids and 36.6% $\pm$ 6.5% for the TOI. A summary of results is presented in **Table 3.3** and **Figure 3.2**.

Late Time Intervals (week eight and pre-operative time interval)

After eight weeks of treatment, the %Lipids and the TOI demonstrated significant differences between response groups ($p<0.001$), but not the %Water parameter ($p=0.062$). However, all tissue parameters demonstrated a significant difference between response groups at the pre-operative time interval ($p<0.001$). At this late time interval (pre-op), responders' tumours showed that the %Water reduced to 57.1% $\pm$ 6.5%, the %Lipids parameter increased to 168.77% $\pm$ 0.8% and the TOI reduced to 6.6% $\pm$ 1.11%. In contrast, non-responders showed the following changes to the %Water, %Lipids and TOI (relative to baseline): %Water=86.9% $\pm$ 10.9%, %Lipids=121.1% $\pm$ 5.6% and TOI=36.6% $\pm$ 9.1%. The late changes are presented in **Figure 3.2** and tests of significance are outlined in **Table 3.3**.

Tests of Significance Over the Treatment Time Course

The results of the repeated measures ANOVA revealed that all tissue parameters demonstrated a significant change over all treatment time intervals for responders, but not for responders. A summary of results is presented in **Table 3.3**.

	Comparison between responders (R) and non-responders (NR) (Independent samples t-test)[1]				Within-subjects comparison (ANOVA)[2]	
	Early Time Intervals		Late Time Intervals		All Time Intervals	
	Week 1	Week 4	Week 8	Pre-Op	R	NR
Tissue Parameters						
	p-value	p-value	p-value	p-value	p-value	p-value
%Water	0.495	**0.008**	0.062	**0.001**	**0.000**	0.241
%Lipids	0.838	**0.000**	**0.000**	**0.000**	**0.000**	0.595
TOI	0.339	**0.000**	**0.000**	**0.000**	**0.000**	0.058

Table 3.3: Summary of measured *p* values for tissue parameters. [1]DOS parameters were tested for significant differences between responders and non-responders using an independent t-test within the 95% confidence level following a test for normality. [2]A repeated-measures ANOVA was used to test for significant changes over time (i.e. repeated measures between time intervals) for DOS and QUS parameters. ***Bold and blue fonts indicate statistically significant results; p<0.05= statistically significant; p<0.01 very statistically significant.***

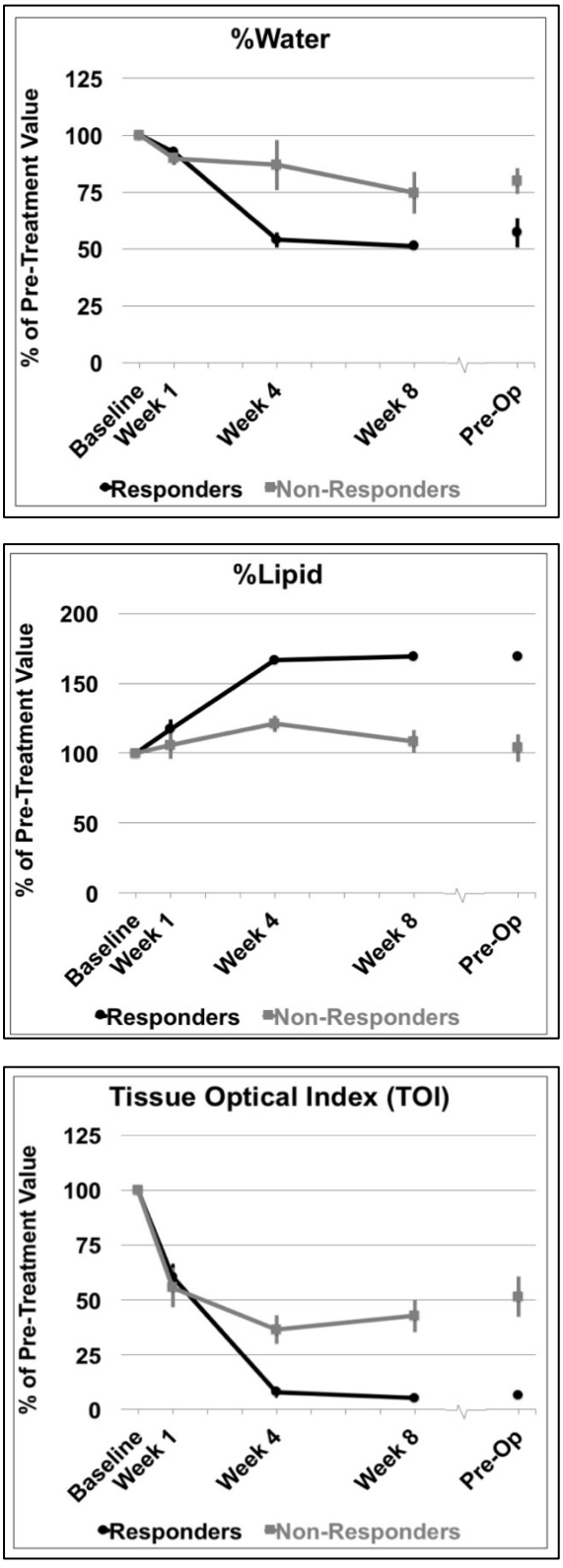

Figure 3.2: DOS tissue parameters measured. Changes in tissue parameters, measured as relative percent changes from baseline values. Error bars = Standard deviation, n = 14 responders and n = 8 non-responders. Significant differences between responders and non-responders were tested at each time interval and parametric changes over time were tested for responders and non-responders (**Table 3.3**).

3.2.4. Results of DOS Measurements- Scattering Parameters

Early Time Intervals (week one and week four)

Scattering parameters included the scattering power (SP) and the scattering amplitude (SA). Early time interval measurements showed significant differences between responders and non-responders in scattering parameters after four weeks of treatment ($p<0.01$) only (i.e. not at week one). After four weeks of treatment, the SP reduced to 42.3% ± 1.4% and the SA increased to 111.5% ± 0.3% for responders; whereas non-responders had a change in the SP to 79.9% ± 5.4% (relative to baseline) and the SA decreased to 97.7% ± 1.8% (relative to baseline). The early changes are presented in **Figure 3.3** and tests of significance are outlined in **Table 3.4**.

Late Time Intervals (week eight and pre-operative time intervals)

Late time intervals showed statistically significant differences in scattering parameters between responders and non-responders after eight weeks of treatment and up to the pre-operative time interval. ($p<0.01$). The SP reduced to 43.0% ± 0.7% and the SA increased to 112.2% ± 0.7% for responders after eight weeks. For non-responders, the SP was 91.9% ± 7.9% and the SA was 91.9% ± 4.4%. The SP and SA did not make a significant change between eight weeks and the pre-operative scan; responders had an SP change to 43.3% ± 0.9% and an SA change to 112.3% ± 0.7%. For non-responders, the SP reduced to 96.3% ± 9.5%; while the SA reduced insignificantly to 99.8% ± 1.8%. The late changes are presented in **Figure 3.3** and tests of significance are outlined in **Table 3.4**.

Tests of Significance Over the Treatment Time Course

A repeated measures ANOVA of the scattering parameters showed that responders had a significant change between the pre-treatment interval and the pre-operative treatment time ($p<0.001$). Non-responders did not have

significant change over treatment ($p>0.05$). A summary of the repeated measures ANOVA test for significance is presented in **Table 3.4**.

	Comparison between responders (R) and non-responders (NR) (Independent samples t-test)				**Within-subjects comparison (ANOVA)**	
	Early Time Intervals		**Late Time Intervals**		**All Time Intervals**	
	Week 1	**Week 4**	**Week 8**	**Pre-Op**	**R**	**NR**
Scattering Parameters						
	p-value	p-value	p-value	p-value	p-value	p-value
SP	0.838	**0.000**	**0.000**	**0.000**	**0.000**	0.595
SA	0.410	**0.002**	**0.002**	**0.001**	**0.000**	0.170

Table 3.4: Summary of measured *p* values for scattering parameters. DOS parameters were tested for significant differences between responders and non-responders and within-groups over the course of chemotherapy. The corresponding data is presented below in **Figure 3.3**. Significant p-values are bolded. *SP (Scattering power) and SA (Scattering amplitude).*

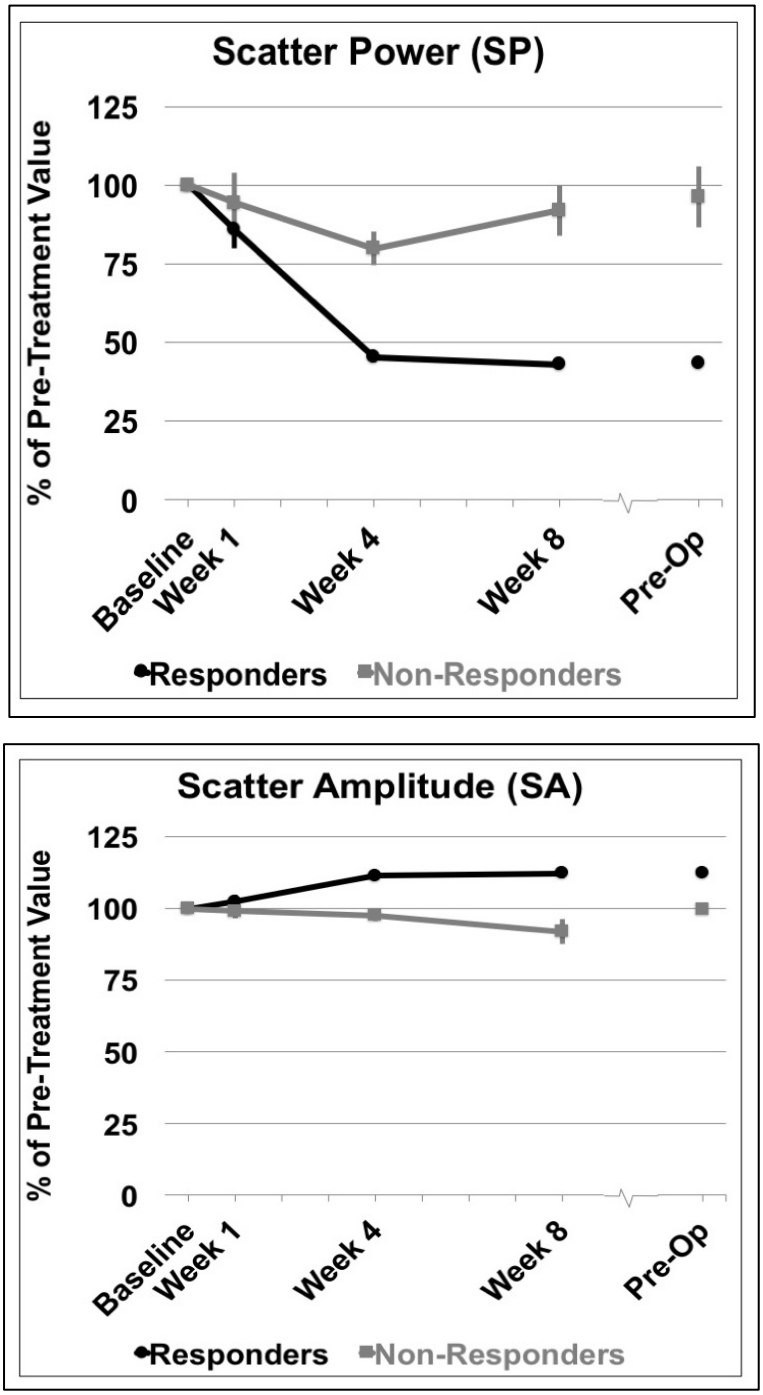

Figure 3.3: DOS scattering parameters (SP and SA) measured during treatment. Changes in scattering parameters, measured as relative percent changes from baseline values. Error bars = Standard deviation, n = 14 responders and n = 8 non-responders. Significant differences are presented in (**Table 3.4**).

3.2.5 Results of QUS Measurements

Early Time Intervals (week one and week four)

After one week of chemotherapy, the difference in the spectral intercept parameter between response groups was statistically significant (*p=0.009*). Responders showed an increase in the mean spectral intercept (∆SI) of +3.93 ± 1.86 [SD] dBr[18]; whereas, non-responders showed a smaller change of +1.83 ± 1.83 dBr (**Figure 3.4**). In comparison, there were no significant differences between responders and non-responders for the mid-band fit (*p=0.413*) and the spectral slope (*p=0.222*) after one week of treatment. The change in the mean mid-band fit (∆MBF) was +3.27 ± 1.40 dBr for responders; while non-responders yielded a change of +2.29 ± 1.53 dBr. For the spectral slope, the change in the mean spectral slope (∆SS) was -0.12 ± 0.17 dBr/MHz for responders and +0.03 ± 0.11 dBr/MHz for non-responders (**Figure 3.4**).

After four weeks of treatment, there were significant differences between responders and non-responders with respect to the ∆MBF and ∆SI parameters (*p<0.001*), but not the ∆SS (*p=0.275*). Responders had a ∆MBF increase of +7.91 ± 1.39 dBr; whereas, non-responders showed a smaller increase of +0.72 ± 1.44 dBr. Similarly, the ∆SI was +8.55 ± 1.84 dBr for responders and +4.40 ± 1.62 dBr for non-responders. The ∆SS was -0.12 ± 0.17 dBr/MHz for responders and -0.67 ± 0.14 dBr/MHz for non-responders. Tests of significance are summarized in **Table 3.5**.

Late Time Intervals (Week eight and Pre-op)

After eight weeks of treatment, there were significant differences in the ∆MBF and ∆SI parameters (*p<0.001*), but not the ∆SS (*p=0.116*). For the ∆MBF, responders and non-responders showed an increase of +10.02 ± 1.48 dBr and +1.60 ± 1.39 dBr, respectively. The ∆SI was +12.27 ± 2.02 dBr for

[18] dBr refers to *decibels* (normalized); it is a measurement of the acoustic intensity.

responders and +2.81 ± 1.58 dBr for non-responders. The ΔSS was -0.41 ± 0.21 dBr/MHz for responders and -0.22 ± 0.13 dBr/MHz for non-responders. Lastly, only the ΔMBF showed a statistically significant difference between response groups at the pre-operative time interval (*p=0.020*). Here, the ΔMBF was +5.44 ± 2.53 dBr for responders and +0.51 ± 1.70 dBr for non-responders.

The mean QUS changes for the MBF, SI and SS within the measured time intervals is presented in **Figure 3.4**. Tests of significance are summarized in **Table 3.5**.

Tests of Significance Over the Treatment Time Course

The significant QUS changes associated with a favourable chemotherapy response showed a similar trend for responders, i.e. for responders, there was an increase in QUS parameters over time (i.e. over course of chemotherapy).

	Comparison between responders (R) and non-responders (NR) (Independent samples t-test)[1]				**Within-subjects comparison (ANOVA)[2]**	
	Early Time Intervals		**Late Time Intervals**		**All Time Intervals**	
	Week 1	**Week 4**	**Week 8**	**Pre-Op**	**R**	**NR**
	p-value	p-value	p-value	p-value	p-value	p-value
MBF	0.413	**0.000**	**0.000**	**0.020**	**0.000**	0.474
SI	**0.009**	**0.001**	**0.000**	0.306	**0.000**	0.113
SS	0.222	0.275	0.116	0.375	0.161	0.127

Table 3.5. [1]QUS parameters were also tested for significant differences between responders and non-responders using an independent t-test. [2]A repeated-measures ANOVA was used to test for significant changes over time (i.e. repeated measures between time intervals) for QUS parameters. ***Bold and blue fonts indicate statistically significant results; p<0.05= statistically significant; p<0.01 very statistically significant.***

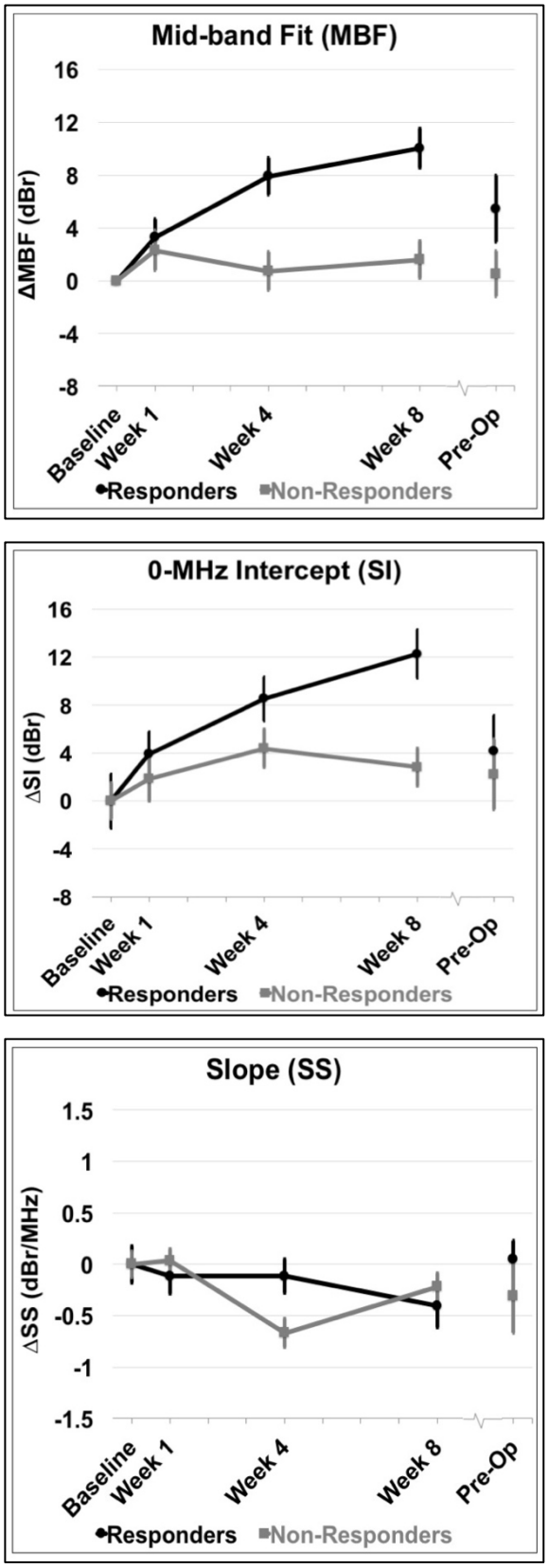

Figure 3.4: QUS parameters measured. Relative changes for all patients grouped by treatment response are presented**. Top,** Mid-band Fit (MBF); **Middle,** 0-MHz Intercept (SI); **Bottom.** Spectral Slope (SS). *Error bars = Standard deviation, n = 14 responders and n = 8 non-responders. Tests of significance are presented in* ***Table 3.5****.*

3.2.6 Representative DOS and QUS Changes During Chemotherapy

DOS and QUS imaging biomarkers demonstrated coincident changes during chemotherapy for patients who were pathologic responders (Miller-Payne Scores 3-5), but not for non-responders (Miller-Payne Score 1,2).

Representative Pathological Responder (Miller-Payne Pathology Response Score 4)

This post-menopausal woman presented with a locally advanced breast tumour in the upper inner quadrant of the right breast that measured 9x9x6 cm by MRI. Core biopsy revealed a high-grade invasive ductal carcinoma that was oestrogen receptor (ER) and progesterone receptor (PR) positive, and negative for HER2-Neu (HER2) overexpression. Neoadjuvant chemotherapy consisted of AC-T. Histological examination at the time of mastectomy revealed pathological response to treatment. **Figure 3.5** presents representative DOS and QUS data for this patient. After four weeks of treatment, this patient demonstrated an increase in the mid-band fit (ΔMBF) of +10.0 ± 1.4 dBr (±SD). At the same time interval, the DOS-measured haemoglobin concentration (Hb) decreased to 29.1% ± 9.5%, relative to the baseline.

Representative Pathological Non-Responder (Miller-Payne Pathology Response Score 2)

A post-menopausal woman presented with a tumour in the right breast, which measured 5 x 4 x 2 cm by MRI. Core biopsy confirmed the presence of invasive ductal carcinoma that was positive for ER, PR negative, and positive for HER2. Chemotherapy treatment consisted of AC-T+Herceptin. Pathological examination after mastectomy demonstrated only minimal response to neoadjuvant treatment (no reduction in tumour size). Representative patient data is shown in **Figure 3.6**. This patient, in contrast to the one above, demonstrated a smaller change in the MBF at week four (ΔMBF = +2.3 ± 1.8 dBr), which was coincident with a reduction in haemoglobin to 64.4% ± 10.9% (SD), relative to baseline values.

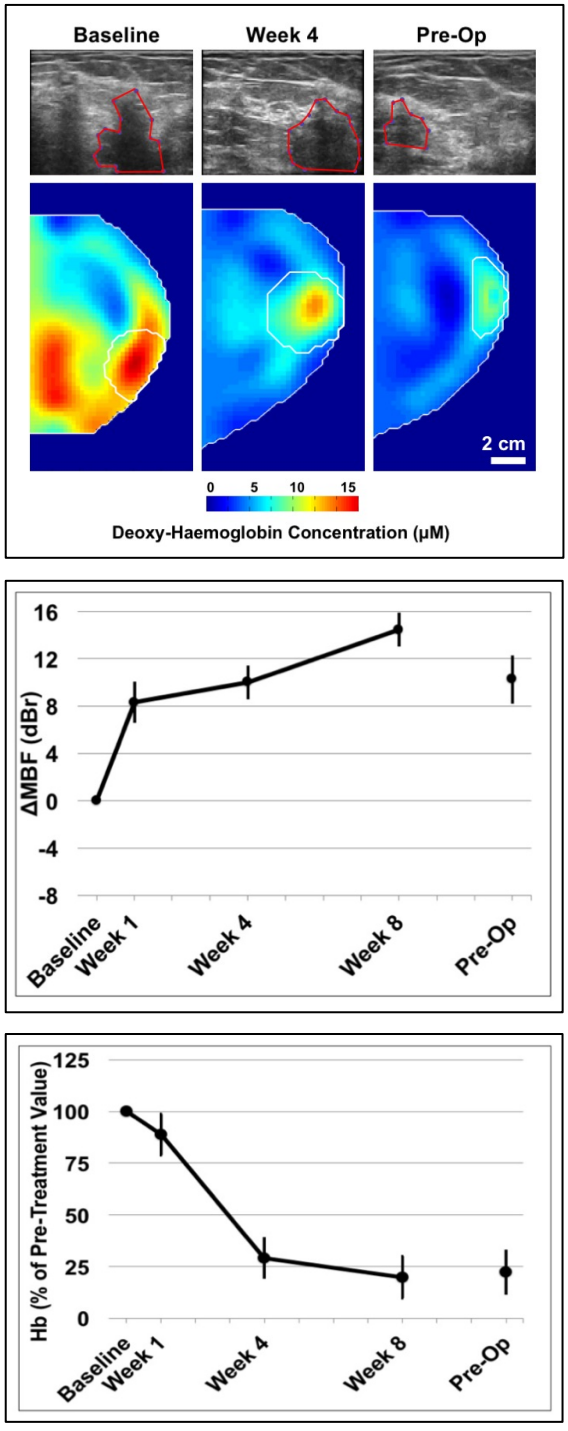

Figure 3.5: Representative DOS and QUS data of a responder (Miller-Payne Pathology Score 4). (Top) Representative B-mode images and DOS parametric maps are presented for baseline, mid-treatment (week four) and pre-operative scans (with contours). This responsive patient showed an overall increase in QUS MBF and an overall reduction in [Hb]. Error bars = Standard deviation, Scale bar; 2 cm. Deoxyhaemoglobin [Hb] colour bar = 0-15 µM (colour bar represents the concentration of deoxyhaemoglobin as shown in top figure; blue=low deoxy-haemoglobin concentration, red=high deoxy-haemoglobin concentration).

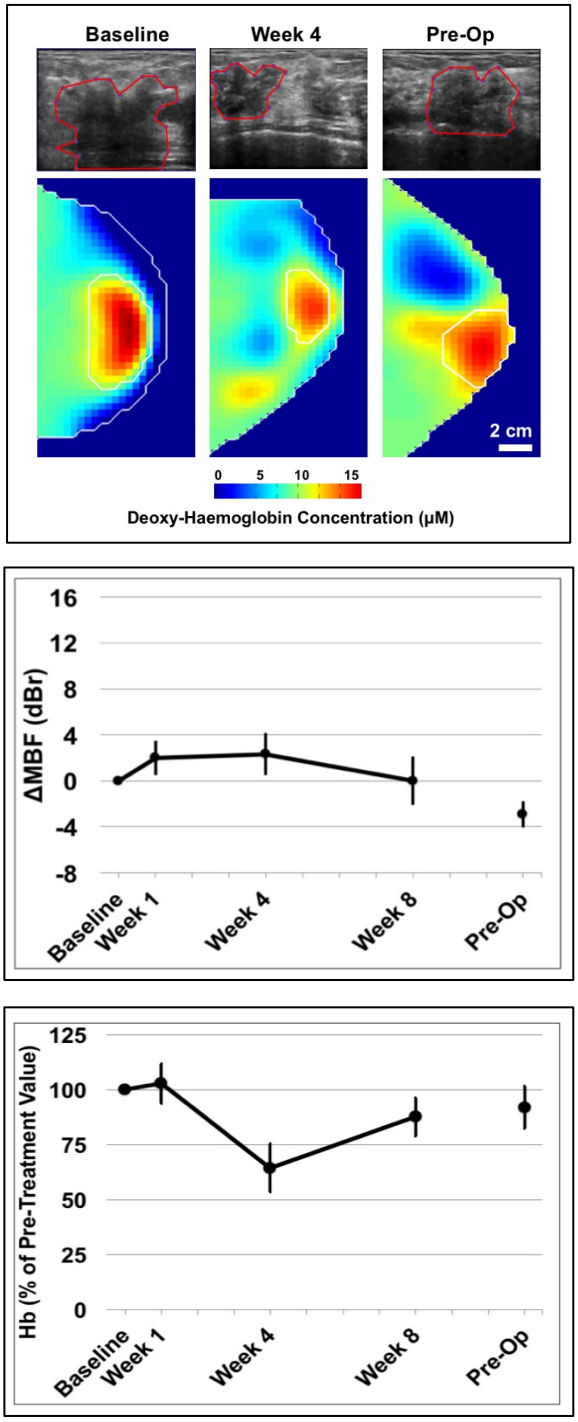

Figure 3.6: Representative DOS-QUS images and data for a non-responder (MP2). Normalized power spectra are presented for baseline and pre-operative scans. This non-responsive patient demonstrated an insignificant change in the mid-band fit (dBr) and lesser changes in DOS parameters (deoxy-haemoglobin presented) during treatment. *Error bars = Standard deviation, Scale bar; 2 cm.* Deoxyhaemoglobin [Hb] colour bar = 0-15 µM (colour bar represents the concentration of deoxyhaemoglobin as shown in top figure; blue=low Hb concentration, red=high Hb concentration). Contours are shown in the ultrasound and optical figures presented.

3.2.7 Overview of Results: Subproject One, Research Question 2

In this section, the following research question is addressed: *"Can DOS and QUS imaging biomarkers be modelled using univariate and multivariate parameters to measure treatment response at early time intervals (i.e. after one or two cycles of chemotherapy)?"*. Evaluating early-response markers is important and clinically relevant because physicians need information at early time intervals in order to modify treatments as necessary. In the following section, the results of both univariate and multiparametric models are presented.

3.2.8 Univariate Analysis of DOS and QUS Parameters

DOS and QUS Analysis at Early Time Intervals

Linear discriminant analysis and ROC analysis of individual DOS and QUS parameters were undertaken to differentiate pathological response, as defined by Miller-Payne pathologic classification during treatment. The area under the curves (AUCs) for individual DOS and QUS parameters (i.e. univariate analysis) during treatment are presented for early time intervals (weeks one and four) in **Table 3.6**. After one week of treatment, the DOS and QUS parameters: SI, HbO_2, and HbT indicated good response classification (AUC range=0.839-0.982), and this corresponded with 64.3-85.7% sensitivity, and 75.0-87.5% specificity. Other DOS and QUS parameters were poorer predicators at this time interval, such as the SS, %Water, % Lipids, and SA (**Table 3.6**). However, after four weeks of treatment, the QUS MBF and SI markers showed an increase in the AUC (range 0.920-0.982) and this corresponded with high sensitivity and specificity (range; 85.7-100.0%).

DOS parameters related to tumour haemoglobin demonstrated high sensitivity and specificity (%Sn=85.7%, %Sp=87.5%), and an AUC of 0.911-0.964. Other DOS parameters such as the TOI demonstrated a sensitivity and specificity of 85.7% and 87.5% respectively, which corresponded to an AUC of 0.973.

Parameters	Early Time Intervals					
	Week 1 (One Chemotherapy Cycle)			Week 4 (Two Chemotherapy Cycles)		
	%Sn	%Sp	AUC	%Sn	%Sp	AUC
QUS						
MBF	50.0	50.0	0.607	**92.9**	**100**	**0.982**
SI	**64.3**	**87.5**	**0.839**	**85.7**	**87.5**	**0.920**
SS	28.6	25.0	0.201	57.1	62.5	0.643
DOS						
Hb	64.3	62.5	0.616	**85.7**	**87.5**	**0.911**
HbO_2	**85.7**	**87.5**	**0.982**	**85.7**	**87.5**	**0.938**
HbT	**78.6**	**75.0**	**0.875**	**85.7**	**87.5**	**0.964**
%Water	50.0	50.0	0.589	**85.7**	**75.0**	**0.848**
%Lipids	50.0	50.0	0.527	**92.9**	**87.5**	**0.982**
SP	50.0	50.0	0.527	**92.9**	**87.5**	**0.982**
SA	57.1	50.0	0.393	**85.7**	**87.5**	**0.897**
TOI	64.3	62.5	0.625	**85.7**	**87.5**	**0.973**

Table 3.6: Sensitivity (%Sn), Specificity (%Sp), and Area Under Curve (AUC) for univariate DOS and QUS parameters. DOS and QUS parameters were estimated from discriminant analysis, and receiver-operating characteristic analysis. DOS and QUS parameters were analysed for weeks 1, 4 and 8 to correspond to response monitoring during treatment. Markers for response classification were detected as early as one week relative to the start of chemotherapy. Highlighted values indicate an AUC threshold of greater than 0.8.

3.2.9 Multivariate Analysis of Pairwise DOS-QUS Parameter Combinations

Multivariate models were formulated using binary (pairwise) DOS and QUS parameters. Pairwise combinations were determined from a statistical

framework that restricts the number of parameters that can be included in a model based on the number of subjects in a sample set[19].

Table 3.7 present results of the ROC analyses of DOS-QUS pairwise combinations during early chemotherapy time intervals (Weeks 1, 4). Parametric combinations increased the sensitivity and specificity for response classification compared to univariate parameters alone after one week of chemotherapy and is represented in **Figure 3.7**. At week one, combining the SI parameter with the %Water parameter demonstrated a sensitivity and specificity of 71.4-75.0% (AUC=0.866). Also, combining the SS+TOI resulted in an AUC of (AUC=0.982). At week one, the combination of the MBF with total haemoglobin (HbT) demonstrated an AUC value of 0.857. All of these combinations demonstrated an increase in the classification performance compared to using the individual (univariate) parameters alone, i.e. the best univariate AUC was 0.839, compared to multivariate models which demonstrated an AUC of 0.857-1.0.

At week four, response classification was enhanced when the MBF, SI, and SS were combined with the following DOS parameters: Hb, HbO_2, %Water, SA, TOI. Representative combinations are presented in **Figure 3.8** and significant DOS and QUS combinations are presented in **Table 3.7**. The combination of the MBF and Hb, or HbO_2, or %Water resulted in an AUC of 1.0, and a sensitivity and specificity of 100% (**Figure 3.8**). The SI showed an increase in sensitivity and specificity when combined with either HbO_2, %Water, or SA. Lastly, the SS showed an improvement with combinations with the TOI or %Water. The performance of these combinations is presented in **Table 3.7**.

---

[19] This statistical framework indicates that the number of parameters permitted into a model is limited by the sample size; defined as 1/10 of the sample size Jain et al., 2000). All possible forward combinations between DOS and QUS parameters were included in the statistical analysis using a brute-force search. Parametric combinations that yielded an AUC>0.8 were reported, as the likelihood ratio of 0.8 (true positive fraction)/0.2 (false positive fraction) was chosen (Zweig et al., 1993).

Multivariate Features	%Sn	%Sp	AUC (Logistic)	*p-value*
Week 1 (One Cycle of Chemotherapy)				
MBF+HbO_2	85.7	87.5	0.973	0.000
MBF+HbT	71.4	75.0	0.857	0.006
SI+HbO2	100	100	1.000	0.000
SI+HbT	85.7	87.5	0.929	0.001
SI+%Water	71.4	75.0	0.866	0.005
SS+HbO_2	100	100	1.000	0.000
SS+HbT	85.7	87.5	0.955	0.000
Week 4 (Two Cycles of Chemotherapy)				
MBF+Hb	100	100	1.000	0.000
MBF+HbO_2	100	100	1.000	0.000
MBF+%Water	100	100	1.000	0.000
SI+SA	100	100	1.000	0.000
SI+HbO_2	85.7	87.5	0.982	0.000
SI+%Water	85.7	87.5	0.964	0.000
SS+SA	100	100	1.000	0.000
SS+TOI	92.9	87.5	0.982	0.000
SS+%Water	85.7	87.5	0.955	0.000

Table 3.7: Sensitivity (%Sn), Specificity (%Sp) and AUC for representative multivariate (pairwise) DOS and QUS parameters. Pairwise combinations were reported with AUC >0.8. Analyses were performed at week one and 4 for combined parameters (i.e. during treatment). Combining DOS and QUS parameters together demonstrated an increase in sensitivity and specificity compared to univariate models.

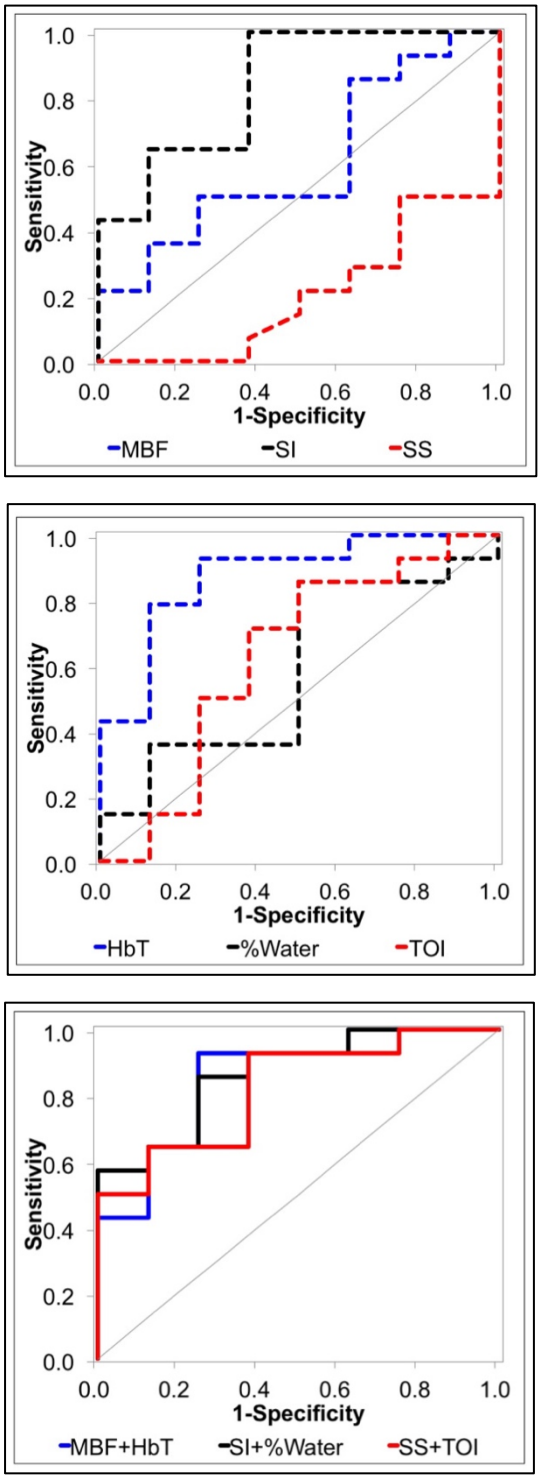

Figure 3.7: Sensitivity (%Sn), Specificity (%Sp) and AUC for representative multivariate (pairwise) DOS and QUS parameters at week one. ROC curves: **(Top)** QUS alone; **(Middle)** DOS alone; **(Bottom).** Combination DOS+QUS. Combining DOS and QUS parameters demonstrated an increase in sensitivity and specificity compared to the univariate parameters alone at this time interval. The parameters presented here are representative; the performances of all multivariate models are presented in **Table 3.7.**

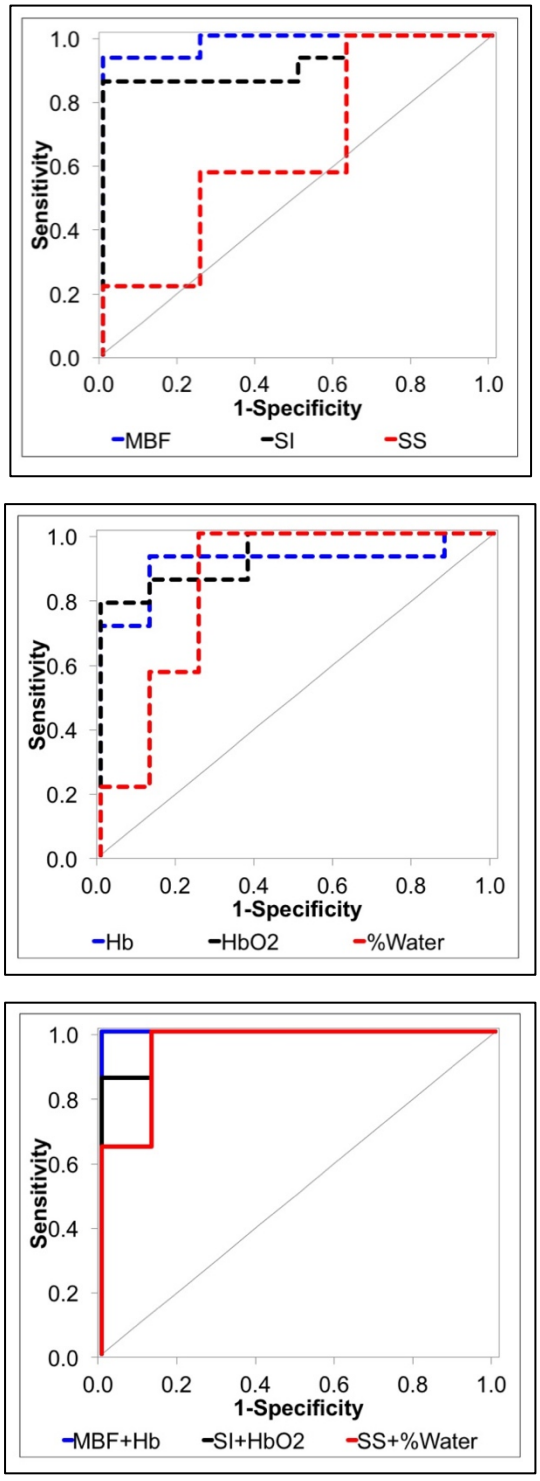

Figure 3.8: Sensitivity (%Sn), Specificity (%Sp) and AUC for representative multivariate (pairwise) DOS and QUS parameters at week four. ROC curves: **(Top)** QUS alone; **(Middle)** DOS alone; **(Bottom).** Combination DOS+QUS. The parameters presented here are representative; the performances of all multivariate models are presented in **Table 3.7**.

3.2.10 Summary of Results and Responses to Research Questions (Subproject One)

DOS and QUS imaging biomarkers were studied in breast cancer patients to report first accounts of coincident markers for tumour response during neoadjuvant chemotherapy. The results of subproject one showed that the changes in DOS and QUS imaging biomarkers represented the biological alternations in the tumour and could be used to measure the tumour's pathologic response. The biological changes, as measured by QUS, include markers for cell death (i.e. MBF, SI); while DOS parameters showed that there were significant changes in the haematological properties (Hb, HbO_2, HbT) and tissue composition (%Water, %Lipids, TOI). The responses to the research questions are presented below:

- ***Research Question 1:*** *Do DOS and QUS imaging biomarkers demonstrate statistically significant changes over the course of chemotherapy?*

Over the entire course of chemotherapy (i.e. from pre-chemotherapy to pre-surgery), the following QUS parameters showed significant increases in responders only: MBF and SI. For DOS parameters, the following parameters showed significant decreases over chemotherapy in responders: Hb, HbO_2, HbT, %Water, SP, TOI; while the following parameters showed significant increases in responders: SA, %Lipids. There were parallel temporal changes in the DOS and QUS parameters.

- ***Research Question 2:*** *Can DOS and QUS imaging biomarkers be modelled together to measure treatment response at early time intervals (i.e. after one or two cycles of chemotherapy)?*

The results indicated that univariate DOS and QUS imaging parameters were good surrogate markers for pathologic endpoints (i.e. Miller-Payne pathologic response criteria) as early as one week after the start of chemotherapy (corresponding to one chemotherapy cycle). At week one, the

QUS-spectral intercept (SI) showed a sensitivity of 64.3% and specificity of 87.5% (AUC=0.839). Similarly, the DOS-haemoglobin parameters, HbO_2 demonstrated a sensitivity of 85.6% and specificity of 87.5%, and the HbT had a sensitivity and specificity of 78.6% and 75%, respectively.

In multivariate models, the results demonstrated that the following DOS and QUS values can be predictive of chemotherapy response at early time intervals, as measured after one week (i.e. one cycle) of chemotherapy: QUS [MBF, SI, SS] and DOS [HbO_2, HbT, %Water]. A logistic regression model was used for multivariate DOS and QUS models and showed that DOS and QUS parameters could be used as surrogate endpoint markers to Miller-Payne pathologic response criteria, which demonstrated an accuracy of up to 100%.

3.3 Results of Subproject Two

3.3.1. Overview and Link to subproject one

The aim of this thesis was to investigate DOS and QUS imaging biomarkers to detect early indicators of chemotherapy response defined as:

1. Early-response markers after one or two cycles of chemotherapy;
2. Predictive markers that are measured before starting chemotherapy.

Subproject two was motivated from the results obtained from subproject one. In subproject one, it was shown that early-response markers could be obtained by modelling DOS and QUS imaging biomarkers as univariate and multivariate models within one or two cycles of chemotherapy. The results indicated that DOS and QUS imaging biomarkers demonstrated high sensitivity and specificity as early as one week after the start of chemotherapy. Thus, the goal of subproject two was to then investigate predictive markers using DOS imaging only; using DOS alone was based on the following rationale:

1. Previous studies have already investigated pre-treatment QUS imaging biomarkers (both mean QUS and texture-based QUS imaging biomarkers) and have shown a high prediction accuracy (88%) to treatment response (Tadayyon et al., 2017); thus, this area of research has already been studied with promising results.
2. Previous studies have indicated that pre-treatment DOS parameters related to tumour haemoglobin and oxygen saturation can predict chemotherapy response; however, these studies had not investigated DOS-texture based imaging biomarkers (Ueda et al., 2012, Tromberg et al., 2016).

Thus, the work in subproject two is motivated by exploring pre-treatment DOS-texture features within a region-of-interest of the tumour-bed only.

3.3.2 Overview of Results: Subproject Two, Research Question 1

The first research question for subproject two was: *Do breast tumours demonstrate significant differences in DOS-texture parameters between responders and non-responders, as measured before chemotherapy?* All DOS-texture parameters were tested for statistically significant differences between Miller-Payne pathologic responders (MP 3-5) and non-responders (MP1,2). The results demonstrated that only DOS-haemoglobin parameters and DOS-oxygen parameters demonstrated significant differences between responders and non-responders and are presented below.

The data are presented as box-and-whisker plots, which show the median DOS-texture values, the lower extreme, the lower quartile, upper quartile and the upper extreme. Since grey-level co-occurrence texture features do not have a unit of measure[20], the DOS-texture values are indicated as A.U. (arbitrary units). The data in the following section is presented in two parts: 1) DOS-haemoglobin parameters are presented and represented in **Figures 3.9, 3.10, 3.11** and; 2) DOS-oxygen features, which correspond to **Figure 3.12** and **Figure 3.13**.

3.3.3 Pre-treatment Tumour Haemoglobin-Texture Features Demonstrated Significant Differences Between Miller-Payne Pathologic Response Groups

Pre-treatment Deoxy-haemoglobin (Hb) Texture Features

The deoxyhaemoglobin-homogeneity (Hb-hom) feature demonstrated a significant difference between responders and non-responders; *(p=0.030).* The Hb-hom feature was greater in non-responders (i.e. Miller-Payne pathology score 1-2) compared to responders (i.e., Miller-Payne pathology score 3-5). Non-responders had a median value of 0.351 A.U.; 95% CI [0.288, 0.370]; whereas responders had a median Hb-hom value of 0.275; 95% CI [0.260,

[20] The calculations for the grey-level co-occurrence matrix uses a probability score that is the sum of the elements in the matrix; thus, having no units and expressed as arbitrary units (A.U.).

0.304]. However, other texture features such as the deoxyhaemoglobin-contrast (Hb-con), correlation (Hb-cor) and energy (Hb-ene) did not demonstrate a significant difference between groups (p >0.05) **(Figure 3.9)**. However, the Hb-con demonstrated near significance between response groups ($p=0.066$).

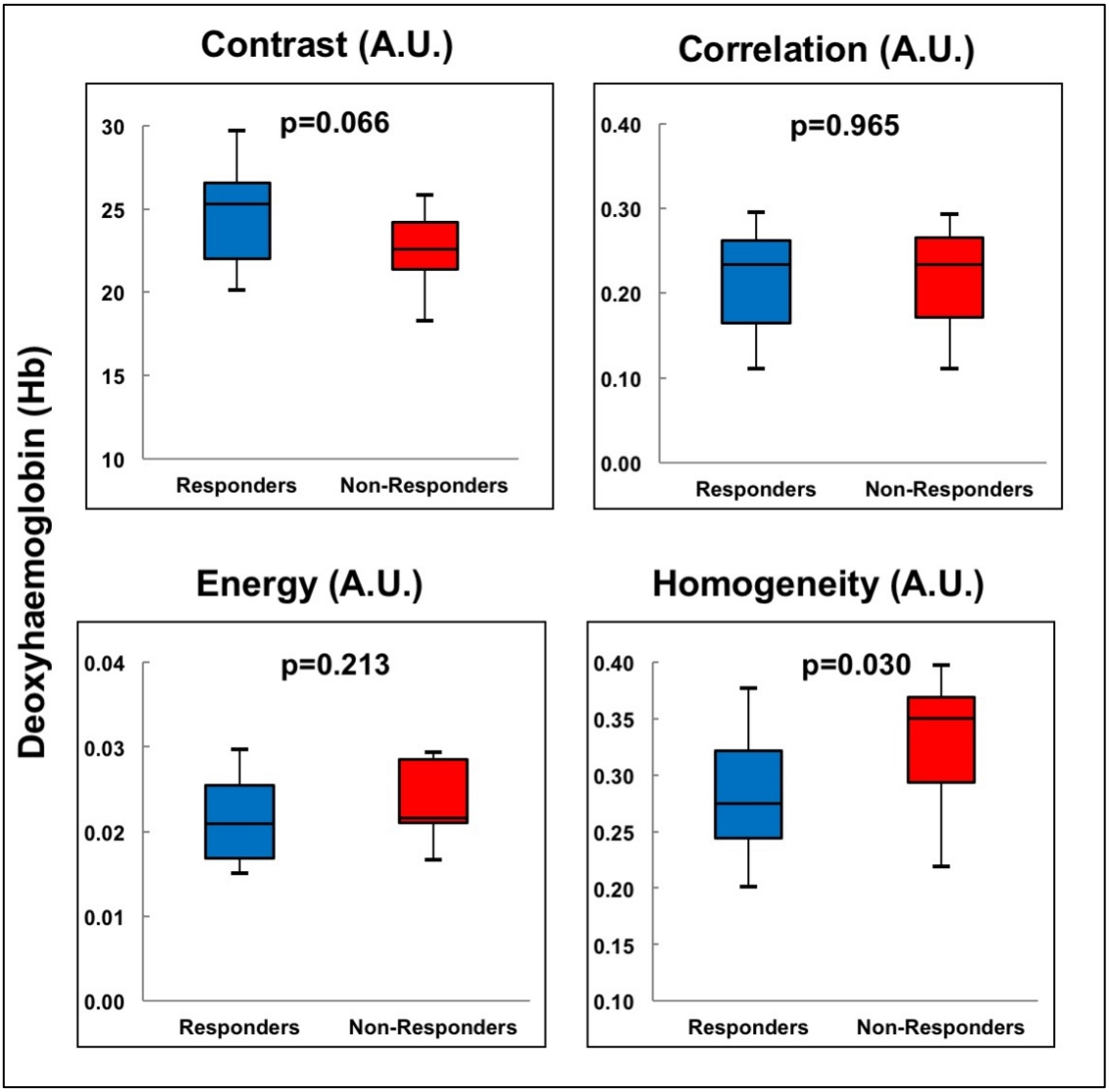

Figure 3.9: GLCM texture features for deoxy-haemoglobin texture features. Box-and-whisker plots showing significant differences in DOS textural markers for responders and non-responders (p values indicated).

Pre-Treatment Oxy-haemoglobin (HbO_2*) Texture Features*

For the HbO_2-texture features, the HbO_2-cor feature was significantly different between response groups; the HbO_2-cor was greater for responders

compared to non-responders (*p<0.024*) (**Figure 3.10**). Responders had a median HbO_2-cor value of 0.195 A.U.; 95% CI [0.182, 0.228] and non-responders showed a median HbO_2-cor value of 0.136 A.U.; 95% CI [0.118, 0.193], *p*<0.024. The HbO_2-con approached a significant difference between response groups (*p=0.058*). For responders, the median value for the HbO_2-con feature was 20.180 A.U.; 95% CI [19.191, 21.337]; whereas for non-responders, the median value was 23.393 A.U.; 95% CI [20.018, 24.651]. The HbO_2-ene and HbO_2-hom was not significantly different between response groups (*p>0.05*).

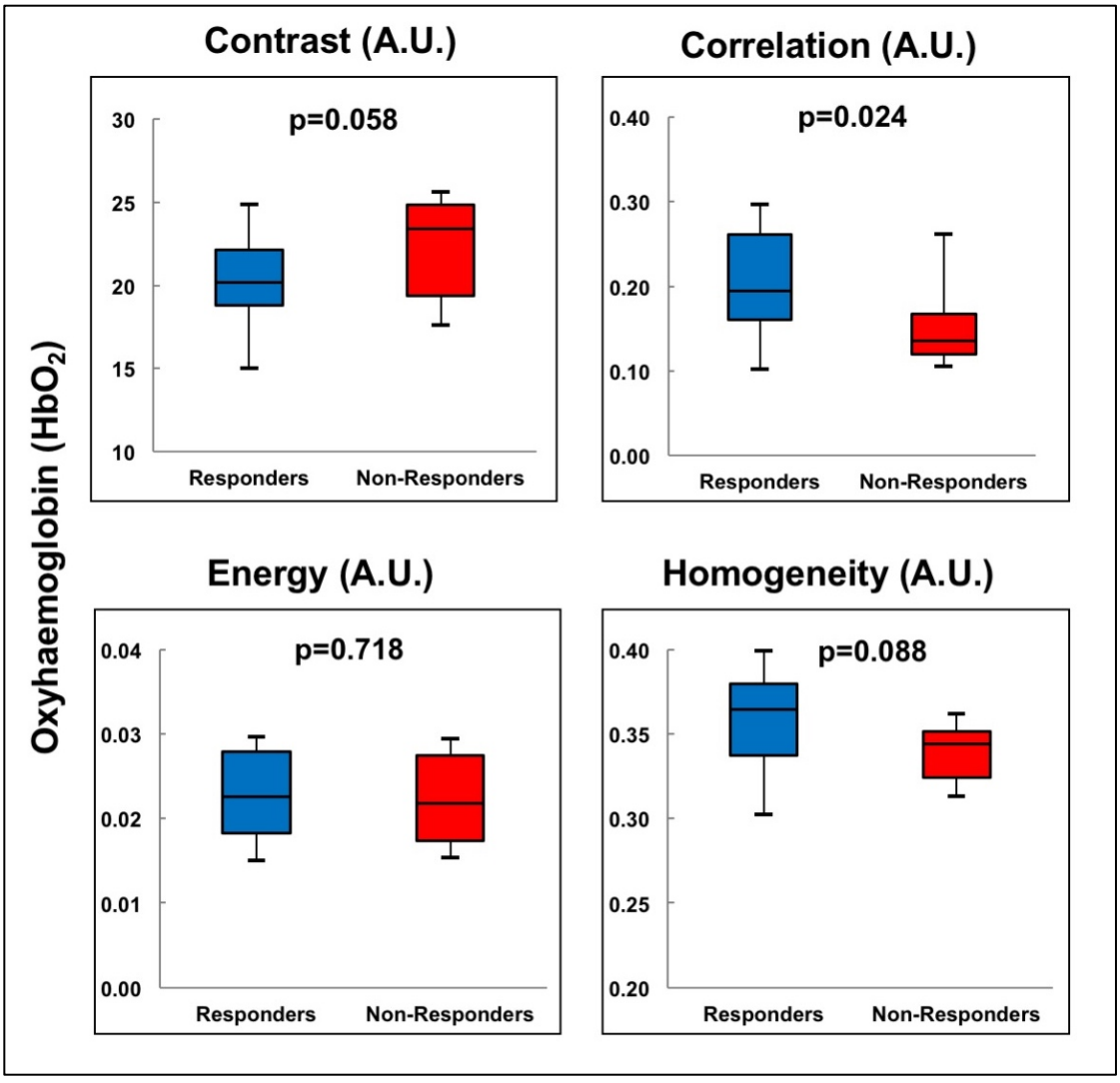

Figure 3.10: GLCM texture features for oxy-haemoglobin texture features. Box-and-whisker plots showing significant differences in DOS textural markers for responders and non-responders (*p* values indicated).

Pre-Treatment Total Haemoglobin (HbT) Texture Features

The total haemoglobin (HbT) texture measurements in tumours demonstrated significant differences in homogeneity (HbT-hom) *(p* = 0.047*)*. The median HbT-hom value was 0.356 A.U.; 95% CI [0.340, 0.362] for responders and 0.373 A.U.; 95% CI [0.345, 0.377] for non-responders. Additionally, the HbT-con feature approached significance (*p* = 0.055); responders had a median value of 18.876 A.U.; 95% CI [17.729, 20.803]; whereas for non-responders, the median value was 16.399 A.U.; 95% CI [13.351, 19.353]. The HbT-con was close to being significantly different between responders and non-responders; the median value was 18.876 A.U.; 95% CI [17.729, 20.803] for responders and non-responders had a median HbT-con value of 16.399 A.U.; 95% CI [13.351, 19.353]. The HbT-ene and HbT-cor features were not significantly different between response groups (p>0.05) (**Figure 3.11**).

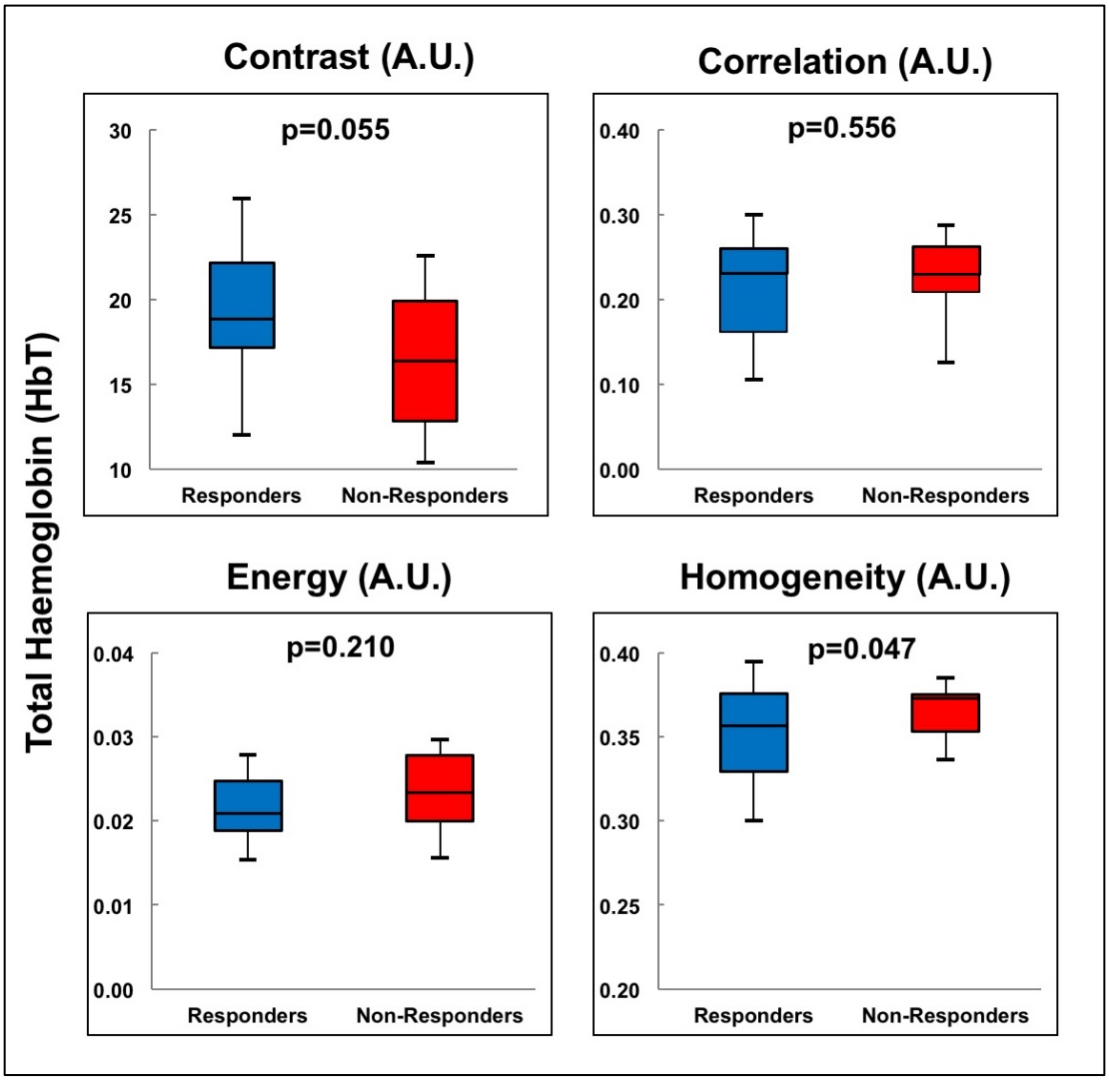

Figure 3.11: GLCM texture features for total haemoglobin texture features. Box-and-whisker plots showing significant differences in DOS textural markers for responders and non-responders (*p* values indicated).

3.3.4 Pre-treatment Tumour Oxygen-Texture Features Demonstrated Significant Differences Between Miller-Payne Pathologic Response Groups

Oxygen Desaturation (St) Texture Features

The St-con was significantly different between response groups (p = 0.044); while other features such as St-hom were close to being significantly different (p = 0.058). Features are presented in **Figure 3.12**. St-con measurements were greater in responders (median value: 21.535 A.U.; 95% CI [20.800, 22.940] versus non-responders (median value: 20.306 A.U.; 95% CI

[19.416, 21.436], *p=0.044*). The St-hom approached statistical significance between groups (*p=0.058*) and other features such as St-cor and St-ene were not statistically different between response groups (*p>0.05*).

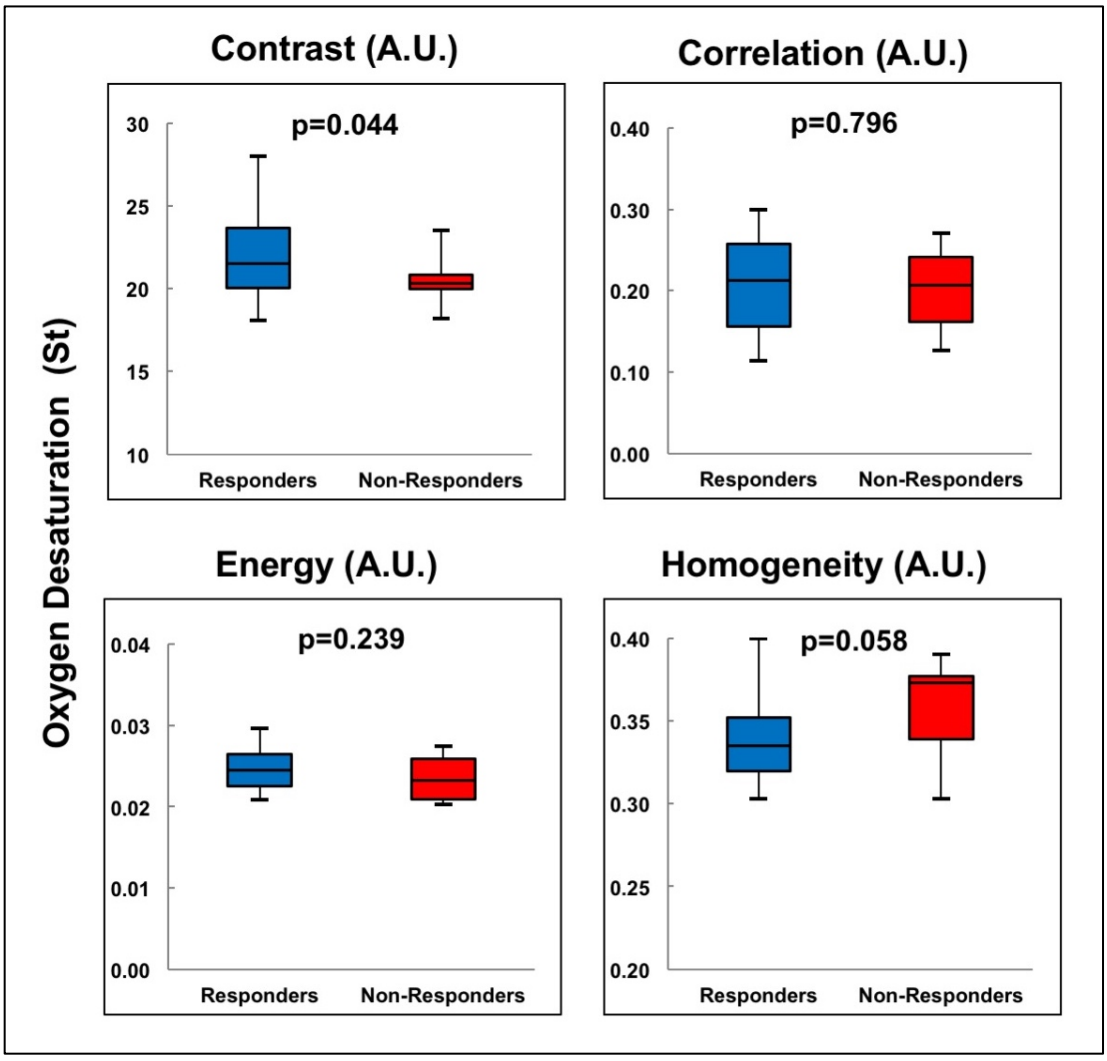

Figure 3.12: GLCM texture features for oxygen desaturation. The St-con was statistically different between response groups (*p=0.044*).

Oxygen Saturation

Tumour oxygen saturation (StO_2) texture features were analysed for significant differences between response groups and showed that only the StO_2-con was significantly different (*p=0.044*) **(Figure 3.13**). The StO_2-con feature was 19.652 A.U.; 95% CI [18.681, 21.067] for responders and non-responders had an StO_2-con value of 21.932 A.U.; 95% CI [20.250-24.010]. Other StO_2 features (StO_2-cor, StO_2-ene, StO_2-hom) were not significantly different between responders and non-responders (*p>0.05*).

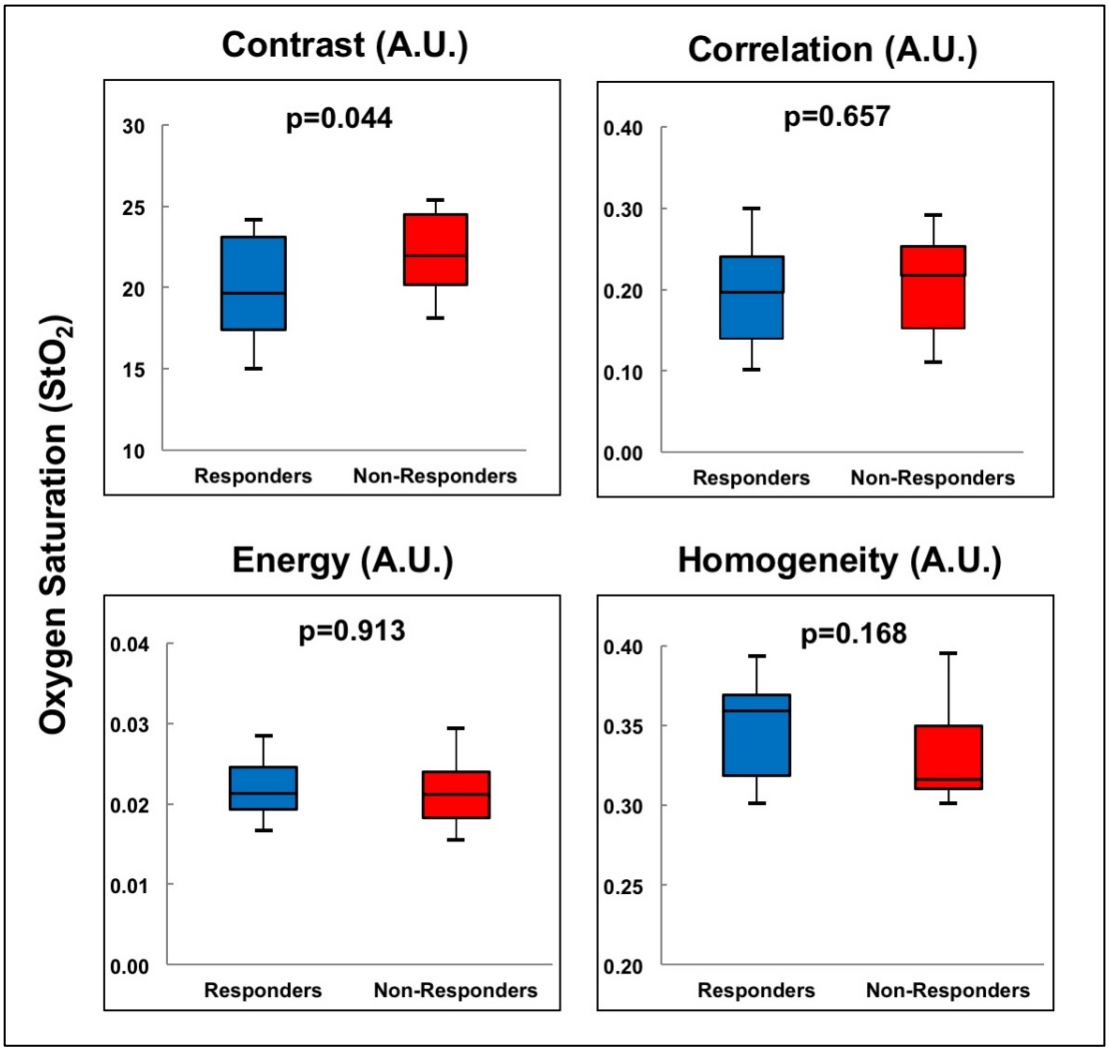

Figure 3.13: GLCM texture features for oxy-haemoglobin texture features. Box-and-whisker plots showing significant differences in DOS textural markers for responders and non-responders (*p* values indicated).

Representative Pre-Chemotherapy DOS Parametric Maps

Representative responder and non-responder pre-chemotherapy DOS images are presented in **Figure 3.14** and **Figure 3.15**, respectively. The corresponding MRI images that were also acquired before treatment are also presented for tumour referencing. Case descriptions are presented below as typical patient pathways for locally advanced breast cancer.

*Responder Patient (Presented in **Figure 3.14**)*

This patient was a 51-year-old woman with right sided breast cancer. At the time of diagnosis her tumour measured 2.2 cm and involved lymph nodes, as indicated from her MRI scan. The breast cancer was hormone receptor positive (oestrogen and progesterone positive), and HER2-negative. Histologically, it was an invasive ductal carcinoma. The patient underwent AC-T chemotherapy (Adriamycin, Cyclophosphamide for four cycles followed by four additional cycles of Taxol). During the course of chemotherapy, the patient showed clinical response (i.e., the tumour was shrinking according to physical palpation). At the time of surgery, the tumour was resected, and pathologic evaluation was completed; the results showed a Miller-Payne pathologic response grade of four (responder), i.e., having greater than a 90% loss of tumour cells.

*Non-Responder Patient (Presented in **Figure 3.15**).*

This was a 38-year-old woman with a large 5.0 cm, left sided breast tumour at the time of diagnosis. Her tumour was “triple negative” (ER-, PR-, HER2-) and was an invasive ductal carcinoma. Her treatment consisted of four cycles of AC (Adriamycin, and Cyclophosphamide), followed by four cycles of Taxol. Her tumour did not respond to chemotherapy, as assessed at the time of surgery. Pathology evaluation of her tumour showed that there was no response to treatment and no overall reduction in the overall cellularity (i.e. Miller Payne grade 1).

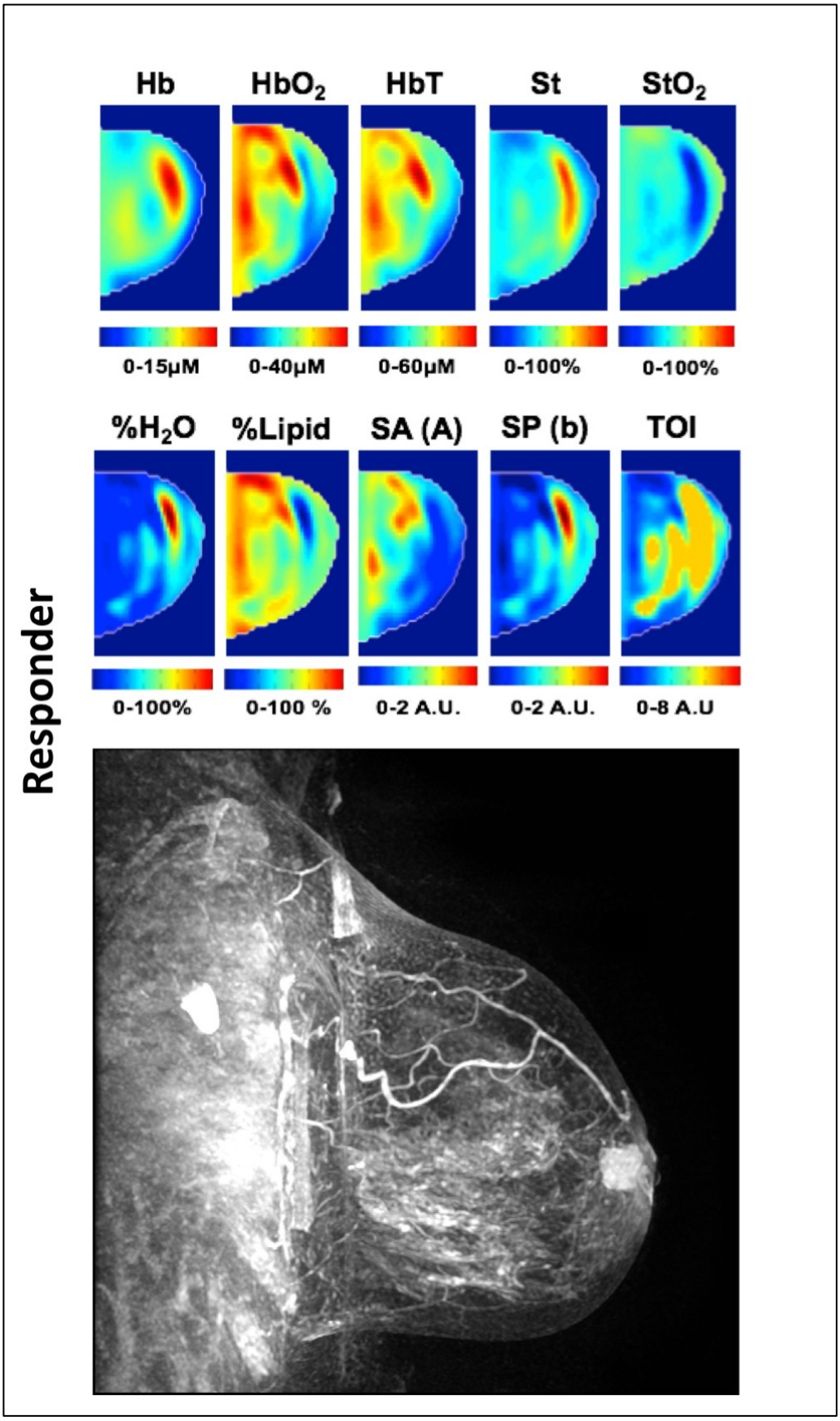

Figure 3.14: Representative DOS parametric maps and contrast-enhanced MRI for a responder, acquired before chemotherapy. All parametric data were acquired and used for texture analyses. Colour washes and colour bars indicate the intensity and concentration of parameters in the image.

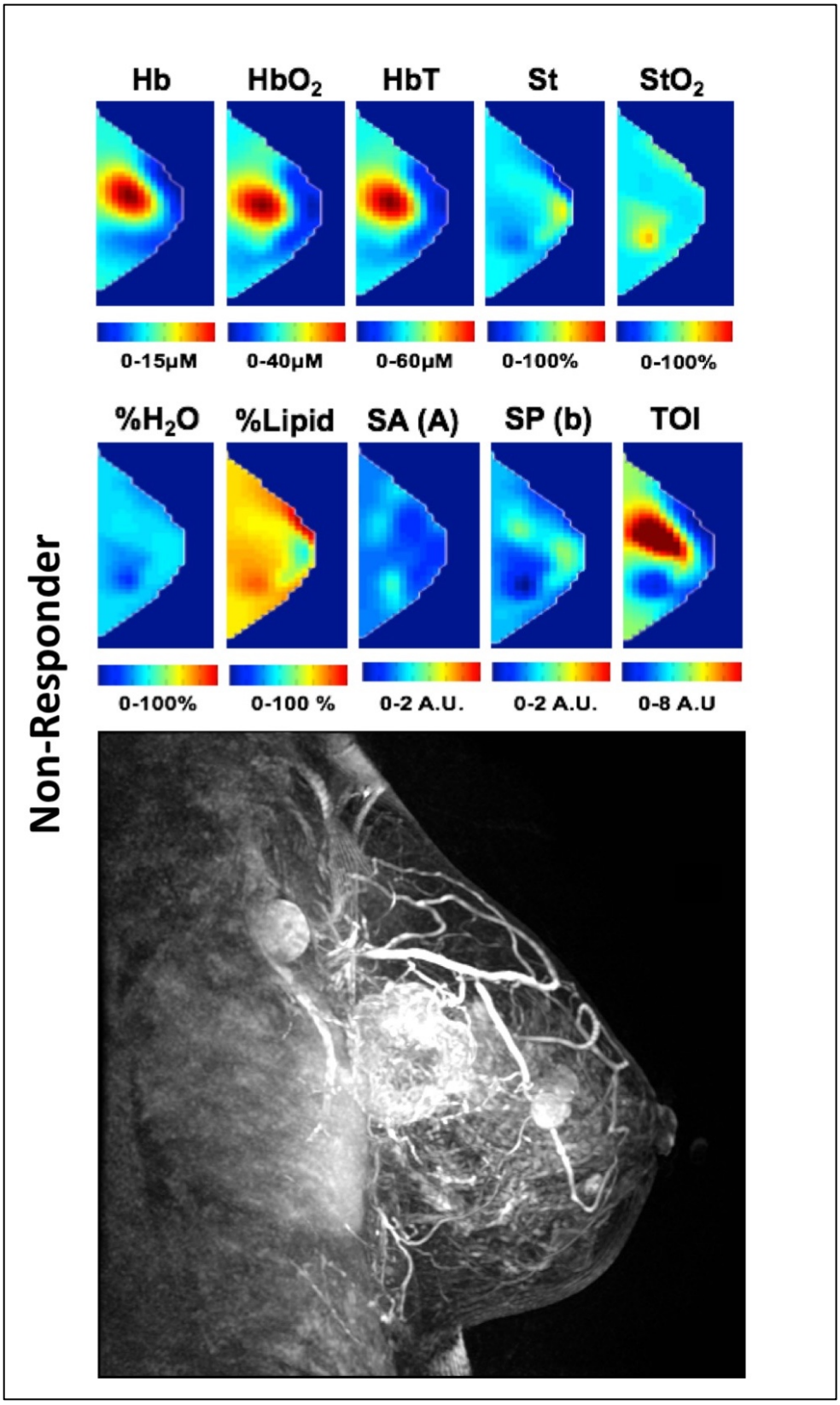

Figure 3.15: Representative DOS parametric maps and contrast-enhanced MRI for a non-responder, acquired before chemotherapy. All parametric data were acquired and used for texture analyses. Colour washes and colour bars indicate the intensity and concentration of parameters in the image.

3.3.5 Overview of Results: Subproject Two, Research Question 2

In this section the results of the following research question are presented: *Can DOS markers predict chemotherapy response before starting chemotherapy?* The results of the section are presented in two sections; 1) classification results for univariate DOS-texture features and; 2) classification results of multivariate DOS-texture features. The models used to predict the classification of patients included a logistic regression model, a naïve Bayes model, and a k-NN model. Results are presented below.

3.3.6 Classification Results of Univariate DOS-texture features

DOS-texture features that were significantly different between response groups (N versus NR) were analysed using the classifier models: Logistic Regression, naïve Bayes and k-NN (**Table 3.8).** The naïve Bayes classification performed the best among the classifier models used in this study. For the HbT-hom, naïve Bayes classification resulted in a sensitivity of 84%, and specificity of 85% (AUC = 0.813), in comparison to k-NN classification which resulted in a classification of only %Sn = 74%, %Sp = 47%, and AUC of 0.552 (**Table 3.8**).

Significant Univariate Feature	Classifier/Model	%Sn	%Sp	AUC	*p*-value	Statistical Power (n_2)
Hb-Homogeneity	Log. Regression	60.0	60.0	0.726	0.030	71.8 (14)
	naïve Bayes	**82.0**	**82.0**	**0.799**		
	k-NN	61.5	67.5	0.577		
HbO_2-Correlation	Log. Regression	70.0	70.0	0.756	0.024	78.9 (11)
	naïve Bayes	**80.0**	**81.0**	**0.778**		
	k-NN	66.5	74.5	0.602		
HbT-Homogeneity	Log. Regression	60.0	60.0	0.657	0.047	79.9 (11)
	naïve Bayes	**84.0**	**85.0**	**0.813**		
	k-NN	74.0	47.0	0.552		
St-Contrast	Log. Regression	60.0	63.0	0.670	0.044	73.5 (13)
	naïve Bayes	**79.5**	**82.0**	**0.779**		
	k-NN	70.5	64.5	0.582		
StO_2-Contrast	Log. Regression	70.0	63.0	0.715	0.044	85.6 (Enough)
	naïve Bayes	**83.0**	**85.5**	**0.803**		
	k-NN	70.0	66.5	0.610		

Table 3.8: Results of univariate analysis using a logistic regression model, naïve Bayes and k-NN classifiers. The bolded-blue values demonstrate the best predictors for each parameter. The numbers in parenthesis indicate the required number of additional patients needed to reach a statistical power of 80%).

Analysis of all DOS-texture features was also performed, independent of statistical significance between groups, using the three classifiers (logistic regression analysis, the naïve-Bayes model, or *k*-NN classifier). However, **Table 3.9** presents the DOS-texture features that demonstrated the highest classification prediction from all possible univariate features (d=40) extracted from each classifier model (i.e. best predictive feature for logistic regression, naïve Bayes, and k-NN).

Classifier Model	Best Predictive Feature of Model	%Sn	%Sp	%Acc
Log. Regression	HbO_2-Correlation	70.0	70.0	70.0
naïve Bayes	HbO_2-Homogeneity	86.5	89.0	87.8
k-NN	HbO_2-Contrast	81.0	73.0	77.0

Table 3.9: Model Prediction Parameters. Summary of best predictive univariate features of each of the classification methods. The corresponding AUCs are presented in **Figure 3.16**.

The corresponding ROC curves with AUCs are presented in **Figure 3.16**. Classification results from significant univariate-texture features indicated an AUC range between 0. 756-0.821 **(Figure 3.16)**. A maximum AUC was observed for HbO_2-hom (AUC = 0.821) using a naïve Bayes model. Cross validated %Sn and %Sp were 86.5%, and 89.0%, respectively and corresponded to an accuracy of 87.8% for the HbO_2-homogeneity feature classified using the naïve Bayes model **(Table 3.9)**.

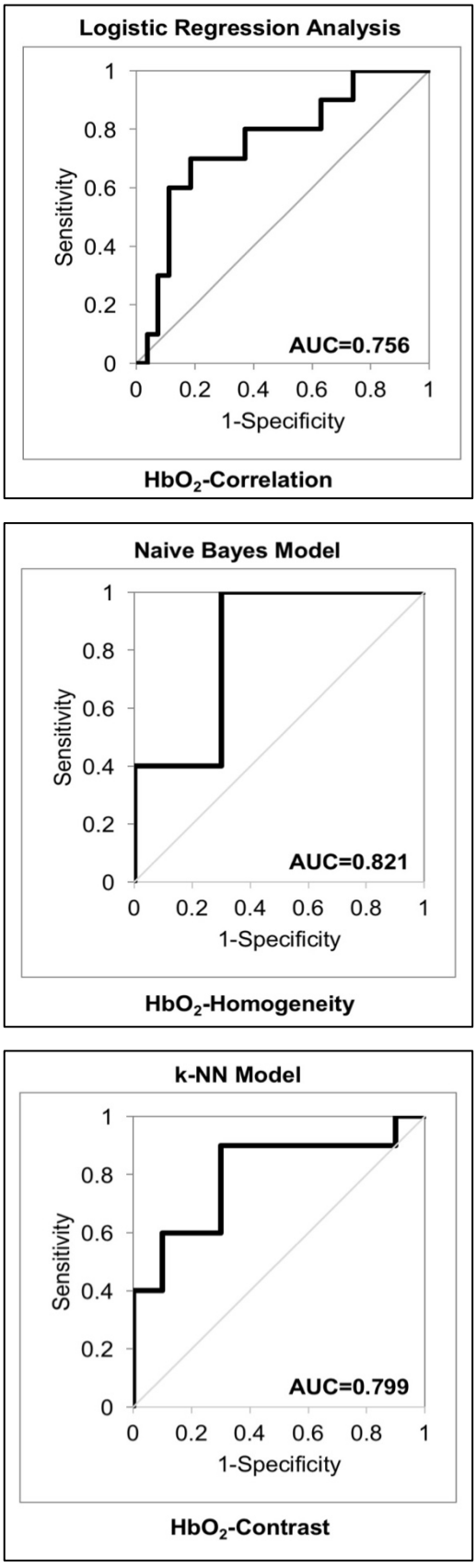

Figure 3.16: Receiver-Operating Characteristic (ROC) curves for univariate DOS-texture features. ROC curves for the best-performing single DOS-texture parameter are presented according to the classification model.

3.3.7 Classification Results of Multivariate DOS-texture features

Table 3.10 presents classification results for the maximum pairwise DOS-GLCM feature combinations. The accuracy of optimal pairwise combinations was 77.8-79.5% for classifying Miller-Payne pathologic responses (responders versus non-responders). Using a logistic regression analysis, the combination of HbO_2-cor + Hb-hom demonstrated a sensitivity of 80%, and specificity of 78.0%. This corresponded to an AUC of 0.815, and an accuracy of 79.5%. In comparison to the naïve Bayes model, the optimal pairwise combination was observed using Hb-con + HbO_2-hom, which indicated a sensitivity and specificity of 78.0%, and 81.0%, respectively. The AUC for these combined parameters was 0.773, and the accuracy was 79.5% **(Figure 3.17 and Table 3.10)**. Lastly, using the *k*-NN classifier, the best pairwise combination resulted from Hb-cor, and HbO_2-con, which showed a sensitivity and specificity of 79.5%, and 76.0%, respectively. The corresponding AUC was 0.802 and the accuracy was 77.8%.

Multivariate Features	Classifier/Model	%Sn	%Sp	%Acc
HbO_2-Correlation + Hb-Homogeneity	Logistic Regression	80.0	78.0	79.5
Hb-Contrast + HbO_2-Homogeneity	naïve Bayes	78.0	81.0	79.5
Hb-Correlation + HbO_2-Contrast	*k*-NN	79.5	76.0	77.8

Table 3.10: Multivariate Analysis for Optimal DOS-texture Pairwise Combinations. Results of multivariate analysis (using three classification models: Logistic regression analysis, naïve Bayes classifier, and *k*-NN.

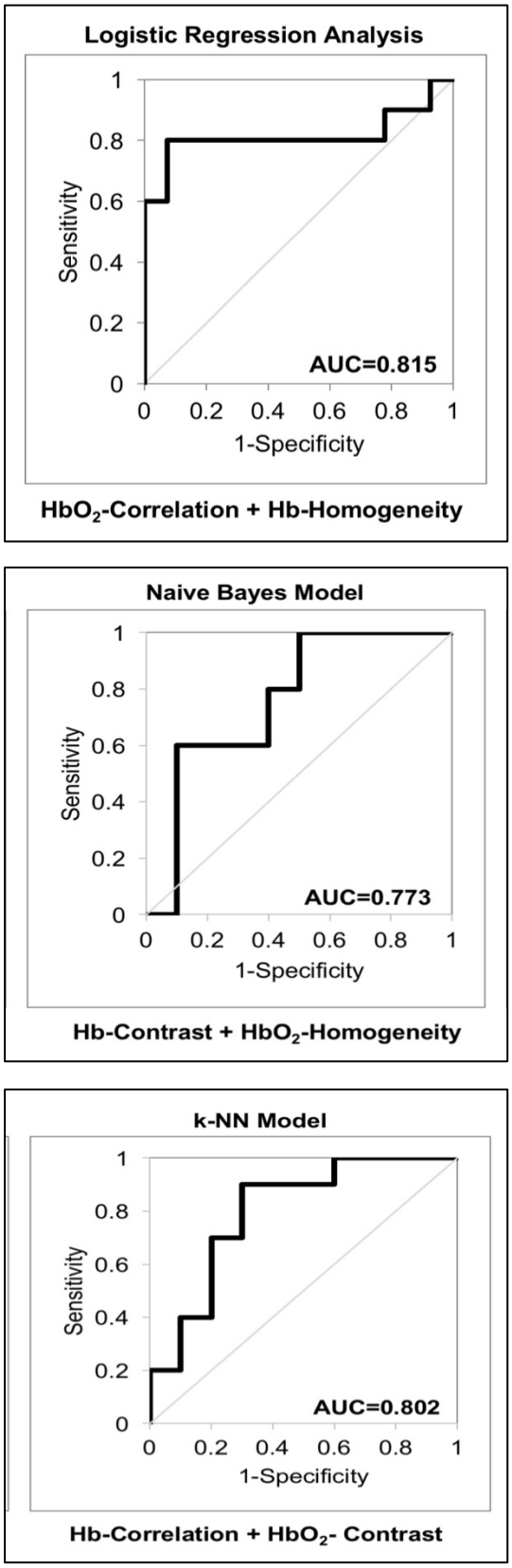

Figure 3.17: Receiver-Operating Characteristic (ROC) curves for multivariate DOS-texture features. ROC curves for the best-performing pairwise DOS-texture parameters are presented.

3.3.8 Overview of Results of Subproject two, Research Question 3

In this section, the results of the following research question are presented: *Are there differences in DOS-texture prediction models for breast cancer subtypes (i.e., ER+ and triple negative) and chemotherapy treatments (i.e. FEC-D and AC-T)?* Firstly, the results of subgroup analysis are presented with respect to each tumour molecular subtype and treatment regimen. The results of this section are presented using a logistic regression analysis, a naïve Bayes classifier and a k-NN algorithm. Secondly, the results from a linear regression model are presented. Here, DOS-GLCM features are tested for correlation to age, molecular and intrinsic subtype, tumour size and final pathological grading (Miller-Payne).

3.3.9 Results of Subgroup Analysis

Subgroup analysis showed that the HbO_2-hom feature was the best predictor in ER+ patients using a naïve Bayes classifier **(Table 3.11)**. For patients with triple-negative tumours, the Hb-hom was the best predictor resulting in an AUC of 0.917 (%Sn=75.0%, 66.7%) using a k-NN classifier. Patients separated according to chemotherapy groups also showed variances in optimal features; FEC-D treated patients classified into responders and non-responders with a sensitivity of 100.0% and specificity of 92.3% using a logistic regression analysis for TOI-hom. Patients treated with AC-T based chemotherapy demonstrated an AUC of 0.896 using the HbO_2-hom feature with k-NN classification (**Table 3.11**).

Subgroup (n=sample size)	Best Feature	Model	%Sn	%Sp	AUC
ER+	Hb-con	Log. Regression	76.2	66.7	0.746
n=27	**HbO_2-hom**	**Naïve Bayes**	**93.3**	**90.1**	**0.883**
	HBO_2-con	**k-NN**	**85.8**	**82.5**	**0.851**
Triple Negative	**Hb-hom**	**Log. Regression**	**100.0**	**33.3**	**0.917**
n=7	Hb-ene	Naïve Bayes	100.0	66.7	0.667
	Hb-hom	**k-NN**	**75.0**	**66.7**	**0.917**
FEC-D	**TOI-hom**	**Log. Regression**	**100.0**	**92.3**	**0.949**
n=16	Hb-con	Naïve Bayes	60.0	81.7	0.722
	Hb-hom	**k-NN**	**80.0**	**80.0**	**0.806**
AC-T	**HbO_2-cor**	**Log. Regression**	**100.0**	**71.4**	**0.837**
n=21	**HbO_2-hom**	**Naïve Bayes**	**96.4**	**90.7**	**0.882**
	HbO_2-hom	**k-NN**	**83.6**	**85.0**	**0.896**

Table 3.11: Subgroup analysis according to molecular subtype and chemotherapy treatment type. Three classification models were used (logistic regression, naïve Bayes and k-NN) and the best predictive features are presented. The best features for each classification model are presented and bolded in blue for those parameters that showed an AUC of greater than 0.80.

3.3.10 Results of Multiple Linear Regression Analysis

The results of the multiple linear regression demonstrated insignificant correlations between clinical features (Age, ER/PR status, HER2 status and tumour size) and DOS-GLCM features for this patient cohort. In particular, the Hb-hom, HbO2-cor, and StO_2-con features demonstrated significant correlations to Miller-Payne grading, corresponding to a regression coefficient value (r) of -0.358, +0.375 and -0.325 respectively ($p<0.05$). Results of the multiple regression analysis are presented in **Table 3.12**.

DOS-GLCM Feature	Comparison	r	F Value	P Value
Hb-Homogeneity	Age	-0.130	0.599	0.444
	ER/PR Status	-0.087	0.267	0.608
	HER2 Status	-0.104	0.382	0.540
	Tumour Size	+0.231	1.967	0.170
	Miller-Payne Grade	**-0.358**	**5.137**	**0.030**
HbO_2-Correlation	Age	-0.116	0.475	0.495
	ER/PR Status	-0.003	0.000	0.988
	HER2 Status	-0.109	0.418	0.522
	Tumour Size	-0.295	3.335	0.076
	Miller-Payne Grade	**+0.375**	**5.172**	**0.022**
HbT-Homogeneity	Age	-0.142	0.715	0.403
	ER/PR Status	+0.007	0.002	0.969
	HER2 Status	+0.206	1.544	0.222
	Tumour Size	+0.085	0.257	0.616
	Miller-Payne Grade	-0.233	2.015	0.165
St-Contrast	Age	-0.231	1.972	0.169
	ER/PR Status	+0.056	0.111	0.741
	HER2 Status	+0.095	0.322	0.574
	Tumour Size	-0.164	0.971	0.331
	Miller-Payne Grade	+0.177	1.138	0.293
StO_2-Contrast	Age	-0.083	0.241	0.626
	ER/PR Status	-0.074	0.190	0.665
	HER2 Status	-0.213	1.661	0.206
	Tumour Size	+0.279	2.966	0.094
	Miller-Payne Grade	**-0.325**	**4.140**	**0.050**

Table 3.12: Regression coefficients (r) of the multiple regression analysis for DOS-GLCM features and corresponding regression F-value are presented. Significantly correlated features are bolded in blue.

3.3.11 Summary of Results and Responses to Research Questions (Subproject two)

Employing texture-based analyses of the DOS parameters showed significant differences in haemoglobin- and oxygen saturation-texture features using a grey-level co-occurrence matrix algorithm (GLCM features: contrast, correlation, energy and homogeneity). Three classification methods were used to analyse data which included a logistic regression analysis (LRA), naïve Bayes classifier, and k-NN algorithm. Both univariate and multivariate models were considered. The results of subproject two are summarized according to the research questions below:

- ***Research Question 1:*** *Do breast tumours demonstrate significant differences in DOS-texture parameters between responders and non-responders, as measured before chemotherapy?*

Texture analysis was completed on all DOS parameters using grey-level co-occurrence (GLCM) algorithm, which included the following texture features: contrast, correlation, energy and homogeneity. Texture analysis of the following DOS parameters were carried out: deoxy-haemoglobin, oxy-haemoglobin, total haemoglobin, oxygen saturation, oxygen desaturation, lipid content, water content, scattering power, scattering amplitude, and the tissue optical index. The results showed that LABC tumours demonstrated significant differences in the following DOS-texture parameters between responders and non-responders, as measured before chemotherapy: deoxy-haemoglobin-homogeneity, oxy-haemoglobin-correlation, total haemoglobin-homogeneity, oxygen desaturation-contrast, oxygen saturation-contrast.

- ***Research Question 2:*** *Can DOS markers predict chemotherapy response prior to starting chemotherapy?*

The results of the subproject two study demonstrated that the pre-chemotherapy DOS-texture parameters demonstrated high sensitivity and specificity for predicting Miller-Payne pathologic response endpoints. The best

DOS-texture univariate model (predictor) was the HbO2-homogeneity feature using the naïve Bayes classifier; the sensitivity, specificity and accuracy was 86.5%, 89.0% and 87.8%, respectively. The best multivariate (pairwise) DOS-texture models were the following: HbO_2-Correlation + Hb-Homogeneity (%Sn=80.0%, %Sp=78.0%, %Acc=79.5%) and Hb-Contrast + HbO_2-Homogeneity (%Sn=78.0%, %Sp=81.0%, %Acc=79.5%).

- ***Research Question 3****: Are there differences in DOS-texture prediction models for breast cancer subtypes (i.e., ER+ and triple negative) and chemotherapy treatments (i.e. FEC-D and AC-T)?*

Within each subgroup, as analysed by tumour molecular features and the treatment regimen, prediction models demonstrated that there were varying optimal DOS-texture features as surrogate markers for Miller-Payne pathologic endpoints. The ER+ subgroup showed that the naive Bayes classifier using the HbO_2-hom feature yielded an optimal AUC of 0.883. Triple negative (i.e. basal-like) patients (ER-/PR-/HER2-) had a maximum AUC of 0.917 using the Hb-hom feature, modelled with a logistic regression. Patients treated with varying chemotherapies showed differences in the best prediction models; FEC-D patients optimal prediction results with the TOI-hom feature using a logistic regression (AUC=0.949); whereas, AC-T treated patients showed maximum results using the HbO2-hom feature with the k-NN algorithm (AUC=0.896).

Chapter 4

Discussion

4.0 Chapter Overview

Chapter 4 highlights the results of the study with a discussion of the significance of DOS and QUS measurements for breast tumour response evaluation to chemotherapy. This chapter is divided into seven sections. In the section one (**Section 4.1**), a thesis overview is presented to outline the research aims and underscore the clinical motivations behind the study. In section two (**Section 4.2**), the results are compared to previous research from diffuse optical spectroscopy and quantitative ultrasound spectroscopy studies. Further to this, a summary of the new contributions to knowledge from this thesis are discussed. In section three (**Section 4.3**), a discussion of DOS and QUS markers are examined with respect to the translational challenges, i.e. the present status of DOS and QUS imaging biomarker research and the steps needed for data validation before it can be implemented into the oncology clinic. Concepts such as, imaging biomarker statistical modelling and the translational gaps of current and previous studies are discussed. In **Section 4.4**, the potential impact to patient care is discussed in terms of using DOS and QUS imaging biomarkers as a treatment decision-making tool by physicians. In **Section 4.5** and **Section 4.6**, the limitations of the study and future work for DOS and QUS in breast cancer imaging are discussed, followed by the final conclusions to the study in **Section 4.7**.

4.1 Summary of Thesis and Study Motivations

In this thesis, DOS and QUS imaging were studied to address two significant clinical problems for breast cancer patients treated with neoadjuvant chemotherapy:

1. Breast cancer response to chemotherapy is variable and this negatively impacts subsequent treatment options and survival for patients. New technologies, preferably non-invasive imaging would be advantageous in the clinic to guide clinicians and inform patients about the most appropriate treatment based on early-response biomarkers for the presumed pathological outcomes.
2. Breast tumours are biologically heterogeneous; even so, a standard "one-size-fits-all" chemotherapy regime is given to patients. As patients respond to treatment in different ways, the overall effect of chemotherapy is that of variability in the treatment response outcomes. Predictive markers are needed before the start of treatment to determine if the tumour is likely to respond favourably (tumour regression) or not, in which case the response to chemotherapy would be considered unfavourable.

The uncertainties surrounding tumour responses to chemotherapy presents a real clinical problem, for the clinician as well as for the patient receiving the treatment, for their survival outcome will be determined by the chemotherapy's efficacy. In this study, the first approach to unravelling this treatment response uncertainty was to develop a framework for study and to begin with a systematic review of the literature; examining previous imaging methods, outcomes and research gaps from comparable studies using imaging biomarkers to measure breast tumour response to neoadjuvant chemotherapy. The results of the literature review yielded 194 reports that had included MRI, PET, CT, conventional X-Ray and ^{99m}-Tc imaging modalities as imaging options to measure the biological and functional activities of breast tumours treated with neoadjuvant chemotherapy. Those studies showed variable accuracies for testing tumour response using imaging (AUC range=0.59-1.00). The major limitations of previous studies included heterogeneities in the patient population, limited analyses completed in tumour subtypes, variable response endpoints

(i.e., radiological endpoints versus pathology endpoints) and differences in the statistical methods to discriminate responders and non-responders. Technical limitations included imaging systems such as MRI and CT that are costly, require invasive procedures (i.e. injection of contrast agents) and the limited repeatability and reproducibility of results between studies. However, the literature search also indicated that there were two major hallmarks of chemotherapy response mechanisms in tumours that could be detected using imaging: 1) QUS imaging biomarkers, previously shown to measure the rate of apoptotic cell death in cancer cells and; 2) DOS imaging biomarkers, shown to measure the changes to the tumour physiology, such vascular density and tissue composition (Czarnota et al., 1999, Cerussi et al., 2011). Research has also suggested that both DOS and QUS imaging may help identify the changes in the tumour's structural matrix during tumour response to chemotherapy. Therefore, the study here, aimed to combine these markers and map out statistical models using DOS and QUS to measure chemotherapy response. Therefore, the motivation of this study was to investigate the tumour response to chemotherapy using DOS and QUS and explore their role as putative biomarkers of tumour response mechanisms. In this thesis, two approaches were used to address the following two overarching research questions:

1) Can DOS and QUS imaging biomarkers be modelled to monitor chemotherapy response in breast cancer at early times after initiation of treatment intervals (i.e. after one or two cycles of chemotherapy)?
2) Can pre-treatment DOS imaging be used to predict chemotherapy response before the initiation of treatment?

To address the first research question (i.e. subproject one), patients were imaged at several time intervals during chemotherapy: before the start of chemotherapy (i.e. baseline), then at week one, week four, week eight during chemotherapy, and one week before surgery. Locally advanced breast cancer patients demonstrated for the first time, coincident changes in the DOS and QUS imaging biomarkers during neoadjuvant chemotherapy. Univariate and multivariate analyses indicated good sensitivity and specificity as early as one week after the start of chemotherapy. The results of the first study (subproject one) indicated that markers of apoptotic cell death could be identified using QUS imaging and were associated with a decrease in tumour haemoglobin

markers on DOS imaging. The results suggested that QUS cell death markers (i.e. ΔSI) increased in responsive tumours which was temporally aligned with a decrease in the haematological parameters (Hb, HbO_2, HbT), as measured by DOS. In the multivariate analyses conducted in the first subproject, the combination of DOS and QUS imaging markers provided a greater number of imaging signatures that could be used to measure early-responses in breast tumours; for example, after one week after initiating chemotherapy (i.e., one cycle of chemotherapy), there were seven DOS-QUS imaging signatures that classified tumour responses compared to only three univariate DOS or QUS parameters at the same time interval.

In subproject two of the study, *pre*-treatment DOS images were studied to predict the pathological response (i.e. Miller-Payne grade) to neoadjuvant chemotherapy. Here, LABC patients were imaged before treatment to measure the tumour's physiological features such as, oxygenation, haemoglobin content and tissue composition (lipids and water content). DOS data were analysed using a texture analysis approach (GLCM from second-order statistical methods). The results demonstrated that DOS-texture maps of the tumour were significantly different between tumour's responding to chemotherapy (i.e. pathological responders) and non-responders as measured using Miller-Payne pathological response criteria. DOS-texture features showed a high discrimination performance between responders and non-responders using the following classification methods: a logistic regression model, a naïve Bayes machine-learning approach and a k-NN algorithm. Additionally, in subproject two, a subgroup analysis was performed of tumours that were ER+, triple negative and patient groups that received either AC-T or FEC-D chemotherapy. Classification models such as Naive Bayes and k-NN machine-learning algorithms were also useful in discriminating patient responses (i.e. responders and non-responders) before treatment. The results of subprojects one and two suggest a correlation between DOS and QUS imaging biomarkers and the tumour's biological layout. The results of subproject two also indicated that the pre-treatment DOS parameters can be used to predict breast tumour response to chemotherapy.

4.2 Comparison to Previous DOS and QUS Studies

4.2.1 Overview

The results presented in the thesis agree with previous reports that show a strong correlation between tumour biology, breast cancer response to chemotherapy, and imaging biomarkers obtained from DOS and QUS imaging. It has been shown that the tumour's biological composition, as measured by DOS and QUS, over the course of chemotherapy or before treatment, can be used as early-response, or predictive markers to pathological endpoints as measured by Miller-Payne pathologic response criteria. Underpinning these criteria, are a series of biological characteristics; haematological features, changes in tissue parameters (i.e., interstitial fluid (water content), lipid measurements and tumour cellularity).

Of the 16 DOS studies identified in Chapter 1 (Literature Review), four studies demonstrated predictive DOS markers using various physiological measurements and one study showed that both predictive and early-response DOS markers were correlated with pathologic endpoints (various endpoints were used across several studies). The remaining 11 DOS studies reported significant differences between responders and non-responders during treatment. For QUS only, one study (Taddayyon et al. 2017) showed that QUS *could* be used to predict treatment response before starting chemotherapy; while the remaining five studies reported that QUS imaging biomarkers could be used as markers for final pathological outcomes[21]. The present study (subproject one of this thesis) demonstrated for the first time, that there were coincident temporal changes in the DOS parameters with QUS imaging markers. It was also shown that DOS and QUS parameters could be used to measure intra-treatment changes in the tumour as a link to the patient's treatment response. Also, for the first time, this was completed using a

[21] Pathologic response endpoints in these previous QUS studies were either systematically assessed (i.e. Miller-Payne pathologic response criteria) or by using non-systematic evaluation (assessment from pathologist based cellular features and identification of residual cancer cells).

systematic pathological response criteria endpoint and here, the Miller-Payne pathological response grading system was used.

The work in subproject two in this thesis used a novel technique by employing a GLCM analysis (i.e. texture) to the tumour-only ROI of baseline (pre-treatment) DOS images. The pre-treatment DOS-texture features were analysed and showed a correlation to Miller-Payne pathological response in patients with locally advanced breast cancer. A discussion about this present study, in comparison to other major DOS and QUS works is presented in the following sections.

4.2.2 Comparisons to other DOS Studies

Previous DOS studies have confirmed that there are significant biophysical and biochemical alterations in breast tumours during chemotherapy that can be optically measured (Enfield et al., 2009). Additionally, previous results have shown that the tumour's biochemical composition, as measured by DOS before treatment, can be used to predict chemotherapy response in tumours, as measured either by radiological or pathological endpoints. However, this present study is unique from previous DOS studies in terms of using volumetric tumour analysis, GLCM-texture analysis in pre-treatment DOS images, using a systematic pathological response criteria and machine learning algorithms for predicting tumour response. This following section compares the results of the present study and previous DOS studies. A summary is presented at the end of the section, in **Table 4.1A, B, C**.

Comparison of DOS-measured Haemoglobin Content

One significant alteration in the biology of the tumour during and after treatment includes significant reductions in haemoglobin content in tumours responding to chemotherapy. These alterations represent a diminution in the vascular density and the decreased metabolic activity of tumours (Roblyer et al., 2011). Thus, the reductions in deoxy-haemoglobin, oxy-haemoglobin and the total haemoglobin can be strong indicators for chemotherapy response. Several studies have indicated that these changes occur early, after the initiation of treatment. Roblyer et al. (2011) reported an "oxy-haemoglobin flare"

in responsive tumours with an increase of 38% in HbO_2 compared to non-responders within the first 24 hours (*p<0.0001*) (Roblyer et al., 2011). The data also showed a significant change in the HbO_2 up to seven days after the start of chemotherapy for responders (Roblyer et al., 2011). When whole-breast parametric haemoglobin maps were analysed using texture analysis, Sadeghi-Naini et al. (2015) showed that the oxy-haemoglobin, deoxy-haemoglobin, and the total haemoglobin parameters could discriminate treatment responses with high sensitivities and specificities (80%-100%) within the first week of treatment (Sadeghi-Naini et al., 2015). Cerussi et al. (2007) previously reported a significant difference in haemoglobin content between responders and non-responders after 7 days of initiating chemotherapy. The relative (normalized) differences in deoxy-haemoglobin between responders and non-responders were 0.73 ± 0.17 and 1.02 ± 0.05, respectively, and the oxy-haemoglobin measured 15% less in responders compared to non-responders at the same time interval (Cerussi et al., 2007). By comparison, the data from the present study supports previous work demonstrating a significant difference in the haemoglobin content between responders and non-responders (*p<0.01*). However, it should be noted that in the present study, the oxy-haemoglobin content for non-responders increased to $110.7\% \pm 5.4\%$ after 7 days and this contrasts with a previous report by Cerussi et al. (2007) where increases in Hb (but not HbO_2) were shown. This is possibly explained by differences in the metabolic activity of tumours, as the rate by which the HbO_2 converts to Hb during tumour activity (and metabolism) within the first week of therapy.

The haematological differences between responders and non-responders are also evident after chemotherapy. The results from several studies have indicated a significantly higher haemoglobin content in patients who did not achieve pathological complete response (pCR) compared to those patients who had chemoresistant tumours (Cerussi et al., 2011). Cerussi et al. (2011) showed that the deoxy-haemoglobin concentration significantly differed in pCR patients compared to non-pCR patients. The relative changes were a 1.01-fold in increase in pCR compared to a 1.32-fold increase in non-pCR patients (*p<0.05*); suggesting that a lower vascularity is associated with better pathologic response to chemotherapy. Similar trends were also observed for oxy-haemoglobin after therapy and showed a 20% lower value in pCR patients compared to non-pCR patients (Cerussi et al., 2011). A comparable report by

Soliman et al. (2010) and Falou et al. (2012) showed a reduction in haemoglobin parameters, however there was a notable difference in the measured values and thus showed that there was a greater reduction in haemoglobin measured at the end of chemotherapy compared to other groups. Responders' deoxy-haemoglobin concentration reduced to 20%-25% of the baseline value (i.e. an ~80% reduction); while the oxy-haemoglobin dropped considerably more to only 5% of the baseline value (Soliman et al., 2010). By contrast, although there was a change in the haemoglobin in non-responders, those changes were statistically insignificant (Falou et al., 2012, Soliman et al., 2010). The results in this present study (subproject one of thesis) agreed with reports by Falou et al. (2012) and Soliman et al. (2010). In this thesis, a significant reduction in haemoglobin was also observed after therapy and in general, responders had a lower tumour haemoglobin concentration compared to non-responders. Tumour deoxy-haemoglobin was reduced to 25.39% $\pm$ 4.50% in responders compared to non-responder tumours which showed a greater relative concentration of 82.99% $\pm$ 7.87%. Similarly, oxy-haemoglobin was 10.46% $\pm$ 2.57% for responders and non-responders had a relative concentration of 84.87% $\pm$ 7.63%. Total haemoglobin at the end of chemotherapy was 13.85% $\pm$ 2.11% in responders and 84.36% $\pm$ 6.83% in non-responders. Although the measured haemoglobin concentrations varied between studies, it is important to note that there were similar trends observed in terms of an overall reduction in responders and insignificant changes in non-responders after starting therapy.

Some exploratory studies have indicated that pre-treatment DOS markers were good predictors for tumour response. Zhu et al. (2013) used the pre-treatment HbT measurements and the data showed that the AUC reached as high as 0.87, which was a strong predictor to pathologic endpoints (Zhu et al., 2013). Similarly, data from Jiang et al. (2014) showed that the pre-treatment HbT was significantly different between responders and non-responders; also showing that the HbT was a strong predictor for treatment response (AUC=0.92) (Jiang et al., 2014). Other DOS studies that examined the pre-treatment haemoglobin content did not show a significant predictive value at the pre-treatment time interval (Sadeghi-Naini et al., 2015). In comparison to these other studies, the average haemoglobin measurements from tumours did not demonstrate a significant result in this study. However, by

employing texture analysis to the parametric maps of tumours, a significant difference was observed between responders and non-responders using the deoxy-haemoglobin-homogeneity (*p=0.030*), the oxy-haemoglobin-correlation (*p=0.024*) and the total haemoglobin-homogeneity (*p=0.047*) parameters. To our knowledge, only one other study to date has used texture-based techniques to analyse DOS data for breast cancer response to chemotherapy (Sadeghi-Naini et al., 2015). In this previous study by Sadeghi et al. (2015), the baseline haemoglobin content did not demonstrate a significant difference between groups before chemotherapy (i.e. pre-treatment). An important difference between this study and the previous work from colleagues at the University of Toronto include differences to their analysis approach. Specifically, their work involved whole breast ROIs; whereas here, textural features were analysed within the parametric maps of tumours only (i.e. tumour-only ROI) (Sadeghi-Naini et al., 2015, Tran et al., 2017). Here, it is also reported that multivariate analysis using DOS-texture features demonstrated an increase in the predictive accuracy using DOS-haemoglobin parameters. The best combination feature sets yielded an accuracy of 79.5% from the GLCM-deoxy-haemoglobin and oxy-haemoglobin parameters. Comparable studies that used multivariate DOS features were conducted by Cerussi et al. (2007) and Sadeghi-Naini et al. (2015). Cerussi et al. (2007) used a discriminant function to predict treatment outcomes from multivariate DOS features. Their analysis yielded an accuracy of 100% after one week of treatment (Cerussi et al., 2007) from the deoxy-haemoglobin using binary DOS feature sets. Similarly, Sadeghi-Naini et al. (2015) used multivariate texture features and showed a significant result after one week.

Comparison of DOS Tissue Composition Parameters

Tissue composition parameters included %Lipids, %Water, TOI, oxygen saturation (StO_2) and oxygen desaturation (St). In the present study, analysis of the absolute DOS parameters, %Lipids, TOI, oxygen saturation and oxygen desaturation demonstrated a significant difference (*p<0.01*) between responders and non-responders after the second cycle of chemotherapy (week four) and up to the pre-operative time-point (*p<0.01*). The %Water was significantly different between response groups after week four, and at pre-

surgery. However, at week eight the water content only approached significance (*p=0.062*) between groups. The research here also analysed tissue composition parameters at baseline (pre-treatment) using a GLCM algorithm. Responders and non-responders had a significant difference in the baseline oxygen saturation-contrast (*p=0.044*) and the oxygen desaturation-contrast (*p=0.044*). In terms of classification results, univariate discriminant analysis of the absolute DOS parameters performed well at classifying responders from non-responders after four weeks of treatment. The best DOS feature was the %Lipids which showed an AUC of 0.982. For all time intervals, the maximum AUC was observed again in the %Lipids parameter after chemotherapy was completed (pre-surgery) (AUC=1.00). Other analyses included studying the textural features of baseline oxygen saturation and oxygen desaturation parameters. The results showed that the oxygen-saturation-contrast was a good marker for pathologic response before chemotherapy (AUC=0.803; %Sn=83.0% and %Sp=85.5%).

In comparison to other reports, the measured changes in tissue-based parameters, %Water and % Lipid did not agree with the results of two previous studies that measured those parameters during chemotherapy. Cerussi and colleagues showed insignificant differences (*z=0.41*) after one week of treatment for %Water and % Lipid (Cerussi et al., 2007). However, it should be noted that the same group reported a significant difference in the %Water at the end of treatment in a follow up study with a larger patient set (n=36) (Cerussi et al., 2011). Results from the Dartmouth group (Jiang et al. (2009)) reported insignificant differences between response groups for the %Water (*p=0.41*) after four weeks of treatment (Jiang et al., 2009). These results agreed with a previous report by Soliman et al. (2010) that demonstrated an insignificant difference (*p<0.60*) at the same time interval (Soliman et al., 2010). Other parameters such as the TOI (tissue optical index), which is a ratio between the %Water, %Lipids and deoxy-haemoglobin showed similar data trends between this study, compared to others. The present study showed that there were significant changes in the TOI in responsive tumours after four weeks of treatment (*p<0.0001*). These results compliment previous findings from the ACRIN 6691 trial (Tromberg et al., 2016), that showed intra-treatment differences in the TOI between response groups (Tromberg et al., 2016). However, an important distinction in Tromberg et al.'s work included subjects

that were selected based on a StO_2 threshold cut-off (StO_2 >76.9%). Effectively in that study, only tumours that had high baseline oxygen saturation were used in their analysis (Tromberg et al., 2016). Indeed, tumour hypoxia and oxygen-availability has been shown to affect tumour response to cytotoxic agents; i.e. hypoxic tumours are more chemoresistant compared to well-oxygenated tumours (Ward et al., 2013). The intra-treatment changes in tumour oxygen content was correlated to pathologic response in one DOS study (Falou et al., 2012). Data from this small cohort of patients (n=15) showed that the oxygen desaturation (St) of the whole-breast was significantly different ($p=0.0002$) at intra-treatment (four weeks) between responders and non-responders (Falou et al., 2012). Their study also showed that the tumour oxygen saturation (StO_2) of the whole-breast was not significant between response groups ($p=0.1$) after four weeks of treatment and this agreed with a previous study by Jiang et al. (2009) ($p=0.47$).

The pre-treatment analysis in the present study agrees with previous DOS data showing that baseline oxygen saturation can predict chemotherapy response (Ueda et al., 2012, Jiang et al., 2014). Jiang et al. (2014) showed that the pre-treatment StO_2 could reach an AUC of 0.8. Similarly, data from Ueda et al. (2012) were comparable; the tumour StO_2 showed an AUC of 0.72 (Ueda et al., 2012). In their study also, when the StO_2 was modelled with intrinsic molecular features (ER+ and PR+) in a linear discriminant function, the AUC increased to 0.80-0.93 (Ueda et al., 2012).

Data Comparison of Optical Scattering Parameters

Optical scattering parameters included the scattering power (SP) and the scattering amplitude (SA). These features correspond to the size of the scattering particle, relative to the wavelength (Cerussi et al., 2007). Tumours have been shown to have higher optical scattering (i.e. larger scattering power) compared to the surrounding normal tissue and this is due to the complex cellular and stromal organization within the tumour's microenvironment that act as scatterers (Tromberg et al., 2005, Cerussi et al., 2007, Soliman et al., 2010).

In the present study, the scatter power and the scatter amplitude demonstrated a significant difference between response groups after four weeks of treatment ($p<0.01$) and there was a significant decrease in the scatter

power in responders during treatment. This corresponded to a high predictive value (AUC range=0.897-0.982). The results of this study agree with other studies that also showed a significant difference in the scattering power between responders and non-responders; Soliman et al. (2010) reported a 48% difference in the scattering power after four weeks of treatment ($p<0.036$). In the present study, the difference in the scattering power parameter was 34.7% only between groups ($p<0.05$); in comparison to another study by Falou et al. (2012), their data indicated a difference of 35% between response groups after four weeks of treatment ($p<0.046$), which was similar to this present work (Falou et al., 2012). On the other hand, in a study by Jiang et al. (2009), there was no difference in scattering parameters (scatter amplitude and scatter power) after four weeks of treatment, although the scattering power approached significance ($p=0.06$) at this time interval (Jiang et al., 2009). Another study by Cerussi et al. (2007) examined earlier time intervals (i.e. after one week of treatment) in the scattering parameters and there were no significant results, differences in the scattering parameters, which corresponded with the data in this study (Cerussi et al., 2007).

4.2.3 Analysis of Data Variances in DOS

DOS Topography versus Tomography

DOS systems can be built as topography systems (2D-image acquisition) or tomography systems (3D-image reconstructions) which can yield varying DOS datasets (i.e. 2D planar images may carry limited DOS data since only a portion of the tumour is measured, depending on the size). Systems developed by the UC Irvine group (Cerussi, Tromberg, Ueda) and the University of Connecticut (Zhu, Hegde) used handheld topography devices that employs a reflectance geometry (Zhu et al., 2014). Other research groups from Dartmouth University (Jiang, Paulsen, Pogue) and the University of Toronto (Falou, Soliman, Czarnota) used tomographic systems which provide cross-sectional, volumetric DOS datasets of the breast. The differences between the two systems are that one produces 2-D maps (topographic); whereas the other, 3-D maps (tomographic) of the chromophores of interest (i.e. haemoglobin, water and lipids) are constructed.

Hand-held topography devices and DOS tomography systems have their respective advantages and disadvantages. Hand-held systems are portable and are advantageous for imaging lesions in harder-to-reach areas such as the axilla. It uses reflectance geometries that have an average imaging penetration depth of 10-22 mm below the skin surface (Cerussi et al., 2011). As a result, the penetration depth limits the imaging of large locally advanced breast tumours that are bigger than 5 cm in the posterior dimension. Since there are often intratumoural heterogeneities in breast tumours, topography systems are potentially constrained by under-sampling, i.e. the entire tumour volume is not measured due to limited penetration depth or limited field-of-view from the geometry of the imaging device. Thus, errors can arise for tumours with deep posterior margins and the major consequence is that it may not represent the tumour's entire biological properties given the limitations in device geometry. In contrast, tomographic systems provide volumetric data (3-D), for it uses light transport calculations that are captured across the breast tissue (Dehghani et al., 2009). DOS tomography is capable of high imaging contrast and yields more data points; yet the major disadvantage is the coarse spatial resolution (i.e. large voxel sizes) as a result of limitations in reconstructing data from diffuse light propagation in tissue (i.e. greater scattering during light transport across the longer tissue distance) (Dehghani et al., 2009). Given these differences in technology, 2-D versus 3-D DOS imaging can yield varying results and this was apparent between research studies. Analysis conducted by the UC Irvine and University of Connecticut group, who used hand-held 2D-planar imaging demonstrated higher haemoglobin levels at the conclusion of therapy. This may have been caused by measuring only a fraction of the tumour's total bulk volume (i.e. anterior aspect). In those studies, tumour analysis was based on two-dimensional datasets that had a fixed depth and area. In comparison, researchers at the University of Toronto (the present study) and at Dartmouth University used DOS tomography which measured the optical properties of the whole tumour and the entire breast; thus, the chromophore concentrations were based on the sum of measurements in all spatial directions across the entire breast volume in some studies. Measuring the whole tumour (and whole breast) versus a smaller tumour segment may have resulted in the variances in changes at the end of treatment; known as signal "washout". Other contributing factors to data variance include a partial-

volume effect which is the loss of quantitative accuracy based on the DOS resolution (Santago and Gage, 1995, Durduran et al., 2010). The result is an underestimation of the chromophore concentration changes and problems with assigning absolute optical properties within the region of interest (Durduran et al., 2010). The lower haemoglobin values calculated from this present study and other studies by Soliman et al. (2010) and Falou et al. (2012) could have been caused by a partial-volume effect (Falou et al., 2012, Soliman et al., 2010). The partial-volume effect is highly possible given the resolution of the DOS tomography system used here (3 mm x 3 mm) is large in comparison to the size of chromophores (i.e. haemoglobin) (Durduran et al., 2010).

DOS Regions of Interest

An important comparison between research reports involves discussing the methods in selecting the region-of-interest. Indeed, there is great interest in studying the effects of adjusting the size, boundary and computing methods to contour the ROI in DOS data processing and analysis since it can impact the measured and absolute DOS values (Hylton, 2009). Jiang et al. (2009) report results on using two ROI segmentation schemes that compared fixed-sized versus variable-sized ROIs (Jiang et al., 2009). In the first approach, a radiologist selected the ROI with *a priori* knowledge of the tumour's location based on MRIs. The size and dimension of the ROI was kept constant for the duration of the imaging series during the patients' treatment. In the second approach, an automated and computer-assisted method was utilized using the intensity distribution of the DOS image maps. The ROI was determined based on the position of the chromophore's maximum intensity and a contour boundary was calculated around that position for values that were above the half of the maximum value. This method is referred to as the full-width-half-maximum (FWHM) approach (Jiang et al., 2009). In a small dataset (n=7), Jiang and colleagues showed that variable-sized ROIs showed a greater normalized decrease in the total haemoglobin in pCR patients compared to using a fixed-sized ROI ($HbT_{fixed} = -64.2 \pm 50.8$ versus $HbT_{variable} = -96.7 \pm 91.8$) (Jiang et al., 2009).

Another study by Falou et al. (2012) reported results using whole-breast analysis versus volume-adjusted ROIs using tomographic datasets. Whole-breast analysis involved calculating the integrated optical parameters across the entire breast, which included tumour and normal breast tissue. For volume-weighted analysis, the tumour volume was determined by referencing clinical imaging (i.e. MRI, CT) and the ROI was placed manually. The optical parameters were calculated within the region of interest only. The major advantages to whole-breast analysis is that it can be done without any knowledge of the size and location of the tumour and thus mitigates inter-user variability. A major disadvantage however is that as tumours regress during treatment the optical parameters may reflect a greater ratio of breast to the tumour optical properties, thus "washing out" the tumour optical measurements. Falou et al. (2012) showed a significant difference in optical properties between whole-breast analysis and volume-weighted analysis. Measuring the deoxy-haemoglobin in responders after four weeks of treatment showed a reduction to 32% $\pm$ 7% for volume-weighted ROIs; while whole-breast ROIs showed an increase of 114% $\pm$ 6% relative to the baseline concentration (Falou et al., 2012). These studies demonstrated that ROI placement and contouring methods have a significant impact on the reported optical properties in tumours. Importantly, other tissue composition features such as %Lipids demonstrated insignificant changes over the course of treatment and did not discriminate responders and non-responders. This could be explained since breast tissue is highly composed of adipose tissue which could "wash out" any measurable changes in the tumour.

Schaafsma et al. (2015) showed that displacing the ROI by 5 mm could result in a 2% change in the deoxyhaemoglobin and oxy-haemoglobin measurements for tumours that are 30 cm^3 and an 8% change for tumours approximately 5 cm^3. Their data suggests that smaller tumour sizes (either on initial presentation or regressing from treatment) are susceptible to greater variability depending on the ROI placement (Schaafsma et al., 2015). This phenomenon may explain some of the data variability in the haemoglobin changes at the end of treatment since tumour dimensions are generally smaller (for responsive patients) and therefore positioning the ROI around these smaller lesions may cause variability; caused also by the lower resolution of DOS images.

Summary of Comparisons of DOS Studies to Thesis	Specific Features		DOS Studies						
			Thesis Study	Cerussi et al. (2007)	Zhu et al. (2008)	Jiang et al. (2009)	Soliman et al. (2010)	Cerussi et al. (2011)	Pakalniskis et al. (2011)
Wavelength (nm)	Near Infrared (600-1100)		x	x	x	x	x	x	x
Image Type	Topographic (2D)			x	x	x		x	
	Tomographic (3D)		x				x		x
ROI Analysed	Tumour		x	x	x	x	x	x	x
	Whole-Breast								
Time Measures	Pre-Treatment		x		x	x		x	x
	Intra-Treatment			x	x	x	x	x	
Imaging Parameters Studied	Haemoglobin		x	x	x	x	x	x	x
	Oxygen Saturation		x	x		x			
	Tissue Parameters		x	x		x	x	x	
	Scattering Parameters		x	x		x	x		
	GLCM-Textures		x						
Tumour Parameters	ER/PR		x		x	x	x		x
	HER2		x		x	x	x		x
	Triple Negative		x		x		x		x
Multimodalities	Other biomarkers		x						
Classification Models	Logistic Regression		x						
	Linear Discriminant			x					
	Machine Learning	k-NN	x						
		SVM							
		N. Bayes	x						
		Others							
	Univariate Models		x	x					
	Multivariate Models		x	x					
Tumour Response Endpoints	RECIST 1.1 (Radiology)								
	Miller-Payne (Pathology)		x		x				
	Residual Cancer Burden								
	NSABP Protocol								
	Other Radiological							x	
	Other Pathological			x		x	x	x	x

Table 4.1A. Summary of comparisons between DOS studies. A significant difference between the present study (thesis) and previous studies include using GLCM-texture analysis on baseline DOS parameters. *Yellow boxes represent the major differences and limitations of previous studies.*

Summary of Comparisons of DOS Studies to Thesis	Specific Features		DOS Studies 'cont (2)						
			Roblyer et al. (2011)	Falou et al. (2011)	Ueda et al. (2012)	Zhu et al. (2013)	O' Sullivan et al. (2013)	Jiang et al. (2014)	Schaafsma et al. (2015)
Wavelength (nm)	Near Infrared (600-1100)		x	x	x	x	x	x	x
Image Type	Topographic (2D)		x		x		x		
	Tomographic (3D)			x		x		x	x
ROI Analysed	Tumour		x	x	x	x	x	x	
	Whole-Breast			x					
Time Measures	Pre-Treatment				x	x		x	
	Intra-Treatment		x	x			x	x	
Imaging Parameters Studied	Haemoglobin			x	x	x	x	x	x
	Oxygen Saturation		x	x	x	x	x	x	
	Tissue Parameters			x			x	x	
	Scattering Parameters			x			x		
	GLCM-Textures								
Tumour Parameters	ER/PR		x	x	x	x		x	x
	HER2		x	x	x	x		x	x
	Triple Negative		x	x	x	x		x	x
Multimodalities	Other biomarkers				x				
Classification Models	Logistic Regression				x	x			x
	Linear Discriminant			x	x			x	
	Machine Learning	k-NN							
		SVM							
		N. Bayes							
		Others							
	Univariate Models			x	x			x	x
	Multivariate Models				x	x			
Tumour Response Endpoints	RECIST 1.1 (Radiology)								x
	Miller-Payne (Pathology)					x			x
	Residual Cancer Burden								
	NSABP Protocol		x						
	Other Radiological						x		
	Other Pathological			x	x			x	

Table 4.1B. Other DOS studies demonstrated significant differences in the classification algorithms used (i.e. machine learning) to predict treatment response. *Yellow boxes represent the major limitations and differences of previous studies.*

Summary of Comparisons of DOS Studies to Thesis	Specific Features		DOS Studies 'cont (3)						
			Sadeghi et al. (2015)	Tromberg et al. (2016)	Ueda et al. (2016)				
Wavelength (nm)	Near Infrared (600-1100)		x	x	x				
Image Acquisition	Topographic (2D)			x	x				
	Tomographic (3D)		x						
ROI Analysed	Tumour			x	x				
	Whole-Breast		x						
Time Measures	Pre-Treatment			x					
	Intra-Treatment		x	x	x				
Imaging Parameters Studied	Haemoglobin		x	x	x				
	Oxygen Saturation		x						
	Tissue Parameters		x	x					
	Scattering Parameters		x						
	GLCM-Textures		x						
Tumour Parameters	ER/PR		x		x				
	HER2		x		x				
	Triple Negative				x				
Multimodalities	Other biomarkers								
Classification Models	Logistic Regression								
	Linear Discriminant		x	x	x				
	Machine Learning	k-NN							
		SVM							
		N. Bayes							
		Others							
	Univariate Models		x	x	x				
	Multivariate Models		x						
Tumour Response Endpoints	RECIST 1.1 (Radiology)								
	Miller-Payne (Pathology)								
	Residual Cancer Burden								
	NSABP Protocol								
	Other Radiological		x						
	Other Pathological		x	x	x				

Table 4.1C: The significant contribution of this thesis includes modelling QUS parameters with DOS features during chemotherapy. *Yellow boxes represent the major limitations and differences of previous studies.*

4.2.4 Comparison of QUS studies

Quantitative ultrasound spectroscopy in breast cancer is a relatively new technique under clinical investigation. Current research is underway for its use in classifying tumour response to treatment and also as a method for identifying malignant and benign breast lesions at diagnosis. To our knowledge, the research group from the University of Toronto is unique in conducting clinical (human) research in breast cancer response to neoadjuvant chemotherapy. Indeed, other researchers have used QUS in the clinical research setting for other aims such as characterizing liver disease (Lu et al., 1999); (Lin et al., 2015); however a large body of this other work is still focused on laboratory and animal-based research.

The previous breast studies presented from the University of Toronto demonstrated promising clinical results; the aims being to acquire both pre-treatment and intra-treatment QUS parameters to measure breast cancer response to chemotherapy. Taking the work of our group forward, the analysis in this thesis aimed to measure intra-treatment QUS changes and to use QUS parameters for combined DOS parametric models; whereas previously our group had included analysis of QUS alone, on both pre-treatment and intra-treatment QUS parameters. The forward innovation here, sought to correlate the biological measurements such as haemoglobin and tissue composition changes with the previous QUS work. Additionally, this work differs from previous intra-treatment QUS studies since now, QUS imaging biomarkers were studied for correlation to a systematic pathological response criteria (i.e. Miller-Payne grading); whereas previously QUS studies have used a non-standard pathological method or relied principally on radiological endpoints. **Table 4.2** outlines the significant differences in methods and approaches between the present study, and previous QUS studies. As indicated from **Table 4.2**. The work here is novel since to date, no other QUS study has included a multiparametric model using other imaging modalities.

In comparing the QUS data only, the results here were consistent with data from Sadeghi-Naini et al. (2013), where there were similar temporal QUS changes observed in responders after four weeks of treatment. Responders also showed a significant increase in the mid-band fit and spectral intercept; whereas non-responders showed insignificant change throughout the course of

treatment (Sadeghi-Naini et al., 2013b). In comparison to the study by Sadeghi et al. (2013), there were two important distinctions in the methods and analysis; the first being a probability density function analysis of the MBF feature. This analysis was carried out by analysing the MBF parametric maps and fitting a generalized gamma (GG) distribution of the MBF intensity histogram for feature extraction (Sadeghi-Naini et al., 2013b). The second, multiparametric QUS-features analysis was performed using combinations of QUS features only. It was shown in their study that the generalized gamma distribution did not improve the accuracy of measuring chemotherapy response at intra-treatment; the sensitivity and specificity of the MBF was 100% and 72.2% at week four, respectively, compared to the 66.7% and 66.7% for the generalized gamma model (Sadeghi-Naini et al., 2013b). Also, by using a multiparametric model (mid-band fit and the 0-MHz intercept), their study showed an improvement in discriminating responses (%Sn=100.0% and %Sp=83.3), compared to using those individual features alone (Sadeghi-Naini et al., 2013b). A follow-up study by the same author used QUS-texture analysis and showed that alterations in the texture features separated responders and non-responders as early as one week after starting chemotherapy (Sadeghi-Naini et al., 2014). This study also showed that QUS-textural biomarkers were significantly correlated to patient survival ($p=0.0007$) (Sadeghi-Naini et al., 2014). By comparison, in this thesis, texture analyses were not completed since the focus here, was to explore the coincidence between mean DOS and QUS biomarkers only. Additionally, survival analysis could not be completed for this patient cohort since the current follow up time is insufficient for long-term analysis (i.e. a minimum of 5-years is typically reported).

Recently, Tadayyon et al. (2016) examined a larger patient cohort (n=58) and expanded QUS analysis to include predictive modelling with acoustic backscatter parameters (Tadayyon et al., 2016). This analysis was developed from a previous study by Sannachi et al. (2015) where 30 LABC patients were studied. The methods included a machine-learning algorithm (k-NN) for tumour-response classification, in addition to modelling intra-treatment and pre-treatment QUS parameters together. The results of that study showed a significant increase in QUS parameters (MBF, SI, ACE) after one week of treatment for responders; however, the diagnostic accuracies were poor for measuring treatment response (%Acc range = 54%-61%). When more than

one parameter was employed (multiparameters), it was shown that the combination of intra- (week one)- and pre-treatment QUS features improved the diagnostic accuracy (%Acc=70.0%) (Tadayyon et al., 2016). It should be noted however that this combination model did not show a significant result after four weeks of treatment. In a subsequent QUS-based study by Tadayyon et al. (2017), pre-treatment QUS parameters were studied further to improve QUS analysis techniques (Tadayyon et al., 2017). There were three important methodological differences to this present study: 1) a modified segmentation scheme of the tumour was used in their study, which included an expansion margin (5-10 mm) around the peritumour region (Tadayyon et al., 2017); 2) molecular tumour markers were used in their predictive models; and 3) machine learning techniques were used for response classification. Their study showed that expanding the ROI margin by 5 mm around the tumour predicted response with an accuracy of 88%; yet including molecular subtypes did not improve the accuracy (%Acc=82%) (Tadayyon et al., 2017). The ROI-expansion technique was not employed in the current study since the scope of the research was to compare coincident DOS and QUS markers of the tumour-volume only. Additionally, the image resolution for QUS is finer compared to DOS; where the in-plane resolution for DOS was 3 x 3 mm^2 and thus an expansion margin would not permit a geometric comparison between DOS and QUS images.

Other QUS studies in breast cancer include a study by Gangeh et al. (2015); where the focus was based on using QUS parameters within the framework of computer-assisted theragnostics (CAT) (Gangeh et al., 2016). CAT is centred around complex machine-learning computations that are used to measure tumour response to therapies (i.e. theragnosis) (Gangeh et al., 2016). It works by implementing pattern-recognition algorithms within a feature space; using attributes or biomarkers, such as those found in QUS parameters, texture features, or morphological tumour characteristics (Gangeh et al., 2016). The scope of that study was primarily exploratory and focused on computational theory that is beyond the scope of the current thesis. In the next section, is a summary of comparisons between this present study and previous QUS studies presented.

4.2.5 Analysis of data variances in QUS Studies

The data variance between the results presented in this thesis and previous QUS reports can be explained by the different methodological approaches used.

Ultrasound Imaging Parameters

Two reports (Tadayyon et al., 2016, 2017) used lower-frequency ultrasound (transducer frequency = 6 MHz, central frequency = 5.5 MHz), compared to the present study that used a transducer frequency of 10 MHz, central frequency = 7 MHz. The differences in ultrasound parameters changes the resolution and thus affects the absolute changes measured in the QUS parameters.

In terms of ROI selection, all studies analysed the tumour volume except for one study by Tadayyon et al. (2017) which used an expansion volume (3-10 mm) around the peritumour region. This method contributed to a better prediction value for pre-treatment QUS parameters based on backscatter co-efficient parameters and spectral parameters. The data variance between this study and the work by Tadayyon et al. (2017) was due to the differences in computing different anatomical volumes. In their study, QUS parameters were calculated on both malignant lesions and the normal breast parenchyma which alters the acoustic scattering measurements.

Parameters of Interest and Modelling Features

All studies but one (Sannachi et al., 2016) reported the linear fit parameters of the power spectrum (MBF, SI, SS). The linear-fit model parameters that were measured in patients for this present study agreed with previous studies in terms of the observed trends and relative changes measured in response groups during chemotherapy. However, there were variances in the predictive values for univariate and multivariate models between studies (sensitivity, specificity, accuracy, AUC) and this was caused from differences in the statistical frameworks used (i.e. classification algorithms used). Univariate and multivariate analysis of the QUS linear-fit parameters

included a linear discriminant function, a logistic regression model and a k-nearest neighbour classification algorithm among studies (Sadeghi-Naini et al., 2013b, Tadayyon et al., 2016). The predictive values are calculated from several factors: 1) the number of variables included into the model; 2) the sample size; and 3) the distribution of data samples. Multivariate models from previous reports have included tumour molecular features and a combination of other QUS features together (Tadayyon et al., 2017, Sadeghi-Naini et al., 2013b)

Summary of Comparisons of QUS Studies to Thesis	Specific Features		QUS Studies						
			Thesis Study	Sadeghi-Naini et al. 2013	Sadeghi-Naini et al. 2014	Sannachi et al. 2015	Tadayyon et al. 2016	Gangeh et al. 2016	Tadayyon et al. 2017
US Transducer Frequency (MHz)	10 MHz (central f = 7 MHz)		x	x	x	x		x	
	6 MHz (central f = 5.5 MHz)						x		x
ROI Analysed	Tumour Volume		x	x	x	x	x	x	x
	Other Volumes								x
Time Measures	Pre-Treatment								x
	Intra-Treatment		x	x	x	x	x	x	
Imaging Parameters Studied (Spectral Analysis)	Linear Fit (MBF, SI, SS)		x	x	x		x		x
	Backscatter coefficient model parameters	ACE					x		x
		ASD				x	x		
		AAC				x	x		
		BSC				x			
		SAS					x		
	GLCM-Textures				x				x
	LBP-Textures							x	
Tumour Parameters	ER/PR		x	x	x	x	x	x	x
	HER2		x	x	x	x	x	x	x
	Triple Negative		x	x	x	x	x	x	
Multimodalities	Other imaging		x						
Classification Models	Logistic Regression		x						
	Linear Discriminant		x	x	x	x			x
	Machine Learning	k-NN					x		x
		SVM							x
		N. Bayes						x	
		Other						x	
	Univariate Models		x	x	x	x	x	x	x
	Multivariate Models		x	x	x	x	x		x
Tumour Response Endpoints	RECIST 1.1 (Radiology)			x			x	x	
	Miller-Payne (Pathology)		x						x
	Other Radiological					x			
	Other Pathological				x			x	

Table 4.2: QUS study comparisons. Significant differences between the present study and previous QUS studies include the methods for spectral analysis (linear fit model compared to backscatter co-efficient model). Other major differences include using concurrent DOS imaging and statistical modelling. Lastly, this study used a systematic approach to pathological response criteria (i.e., Miller-Payne criteria). LBP=local binary pattern. *Yellow boxes represent the major differences and limitations of previous studies.*

4.2.6 Modelling DOS and QUS Parameters as Complementary Response Markers

In the present study, combined analysis was completed for DOS-QUS parameters to measure NAC response at early time intervals in locally advanced breast cancer. To our knowledge, this is the first study that has completed serial and coincident imaging with DOS and QUS in locally advanced breast cancer. The coincident biomarkers measured from DOS and QUS show that there are also coincident cellular, biochemical, haematological and morphological changes with treatment (Jakubowski et al., 2004, Srinivasan et al., 2006, Jiang et al., 2009). Of note, QUS parameters have been demonstrated in tumours that exhibit apoptotic cell death from chemotherapy (Kolios et al., 2002, Sadeghi-Naini et al., 2013b). These DOS and QUS parameters have also been correlated to pathologic characteristics and outcomes (Cerussi et al., 2011, Cerussi et al., 2007, Sadeghi-Naini et al., 2013b, Tadayyon et al., 2014). Previous work by Cerussi et al., (2011) used DOS to measure tumour water content, and tumour haemoglobin concentration at multiple times during chemotherapy treatment (Cerussi et al., 2011). The results of that study indicated a significant reduction in %Water and tumour haemoglobin at the end of chemotherapy when compared to the baseline measurements, and this corresponded to patients who demonstrated pathological complete response (Cerussi et al., 2011). The results in the study here are consistent with their findings and in addition, DOS data is supplemented with QUS biomarkers (MBF, SI) that indicated an increase in cell death within the tumour region. Specifically, after four weeks, where there is an increase in the MBF and SI in responders, the total haemoglobin (HbT) in responders reduced significantly. A possible explanation in responders could be due to decreased vessel viability within the tumour (measured by DOS), which also corresponded to an increase in cell death that resulted in spatial changes within the tumour (measured by QUS) (Zhu et al., 2008, Ueda et al., 2012). Conversely, non-responding patients may have had tumours with more aggressive malignant cells that prompted blood vessel growth to support the metabolic demands.

In principle, tumour metabolic information, reflected by markers for deoxy-haemoglobin and oxy-haemoglobin parameters is closely linked to

tumour cellular activity (Roblyer et al., 2011, Falou et al., 2012). This is explained by the conversion of oxy-haemoglobin to deoxy-haemoglobin during tumour cell cycling, and activity (i.e. metabolism). After eight weeks of treatment, responders demonstrated a significant reduction of HbO_2 and Hb and this corresponded with an increase in MBF of +10.0 ± 1.5 dBr, suggesting a coincident increase in dying cells within the tumour bed. Non-responders however, demonstrated less significant decreases in the tumour haemoglobin, relative to the pre-treatment value and this was also correlated to a lesser change in the MBF and SI. Together, DOS and QUS data suggest that chemotherapy-responsive tumours decrease in metabolism as linked to blood-based parameters in comparison to non-responding tumours; potentially because of dying tumour cells. QUS parameters, such as the SI and SS were not significantly different at the pre-operative time-point. This was expected since QUS measurement are sensitive to cell death induced by treatment which occurs in responsive patients early on, rather than many months later after chemotherapy. Pre-operative measurements were obtained 4-6 weeks after the last chemotherapy infusion and therefore, cell death is expected to diminish within the tumour bed in responsive patients, due to a large reduction in tumour cells after many months of chemotherapy.

Tumour structure was further characterized by measuring the tissue optical index (TOI) parameter which has been shown to demonstrate contrast between tissue types (Fantini and Sassaroli, 2012, Cerussi et al., 2006). The TOI reflects the optical properties of breast tumours in reference to its pathological state (Fantini and Sassaroli, 2012). In the work here, the TOI demonstrated significant differences ($p=0.000$) between responders and non-responders after four weeks of chemotherapy and differed significantly $(p<0.001)$ after completing chemotherapy (pre-surgery). The change in TOI is dependent on the concentration of water and lipid content within the tumour and thus responsive tumours that demonstrated a larger reduction in water content would also result in a diminished TOI value (Fantini and Sassaroli, 2012, Tromberg et al., 2005). Cerussi et al. 2007 previously suggested that this reduction in water fraction in responsive tumours might represent variations in tumour cell density, and cellularity within the tumour bed (Cerussi et al., 2007), and this was supported by clinically reported histological data that demonstrated cellular changes in the tumour after NAC. Although the

relationship between water fraction and tumour cellularity is not entirely clear; it may be related to inflammatory response mechanisms within the tumour parenchyma (Coussens and Werb, 2002). Further, in the work here the %Lipid also increased for responders, which can affect the TOI. The increase in lipid content within the tumour bed could represent the changes in lipid composition closer to that of normal breast tissue and its relationship to QUS markers would suggest that there were cellular changes concurrently.

DOS-QUS combined parameters enhanced chemotherapy response classification in comparison to single modality parameters as early as one week after the start of NAC. However, it should be noted that not all combinations increased the sensitivity and specificity of response assessment, and this could likely be caused by the relatively small sample size in this first study. Many single parameters classified patients with higher accuracy at weeks four and eight. This is likely due to the cumulative effects of treatment and the concurrent biological changes in tumours at those times. However, some parameters such as the SS benefited from multivariate DOS-QUS combinations. It was expected that combining highly sensitive and/or specific parameters would increase the accuracy and prediction of treatment outcomes. In contrast, weaker predictors (such as the slope) would benefit from pairing with stronger predictive parameters with increases in sensitivity and specificity because more parameters carry complementary information about tumour physiology or cell death. The results of this study suggest that DOS-QUS pairwise combinations may be useful for clinical application when modelled at one week of NAC treatment, using a combination of parameters that include: SI, SS, HbO_2, HbT, SP, SA, %Water, and TOI, since many of these parameters demonstrate poor sensitivity and specify on their own at that time. This may potentially be followed by treatment response verification and validation by using several other DOS-QUS parameters at weeks four and eight.

Other strategies for combined systems to compliment tumour response measurements include US-guided optical imaging developed by Zhu et al., from the University of Connecticut (Xu et al., 2015, Zhu et al., 2013, Zhu et al., 2008). These systems have been studied to measure NAC response in breast tumours. US grey-scale imaging was used there to localize breast tumours, and optical tomography to map tumour haemoglobin changes during treatment (Zhu et al., 2013, Zhu et al., 2008). The technical benefits of that approach use

co-registered US images to verify posterior (deeper) tumour margins, where optical image resolution is poorer (Zhu et al., 2008). For the current study, conventional US and DOS images were not co-registered since there were differences in the spatial geometries of the DOS and QUS images but averaged values over the tumour volume were used. This was due to patient positioning for each scan modality (i.e. supine versus prone), and breast shape from DOS breast compression. Another study from Ueda *et al*. used multivariate analyses for baseline DOS parameters combined with tissue biomarkers from immunohistochemistry (Ueda et al., 2012). Markers for cell proliferation (Ki67), and molecular features (oestrogen and progesterone receptor) were combined with optical measurements such as (HbO_2), (Hb), or the tumour oxygen saturation (StO_2). Multivariate discriminant analysis of the combined parameters demonstrated an increase in the sensitivity and specificity for predicting NAC response. The results of this study from Ueda *et al.* support the need for further exploration into combination analysis to improve the predictive performance of multiple imaging and clinical biomarkers (Ueda et al., 2012).

4.2.7 Significance of Texture-Analysis of Pre-Treatment DOS parameters

Texture analysis is a general term for mathematical methods and models used to analyse images based on the image pixels' spatial relationship to other neighbouring pixels (Davnall et al., 2012). It has been used as a second-order statistical approach to analyse DOS parametric images; yielding DOS-texture features to aid in discriminating tumour response during NAC (Sadeghi-Naini et al., 2015, Davnall et al., 2012). Texture feature-extraction methods such as those based on grey-level co-occurrence matrices (GLCM) can be applied to compute the probabilities of relative pixel intensities of images from the spatial distribution of their voxels (Haralick et al., 1973). In discussing the advantages of applying texture analysis to DOS images, it is important to emphasize that the texture of the image carries important information about the images' properties; specifically, between one pixel region to the next and giving insight about the "roughness", "softness" or "smoothness" of the image itself. In medical imaging, these qualities can help discern tumour heterogeneity which is represented by the biological measurements captured within the breast image (Gupta and Undrill, 1995).

There are several GLCM texture features but recently studied parameters in DOS include the following GLCM-textural features: contrast (*con*), correlation (*cor*), homogeneity (*hom*), and energy (*ene*). These features are dependent on the number of grey-levels (N_g) in the image or within the region of interest (ROI). Such techniques have been applied in computer-assisted diagnostics in mammographic imaging and have been extended for use in several modalities, such as X-ray mammography (Li et al., 2005), MRI (Chen et al., 2007, Lerski et al., 1993), positron-emission tomography (PET) (Chicklore et al., 2013), and ultrasound (Yang et al., 2012). Its use has also shown promising results for discriminating and characterizing tissue types (Castellano et al., 2004). In breast studies, GLCM analysis has been able to classify benign and malignant lesions using planar (2D) and volumetric (3D) MRI images (Chen et al., 2007, Gibbs and Turnbull, 2003). For X-ray mammography, GLCM analysis has been used to segment lesion borders of stellate (malignant) breast masses (Gupta and Undrill, 1995). As previously shown, it was also reported that texture-based features from quantitative ultrasound (QUS) imaging can be used to classify responders and non-responders early during NAC treatment (Sadeghi-Naini et al., 2014). These previous findings suggested that textural features may detect the acute, heterogeneous microstructural features carried in the parametric layout not otherwise detected using the mean measurements (Sadeghi-Naini et al., 2014).

4.2.8 Summary of Novel Contributions

Novel contributions for Subproject One

In terms of the novelty of the work presented in this thesis, there were three significant and new contributions in subproject one[22]:

1. New DOS and QUS imaging marker signatures were identified for the first time, at early treatment time intervals (i.e. after one cycle of chemotherapy), by combining DOS and QUS parameters together in a

[22] A summary of published contributions for subproject one is presented in **Appendix 4** and **Appendix 5.**

pairwise model; these included, MBF+HbO_2, MBF+HbT, SI+HbO_2, SI+HbT, SI+%Water, SS+HbO_2, SS+HbT.

2. *Intra-treatment* DOS and QUS parameters were used to demonstrate the likelihood of patients achieving pathologic endpoints, as defined systematically by Miller-Payne pathological response criteria, for the first time. This is novel compared to other QUS studies using radiological endpoints (Sadeghi-Naini et al., 2013b).

3. Combining DOS and QUS parameters into pairwise models improved the classification performance compared to using the univariate parameters alone at early time intervals. For example, the AUC of the QUS-SS parameter was 0.201 after one cycle (i.e. one week) of chemotherapy. The HbO_2 AUC was 0.982 and the HbT AUC was 0.875; whereas combining the SS+HbO_2 resulted in an increase of the AUC to 1.00 and the SS+HbT resulted in an increase of the AUC to 0.955.

The coincident DOS and QUS parameters may have represented concurrent biological responses in the tumour. The findings would suggest that the following coincident biological changes were processed in responsive tumours: 1) tumour cell death; 2) haematological and vascular regression and; 3) tumour morphological changes (i.e. decreases in stromal and cellular properties) and thus suggests that tumour responses to cytotoxic agents involves multiple biological processes as mentioned above (Coley, 2008).

Novel Contributions for Subproject Two[23]

In terms of novel work in subproject two, there were three new and significant contributions:

1. For the first time, a tumour ROI-only GLCM analysis was completed on DOS tomographic images using machine learning classifiers. The pre-

[23] A summary of published contributions for subproject two is presented in **Appendix 4** and **Appendix 5**.

treatment DOS parameters were studied using GLCM texture analysis and showed that for the first time, that there were significant differences between pathologic non-responders (MP1,2) and pathological responders (MP3-5) from DOS-texture features: Hb-homogeneity, HbO_2-correlation, total-haemoglobin-homogeneity, oxygen desaturation-contrast, oxygen saturation-contrast.

2. The second novel contribution included identifying DOS-texture signatures that could predict breast cancer response according to chemotherapy types; for FEC-D chemotherapy, the DOS-texture parameter, TOI-homogeneity demonstrated the highest predictive value (AUC=0.949), whereas the HbO_2-homogeneity showed an optimal AUC of 0.896 for AC-T chemotherapy.

3. The third novel contribution included analysis of DOS-texture parameters to characterize the likelihood of pathological response according to the tumour molecular subtypes. The results demonstrated for the first time, that the HbO_2-homogeneity could optimally predict response in ER+ breast cancers (AUC=0.883) and that the Hb-homogeneity parameter could optimally predict tumour response in triple negative breast cancers (AUC=0.917).

4.3 DOS and QUS Clinical Translation

4.3.1 Current Challenges for DOS and QUS Imaging as a Clinical Tool

Developing imaging biomarkers to produce a clinical decision-making tool (i.e. using biomarker information to guide and adapt treatments) requires several steps that begin with biomarker discovery, followed by validation in the clinical research setting. Subsequently, further steps are needed to test the imaging biomarkers within heterogeneous tumour subtypes in order to determine if the biomarkers are generalizable. These steps are referred to as the imaging biomarker pathway and this is analogous to the processes involved in clinical and translational research. The similarities include moving laboratory-based discoveries along a pipeline that is ultimately validated for either diagnostic or therapeutic interventions in patients and diseases (Drucker and Krapfenbauer, 2013, O'Connor et al., 2016). The processes involved in the imaging biomarker pathway require a discussion about the current demand by physicians and patients for using imaging biomarkers as a clinical tool to help guide physicians and inform patients about the progress of chemotherapy treatments. Also, it is pertinent to explore the challenges in study design and validation from laboratory testing to clinical implementation within the context of DOS and QUS imaging biomarkers.

The clinical demand for imaging biomarkers, and thus using DOS and QUS in oncology, has been highlighted recently by a UK-based working group which identified critical research gaps and translational priorities for breast cancer. Their report highlighted the importance of exploiting both biospecimen-based markers and imaging for guiding breast cancer treatment. Below are the major considerations outlined by their group (Eccles et al., 2013):

1. Selection of therapies should be offered on an individual basis and using level one evidence. Personalized treatments are the best approach. Important considerations include optimizing the treatment time-course from individual tumour and patient data. Currently, overtreatment is a clinical challenge.
2. An assessment for the tumour's underlying biology is essential. Tumour metrics may help assess the patient's metastatic risk and

predict drug resistance. The tumour's behaviours from its cellular characteristics, molecular features, angiogenic pathways and stromal conditions (i.e. hypoxia, altered metabolism) may aid in understanding the impact on therapeutic interventions. This may be achieved by using functional and metabolic medical imaging modalities.

3. Clinical decision-making tools will be integral in the management and treatment of breast cancer patients. For example, imaging biomarkers could be used to predict prognosis and response to chemotherapy. Imaging modalities will permit potentially non-invasive, serial measurements that show the dynamic tumour changes over time.
4. High risk populations include triple negative breast cancer patients and research needs to address prognostic and predictive biomarkers for this patient population. In general, tumour heterogeneity is a treatment challenge and stratification of patients is needed in future studies for better treatment strategies.
5. Both clinical and financial effectiveness should be considered while implementing new decision-making tools for clinical use.

The need for biomarkers in medicine have been identified for decades. In the early 2000s, the human genome project was completed to identify and map out thousands of genes in human cells (Cooper and Psaty, 2003, Chin et al., 2011). Since then, great efforts have been made in cataloguing and identifying gene signatures involved in disease progression, drug metabolism and treatment resistance across several disorders like cardiovascular disease, infectious diseases and cancer (Wang et al., 2011). A major focus in genomic oncology has been to identify predictors for chemotherapy-resistance in breast cancer (Wang et al., 2011, Straver et al., 2010). Indeed, thousands of genes have been studied as predictors to therapy response in cancer. Yet, one notable example of these studies includes the validation of a 21-gene assay (Oncotype-DX) that predicts the probability of patients that would benefit from adjuvant chemotherapy. The assay studies genes that have been shown to potentiate higher prognostic risk factors (Straver et al., 2010). The 21-gene signatures included have undergone validation in over 10,000 patients. The NSABP study B-14 trial demonstrated that Oncotype DX shown to predict recurrence in patients treated with Tamoxifen (Paik et al., 2004); while a parallel

study (NSABP study B-20) showed the benefit of the assay for predicting chemotherapy response (Paik et al., 2006). Yet, a meta-analysis demonstrated variability in recurrence data between 23 studies and there were concerns over the test's generalizability (Straver et al., 2010, Carlson and Roth, 2013). Patients who had intermediate risk breast cancer were not shown to benefit from Oncotype DX and it was also shown that only a subset of breast patients benefits from the assay; namely, in hormone-receptor-positive, HER2-negative, axillary node-negative breast cancer (Sparano et al., 2015, Carlson and Roth, 2013). The Oncotype-DX assay is one example of how biomarker discoveries have been adopted by clinicians to guide treatment. It also demonstrates that biomarkers themselves may not be generalizable for all breast cancer subtypes and that it may not be suitable for all patients. To date, no imaging biomarkers (excluding imaging tumour size) have reached the clinical adoption stage equivalent to biospecimen-based markers to monitor or predict breast cancer response to neoadjuvant chemotherapy. The reasons for this are because imaging biomarkers have yet to undergo large-scale clinical studies and the availability of imaging technologies across geographical regions is still limited due to their high costs. Additionally, advancing the use of imaging biomarkers also requires personnel expertise that are not always available (O'Connor et al., 2016). Thus, despite great efforts to investigate imaging biomarkers for clinical use, many studies involving novel imaging methods have not surpassed initial research hypothesis testing; thus, never reaching large-scale clinical trials for robust validation and translation into the clinic. In fact, emerging research that could potentially guide treatments often fall through translational gaps, defined as not sufficiently meeting the following criteria and stages below (O'Connor et al., 2016).

Discovery

This involves the identification, selection and derivation (i.e. calculation) of imaging biomarkers from the imaging modality. Biomarker discovery can be driven by computer-assisted technologies that permit high computing tasks, such as spectral analysis for MRI, CT or US data, which was not possible before the recent developments in high-throughput computing. Other examples of extracting imaging biomarkers include the development of mathematical

models, for example using texture analysis that emerged in the 1970s (Haralick et al., 1973). Only after several years, has texture analysis of medical images been applied to modern imaging from MRI and ultrasound. Thus, biomarker discovery is dependent on technological advances and imaging constraints such as resolution and sensitivity of the detection system (e.g. detection of radiotracers).

Technical Validation

This stage involves ascertaining the repeatability and reproducibility of the imaging biomarkers. Repeatability validation involves measuring the imaging biomarkers from the same subject (i.e. patient), equipment, software and by employing only one operator to ensure that the measurements are similar from one test series to the next. In contrast, reproducibility uses the same subject or multiple subjects, tests multiple imaging devices of the same technology, studies the measurement accuracy with different users, or uses various software. Reproducibility can be evaluated by conducting studies at multiple clinical research sites. Also, system- and user-dependent errors can cause technical biases, defined as the difference between the measured biomarker value and the true value for example, the concentration of a substance such as oxy-haemoglobin in tissue (Kessler et al., 2015). These biases must be reduced within the study design and can be achieved by conducting experiments in phantoms where the measurements can be confirmed based on reference values known about the phantom's imaging properties (O'Connor et al., 2016).

Lastly, technical validation requires that the imaging biomarkers are tested for safety for the intended patient population. For example, important safety considerations include assessing if the imaging modality can induce harmful biological changes (e.g. ionizing radiation causing genetic mutations) or if the imaging procedure causes other health risks or effects (i.e. nausea, physical discomfort, allergies). Subsequently, as the studies become validated for safety, approval for its use in patients must be obtained from the appropriate regulatory bodies such as, Health Canada, The Food and Drug Administration of the United States (FDA), or The Medicines and Healthcare Products Regulatory Agency of the United Kingdom (MHPRA).

Biological Validation, Clinical Validation and Evaluation of Clinical Utility

Biological validation confirms that the imaging biomarker represents an underlying biological process, for example, measuring the rate of apoptosis in tumour cells that have been treated with chemotherapy. An extension of biological validation is clinical validation, which is defined as evidence of a link between the measured imaging biomarkers and the clinical outcomes, such as pathology endpoints (i.e. pathological complete response , defined as a complete disappearance of tumour cells after chemotherapy). Biological and clinical validation lead to building evidence for clinical utility which evaluates the clinical benefits of using the imaging biomarkers in patient care. Clinical utility is measured by improvements in patient outcomes, such as longer survival periods (i.e. >5-year intervals); or by optimizing the therapeutic effect by choosing therapies that are indicated for specific tumour types, for example using antivascular drugs in tumours where imaging biomarkers indicate high vascular density. Recommendations and guidelines to achieve robust clinical validation were previously outlined by the National Cancer Institute and the European Organization for Research and Treatment of Cancer (NCI-EORTC) (McShane et al., 2005). The NCI-EORTC guidelines made recommendations such that results could be compared across multiple studies and that conclusions could be drawn from multiple studies with the same imaging objectives. The recommendations included the following highlights (McShane et al., 2005):

1. Describing the clinical characteristics of patients (i.e. age, sex, disease stage, and the disease laterality where relevant, such as breast cancer).
2. Indicate all treatments to patients.
3. The method for case selection (inclusion and exclusion criteria) and stratification of disease types.
4. Precisely defining the clinical endpoints, for example, pathologic complete response (pCR) and indicate the standard grading systems used. If the endpoints are survival, the survival data should include time intervals from at least 3-5 year intervals (O'Connor et al., 2016).

5. Indicate the statistical methods used. This includes an analysis of the relation of the imaging markers to the endpoints, as defined within the study.

Lastly, for clinical validation and clinical utility, a consensus statement that includes all disciplines (medicine, scientific, technical) should be developed to establish standard imaging protocols that can be used and adapted across any treatment site (O'Connor et al., 2016).

Cost Effectiveness Analysis

Using imaging biomarkers should be aimed for cost-savings to the healthcare system. Using imaging biomarkers to guide chemotherapy and adapt treatments could potentially confer an economic benefit since imaging biomarkers could potentially identify ineffective chemotherapies; therefore, eliminating unnecessary treatments. Additionally, in cases where tumours are highly responsive, the number of chemotherapy cycles could be potentially reduced since the desired therapeutic effect may be achieved earlier than conventionally scheduled treatments. In developing imaging biomarkers, it is important to consider that the costs of imaging should not exceed the cost of the therapy or medical procedure itself. Cost effectiveness analysis also includes a careful evaluation of the research costs associated with developing the imaging biomarkers. Imaging studies are by its inherent nature, very expensive to conduct since there are high costs associated with imaging equipment. With the expenses associated with high equipment costs, and the considerable research time involved in developing imaging biomarkers, translating imaging biomarkers to clinical implementation are a very costly endeavour (O'Connor et al., 2016).

Conclusions of Biomarker Discovery Pathway

Taken together, integrating and using imaging biomarkers in clinical practice requires robust marker validation through single- and multi-institutional testing, establishing the generalizability of the tests to the patient population and cost effectiveness analysis to demonstrate that the imaging biomarkers will have an economic benefit to the healthcare system (O'Connor et al., 2016,

Eccles et al., 2013). These translational stages and the associated challenges are discussed further below with respect to the status of DOS and QUS imaging within the imaging biomarker development pathway.

4.3.2 Status of DOS and QUS Biomarkers for Breast Cancer Treatment

The status of DOS and QUS imaging biomarkers have not reached clinical implementation for locally advanced breast cancer, i.e. clinicians are not currently using DOS and QUS as clinical decision-making tools for guiding and adapting chemotherapy treatments in locally advanced breast cancer. To date, the advantages of using DOS and QUS imaging biomarkers have been well established for locally advanced breast cancer, which include: 1) non-invasive imaging; 2) minimal risk for adverse reactions because contrast agents are not required; 3) no exposure to ionizing radiation; 4) lower-cost instrumentation that permit serial imaging during chemotherapy; and 5) whole-tumour analysis that permits measurements across the heterogeneous tumour volume. Despite these advantages, DOS and QUS studies to date have not undergone sufficient validation and large-scale studies to have gained physician confidence to use as a clinical decision-making tool, i.e. to adapt treatments based on the imaging biomarker information provided by DOS and QUS. The criteria considered for the imaging biomarker development pathway are outlined below with respect to DOS and QUS.

DOS and QUS Biomarkers Discovery

Previous DOS imaging biomarker discoveries originated from continuous wave, time-domain and frequency-domain imaging techniques that emerged in the 1990s (Tromberg et al., 2008). DOS biomarker discoveries at that time included measurements of intrinsic (i.e. naturally occurring) optical absorbers that could be used to characterize tissue components and optical scattering (previously outlined in Chapter 1) (Tromberg et al., 2008). The present status of DOS imaging biomarkers, in terms of new discoveries, has shown new DOS biomarker discoveries that measure metabolic activity. These include the bound water index (BWI), which measures the quantity of bound water molecules to macromolecules such as protein (Chung et al., 2008). Kukreti et

al. (2010) identified another new imaging biomarker, termed the specific tumour component parameter (STC). The STC is capable of characterizing tissue types by comparing the spectral patterns, i.e. the shape of the absorption spectral form between normal breast tissue and tumours (Kukreti et al., 2010). To date however, the BWI and STC have not been used to measure chemotherapy response in breast cancer. It is also important to mention discoveries in exogenous fluorophores (i.e. probes that emit light after optical excitation) used as DOS imaging biomarkers. Exogenous agents in DOS imaging (within the near-infrared spectrum, NIR) include excitable fluorescent agents (NIR-EFAs) (Sevick-Muraca et al., 2002). Examples of NIR-EFAs include tricarbocyanine dye, which absorb NIR wavelengths at ~800-840 nm. Tricarbocyanine dye is readily taken up by blood albumin and thus can serve as a vascular tracer, but has not been found to be useful in cancer studies (Richards-Kortum and Sevick-Muraca, 1996).

Other recent DOS discoveries are using texture-based analysis which can yield hundreds of texture parameters from the DOS parametric layout. The number of possible texture features is dependent on the statistical technique used such as: 1) histograms; 2) absolute gradients; 3) run-length matrix, 4) auto-regressive model; and 5) wavelets (Castellano et al., 2004). Recently, 40 additional texture features were yielded from GLCM analysis of DOS breast images (Sadeghi-Naini et al., 2015).

Previous QUS biomarker discoveries include parameters from the spectral form of the backscatter signal, which was first introduced by Frederic Lizzi in the 1970s (Mamou and Oelze, 2013, Feleppa et al., 2011). Subsequent works by Insana et al. (1990) continued to develop spectral analysis to obtain parameters that represented the scatterer properties, i.e. size, concentration and distribution of scattering particles in tissue, by using estimates of the backscatter co-efficient from the power spectra (Insana and Hall, 1990). The present status of QUS imaging biomarkers, in terms of new discoveries, involve improvements in mathematical models that estimate the size and concentration of scatterers in tissue (Oelze and Mamou, 2016). Other innovative techniques are using texture-based analysis as previously described with DOS features above (Sadeghi-Naini et al., 2014).

DOS and QUS Technical Validation

In terms of technical validation, both DOS and QUS imaging biomarkers have been tested in laboratory studies for decades, thus having shown repeatability and robust methodologies in measuring and extracting biomarkers from biological specimens (Feleppa et al., 2011, Tromberg et al., 2008). Indeed, the evidence supporting the reliability of DOS imaging measurements has led to commercially available DOS mammography systems manufactured from Imaging Diagnostic Systems, (Florida, USA), Philips Healthcare (Amsterdam, Netherlands) and Advanced Research Technologies (Montreal, Canada, currently discontinued) (Leo et al., 2017). However, these devices have been classified under regulatory bodies for use in diagnostic mammography and are not indicated for evaluating treatment response. Similarly, ultrasound imaging systems are ubiquitous in radiology clinics, but are not yet approved for using QUS imaging biomarkers for treatment response assessment.

Validating the utility of DOS and QUS imaging biomarkers for chemotherapy response evaluation is still in its research phase. A limitation of translating these imaging biomarkers into clinical implementation is the need to validate the data reproducibility through multicentre clinical trials. This was identified in the early 2000s for DOS imaging in which the National Cancer Institute (NCI) initiated a consortium of health institutions, physicians and scientists to further develop DOS imaging for breast cancer (Network for Translation Research for Optical Imaging, NCI-NTROI) (Clarke et al., 2003). The NCI-NTROI is currently supporting multicentre trials in the United States by funding core institutions at Washington University, University of Texas, University of Michigan, and Stanford University. Other networks include the American College of Radiology Imaging Network (ACRIN). The ACRIN 6691 trial was completed in 2013 and included six clinical research sites across the USA (Tromberg et al., 2016). The aim of the ACRIN 6691 trial was to measure intratreatment chemotherapy response in LABC patients at the following time intervals: pre-treatment, 5-10 days after the first cycle, mid-therapy, and before surgery (American College of Radiology Imaging Network, 2017). The study however, only reported evaluable cases of only 34 patients; thus, not having sufficient statistical power to translate the results for clinical implementation

(Tromberg et al., 2016). To date, the ACRIN 6691 trial is the only DOS-based multisite trial for LABC response evaluation.

QUS studies for measuring chemotherapy response in LABC is currently led by the University of Toronto (Ontario, Canada). Studies to date have only indicated results from single-institution trials. However, for other disease types such as prostate cancer, and for the purpose of diagnostics, QUS trials have been conducted at other institutions led by Riverside Research (New York, USA) (Feleppa et al., 2011).

DOS and QUS Biological Validation and Clinical Validation

DOS measurements to quantify biological chromophores in tissue, such as haemoglobin, lipids and water are based on mathematical modelling that uses a photon transport model and diffusion theory[24] (Dehghani et al., 2009, Gibson et al., 2005). Biological and clinical validation studies using DOS have indicated that DOS measurements for haemoglobin are linked to vascular abundance in tumours and can serve as indicators for final pathologic endpoints such as pCR at mid-treatment (Choe et al., 2005, Cerussi et al., 2007, Cerussi et al., 2011). There are previous studies that have shown a correlation between DOS imaging parameters and tissue features, as tested histologically (Pogue et al., 2001). Pakalnikis et al. (2011) reported that the total haemoglobin measured in breast tumours (HbT=45 μmol/L) was significantly correlated (*p=0.001*) with the tumour's vascular density as measured using histology (CD105 blood vessel staining) (Pakalniskis et al., 2011). Similarly, data by Zhu et al. (2008) demonstrated a nearly significant correlation (P=0.056) between DOS-measured HbT and vascular density, as stained with CD-31 in the post-treatment breast samples (Zhu et al., 2008).

For QUS studies, biological validation was completed both *in vitro* and *in vivo*. Previous *in vitro* experiments demonstrated an increase in QUS parameters which corresponded to an increase in apoptosis in acute myeloid leukaemia cells treated with chemotherapy (Czarnota et al., 1999, Kolios et al., 2002). Also, Brand et. al (2008) showed that other cancer cell types such as,

[24] These models are used to determine the scattering and absorption co-efficient to measure tissue parameters.

HeLa (human cervical cancer) cells treated with chemotherapy were linked to an increase in QUS features (SI and MBF) (Brand et al., 2008) *In vivo* studies used mouse models that were transplanted with human breast tumours; Tadayyon et al. (2015) showed that QUS biomarkers, such as the average acoustic concentration (AAC) were correlated to increases in cell death, as demonstrated in histological analysis of excised tumours (r^2=0.40) (Tadayyon et al., 2015). Similarly, Sadeghi-Naini et al. (2013) showed that texture analysis of QUS parameters (MBF, SI) demonstrated a high correlation (r^2=0.97) to cell death using the same experimental mouse and treatment model (Sadeghi-Naini et al., 2013a).

DOS and QUS Cost-Effectiveness Analysis

A recent study demonstrated that Americans pay about $34,000 USD per chemotherapy visit for drugs and medical care to treat advanced breast cancer (i.e. stage 3) (Blumen et al., 2016). Over the entire course of the chemotherapy treatment, over $200,000 USD would be spent for 6-8 chemotherapy cycles. Indeed, the cost of health care is dramatically lower in Canada and the United Kingdom; a study by Hall et al. (2015) reported significantly lower costs for the entire chemotherapy treatment for breast cancer, on average, approximately £16,000 GBP (Hall et al., 2015). It can be appreciated that there is a huge economic problem when ineffective chemotherapies are given to cancer patients. Therefore, using imaging biomarkers to evaluate the efficacy of chemotherapy, i.e. prognosticate if the tumours will respond to treatment, has an enormous economic benefit to the health system.

To date, no cost-effectiveness analysis has been completed for QUS imaging. However, Schegerin et al. (2009) previously analysed the cost effectiveness of prognostic DOS imaging in LABC patients treated with neoadjuvant chemotherapy (Schegerin et al., 2009). The cost-effectiveness model was used to test if implementing DOS in the patient's chemotherapy treatment would be cost-beneficial and included the following variables in their cost-model:

1. The cost of the device (operational and capital)
2. The chemotherapy treatment course

3. The prevalence of chemotherapy response in women, defined as pathologic complete response.
4. The sensitivity and specificity of the imaging device and the potential gains in lives saved from adapting treatment based on biomarker information.
5. The life expectancy of patients

The results of their study indicated that a device cost of $1M for a DOS system would be cost-effective under the condition that DOS imaging could increase the cure rate by at least 1%, and that chemoefficacy rates would not exceed 90% (i.e. there is no utility for using DOS imaging biomarkers to guide treatment if chemotherapies are already effective) (Schegerin et al., 2009).

4.4 Potential Impact to Patient Care

The body of research to support using DOS and QUS imaging biomarkers by physicians to evaluate breast tumour response to NAC is limited by small datasets (i.e., not enough patients for sufficient statistical power), variable imaging protocols and identifying biomarkers that yield an optimal correlation to final pathologic endpoints such as, Miller-Payne grade or the Residual Cancer Burden Index.

However, using DOS and QUS parameters to accurately screen patients either before or during chemotherapy for treatment endpoints such as, pCR and partial pathologic response (pPR) can be achieved by increasing multicentre studies with sufficient power and sample size. This will also lead to identifying salient DOS and QUS imaging biomarkers that can be used clinically; in contrast to the current status, where there are hundreds of experimental DOS and QUS imaging biomarkers available for analysis. Before clinical implementation, it is also important to develop a consensus statement from an expert panel that may include imaging scientists, radiologists, oncologists, nurses and technicians. This multidisciplinary approach will result in compiling a standard imaging protocol that outlines the imaging procedures, interpreting test cut-off points and optimal imaging time intervals. This will effectively establish a decision-making algorithm that outlines how physicians would use DOS and QUS biomarker information to guide their treatment decisions. The potential impact of prediction-guided and response-adaptive chemotherapy treatments could significantly improve treatment outcomes for patients, for example, increased pCR rates and improved patient survival from more efficacious treatments. The approach by which treatments are customized for each individual based on biological and patient-based information is termed personalized medicine.

4.4.1 Using Biomarkers to Make Treatment Decisions for Personalized Medicine

Personalized medicine refers to using biological, imaging, or individual patient characteristics to customize and administer the most precise diagnostic procedure or therapeutic intervention in medicine. Personalized medicine is

predicated on gathering the most sensitive, specific and individualized information obtainable. Indeed, access and availability of useful and meaningful information (i.e. biomarkers) is the rate limiting factor since biomarker discovery and validation is highly dependent on the available technology.

In current oncology practice, treatments that are given to patients are to some degree personalized, for example, tailoring the chemotherapy dose based on the patient's height and weight, or discontinuing chemotherapy due to a patient's low blood counts or other toxicities. Medical imaging continues to play an important role in personalized treatments in other specialties like radiation oncology. Imaging modalities like CT, MRI, and PET are being used in the clinic to map tumour response (i.e. size changes, and metabolic data) during radiation treatments and the information is used to adapt radiation treatment plans to conform to the dynamic changes in the tumour (Metcalfe et al., 2013). For personalized treatment in locally advanced breast cancer, existing methods include collecting tissue samples to extract biomarkers such as HER2-expression. Tailored treatments for HER2-overexpressed tumours (i.e. HER2+) include prescribing targeted therapies such as Trastuzumab. Other biomarker screening approaches include testing for oestrogen-receptor positive (ER+) tumours, where endocrine therapies are administered to increase the therapeutic efficacy. In these examples, biomarkers can be used to personalize drugs and the treatment course for patients; yet the challenge currently is to also understand if anticancer therapies are optimally effective. Within this framework, biomarkers can be used in three ways to personalize treatment (below). Understanding the different biomarker types will facilitate the discussion on the potential and future impact of DOS and QUS biomarkers for personalized treatments for patients with locally advanced breast cancer (Hricak, 2011):

1) **Prognostic biomarkers:** Indicators for the likelihood of the tumours to progress (i.e. identifies aggressive disease) without considering treatment interventions. Population-based statistics can be used to identify prognostic biomarkers, for example, observing biomarkers for high proliferation (Ki67) and the prevalence of aggressive cancers within the sample population.

2) **Predictive biomarkers:** Predictive biomarkers indicate the probability of the tumour's response to treatment (usually before treatment), for example, tumours with biomarkers for hypoxia are susceptible to chemoresistance.
3) **Early-response biomarkers:** Early response biomarkers are collected during the treatment course and indicates the likelihood of the tumour's response to the post-treatment gold-standard assessment. For example, breast tumours could be measured using DOS after the 2d cycle of chemotherapy and the output parameters are used to statistically evaluate a link to pathologic complete response in the tumour.

Potential Impact to Patients: Confirming chemotherapy response before and during treatment using DOS and QUS imaging biomarkers

Not all patients are good candidates for chemotherapy because of tumour heterogeneity. The response to chemotherapy can influence the subsequent treatment course for patients, as outlined by the NCCN (USA) or NICE (UK) (National Comprehensive Cancer Network, 2016, National Institute for Health and Care Excellence, 2017, National Institute for Health and Clinical Excellence (NICE), 2009b, National Institute for Health and Clinical Excellence (NICE), 2009a) (**Figure 4.2**). Since these standard therapies are not always effective, clinicians are interested in confirming chemoefficacy for their patients either before or during treatment. To address this problem, this study demonstrated that DOS and QUS imaging biomarkers were potentially useful as either predictive biomarkers or early-response biomarkers in LABC. Here, pre-treatment DOS parameters were shown to be predictive biomarkers for chemotherapy response; whereas both DOS and QUS were modelled as early-response biomarkers (i.e. intratreatment response evaluation). The potential impact to patients by using DOS and QUS imaging biomarkers could personalize the patient's treatment course by mapping out the best therapy at the early onset of treatment planning. Additionally, serial DOS and QUS measurements during chemotherapy can provide physicians with real-time "feedback" to confirm that the treatment is appropriate for the patient and that the course can continue as planned.

In comparison to other biomarker technologies, predictive biomarkers using genes, are currently personalizing the treatment course for patients with early stage breast cancer who undergo surgery first, then are considered for chemotherapy (Straver et al., 2010). Predictive biomarkers include the Mammaprint™ assay, which is a clinically validated assay that extracts 70 gene markers from the surgical tumour specimen. The Mammaprint™ assay provides physicians with an analysis about the potential risk of breast tumour recurrence. Doctors use this analysis to decide on the potential benefit of patients receiving chemotherapy since the risk of recurrence is also linked to lower chemosensitivity and more aggressive tumours (Straver et al., 2010). The Mammaprint™ test provides a framework for using pre-treatment DOS biomarkers to non-invasively evaluate LABC patients before chemotherapy to test if there is a potential clinical benefit for patients. As can be seen in **Figure 4.1**, patients who do not respond to chemotherapy in their "first-line" may go on to receive additional chemotherapy. DOS and QUS imaging biomarkers could also be used to assess the potential clinical benefit during each phase of treatment.

It should be noted that other markers such as the tumour's grade are associated with pathological response to neoadjuvant chemotherapy (Huober et al., 2010). Research from the GeparTrio trial investigated 2,072 breast cancer patients treated with neoadjuvant anthracycline-taxane chemotherapy. The results showed a higher pCR rate in grade three tumours (211 patients, 28.1%) compared to grade one and grade two tumours (156 patients, 13.0%, $p<0.001$) (Huober et al., 2010). The results of the study suggest that there are several biological and clinical variables that are involved in tumour response; thus, using this framework as a guiding principle for well-designed clinical trials can significantly improve the quality of imaging biomarker research. Such frameworks could include stratifying patients by initial tumour grade, hormone-receptor status or by tumour size at the time of diagnosis.

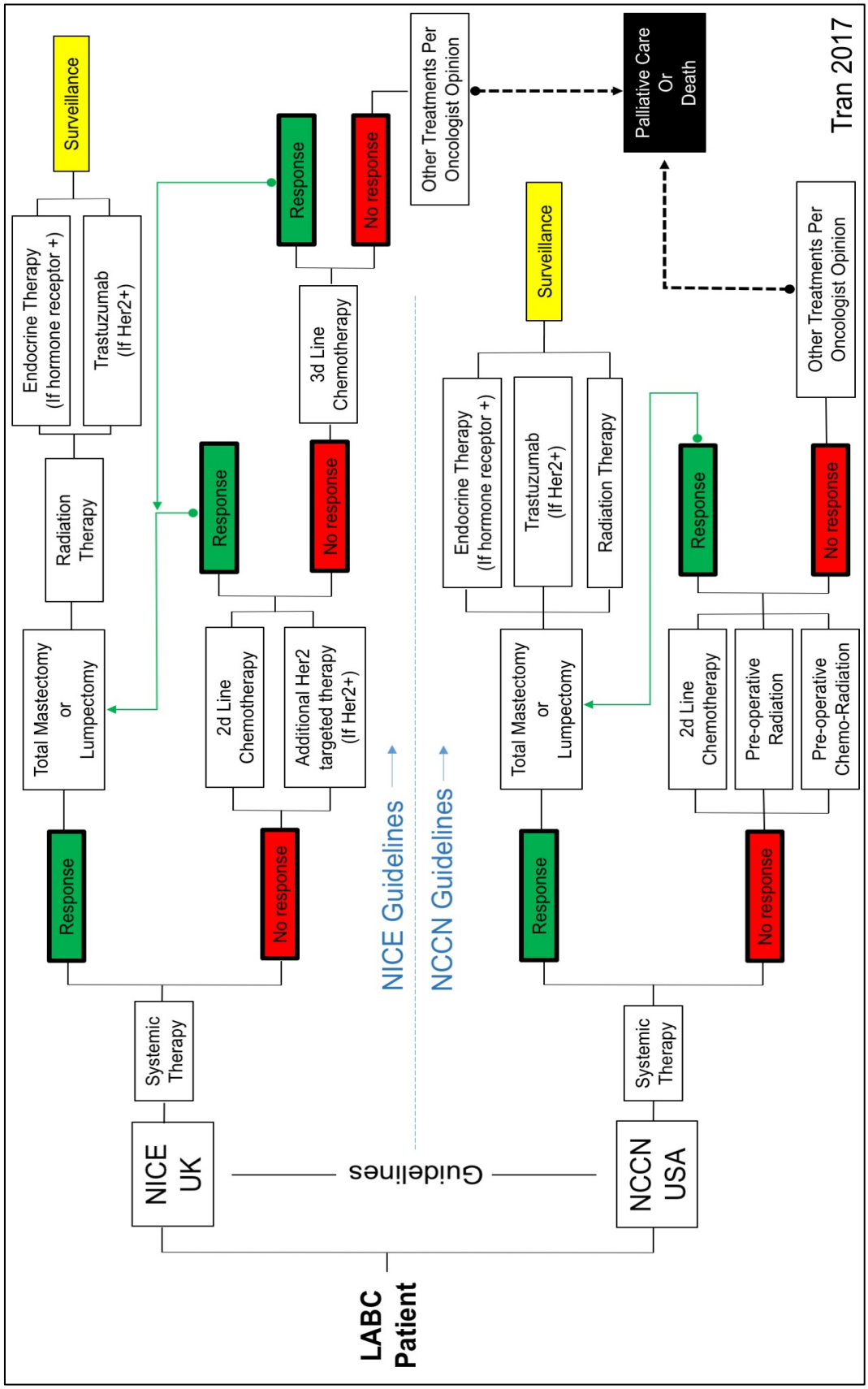

Figure 4.1. LABC patients are treated using a complex treatment decision-tree as outlined by the NCCN (USA) and NICE (UK). For patients who do not respond to first-line chemotherapy, additional chemotherapies may be given, or other targeted therapies (e.g. endocrine therapy) may be offered.

4.4.2 Adapting Chemotherapy Dosing Schedules to Optimize Tumour Response and Survival Outcomes

Using DOS and QUS as early-response biomarkers could help adapt chemotherapy doses (i.e. frequency of dose scheduling) according to tumour response. Tumours that demonstrate early response could be given fewer chemotherapy cycles in contrast to non-responding tumours that could be recommended for more chemotherapy. Adapting the chemotherapy dose according to response using information from radiology, biomarkers, or physical examination is called response-guided therapy (von Minckwitz et al., 2013). A recent phase three randomized study (GeparoTrio) from the German Breast Group recently reported an increase in survival for patients who underwent response-guided neoadjuvant chemotherapy in breast cancer (von Minckwitz et al., 2013). The GeparoTrio study included analysis of 2,072 breast cancer patients who received neoadjuvant chemotherapy. In this study, the standard chemotherapy was defined as 6 cycles of anthracycline-taxane (TAC). Patients were assessed as early responders or early non-responders using conventional ultrasound; early responders were defined as a having a reduction of at least 50% of the tumour size after the second cycle of chemotherapy. Early responders were then randomized into two arms. In the first arm, patients completed the conventional chemotherapy (6 cycles of TAC in total). In the second arm (response-guided arm), patients were given two additional TAC chemotherapy cycles (8 cycles total). For early non-responders, patients were randomized to receive the conventional chemotherapy (6 cycles of TAC) in the first arm; whereas the response-guided arm, patients were switched to other chemotherapy types (vinorelbine and capecitabine) for 4 cycles (von Minckwitz et al., 2013). There were two significant outcomes from this study:

1) **Early response group:** Patients that were randomized to the response-guided treatments (i.e. 8 cycles of TAC) compared to those in conventional treatments, had better survival outcomes (Hazard ratio, 0.78; *P=0.026*).
2) **Early non-response group:** Patients that were randomized to the response-guided treatments (2 cycles of TAC, then switched to 4 cycles of vinorelbine and capecitabine) lived longer compared to patients who

were randomized to receive the conventional treatment (Hazard ratio, 0.59; *P=0.001*).

The results presented by the German Breast Group suggested that response-guided, and response-adapted chemotherapy may improve survival outcomes for patients. Their study has also opened potential opportunities for further studies on using imaging biomarkers to guide chemotherapies, instead of using conventional imaging (e.g. grey-scale ultrasound) that was used previously to guide treatments (von Minckwitz et al., 2013). Using imaging biomarkers such as from DOS and QUS during treatment, that are more sensitive and specific compared to conventional imaging, could thus optimize treatment endpoints such as survival, for both responding and non-responding patients. In terms of adapting the GeparoTrio study's framework into the current study, using DOS and QUS imaging biomarkers after two cycles of chemotherapy (in this present study, indicated as "Week 4"), could potentially impact patients by intratreatment response monitoring and by administering either more chemotherapy or adjusting the types of chemotherapies that could increase the therapeutic index.

4.4.3 Potential Applications for Chemotherapy Drug Trials

Each year, approximately 10,000 new biochemical compounds are identified for potential drug development. It costs $800,000 million USD to develop the compounds into pharmaceutical agents which includes extensive testing and validation along the development pipeline (Willmann et al., 2008). DOS and QUS imaging biomarkers can be a cost-effective validation tool to test drug effectiveness and safety. Implementing DOS and QUS imaging biomarkers during animal and human testing can help measure the biological effects of anticancer drugs such as cell death, vascular regression and changes to tissue composition (Pien et al., 2005). DOS and QUS imaging biomarkers could be used along-side traditional evaluation methods such as biospecimen-based immunohistochemistry to help identify and select those compounds that demonstrate a high therapeutic potential. The impact to patient care includes expediting the drug-development process to bring new anticancer drugs to patients faster (Rudin and Weissleder, 2003). Increased use of imaging

biomarkers in the drug development process has resulted from technological advances; for example, the ability for radiolabelled PET imaging to measure the accumulation of candidate drug compounds in tissue and permitting pharmacokinetic measurements (Pien et al., 2005). Other methods, such as MRI have also been used to measure the reduction in the tumour blood flow and changes to the vascular volume from testing anti-vascular drugs (O'Connor et al., 2008).

The specific uses for DOS and QUS imaging biomarkers in cancer drug development include investigating drug effects in pre-clinical (i.e. animal) models to detect the cellular and physiological characteristics of tumours treated by the new drug compounds. Previous animal experiments using xenografted human tumours have shown that QUS imaging biomarkers could be used for high resolution tumour imaging (50 microns), and that the spectral parameters were correlated to an increase in tumour cell death after 24 hours of treatment from radiation, chemotherapy and novel antivascular agents, such as microbubbles (Vlad et al., 2011, Sadeghi-Naini et al., 2013a, Tran et al., 2016). Thus, QUS analysis of new drug candidates in animal models could permit non-invasive and serial imaging of tumours to understand the effective doses needed to achieve a useful therapeutic index in tumours. For applications in drug development trials in humans, the work presented in this present study could provide a framework to monitor tumour responses to new drug compounds and could provide a useful adjunct tool to assess the physical properties that are related to tumour cellularity. To demonstrate other important tumour-response features such as vascular density, DOS imaging can play an important role in clinical trials by measuring the effects of new drugs to the tumour vasculature. Other parameters such as the scattering power could be used to measure the tumour cellularity and the models presented in this current study could be used to measure the intratreatment response. Therefore, DOS (like QUS) can also evaluate important resistance factors in tumours such as hypoxia and interstitial fluid and this can potentially affect the validation and interpretation of results in drug trials, not otherwise detectable serially using traditional invasive procedures such as biopsies.

4.5 Study Limitations

4.5.1 Sample Size

Limitations for subproject one included a small study (n=22 patients), which could have resulted in an overestimation of the sensitivity and specificity and this is an inherent statistical limitation. For subproject two, a small sample size of n=37 was also an important limitation to the subproject in terms of statistical testing, i.e., the statistical test of significance was performed with a relatively small sample size in each responding group (n_1 = 27 and n_2 = 10) (Siegel and Castellan, 1988, de Winter, 2013). To evaluate the reliability of the performed tests, the statistical power was calculated using PASS[14] (NCSS, LLC. Kaysville, Utah, USA). As can be seen from the results, the statistical power for the statistically significant parameters varied between 71.8% and 85.6%. This was one of the limitations of this study, as a threshold of 70% was chosen for the statistical power, instead of a commonly used threshold of 80%. By fixing the number of responders (n_1 = 27), we have also estimated the number of non-responders (n_2) required to achieve a minimum statistical power of 80%. Analysis showed that at minimum, 4 additional non-responders were needed to achieve an 80% statistical power. This change would permit stronger conclusions to be drawn from this subproject. This limitation could have been addressed by approaching the study in two ways: 1) increasing the recruitment period in order to enrol four non-responders using the chosen Miller-Payne response criteria or; 2) redefining the ground-truth labels; i.e. a modified cut-off point in the Miller-Payne grade to classify responders and non-responders.

4.5.2 Sample Heterogeneity

Patient-related factors that could affect DOS measurements include increased body mass index (BMI[25]), higher breast density, and the larger breasts for imaging (Srinivasan et al., 2003, Intes, 2005, O'Sullivan et al., 2013). A study by Srinivasan et al. (2003) showed a significant negative correlation

[25] Body mass index (BMI) was not recorded in the patient's medical record.

($p<0.05$) between BMI and the total haemoglobin, breast size and the scattering amplitude, and age with the scattering power (Srinivasan et al., 2003). Also, women with radiologically dense breasts showed an increase in the scattering power and scattering amplitude (Srinivasan et al., 2003). The results of these studies demonstrate some potential limitations in the present study in terms of breast and patient heterogeneity that can affect the DOS measurements. However, the advantage of using the DOS tomographic device in the present study is the ability to apply a soft compression to the breast, as to maintain an equal breast thickness during the scanning process to mitigate the scattering effects from light transport across larger distances in the breast.

Patients included in this study also demonstrated differences in molecular features (oestrogen receptor, progesterone receptor, and HER2 status). The major limitations to tumour heterogeneity include patients who were HER2+, who also received Trastuzumab during their second phase (taxane) therapy. Improved treatment response has been observed in HER2+ patients for two reasons: 1) HER2+ tumours are highly responsive to anthracycline and taxane chemotherapies and; 2) data from the German Breast Group (GeparoQuattro trial) showed that targeted therapies given in the neoadjuvant setting, such as Trastuzumab, demonstrate a 16% increase in pCR rates in breast cancer treatment (Untch et al., 2010, Andre et al., 2008). Therefore, the major limitations in having variable tumour subtypes within the study population, and the consequences of variable responses within these tumour subtypes can affect the DOS and QUS measurements.

4.5.3 Pathologic Endpoints (Ground Truth Labels)

Another limitation in this study included classifying patients into binary response categories (i.e. responders versus non-responders) and this approach was necessary for statistical modelling. However, in clinical practice, tumours do not respond to chemotherapy in a binary mode; rather, tumour response to chemotherapy is dynamic and graded within a continuum, i.e. there is a spectrum between pathological complete response (pCR), to partial response, to progressive disease (Marchio and Sapino, 2011). There is added complexity since other classification systems such as the residual cancer burden index (RCBI) and TNM system (tumour, node, metastasis) include lymph node status

within their definitions of pathological complete response and in pathological complete response (Symmans et al., 2007, von Minckwitz et al., 2012). Some response criteria, such as the RCBI and TNM are useful endpoints since those scores have been linked also to long-term survival in some cancer subtypes such as triple negative breast cancers and HER2+ breast cancers (Symmans et al., 2007, von Minckwitz et al., 2012).

In this study, Miller-Payne (MP) response criteria was used. As previously discussed in Chapter 2 (Methods), Miller-Payne response criteria is a five-scale system that measures the reduction in cellularity from before and after chemotherapy in the primary tumour (Ogston et al., 2003). It is defined as: grade 1 (no change to cellularity); grade 2 (up to 30% loss in cellularity); grade 3 (between 30-90% reduction in cellularity); grade 4 (small clusters of tumour cells and greater than 90% loss in cellularity) and; grade 5 (disappearance of tumour cells). In this study, responders were defined as having a MP grade of 3-5; whereas non-responders were defined as having an MP grade of 1-2. This was chosen based on the advice and discussion with the host institution's breast pathologist and also demonstrated good statistical modelling from other DOS studies (Zhu et al., 2014). Also, Miller-Payne criteria is used to evaluate tumour-only response and thus provided a good system as DOS and QUS imaging analysis was only of the tumour alone. Using Miller-Payne criteria here, still has important clinical relevance, i.e., clinicians will still indicate continuing with chemotherapy, if there is partial response in the tumour. The natural follow-up question to this limitation is to inquire about the link between pCR/ pPR and long-term survival and if measuring partial response is still a clinical benefit in terms of survival outcomes to patients. Indeed, pCR has been shown to be linked to long term (+5 years) survival by the German Breast Group (von Minckwitz et al., 2012). However, achieving partial response is also an important clinical indicator; a study by Symmans et al. (2007) showed that up to 80% of patients who achieved partial response to chemotherapy may still live up to 5 years without distant relapse (Symmans et al., 2007).

4.5.4 Limitations of DOS and QUS Imaging

Signal-to-Noise Ratio

A major challenge with all types of imaging (i.e. MRI, CT, PET, ultrasound, optical imaging) involves optimizing the signal-to-noise ratio (SNR) to obtain the intrinsic or "true" measurement. The SNR is defined as the ratio between the strength (power) of the image signal to the strength of the unwanted signal (noise); thus, a greater SNR is desirable in medical imaging. Obtaining a high SNR in DOS imaging can be a challenge since light from the surrounding environment (i.e. room light or background illumination) can cause unwanted light signals detected and this can result in a contaminated DOS measurements or low SNR (Gibson et al., 2005)[26]. Other challenges associated with optimal SNR in optical imaging include measuring the absorption co-efficient across large tissue distances (Gibson et al., 2005). Measurements of DOS imaging parameters such as the total haemoglobin concentration are dependent on the absorption co-efficient; yet the limitation is that scattering dominates over absorption as the photon path length increases (Gibson et al., 2005). It has been shown previously that there is a negative correlation between the path length and the total haemoglobin measurement (r=*-0.34*); thus, as the photon path length (e.g. breast thickness) increases, the total haemoglobin decreases (Intes, 2005, Gibson et al., 2005). To limit these challenges, a maximum breast thickness of 80 mm was used with the DOS tomography system in this thesis study. Another limitation with DOS systems include the need to ensure adequate surface coupling between the light source and the breast. In this study, optical compensation medium was used; but heterogeneities in the medium, such as air bubbles, inhomogeneous distribution of its components (lipid and dye), may result in a lower SNR. However, a quality check was completed before each scan to remove air bubbles in the imaging aquarium and each OCM batch was characterized as described by Intes et al. (2005) prior to DOS imaging (Intes, 2005). One major limitation for

---

[26] Note that in this thesis study, DOS data was acquired in a dark-room.

optical imaging is skin pigmentation since intrinsic chromophores such as melanin in the skin can absorb the transmitted light at the skin surface.

For QUS, a low SNR can be caused by imaging deep (posterior) tumours; large breast tumours that extend into the posterior margin results in increased acoustic attenuation which can affect the quality of the echo signal (Lizzi et al., 1983). The study here used an attenuation correction (i.e. an attenuation co-efficient was calculated per unit depth of QUS imaging) to compensate for the attenuation effects of deeply-located tumours (Lizzi et al., 1997b).

Image Resolution and Region of Interest

The accuracy of DOS and QUS imaging modalities is limited by the finite resolution size, which is greater than the physiological structures being measured (i.e. blood vessels, haemoglobin, cell substructures). In medical imaging, this limitation is called the “partial volume effect”; defined as an underestimation of the measured value (i.e. concentration of a tracer or signal strength) due to the finite information that can be carried within the resolution parameters of a pixel or voxel. For example, high resolution imaging can carry greater information compared to lower resolution imaging since in high resolution imaging, the greater number of pixels (or voxels) within the image can better represent the spatial layout (Soret et al., 2007). For DOS, the voxel size was 3 mm x 3 mm, which can capture information on larger blood vessels and even represent clusters of smaller blood vessels. The limitation here is that image reconstruction is poor, yet the quantitative measurements may still represent the biological properties very well.

Another limitation for DOS and QUS imaging is the repeatability and reproducibility in ROIs; as the resolution of the images were relatively lower compared to other modalities such as MRI and CT imaging. Variations in contouring the ROI could have resulted in differing results. In this study, we employed a semi-automated contouring approach which was software driven (thus, minimizing potential user-variations). Additionally, interuser variability testing was completed to ensure that there was consistency between readers.

Cross-validating DOS and QUS Parameters with Biospecimen Assays

An important limitation was that it was not possible to validate intratreatment tumour biology with histology. Using immunohistochemistry could have correlated biospecimen evaluation of tumour cell death, cell proliferation, vascular changes or hypoxia with DOS and QUS measurements. For example, biological assays for apoptotic cell death could have used TUNEL (Terminal deoxynucleotidyl transferase (TdT) dUTP Nick-End Labelling); while using Ki-67 could have been used to assess the proliferative rate in tumour cells. Vascular assessment could have included serial biopsies to stain tumours with CD-31 (Cluster of differentiation-31); whereas using CA-9 (carbonic anhydrase-9) could have been used to validate hypoxia and tumour oxygenation. The above biological assays could have been used to compare with DOS and QUS markers. However, it should be noted that serial biopsies during chemotherapy is difficult for patients and may also cause discomfort, pain and inflammation in the tumour site which may also cause the patient undue harm. Also, in some patients, invasive procedures such as biopsies may cause breast swelling and injury to the breast which could also affect haematological measurements from DOS.

4.6 Future Work

4.6.1 Future work for Locally Advanced Breast Cancer

Future work could be directed to allow stratification of patients to tumour subtypes based on measures/markers of the tumour responses to chemotherapy using DOS and QUS. Such work could further examine the DOS and QUS imaging biomarker signatures associated with NAC responses in tumour subtypes[27] such as triple negative breast cancer, luminal A, luminal B breast cancer, HER2-positive breast cancer and by tumour grade. This future work is important since previous study results by the German Breast Group indicated that there were significant increases in long-term survival (10 years) for patients with HER2-positive (non-luminal), and triple negative breast tumours (von Minckwitz et al., 2012). Thus, further studies using DOS and QUS could be used to measure the responses in these subtypes and link DOS and QUS imaging biomarkers to other endpoints such as overall survival.

With a larger patient cohort, further work could be completed correlating DOS and QUS parameters within multinomial categories; for example, classifying patients into MP1, MP2, MP3, MP4, and MP5. This graded response classification could increase the information given to clinicians. Also, other response classification models could be used such as TNM, Sataloff index, or residual cancer burden index. These response indices are important since they also consider lymph node status in their response criteria, as involved lymph nodes after chemotherapy have been shown to decrease overall survival (von Minckwitz et al., 2012). Thus, future work could also include DOS and QUS measurements of lymph nodes as surrogate endpoints for overall survival. Evaluating lymph nodes would also give further insight to the risk of metastatic disease. Assessing the risk of metastatic lymph node involvement after neoadjuvant chemotherapy is a subject of great interest to clinicians; as lymph node metastasis after primary treatment is linked to higher mortality (Symmans et al., 2007). A recent study by Hieken et al. (2013) studied sentinel

---

[27] The subtypes are defined as: **Luminal A**: ER+/PR+/HER2-; **Luminal B**: ER+/PR+/HER2+/-/Ki67 high; **Triple Negative**: ER-/PR-/HER2-

lymph node involvement after NAC using conventional ultrasound, MRI, and PET and showed low sensitivity (range; 61.0%-69.8%) to gold-standard biopsy evaluation (Hieken et al., 2013). Thus, there is an opportunity to improve the accuracies from current imaging techniques to assess lymph node metastasis after NAC using QUS.

In terms of developing further clinical relevance using DOS and QUS, further work can be completed for analysing patients who are pCR and non-pCR; since pCR patients have been shown to demonstrate a lower tumour recurrence rate and are also more likely to live longer (i.e. >5 years) (von Minckwitz et al., 2012).

4.6.2 Applications to Early Stage Breast Cancer and Other Cancers

Neoadjuvant chemotherapy is becoming increasingly indicated for early (stage 1 and stage 2), operable invasive breast cancer (Cain et al., 2017). Patients with early breast cancer (EBC) are recommended for neoadjuvant chemotherapy upon presentation of the following clinical characteristics (Cain et al., 2017):

1. large tumours relative to the breast size; as to downstage the tumour for either total mastectomy or lumpectomy (breast conserving surgery)
2. higher risk breast cancer, i.e., positive lymph node status
3. high grade tumours, HER2+ and triple negative disease
4. women of younger age.

In a Japanese study, women with HER2-negative breast cancer (median age; 48 years old) were also indicated for neoadjuvant chemotherapy since in this tumour subgroup, the risk of tumour relapse is high and there is a low rate of pathological complete response (Masuda et al., 2017). The opportunity for future work includes using DOS and QUS to measure the chemotherapy responses in early breast cancer with the primary endpoint of surrogate imaging biomarkers for incomplete pathologic response[28], as opposed to measuring for complete pathologic response. Identifying patients for incomplete pathologic response, (i.e., residual tumour cells after NAC) could build on the recent

[28] Incomplete pathological response is defined as the presence of residual cancer cells after primary treatment.

CREATE-X study by Masuda et al. (2017). In this study, it was shown that incomplete responders benefited from additional chemotherapies, such as capecitabine[29] after surgery (Masuda et al., 2017). The results indicated that the major benefit to administering adjuvant capecitabine increased overall survival (the hazard ratio was 0.70 for patients who received capecitabine versus control group) (Masuda et al., 2017). The potential benefit of using DOS and QUS to collect early-response markers could identify incomplete responders early, so that patients could potentially receive capecitabine upfront before surgery, to downstage tumours and improve tumour response.

QUS could be used to monitor treatment response in other tumours. QUS is more ideal than DOS for imaging in other tumour types, since QUS imaging can achieve high resolution imaging in comparison to the current technology for DOS imaging that has a low resolution. Indeed, current studies are underway to use QUS imaging biomarkers to measure radiotherapy response in head and neck cancer (Tran et al. (2017), unpublished data, under review). Other disease sites, such as prostate cancer and bladder cancer could potentially benefit from using QUS imaging biomarker assessment for radiotherapy response, as pre-clinical studies are demonstrating promising results in mice models (Kim et al., 2014, Tran et al., 2016). However, one major consideration for future projects is the requirement to use high resolution QUS imaging, due to the disease presentation in prostate and bladder tumours (i.e., diffuse cancer cells), which would require intensive work on partitioning the QUS signals between normal and tumour cells.

4.6.3 Other Frameworks for Future Studies

Collaborative Frameworks Toward Biomarkers Validation and Clinical Implementation

Using DOS and QUS as a routine decision-making tool to guide therapy in oncology will require further investigation in terms of validating the results with a greater sample size. Therefore, there is a motivation for future work to

[29] Capecitabine is an antimetabolite chemotherapy drug.

confirm DOS and QUS data reproducibility across several research centres and hospitals. To achieve this, collaborations through imaging networks such as the NCI-based, Quantitative Imaging Network (QIN), Quantitative Imaging Biomarkers Alliance (QIBA), and the American College of Radiology Imaging Network (ACRIN) and Cancer Research UK (CRUK) could help with linking expertise and future work with collaborating scientists and physicians (O'Connor et al., 2016). Collaborative multicentre trials have been carried out to investigate DOS imaging in breast cancer through the ACRIN network. Future work could include participating in those multicentre trials with other research groups (Tromberg et al., 2016).

Technical Frameworks

To address the limitations of correlating DOS and QUS measurements with histological assays during treatment, potential cross validation could be completed by performing parallel imaging with other modalities such as BOLD-MRI[30]; to measure tumour blood perfusion and oxygenation to complement the physiological inferences by DOS parameters that measure haemoglobin and oxygen saturation (Jiang et al., 2013). Additionally, some early imaging studies have shown a link between ^{99m}Tc Annexin V imaging biomarkers and the rate of apoptosis; thus, it would be interesting if complementary QUS and ^{99m}Tc Annexin V imaging biomarkers could be modelled together in multivariate analyses (Blankenberg et al., 1999).

A potential opportunity for future work could be to explore image co-registration using other modalities such as MRI and conventional ultrasound. In previous studies, US-guided optical imaging has been studied and developed by Zhu *et al.,* from the University of Connecticut (Xu et al., 2015, Zhu et al., 2013, Zhu et al., 2008). In these studies, US grey-scale imaging was used to localize breast tumours, and diffuse optical imaging to map tumour haemoglobin changes during treatment (Zhu et al., 2013, Zhu et al., 2008, Xu et al., 2015,

[30] MRI-based functional imaging techniques, such as blood oxygenation-level dependent (BOLD) contrast, have indicated some promising results to measure vascular oxygenation as a marker for treatment response in tumours (Jiang et al. 2013).

Zhu et al., 2014). The technical benefits of that approach use US guidance to verify posterior (deeper) tumour margins, where optical image resolution is poorer (Zhu et al., 2008). Due to the differences in patient positioning in this present study (i.e. prone and supine for DOS and QUS, respectively), it was not possible to use ultrasound images to guide DOS, but MRIs were used to help demonstrate the extent of the tumour since patients were positioned in prone position for both imaging techniques. A future project would investigate image co-registration and fusion, which is different from image guidance. Image co-registration and fusion involves correcting for the geometric transformations between two images; as to match the spatial coordinates between objects in the images.

Lastly, an opportunity exists for modelling DOS and QUS imaging markers with bio-specimen markers, such as oestrogen receptor, progesterone receptor, HER2, proliferation markers such as Ki67, or vascular markers such as CD-31 using the pre-treatment breast biopsies. Previous work by Ueda et al. (2012) used multivariate analyses for baseline DOS parameters combined with tissue biomarkers from immunohistochemistry (Ueda et al., 2012). Markers for cell proliferation (Ki67), and molecular features (oestrogen and progesterone receptor) were combined with optical measurements such as HbO_2, Hb, or the tumour oxygen saturation (StO_2). Multivariate discriminant analysis of the combined parameters demonstrated an increase in the sensitivity and specificity for predicting NAC response. The results from Ueda et al. (2012) support the need for further exploration into combination analysis to improve the predictive performance of multiple imaging and clinical biomarkers (Ueda et al., 2012).

4.7 Conclusion

In this study, DOS and QUS imaging was explored for the potential to extract imaging biomarkers in locally advanced breast cancer patients to report first accounts of coincident expression during neoadjuvant chemotherapy. The results from the present study support, and build on, the previous body of work suggesting that DOS and QUS imaging biomarkers may be extracted from breast tumours either before, or during, chemotherapy.

In this study, baseline DOS functional maps were also examined using GLCM-texture analysis to predict patient response to NAC. The results of this study demonstrated that an increase in cell death markers from QUS correlated with a decrease in tumour haemoglobin markers from DOS; suggesting that cell death and vascular remodelling were typically predictive of a favourable treatment response. The results of subproject two also indicated that DOS-texture features differentiated between response groups before the start of treatment, based on the biological features of breast tumours. Here, high sensitivity and specificity with pathologic endpoints as measured using Miller-Payne pathologic response criteria were shown in this study.

Using DOS and QUS imaging modalities together and deriving combined acoustic and optical spectral data could provide more powerful imaging signatures to help guide treatment decisions and improve outcomes for patients. With further validation studies, it would be plausible to use DOS-QUS markers as biological surrogates to predict tumour response to neoadjuvant chemotherapy. These imaging modalities are lower in cost compared to MRI and CT, non-invasive and can be acquired quickly and in series within the patient's treatment schedule. Coincident DOS and QUS changes are important to understand the pathophysiological traits in tumours for better treatment response evaluation. Although further studies are required, this first report demonstrates promising potential for DOS-based textural parameters to evaluate baseline tumour vascular heterogeneity, and subsequently as markers for response to chemotherapy. The use of DOS and QUS markers may help guide treatments to personalize patient care plans by potentially predicting chemoresponse and to extract early-response indicators to help physicians make decisions about the patient's treatment. Ultimately if used to guide

therapy, validated DOS and QUS imaging biomarkers may help improve breast cancer therapeutics and may be further studied to potentially improve overall disease-free survival.

Appendix 1

Supplementary Information to Chapter 1

A1.1 Radiological Tumour Response Endpoints

A1.1.1 WHO Tumour-response Imaging Guidelines

The standards set by the WHO were developed in the early 1980s and measures the changes in tumour dimensions to classify treatment response (**Figure A1.1**) (Park et al., 2003). Tumour measurements are taken from radiographs, and a value is calculated from the product of the longest overall tumour diameter, and the longest perpendicular diameter (mm x mm). This calculation is known as the sum of the products of diameters (SPD) (**Figure A1.1**). In order to quantify tumour response, a relative percent change from the baseline SPD is computed. Response categories are based on the overall percent changes and are classified as (Tirkes et al., 2013):

1. **Complete response (CR)**. There is no detectable tumour on imaging for at least four weeks.
2. **Partial response (PR)**. There is a ≥50% reduction in the SPD at four weeks relative to baseline.
3. **Progressive disease (PD)**. There is a ≥25% increase in the SPD.
4. **Stable disease (SD)**. There is no significant change; neither partial response, or progressive disease.

A1.1.2 RECIST 1.1 Guidelines

RECIST guidelines were introduced in the early 2000s and have been updated recently to simplify the recommendations on tumour measurement

techniques and to include CT-based imaging (RECIST Version 1.1)(Eisenhauer et al., 2009, Therasse et al., 2000). Significant differences between RECIST 1.1 and WHO guidelines include changes in the classification cut-off points and modifying the way tumours are measured. For breast tumours, RECIST 1.1 guidelines require only unidimensional tumour measurements and optimal analysis is recommended on axial CT images (**Figure A1.1**). Tumour response is classified based on the relative percent changes from the baseline (Eisenhauer et al., 2009):

1. **Complete Response (CR):** Disappearance of all target lesions. Any pathological lymph nodes (both target and non-target lesions) have been reduced to less than 10 mm in the short axis.
2. **Partial Response (PR):** ≥30% decrease in the sum of the longest diameter of the target lesion compared to baseline.
3. **Progressive Disease (PD):** ≥20% increase in the sum of the shortest diameter of the target lesion compared to baseline
4. **Stable Disease (SD):** No significant change to tumour dimension. Neither PR or PD.

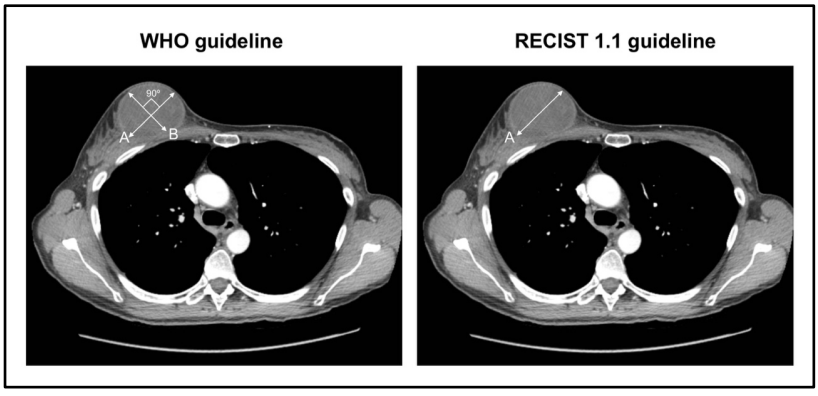

Figure A1.1: CT of the chest indicating a right breast tumour. (Left) WHO guidelines use the cross-product of the longest tumour measurement **(Arrow A)** and the perpendicular longest measurement **(Arrow B).** The sum of the product of diameters (SPD) is used to measure relative percent changes from baseline. **(Right)** RECIST 1.1 guidelines measure the sum of the longest tumour dimension to calculate the relative changes in tumour size during treatment **(Arrow A)**. (Image taken from clinical breast patient at Sunnybrook Health Sciences Centre, Toronto, Canada).

A1.1.3 Limitations of using Radiological Response Endpoints

Limitations for WHO and RECIST 1.1 methods include variability among readers were previously shown in determining the longest tumour measurement and errors increased when readers were measuring multifocal malignant lesions (Kang et al., 2012). Also WHO guidelines have been limited in describing the utility of three-dimensional imaging such as computed tomography (CT) and magnetic resonance imaging (MRI) (Kang et al., 2012). Size-based measurements to monitor treatment response have shifted towards using updated guidelines such as RECIST since it has shown greater applicability with newer imaging modalities such as MRI and CT (Schwartz et al., 2016). Limitations for RECIST criteria include the spatial resolution constraints for CT imaging which restrict imaging for lesions > 1 cm only (Eisenhauer et al., 2009). Other significant limitations include the overestimation of the tumour's size on imaging due fibrosis and scattered residual nodules that can appear as enhanced imaging features on MRI and CT (Pritt and Weaver, 2005).

Appendix 2

Supplementary Information to Chapter 2

A2.1 Institutional Ethics Review Board Approval Letters

Inquiries regarding ethics approval may be sent to:

Human Research Protections Program, Sunnybrook Health Sciences Centre
C825, 2075 Bayview Avenue
Toronto, Ontario, M4N3M5
Tel: 416 480 6100 x 88144
Fax: 416 480 5385

Sunnybrook
HEALTH SCIENCES CENTRE

Research Ethics Office, Room C819
2075 Bayview Avenue
Toronto, ON Canada M4N 3M5
t: 416-480-6100 ext. 4276 or 88144
www.sunnybrook.ca/reo

To: Dr. Gregory Czarnota
Radiation Oncology
Room T2 167

From: Dr. Brian Murray

Date: July 4, 2014

Subject: **A Pilot Study to Evaluate the Effectiveness of Pulsed Time-Domain Optical Spectroscopy for Monitoring the Responses in Neoadjuvant Treatments of Locally-Advanced Breast Cancer**

Project Identification Number: 186-2006

This letter serves as an acknowledgment that Mr. William Tran, Radiation Therapist at Sunnybrook Health Sciences Centre Odette Cancer Centre, has been delegated responsibilities for this study as study personnel by the Principal Investigator within the capacity of his role at Sunnybrook and as a PhD student. Mr. Tran will be analyzing data as part of his role and the analysis will be done in accordance with the REB approved protocol.

Thank you for keeping the Board informed.

Brian Murray, MD FRCP(C) D,ABSM
Chair, Research Ethics Board
/tt

OR

Philip C. Hébert, MD PhD FCFPC
Vice-Chair, Research Ethics Board

Sunnybrook
HEALTH SCIENCES CENTRE

Research Ethics Office, Room C819
2075 Bayview Avenue
Toronto, ON Canada M4N 3M5
t: 416-480-6100 ext. 4276 or 88144
www.sunnybrook.ca/reo

To: Dr. Gregory Czarnota
Radiation Oncology
Room T2 167

From: Dr. Brian Murray

Date: July 4, 2014

Subject: **Pilot Investigation of Ultrasound Imaging and Spectroscopy and Ultrasound Imaging of Vascular Blood Flow as Early Indicators of Locally-Advanced Breast Cancer Response to Neoadjuvant Treatment**

Project Identification Number: 185-2006

This letter serves as an acknowledgment that Mr. William Tran, Radiation Therapist at Sunnybrook Health Sciences Centre Odette Cancer Centre, has been delegated responsibilities for this study as study personnel by the Principal Investigator within the capacity of his role at Sunnybrook and as a PhD student. Mr. Tran will be analyzing data as part of his role and the analysis will be done in accordance with the REB approved protocol.

Thank you for keeping the Board informed.

Brian Murray, MD FRCP(C) D,ABSM
Chair, Research Ethics Board

OR

Philip C. Hébert, MD PhD FCFPC
Vice-Chair, Research Ethics Board

A2.2 Image Processing

A2.2.1 Fast Fourier Transform (FFT) (QUS)

Fast Fourier Transform (FFT) of the amplitude line spectrum;

$$A_l(f,z_l)=\left(\frac{\gamma}{2}\right)^2 \frac{A_s(f,z_l)}{A_r(f,z_l)}$$

Calculation of the power spectrum is done by applying a fast Fourier transform (FFT, $A_s(f,z_l)$) of a gated radiofrequency data line segment (z_l) to obtain the amplitude line spectrum ($A_l(f,z_l)$)

To reduce spectral-noise artefacts, a sliding window algorithm was used with the settings of a Hamming window function for gating, where there was an 80% overlap between adjacent windows in the axial direction. A reference phantom technique was used to remove system transfer effects from the data using a tissue-mimicking agar-embedded glass-bead phantom with known acoustic properties (Tadayyon et al., 2014).

Calibration using a reference signal;

$$S(f)=\log_{10}\frac{1}{N}\sum_{l=1}^{N}/A_l(f,z_l)/^2 e^{-4(\alpha_s-\alpha_r)(R+\frac{\Delta z}{2})}$$

To normalize the tissue sample signal to the reference phantom, the amplitude line spectrum is calculated in the same manner; where $A_r(f,z_l)$ is the FFT of the gated radiofrequency signal from the ROIs of the reference phantom. The log power spectrum $S(f)$ is computed by the average of the squared magnitudes of the amplitude line spectra by lateral windowing. The depth-dependent acoustic attenuation (α) is employed for calculating the power spectrum, where α_s and α_r refer to the attenuation of the tissue and reference, respectively. The resulting normalized power spectrum was calculated; where R is the on-axis distance between the transducer and the proximal gated window, and Δz is the range of the axial distance of the gated window (Insana and Hall, 1990).

A2.2.2 Calculation for Sound Intensity (dB)

$$dB = 10log_{10}\frac{(Z_1 - Z_2)^2}{(Z_1 + Z_2)^2}$$

where; Z_1 and Z_2 corresponds to the characteristic impedance of a medium (1) and medium (2), respectively. The characteristic impedance, Z, is defined as;

$$Z = \rho c$$

where ρ = density of the material, and c = speed of sound in the medium.

A2.2.3 Calculation for Average Speed of Sound in Soft Tissue

$c = \sqrt{\frac{1}{\rho\kappa}}$ (Madsen et al., 1978):

A2.2.4 QUS Axial Resolution

The SPL is expressed as;

$$SPL = N\lambda$$

To determine the "best" axial resolution, a mathematical function is expressed that is derived from the SPL:

$$R_{(axial)} = \frac{c}{4\Delta f}\ (mm)$$

Axial resolution was calculated as:

$$R_{(axial)} = \frac{0.77}{\Delta f}\ ;$$

where the frequency bandwidth was 3-8 MHz, (Δf) = 5 MHz

$$R_{(axial)} = \frac{0.77}{5\ MHz}\ ;$$

therefore,

$$\boldsymbol{R_{(axial)} = 0.154\ mm}$$

Assumptions: The average speed of sound in soft tissue (i.e. breast) is 1540 m/s, the best axial resolution would be expressed mathematically as, $R_{(axial)} = \frac{0.77}{\Delta f}$ (O'Brien, 2007), where Δf is equal to the system bandwidth (frequency range) in MHz.

A2.2.5 QUS Lateral resolution (at focus)

$$R_{lateral} = F \times \lambda\ \ ;$$

where the speed of sound was 1540 m/s and central frequency was 7 MHz and F[31] is the F_{number}:

$$R_{lateral} = 0.98\ x\ 0.22\ mm\ \ ;$$

therefore,

$$\boldsymbol{R_{lateral} = 0.21\ mm}$$

The optimal lateral resolution of the imaging system used was 0.21 mm.

[31] The F number was obtained from the settings profile of the ultrasound system.

Appendix 3

Supplementary Information to Chapter 3

A3.1. Pathological Assessment

A.3.1.1 Pathological responder versus Pathological non-responder

Representative immunohistochemistry staining.

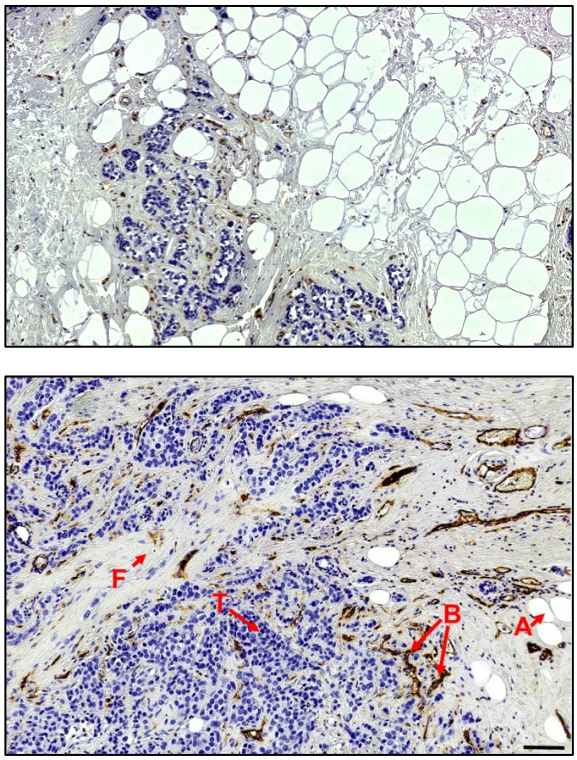

Figure A3.1. Light microscopy of a responder's breast tumour (Patient #10) and a non-responder's breast tumour after chemotherapy (Study Patient # 21). Tumour specimens were stained with haematoxylin and eosin and cluster of differentiation-31 (CD-31) for vascular detection. Biophysical features demonstrated differences in the tissue composition. Spatial heterogeneity between responders and non-responders were observed. **Legend: (A)** Adipocyte; **(B)** Blood Vessels; **(F)** Fibroblasts; **(T)** (Tumour Cells).

A.3.1.2 Mastectomy histology demonstrated a significant difference in vascular density between responders and non-responders as assessed by CD31 immunohistochemistry staining.

Appendix 4

Supplementary Information to Chapter 4

A4.3 Summary of Contributions of Thesis Study

Description of Studies Published from Thesis		
No.	**Reference**	**Summary of Work/Significant Findings/Optimal Markers**
23	Tran et al. (2016)	• DOS and QUS measurements were obtained in parallel, at the same time intervals (baseline, week one, week four, week eight, preoperatively). • Results demonstrated that univariate QUS (SI) and DOS (HbO_2) markers were significantly different between responders and non-responders after one week of treatment (*p<0.01*). The %Sn and %Sp for the SI was 64.3% and 87.5%, respectively and for HbO2, the %Sn and %Sp was 85.7% and 87.5%, respectively. • The best multivariate (pairwise) combinations included the SI + HbO_2 which resulted in an AUC of 1.00 after one week (*p<0.001*)
24	Tran et al. (2017)	• Pre-treatment DOS-texture markers demonstrated significant differences between responders and non-responders. • The HbO_2 homogeneity resulted in the highest accuracy among univariate parameters in predicting response to chemotherapy; corresponding to a %Sn and %Sp were 86.5% and 89.0%, respectively, and accuracy was 87.8%. The highest predictors using multivariate (binary) combination features were the Hb-contrast + HbO_2-homogeneity, which resulted in a %Sn/ %Sp¼78.0/81.0% and an accuracy of 79.5%.

Table A4.4: Significant contributions related to the work outlined in the thesis. The major contributions include using DOS and QUS at the same temporal time intervals, and using pre-treatment DOS-texture features to predict chemotherapy response.

Appendix 5

Academic Output from PhD

A5.1 Overview and Summary

OUTPUT TYPE	COUNT
Primary Author Publications	3
Contributing Author Publications	9
Book Chapters	1
Conference Presentations	6

A5.2 Publications (Primary Author)

1. **Tran WT**, Gangeh MJ, Sannachi L, Chin L, Watkins E, Bruni SG, Rastegar RF, Curpen B, Trudeau M, Gandhi S, Yaffe M, Slodkowska E, Childs C, Sadeghi-Naini A, Czarnota GJ. **Predicting breast cancer response to neoadjuvant chemotherapy using pre-treatment diffuse optical spectroscopic texture analysis.** Br J Cancer. 2017 Apr 18. doi: 10.1038/bjc.2017.97. [Epub ahead of print] PubMed PMID: 28419079. **Impact Factor: 5.57**

2. **Tran WT**, Childs C, Chin L, Slodkowska E, Sannachi L, Tadayyon H, Watkins E, Wong SL, Curpen B, El Kaffas A, Al-Mahrouki A, Sadeghi-Naini A, Czarnota GJ. **Multiparametric monitoring of chemotherapy treatment response in locally advanced breast cancer using quantitative ultrasound and diffuse optical spectroscopy.** Oncotarget. 2016 Apr 12;7(15):19762-80. doi: 10.18632/oncotarget.7844. PubMed PMID: 26942698; PubMed Central PMCID: PMC4991417. **Impact Factor: 5.00**

3. **Tran WT**, Childs C, Probst H, Farhat G, Czarnota GJ. Commentary: Imaging Biomarkers for Precision Medicine in Locally Advanced Breast Cancer. Accepted September 2017. In Press. Journal of Medical Imaging and Radiation Sciences. **Impact Factor: N/A**

A5.3 Publications (Contributing Author)

1. Sadeghi-Naini A, Sannachi L, Tadayyon H, **Tran WT**, Slodkowska E, Trudeau M, Gandhi S, Pritchard K, Kolios MC, Czarnota GJ. Chemotherapy-Response Monitoring of Breast Cancer Patients Using Quantitative Ultrasound-Based Intra-Tumour Heterogeneities. Sci Rep. 2017 Sep 4;7(1):10352. doi: 10.1038/s41598-017-09678-0. PMID: 28871171. **Impact Factor: 5.23**

2. Tadayyon H, Sannachi L, Gangeh MJ, Kim C, Ghandi S, Trudeau M, Pritchard K, **Tran WT**, Slodkowska E, Sadeghi-Naini A, Czarnota GJ. **A priori Prediction of Neoadjuvant Chemotherapy Response and Survival in Breast Cancer Patients using Quantitative Ultrasound**. Sci Rep. 2017 Apr 12;7:45733. doi: 10.1038/srep45733. PubMed PMID: 28401902; PubMed Central PMCID: PMC53 50. **Impact Factor: 5.23**

3. Pasternak M, Doss L, Farhat G, Al-Mahrouki A, Kim CH, Kolios M, **Tran WT**, Czarnota GJ. **Effect of chromatin structure on quantitative ultrasound parameters**. Oncotarget. 2017 Mar 21;8(12):19631-19644. doi: 10.18632/oncotarget.14816. PubMed PMID: 28129644; PubMed Central PMCID: PMC5386710. **Impact Factor: 5.00**

4. Tadayyon H, Sannachi L, Gangeh M, Sadeghi-Naini A, **Tran W**, Trudeau ME, Pritchard K, Ghandi S, Verma S, Czarnota GJ. **Quantitative ultrasound assessment of breast tumour response to chemotherapy using a multi-parameter approach.** Oncotarget. 2016 Jul 19;7(29):45094-45111. doi: 10.18632/oncotarget.8862. PubMed PMID: 27105515; PubMed Central PMCID: PMC5216708. **Impact Factor: 5.00**

5. Tadayyon H, Sannachi L, Sadeghi-Naini A, Al-Mahrouki A, **Tran WT**, Kolios MC, Czarnota GJ. Quantification of Ultrasonic Scattering **Properties of In Vivo Tumour Cell Death in Mouse Models of Breast Cancer.** Transl Oncol. 2015 Dec;8(6):463-73. doi: 10.1016/j.tranon.2015.11.001. PubMed PMID: 26692527; PubMed Central PMCID: PMC4701005. **Impact Factor: 3.01**

6. Gangeh MJ, Tadayyon H, Sannachi L, Sadeghi-Naini A, **Tran WT**, Czarnota GJ. **Computer Aided Theragnosis Using Quantitative Ultrasound Spectroscopy and Maximum Mean Discrepancy in Locally Advanced Breast Cancer.** IEEE Trans Med Imaging. 2016 Mar;35(3):778-90. doi: 10.1109/TMI.2015.2495246. Epub 2015 Oct 27. PubMed PMID: 26529750.

Impact Factor: 3.76

7. Sadeghi-Naini A, Vorauer E, Chin L, Falou O, **Tran WT**, Wright FC, Gandhi S, Yaffe MJ, Czarnota GJ. **Early detection of chemotherapy-refractory patients by monitoring textural alterations in diffuse optical spectroscopic images.** Med Phys. 2015 Nov;42(11):6130-46. doi: 10.1118/1.4931603. PubMed PMID: 26520706.
Impact Factor: 2.64

8. Sannachi L, Tadayyon H, Sadeghi-Naini A, **Tran W**, Gandhi S, Wright F, Oelze M, Czarnota G. **Non-invasive evaluation of breast cancer response to chemotherapy using quantitative ultrasonic backscatter parameters.** Med Image Anal. 2015 Feb;20(1):224-36. doi: 10.1016/j.media.2014.11.009. Epub 2014 Nov 25. PubMed PMID: 25534283.
Impact Factor: 4.57

9. Sadeghi-Naini A, Falou O, Tadayyon H, Al-Mahrouki A, **Tran W,** Papanicolau N, Kolios MC, Czarnota GJ. **Conventional frequency ultrasonic biomarkers of cancer treatment response in vivo.** Transl Oncol. 2013 Jun 1;6(3):234-43. Print 2013 Jun. Erratum in: Transl Oncol. 2013 Dec;6(6):erratum. PubMed PMID: 23761215; PubMed Central PMCID: PMC3678128.
Impact Factor: 3.01

A5.4 Conference Presentations and Posters

1. **Tran W.** and Czarnota GJ. DOS and QUS imaging biomarkers in locally advanced breast cancer. Canadian Consensus Meeting on Locally Advanced Breast Cancer. 2017. **Podium Presentation.**

2. **Tran WT**, Gangeh M, Suraweera H., Hadizad F., Watkins E., Czarnota GJ. DOS and QUS multiparametric modelling to measure neoadjuvant chemotherapy response in locally advanced breast cancer. Terry Fox Research Institute Cancer Symposium. Vancouver BC. 2016. **Poster Presentation.**

3. **Tran WT**, Gangeh M, Suraweera H., Hadizad F., Watkins E., Czarnota GJ. Multiparametric analysis of DOS and QUS imaging biomarkers to monitor chemotherapy response in breast cancer. Ultrasonic Imaging and Tissue Characterization Symposium. Washington DC, USA. 2015. **Podium Presentation.**

4. **Tran W.,** Kim C. Czarnota GJ. Cell death detection in locally advanced breast cancer using quantitative ultrasound and diffuse optical spectroscopy. IEEE International Ultrasonics Symposium, Chicago USA. 2014. **Poster Presentation**

5. Gangeh M, Tadayyon H., Sannachi L., Sadeghi-Naini A., **Tran W**., Czarnota GJ. Texton-Based Method in Clinical Cancer Response Monitoring. IEEE International Ultrasonics Symposium, Chicago USA. 2014. **Poster Presentation**

6. Gangeh M, Tadayyon H., Sannachi L., Sadeghi-Naini A., **Tran W**., Czarnota GJ. Computer-Aided Theragnosis Using Quantitative Ultrasound Spectroscopy and Maximum Mean Discrepancy in Locally Advanced Breast Cancer. IEEE International Ultrasonics Symposium, Chicago USA. 2014. **Poster Presentation**

A5.5 Book Chapters

1. Gangeh M., Tadayyon H., **Tran W**., Czarnota G. Machine Learning Applications in Cancer Therapy Assessment and Implications on Clinical Practice. Handbook of research on data science for effective healthcare practice and administration. Editors: Far, Behrouz H, 1959-; Albadvi, Amir, 1961-; Raahemi, Bijan, 1964-; Noughabi, Elham Akhond Zadeh. Hershey, PA: Medical Information Science Reference, [2017]. NLM ID: 101699768. ISBN13: 9781522525158|ISBN10: 1522525157|EISBN13: 9781522525165|DOI: 10.4018/978-1-5225-2515-8

Bibliography

ABRAMSON, R. G., LI, X., HOYT, T. L., SU, P. F., ARLINGHAUS, L. R., WILSON, K. J., ABRAMSON, V. G., CHAKRAVARTHY, A. B. & YANKEELOV, T. E. 2013. Early assessment of breast cancer response to neoadjuvant chemotherapy by semi-quantitative analysis of high-temporal resolution DCE-MRI: preliminary results. *Magn Reson Imaging,* 31**,** 1457-64.

AGHAEI, F., TAN, M., HOLLINGSWORTH, A. B. & ZHENG, B. 2016. Applying a new quantitative global breast MRI feature analysis scheme to assess tumor response to chemotherapy. *J Magn Reson Imaging,* 44**,** 1099-1106.

AH-SEE, M. L., MAKRIS, A., TAYLOR, N. J., HARRISON, M., RICHMAN, P. I., BURCOMBE, R. J., STIRLING, J. J., D'ARCY, J. A., COLLINS, D. J., PITTAM, M. R., RAVICHANDRAN, D. & PADHANI, A. R. 2008. Early changes in functional dynamic magnetic resonance imaging predict for pathologic response to neoadjuvant chemotherapy in primary breast cancer. *Clin Cancer Res,* 14**,** 6580-9.

AHMED, A., GIBBS, P., PICKLES, M. & TURNBULL, L. 2013. Texture analysis in assessment and prediction of chemotherapy response in breast cancer. *J Magn Reson Imaging,* 38**,** 89-101.

ALVARADO-CABRERO, I., ALDERETE-VAZQUEZ, G., QUINTAL-RAMIREZ, M., PATINO, M. & RUIZ, E. 2009. Incidence of pathologic complete response in women treated with preoperative chemotherapy for locally advanced breast cancer: correlation of histology, hormone receptor status, Her2/Neu, and gross pathologic findings. *Ann Diagn Pathol,* 13**,** 151-7.

AMERICAN COLLEGE OF RADIOLOGY IMAGING NETWORK, A. 2017. *ACRIN 6691 Participating Sites* [Online]. Available: https://www.acrin.org/PROTOCOLSUMMARYTABLE/PROTOCOL6691/6691ParticipatingSites/tabid/745/Default.aspx [Accessed July 15 2017 2017].

AMIOKA, A., MASUMOTO, N., GOUDA, N., KAJITANI, K., SHIGEMATSU, H., EMI, A., KADOYA, T. & OKADA, M. 2016. Ability of contrast-enhanced ultrasonography to determine clinical responses of breast cancer to neoadjuvant chemotherapy. *Jpn J Clin Oncol,* 46**,** 303-9.

ANDRADE, W. P., LIMA, E. N., OSORIO, C. A., DO SOCORRO MACIEL, M., BAIOCCHI, G., BITENCOURT, A. G., FANELLI, M. F., DAMASCENA, A. S. & SOARES, F. A. 2013. Can FDG-PET/CT predict early response to neoadjuvant chemotherapy in breast cancer? *Eur J Surg Oncol,* 39**,** 1358-63.

ANDRE, F., MAZOUNI, C., LIEDTKE, C., KAU, S. W., FRYE, D., GREEN, M., GONZALEZ-ANGULO, A. M., SYMMANS, W. F., HORTOBAGYI, G. N. & PUSZTAI, L. 2008. HER2 expression and efficacy of preoperative paclitaxel/FAC chemotherapy in breast cancer. *Breast Cancer Res Treat,* 108**,** 183-90.

ANTONIOU, A., PHAROAH, P. D., NAROD, S., RISCH, H. A., EYFJORD, J. E., HOPPER, J. L., LOMAN, N., OLSSON, H., JOHANNSSON, O., BORG, A., PASINI, B., RADICE, P., MANOUKIAN, S., ECCLES, D. M., TANG, N., OLAH, E., ANTON-CULVER, H., WARNER, E., LUBINSKI, J.,

GRONWALD, J., GORSKI, B., TULINIUS, H., THORLACIUS, S., EEROLA, H., NEVANLINNA, H., SYRJAKOSKI, K., KALLIONIEMI, O. P., THOMPSON, D., EVANS, C., PETO, J., LALLOO, F., EVANS, D. G. & EASTON, D. F. 2003. Average risks of breast and ovarian cancer associated with BRCA1 or BRCA2 mutations detected in case Series unselected for family history: a combined analysis of 22 studies. *Am J Hum Genet,* 72**,** 1117-30.

ARGYRIOU, A. A., POLYCHRONOPOULOS, P., ICONOMOU, G., KOUTRAS, A., KALOFONOS, H. P. & CHRONI, E. 2005. Paclitaxel plus carboplatin-induced peripheral neuropathy. A prospective clinical and electrophysiological study in patients suffering from solid malignancies. *J Neurol,* 252**,** 1459-64.

ARPINO, G., CIOCCA, D. R., WEISS, H., ALLRED, D. C., DAGUERRE, P., VARGAS-ROIG, L., LEUZZI, M., GAGO, F., ELLEDGE, R. & MOHSIN, S. K. 2005. Predictive value of apoptosis, proliferation, HER-2, and topoisomerase IIalpha for anthracycline chemotherapy in locally advanced breast cancer. *Breast Cancer Res Treat,* 92**,** 69-75.

ATCHLEY, D. P., ALBARRACIN, C. T., LOPEZ, A., VALERO, V., AMOS, C. I., GONZALEZ-ANGULO, A. M., HORTOBAGYI, G. N. & ARUN, B. K. 2008. Clinical and pathologic characteristics of patients with BRCA-positive and BRCA-negative breast cancer. *J Clin Oncol,* 26**,** 4282-8.

ATHANASIOU, A., TARDIVON, A., OLLIVIER, L., THIBAULT, F., EL KHOURY, C. & NEUENSCHWANDER, S. 2009. How to optimize breast ultrasound. *Eur J Radiol,* 69**,** 6-13.

ATUEGWU, N. C., ARLINGHAUS, L. R., LI, X., CHAKRAVARTHY, A. B., ABRAMSON, V. G., SANDERS, M. E. & YANKEELOV, T. E. 2013. Parameterizing the Logistic Model of Tumor Growth by DW-MRI and DCE-MRI Data to Predict Treatment Response and Changes in Breast Cancer Cellularity during Neoadjuvant Chemotherapy. *Transl Oncol,* 6**,** 256-64.

AUSTOKER, J. 2003. Breast self examination. *BMJ,* 326**,** 1-2.

BABYSHKINA, N., MALINOVSKAYA, E., PATALYAK, S., BRAGINA, O., TARABANOVSKAYA, N., DOROSHENKO, A., SLONIMSKAYA, E., PERELMUTER, V. & CHERDYNTSEVA, N. 2014. Neoadjuvant chemotherapy for different molecular breast cancer subtypes: a retrospective study in Russian population. *Med Oncol,* 31**,** 165.

BAEK, H. M., CHEN, J. H., NIE, K., YU, H. J., BAHRI, S., MEHTA, R. S., NALCIOGLU, O. & SU, M. Y. 2009. Predicting pathologic response to neoadjuvant chemotherapy in breast cancer by using MR imaging and quantitative 1H MR spectroscopy. *Radiology,* 251**,** 653-62.

BAGLEY, C. M., JR., DEVITA, V. T., JR., BERARD, C. W. & CANELLOS, G. P. 1972. Advanced lymphosarcoma: intensive cyclical combination chemotherapy with cyclophosphamide, vincristine, and prednisone. *Ann Intern Med,* 76**,** 227-34.

BALLEYGUIER, C., AYADI, S., VAN NGUYEN, K., VANEL, D., DROMAIN, C. & SIGAL, R. 2007. BIRADS classification in mammography. *Eur J Radiol,* 61**,** 192-4.

BANIHASHEMI, B., VLAD, R., DEBELJEVIC, B., GILES, A., KOLIOS, M. C. & CZARNOTA, G. J. 2008. Ultrasound imaging of apoptosis in tumor response: novel preclinical monitoring of photodynamic therapy effects. *Cancer Res,* 68**,** 8590-6.

BARER, R. 1957. Refractometry and interferometry of living cells. *J Opt Soc Am,* 47**,** 545-56.
BECKMANN, M. W., NIEDERACHER, D., SCHNURCH, H. G., GUSTERSON, B. A. & BENDER, H. G. 1997. Multistep carcinogenesis of breast cancer and tumour heterogeneity. *J Mol Med (Berl),* 75**,** 429-39.
BEDWINEK, J., RAO, D. V., PEREZ, C., LEE, J. & FINEBERG, B. 1982. Stage III and localized stage IV breast cancer: irradiation alone vs irradiation plus surgery. *Int J Radiat Oncol Biol Phys,* 8**,** 31-6.
BELLI, P., COSTANTINI, M., IERARDI, C., BUFI, E., AMATO, D., MULE, A., NARDONE, L., TERRIBILE, D. & BONOMO, L. 2011. Diffusion-weighted imaging in evaluating the response to neoadjuvant breast cancer treatment. *Breast J,* 17**,** 610-9.
BERGERS, G. & BENJAMIN, L. E. 2003. Tumorigenesis and the angiogenic switch. *Nat Rev Cancer,* 3**,** 401-10.
BERRIOLO-RIEDINGER, A., TOUZERY, C., RIEDINGER, J. M., TOUBEAU, M., COUDERT, B., ARNOULD, L., BOICHOT, C., COCHET, A., FUMOLEAU, P. & BRUNOTTE, F. 2007. [18F]FDG-PET predicts complete pathological response of breast cancer to neoadjuvant chemotherapy. *Eur J Nucl Med Mol Imaging,* 34**,** 1915-24.
BLAMEY, R. W. 2002. Estimation of prognosis of the individual with primary breast cancer and its applications. *Scand J Surg,* 91**,** 273-8.
BLANKENBERG, F. G., KATSIKIS, P. D., TAIT, J. F., DAVIS, R. E., NAUMOVSKI, L., OHTSUKI, K., KOPIWODA, S., ABRAMS, M. J. & STRAUSS, H. W. 1999. Imaging of apoptosis (programmed cell death) with 99mTc annexin V. *J Nucl Med,* 40**,** 184-91.
BLOMLEY, M. J., COOKE, J. C., UNGER, E. C., MONAGHAN, M. J. & COSGROVE, D. O. 2001. Microbubble contrast agents: a new era in ultrasound. *BMJ,* 322**,** 1222-5.
BLUMEN, H., FITCH, K. & POLKUS, V. 2016. Comparison of Treatment Costs for Breast Cancer, by Tumor Stage and Type of Service. *Am Health Drug Benefits,* 9**,** 23-32.
BOAS, D. A., PITRIS, C. & RAMANUJAM, N. 2011. *Handbook of biomedical optics,* Boca Raton, CRC Press.
BOLD, R. J., TERMUHLEN, P. M. & MCCONKEY, D. J. 1997. Apoptosis, cancer and cancer therapy. *Surg Oncol,* 6**,** 133-42.
BOSSUYT, P. M., REITSMA, J. B., BRUNS, D. E., GATSONIS, C. A., GLASZIOU, P. P., IRWIG, L. M., MOHER, D., RENNIE, D., DE VET, H. C., LIJMER, J. G. & STANDARDS FOR REPORTING OF DIAGNOSTIC, A. 2003. The STARD statement for reporting studies of diagnostic accuracy: explanation and elaboration. *Ann Intern Med,* 138**,** W1-12.
BOUSSIOS, S., PENTHEROUDAKIS, G., KATSANOS, K. & PAVLIDIS, N. 2012. Systemic treatment-induced gastrointestinal toxicity: incidence, clinical presentation and management. *Ann Gastroenterol,* 25**,** 106-118.
BRAND, S., WEISS, E. C., LEMOR, R. M. & KOLIOS, M. C. 2008. High frequency ultrasound tissue characterization and acoustic microscopy of intracellular changes. *Ultrasound Med Biol,* 34**,** 1396-407.
BROADWATER, J. R., EDWARDS, M. J., KUGLEN, C., HORTOBAGYI, G. N., AMES, F. C. & BALCH, C. M. 1991. Mastectomy following preoperative chemotherapy. Strict operative criteria control operative morbidity. *Ann Surg,* 213**,** 126-9.
BUCHBENDER, C., KUEMMEL, S., HOFFMANN, O., STAHL, A. R., KIMMIG, R., OTTERBACH, F., LADD, S., KOENINGER, A., FORSTING, M.,

BOCKISCH, A., ANTOCH, G. & HEUSNER, T. A. 2012. FDG-PET/CT for the early prediction of histopathological complete response to neoadjuvant chemotherapy in breast cancer patients: initial results. *Acta Radiol,* 53**,** 628-36.

BUCHHOLZ, T. A., DAVIS, D. W., MCCONKEY, D. J., SYMMANS, W. F., VALERO, V., JHINGRAN, A., TUCKER, S. L., PUSZTAI, L., CRISTOFANILLI, M., ESTEVA, F. J., HORTOBAGYI, G. N. & SAHIN, A. A. 2003. Chemotherapy-induced apoptosis and Bcl-2 levels correlate with breast cancer response to chemotherapy. *Cancer J,* 9**,** 33-41.

BURCOMBE, R. J., MAKRIS, A., PITTAM, M., LOWE, J., EMMOTT, J. & WONG, W. L. 2002. Evaluation of good clinical response to neoadjuvant chemotherapy in primary breast cancer using [18F]-fluorodeoxyglucose positron emission tomography. *Eur J Cancer,* 38**,** 375-9.

BURSTEIN, H. J., POLYAK, K., WONG, J. S., LESTER, S. C. & KAELIN, C. M. 2004. Ductal carcinoma in situ of the breast. *N Engl J Med,* 350**,** 1430-41.

BUTCHER, D. T., ALLISTON, T. & WEAVER, V. M. 2009. A tense situation: forcing tumour progression. *Nat Rev Cancer,* 9**,** 108-22.

CAIN, H., MACPHERSON, I. R., BERESFORD, M., PINDER, S. E., PONG, J. & DIXON, J. M. 2017. Neoadjuvant Therapy in Early Breast Cancer: Treatment Considerations and Common Debates in Practice. *Clin Oncol (R Coll Radiol),* 29**,** 642-652.

CAMPBELL, J. D. & RAMSEY, S. D. 2009. The costs of treating breast cancer in the US: a synthesis of published evidence. *Pharmacoeconomics,* 27**,** 199-209.

CAMPISI, J. 2013. Aging, cellular senescence, and cancer. *Annu Rev Physiol,* 75**,** 685-705.

CANCE, W. G., CAREY, L. A., CALVO, B. F., SARTOR, C., SAWYER, L., MOORE, D. T., ROSENMAN, J., OLLILA, D. W. & GRAHAM, M., 2ND 2002. Long-term outcome of neoadjuvant therapy for locally advanced breast carcinoma: effective clinical downstaging allows breast preservation and predicts outstanding local control and survival. *Ann Surg,* 236**,** 295-302; discussion 302-3.

CANCER RESEARCH UK. 2016a. *About breast cancer chemotherapy* [Online]. Cancer Research UK. Available: http://www.cancerresearchuk.org/about-cancer/type/breast-cancer/treatment/chemotherapy/about-breast-cancer-chemotherapy [Accessed January 17 2017 2017].

CANCER RESEARCH UK. 2016b. *Breast Cancer (C50): 2002-2006; Five-Year Relative Survival (%) by Stage, Adults Aged 15-99, Former Anglia Cancer Network* [Online]. Available: http://www.cancerresearchuk.org/sites/default/files/cstream-node/surv_5yr_stage_w_breast_0.pdf [Accessed January 17 2017 2016].

CANCER RESEARCH UK. 2016c. *Proportion of Cancers Diagnosed at Each Stage, All Ages, England* [Online]. Available: http://www.cancerresearchuk.org/sites/default/files/cstream-node/inc_stage_breast_0.pdf [Accessed January 17 2017 2016].

CANCER RESEARCH UK. 2016d. *Routes to diagnosis of breast cancer* [Online]. Cancer Research UK. Available: http://www.cancerresearchuk.org/health-professional/cancer-statistics/statistics-by-cancer-type/breast-cancer/diagnosis-and-treatment#heading-Zero [Accessed January 17 2016 2016].

CANCER RESEARCH UK. 2017. *Cancer Incidence Statistics* [Online]. Available: http://www.cancerresearchuk.org/health-professional/cancer-statistics/incidence#heading-Zero [Accessed October 2017 2017].
CANELLOS, G. P., DEVITA, V. T., GOLD, G. L., CHABNER, B. A., SCHEIN, P. S. & YOUNG, R. C. 1974. Cyclical combination chemotherapy for advanced breast carcinoma. *Br Med J,* 1**,** 218-20.
CAO, M. D., GISKEODEGARD, G. F., BATHEN, T. F., SITTER, B., BOFIN, A., LONNING, P. E., LUNDGREN, S. & GRIBBESTAD, I. S. 2012a. Prognostic value of metabolic response in breast cancer patients receiving neoadjuvant chemotherapy. *BMC Cancer,* 12**,** 39.
CAO, X., XUE, J. & ZHAO, B. 2012b. Potential application value of contrast-enhanced ultrasound in neoadjuvant chemotherapy of breast cancer. *Ultrasound Med Biol,* 38**,** 2065-71.
CAREY, L. A., DEES, E. C., SAWYER, L., GATTI, L., MOORE, D. T., COLLICHIO, F., OLLILA, D. W., SARTOR, C. I., GRAHAM, M. L. & PEROU, C. M. 2007. The triple negative paradox: primary tumor chemosensitivity of breast cancer subtypes. *Clin Cancer Res,* 13**,** 2329-34.
CARLSON, J. J. & ROTH, J. A. 2013. The impact of the Oncotype Dx breast cancer assay in clinical practice: a systematic review and meta-analysis. *Breast Cancer Res Treat,* 141**,** 13-22.
CARMELIET, P. & JAIN, R. K. 2000. Angiogenesis in cancer and other diseases. *Nature,* 407**,** 249-57.
CASTELLANO, G., BONILHA, L., LI, L. M. & CENDES, F. 2004. Texture analysis of medical images. *Clin Radiol,* 59**,** 1061-9.
CASTELLS, M., SANCHO-SERRA MDEL, C. & SIMARRO, M. 2012. Hypersensitivity to antineoplastic agents: mechanisms and treatment with rapid desensitization. *Cancer Immunol Immunother,* 61**,** 1575-84.
CERUSSI, A., BERGER, A. J., BEVILACQUA, F., SHAH, N., JAKUBOWSKI, D., BUTLER, J., HOLCOMBE, R. F. & TROMBERG, B. J. 2001. Sources of absorption and scattering contrast for near-infrared optical mammography. *Acad Radiol,* 8**,** 211-8.
CERUSSI, A., HSIANG, D., SHAH, N., MEHTA, R., DURKIN, A., BUTLER, J. & TROMBERG, B. J. 2007. Predicting response to breast cancer neoadjuvant chemotherapy using diffuse optical spectroscopy. *Proc Natl Acad Sci U S A,* 104**,** 4014-9.
CERUSSI, A., SHAH, N., HSIANG, D., DURKIN, A., BUTLER, J. & TROMBERG, B. J. 2006. In vivo absorption, scattering, and physiologic properties of 58 malignant breast tumors determined by broadband diffuse optical spectroscopy. *J Biomed Opt,* 11**,** 044005.
CERUSSI, A., TANAMAI, V. W., HSIANG, D., BUTLER, J., MEHTA, R. S. & TROMBERG, B. J. 2011. Diffuse optical spectroscopic imaging correlates with final pathological response in breast cancer neoadjuvant chemotherapy. *Philos Trans A Math Phys Eng Sci,* 369**,** 4512-30.
CHANG, H. R., GLASPY, J., ALLISON, M. A., KASS, F. C., ELASHOFF, R., CHUNG, D. U. & GORNBEIN, J. 2010. Differential response of triple-negative breast cancer to a docetaxel and carboplatin-based neoadjuvant treatment. *Cancer,* 116**,** 4227-37.
CHANG, J., ORMEROD, M., POWLES, T. J., ALLRED, D. C., ASHLEY, S. E. & DOWSETT, M. 2000. Apoptosis and Proliferation as Predictors of Chemotherapy Response in Patients with Breast Carcinoma. *Cancer,* 89**,** 2145-2152.

CHANG, Y. C., HUANG, C. S., LIU, Y. J., CHEN, J. H., LU, Y. S. & TSENG, W. Y. 2004. Angiogenic response of locally advanced breast cancer to neoadjuvant chemotherapy evaluated with parametric histogram from dynamic contrast-enhanced MRI. *Phys Med Biol,* 49**,** 3593-602.
CHEN, W., GIGER, M. L., LI, H., BICK, U. & NEWSTEAD, G. M. 2007. Volumetric texture analysis of breast lesions on contrast-enhanced magnetic resonance images. *Magn Reson Med,* 58**,** 562-71.
CHEN, W. Y., ROSNER, B., HANKINSON, S. E., COLDITZ, G. A. & WILLETT, W. C. 2011. Moderate alcohol consumption during adult life, drinking patterns, and breast cancer risk. *JAMA,* 306**,** 1884-90.
CHEVALLIER, B., ROCHE, H., OLIVIER, J. P., CHOLLET, P. & HURTELOUP, P. 1993. Inflammatory breast cancer. Pilot study of intensive induction chemotherapy (FEC-HD) results in a high histologic response rate. *Am J Clin Oncol,* 16**,** 223-8.
CHICKLORE, S., GOH, V., SIDDIQUE, M., ROY, A., MARSDEN, P. K. & COOK, G. J. 2013. Quantifying tumour heterogeneity in 18F-FDG PET/CT imaging by texture analysis. *Eur J Nucl Med Mol Imaging,* 40**,** 133-40.
CHIN, L., ANDERSEN, J. N. & FUTREAL, P. A. 2011. Cancer genomics: from discovery science to personalized medicine. *Nat Med,* 17**,** 297-303.
CHIVERS, R. C. 1977. The scattering of ultrasound by human tissues--some theoretical models. *Ultrasound Med Biol,* 3**,** 1-13.
CHOE, R., CORLU, A., LEE, K., DURDURAN, T., KONECKY, S. D., GROSICKA-KOPTYRA, M., ARRIDGE, S. R., CZERNIECKI, B. J., FRAKER, D. L., DEMICHELE, A., CHANCE, B., ROSEN, M. A. & YODH, A. G. 2005. Diffuse optical tomography of breast cancer during neoadjuvant chemotherapy: a case study with comparison to MRI. *Med Phys,* 32**,** 1128-39.
CHOLLET, P., AMAT, S., CURE, H., DE LATOUR, M., LE BOUEDEC, G., MOURET-REYNIER, M. A., FERRIERE, J. P., ACHARD, J. L., DAUPLAT, J. & PENAULT-LLORCA, F. 2002. Prognostic significance of a complete pathological response after induction chemotherapy in operable breast cancer. *Br J Cancer,* 86**,** 1041-6.
CHON, S. Y., CHAMPION, R. W., GEDDES, E. R. & RASHID, R. M. 2012. Chemotherapy-induced alopecia. *J Am Acad Dermatol,* 67**,** e37-47.
CHUNG, S. H., CERUSSI, A. E., KLIFA, C., BAEK, H. M., BIRGUL, O., GULSEN, G., MERRITT, S. I., HSIANG, D. & TROMBERG, B. J. 2008. In vivo water state measurements in breast cancer using broadband diffuse optical spectroscopy. *Phys Med Biol,* 53**,** 6713-27.
CIANFROCCA, M. & GOLDSTEIN, L. J. 2004. Prognostic and predictive factors in early-stage breast cancer. *Oncologist,* 9**,** 606-16.
CIARMIELLO, A., DEL VECCHIO, S., SILVESTRO, P., POTENA, M. I., CARRIERO, M. V., THOMAS, R., BOTTI, G., D'AIUTO, G. & SALVATORE, M. 1998. Tumor clearance of technetium 99m-sestamibi as a predictor of response to neoadjuvant chemotherapy for locally advanced breast cancer. *J Clin Oncol,* 16**,** 1677-83.
CLARKE, L. P., BAKER, H. & KELLOFF, G. 2003. Foreword: Potential of Optical Imaging for Early Cancer Detection, Screening, Diagnosis and Image Guided Treatment. *Technology in Cancer Research and Treatment,* 2**,** 487-489.
CLEMENTI, M. E., GIARDINA, B., DI STASIO, E., MORDENTE, A. & MISITI, F. 2003. Doxorubicin-derived metabolites induce release of cytochrome C

and inhibition of respiration on cardiac isolated mitochondria. *Anticancer Res,* 23**,** 2445-50.
COLEY, H. M. 2008. Mechanisms and strategies to overcome chemotherapy resistance in metastatic breast cancer. *Cancer Treat Rev,* 34**,** 378-90.
COLLABORATIVE GROUP ON HORMONAL FACTORS IN BREAST, C. 2001. Familial breast cancer: collaborative reanalysis of individual data from 52 epidemiological studies including 58,209 women with breast cancer and 101,986 women without the disease. *Lancet,* 358**,** 1389-99.
COLLABORATIVE GROUP ON HORMONAL FACTORS IN BREAST, C. 2002. Breast cancer and breastfeeding: collaborative reanalysis of individual data from 47 epidemiological studies in 30 countries, including 50302 women with breast cancer and 96973 women without the disease. *Lancet,* 360**,** 187-95.
COLLABORATIVE GROUP ON HORMONAL FACTORS IN BREAST, C. 2012. Menarche, menopause, and breast cancer risk: individual participant meta-analysis, including 118 964 women with breast cancer from 117 epidemiological studies. *Lancet Oncol,* 13**,** 1141-51.
COOPER, R. S. & PSATY, B. M. 2003. Genomics and medicine: distraction, incremental progress, or the dawn of a new age? *Ann Intern Med,* 138**,** 576-80.
CORBEN, A. D., ABI-RAAD, R., POPA, I., TEO, C. H., MACKLIN, E. A., KOERNER, F. C., TAGHIAN, A. G. & BRACHTEL, E. F. 2013. Pathologic response and long-term follow-up in breast cancer patients treated with neoadjuvant chemotherapy: a comparison between classifications and their practical application. *Arch Pathol Lab Med,* 137**,** 1074-82.
COUSSENS, L. M. & WERB, Z. 2002. Inflammation and cancer. *Nature,* 420**,** 860-7.
CRACIUNESCU, O. I., BLACKWELL, K. L., JONES, E. L., MACFALL, J. R., YU, D., VUJASKOVIC, Z., WONG, T. Z., LIOTCHEVA, V., ROSEN, E. L., PROSNITZ, L. R., SAMULSKI, T. V. & DEWHIRST, M. W. 2009. DCE-MRI parameters have potential to predict response of locally advanced breast cancer patients to neoadjuvant chemotherapy and hyperthermia: a pilot study. *Int J Hyperthermia,* 25**,** 405-15.
CRAWFORD, J., DALE, D. C. & LYMAN, G. H. 2004. Chemotherapy-induced neutropenia: risks, consequences, and new directions for its management. *Cancer,* 100**,** 228-37.
CZARNOTA, G. J., KOLIOS, M. C., ABRAHAM, J., PORTNOY, M., OTTENSMEYER, F. P., HUNT, J. W. & SHERAR, M. D. 1999. Ultrasound imaging of apoptosis: high-resolution non-invasive monitoring of programmed cell death in vitro, in situ and in vivo. *Br J Cancer,* 81**,** 520-7.
CZARNOTA, G. J., KOLIOS, M. C., HUNT, J. W. & SHERAR, M. D. 2002. Ultrasound imaging of apoptosis. DNA-damage effects visualized. *Methods Mol Biol,* 203**,** 257-77.
DAMIA, G. & GARATTINI, S. 2014. The pharmacological point of view of resistance to therapy in tumors. *Cancer Treat Rev,* 40**,** 909-16.
DAVNALL, F., YIP, C. S., LJUNGQVIST, G., SELMI, M., NG, F., SANGHERA, B., GANESHAN, B., MILES, K. A., COOK, G. J. & GOH, V. 2012. Assessment of tumor heterogeneity: an emerging imaging tool for clinical practice? *Insights Imaging,* 3**,** 573-89.

DE LOS SANTOS, J. F., CANTOR, A., AMOS, K. D., FORERO, A., GOLSHAN, M., HORTON, J. K., HUDIS, C. A., HYLTON, N. M., MCGUIRE, K., MERIC-BERNSTAM, F., MESZOELY, I. M., NANDA, R. & HWANG, E. S. 2013. Magnetic resonance imaging as a predictor of pathologic response in patients treated with neoadjuvant systemic treatment for operable breast cancer. Translational Breast Cancer Research Consortium trial 017. *Cancer,* 119**,** 1776-83.

DE WINTER, J. C. F. 2013. Using the Student's t-test with extremely small sample sizes. *Practical Assessment, Research & Evaluation,* 18.

DEHGHANI, H., SRINIVASAN, S., POGUE, B. W. & GIBSON, A. 2009. Numerical modelling and image reconstruction in diffuse optical tomography. *Philos Trans A Math Phys Eng Sci,* 367**,** 3073-93.

DESMEDT, C., HAIBE-KAINS, B., WIRAPATI, P., BUYSE, M., LARSIMONT, D., BONTEMPI, G., DELORENZI, M., PICCART, M. & SOTIRIOU, C. 2008. Biological processes associated with breast cancer clinical outcome depend on the molecular subtypes. *Clin Cancer Res,* 14**,** 5158-65.

DEVITA, V. T., JR. & CHU, E. 2008. A history of cancer chemotherapy. *Cancer Res,* 68**,** 8643-53.

DOSSUS, L. & BENUSIGLIO, P. R. 2015. Lobular breast cancer: incidence and genetic and non-genetic risk factors. *Breast Cancer Res,* 17**,** 37.

DRUCKER, E. & KRAPFENBAUER, K. 2013. Pitfalls and limitations in translation from biomarker discovery to clinical utility in predictive and personalised medicine. *EPMA J,* 4**,** 7.

DUCH, J., FUSTER, D., MUNOZ, M., FERNANDEZ, P. L., PAREDES, P., FONTANILLAS, M., GUZMAN, F., RUBI, S., LOMENA, F. J. & PONS, F. 2009. 18F-FDG PET/CT for early prediction of response to neoadjuvant chemotherapy in breast cancer. *Eur J Nucl Med Mol Imaging,* 36**,** 1551-7.

DUDA, R. O., HART, P. E. & STORK, D. G. 2001. *Pattern classification,* New York, Wiley.

DUDANI, S. A. 1976. The Distance-Weighted k-Nearest-Neighbor Rule. *IEEE Transactions on Systems, Man, and Cybernetics,* 6**,** 325-327.

DUMONTET, C. & JORDAN, M. A. 2010. Microtubule-binding agents: a dynamic field of cancer therapeutics. *Nat Rev Drug Discov,* 9**,** 790-803.

DURDURAN, T., CHOE, R., BAKER, W. B. & YODH, A. G. 2010. Diffuse Optics for Tissue Monitoring and Tomography. *Rep Prog Phys,* 73.

DVORAK, H. F., NAGY, J. A., DVORAK, J. T. & DVORAK, A. M. 1988. Identification and characterization of the blood vessels of solid tumors that are leaky to circulating macromolecules. *Am J Pathol,* 133**,** 95-109.

EASTWOOD, J. D., LEV, M. H. & PROVENZALE, J. M. 2003. Perfusion CT with iodinated contrast material. *AJR Am J Roentgenol,* 180**,** 3-12.

ECCLES, S. A., ABOAGYE, E. O., ALI, S., ANDERSON, A. S., ARMES, J., BERDITCHEVSKI, F., BLAYDES, J. P., BRENNAN, K., BROWN, N. J., BRYANT, H. E., BUNDRED, N. J., BURCHELL, J. M., CAMPBELL, A. M., CARROLL, J. S., CLARKE, R. B., COLES, C. E., COOK, G. J., COX, A., CURTIN, N. J., DEKKER, L. V., SILVA IDOS, S., DUFFY, S. W., EASTON, D. F., ECCLES, D. M., EDWARDS, D. R., EDWARDS, J., EVANS, D., FENLON, D. F., FLANAGAN, J. M., FOSTER, C., GALLAGHER, W. M., GARCIA-CLOSAS, M., GEE, J. M., GESCHER, A. J., GOH, V., GROVES, A. M., HARVEY, A. J., HARVIE, M., HENNESSY, B. T., HISCOX, S., HOLEN, I., HOWELL, S. J., HOWELL, A.,

HUBBARD, G., HULBERT-WILLIAMS, N., HUNTER, M. S., JASANI, B., JONES, L. J., KEY, T. J., KIRWAN, C. C., KONG, A., KUNKLER, I. H., LANGDON, S. P., LEACH, M. O., MANN, D. J., MARSHALL, J. F., MARTIN, L., MARTIN, S. G., MACDOUGALL, J. E., MILES, D. W., MILLER, W. R., MORRIS, J. R., MOSS, S. M., MULLAN, P., NATRAJAN, R., O'CONNOR, J. P., O'CONNOR, R., PALMIERI, C., PHAROAH, P. D., RAKHA, E. A., REED, E., ROBINSON, S. P., SAHAI, E., SAXTON, J. M., SCHMID, P., SMALLEY, M. J., SPEIRS, V., STEIN, R., STINGL, J., STREULI, C. H., TUTT, A. N., VELIKOVA, G., WALKER, R. A., WATSON, C. J., WILLIAMS, K. J., YOUNG, L. S. & THOMPSON, A. M. 2013. Critical research gaps and translational priorities for the successful prevention and treatment of breast cancer. *Breast Cancer Res,* 15**,** R92.

EEROLA, H., HEIKKILA, P., TAMMINEN, A., AITTOMAKI, K., BLOMQVIST, C. & NEVANLINNA, H. 2005. Histopathological features of breast tumours in BRCA1, BRCA2 and mutation-negative breast cancer families. *Breast Cancer Res,* 7**,** R93-100.

EISENHAUER, E. A., THERASSE, P., BOGAERTS, J., SCHWARTZ, L. H., SARGENT, D., FORD, R., DANCEY, J., ARBUCK, S., GWYTHER, S., MOONEY, M., RUBINSTEIN, L., SHANKAR, L., DODD, L., KAPLAN, R., LACOMBE, D. & VERWEIJ, J. 2009. New response evaluation criteria in solid tumours: revised RECIST guideline (version 1.1). *Eur J Cancer,* 45**,** 228-47.

EL SAGHIR, N. S., ENIU, A., CARLSON, R. W., AZIZ, Z., VOROBIOF, D., HORTOBAGYI, G. N. & BREAST HEALTH GLOBAL INITIATIVE SYSTEMIC THERAPY FOCUS, G. 2008. Locally advanced breast cancer: treatment guideline implementation with particular attention to low- and middle-income countries. *Cancer,* 113**,** 2315-24.

ELLIS, SHNITT, SASTRE-GARAU, BUSSOLATI, TAVASSOLI & EUSEBI 2003. World Health Organization Classification of Tumours. *In:* TAVASSOLI, F. & DEVILEE, P. (eds.) *Invasive Breast Carcinoma.* Lyon, France: World Health Organization.

ELLIS, P. A., SMITH, I. E., MCCARTHY, K., DETRE, S., SALTER, J. & DOWSETT, M. 1997. Preoperative chemotherapy induces apoptosis in early breast cancer. *Lancet,* 349**,** 849.

ELMORE, S. 2007. Apoptosis: a review of programmed cell death. *Toxicol Pathol,* 35**,** 495-516.

ELSAMANY, S., ALZAHRANI, A., ABOZEED, W. N., RASMY, A., FAROOQ, M. U., ELBIOMY, M. A., RAWAH, E., ALSALEH, K. & ABDEL-AZIZ, N. M. 2015. Mammographic breast density: Predictive value for pathological response to neoadjuvant chemotherapy in breast cancer patients. *Breast,* 24**,** 576-81.

ELSTON, C. W. & ELLIS, I. O. 1991. Pathological prognostic factors in breast cancer. I. The value of histological grade in breast cancer: experience from a large study with long-term follow-up. *Histopathology,* 19**,** 403-10.

ENFIELD, L. C., GIBSON, A. P., HEBDEN, J. C. & DOUEK, M. 2009. Optical tomography of breast cancer-monitoring response to primary medical therapy. *Target Oncol,* 4**,** 219-33.

ESCUIN, D. & ROSELL, R. 1999. The anti-apoptosis survivin gene and its role in human cancer: an overview. *Clin Lung Cancer,* 1**,** 138-43.

ESSAYAN, D. M., KAGEY-SOBOTKA, A., COLARUSSO, P. J., LICHTENSTEIN, L. M., OZOLS, R. F. & KING, E. D. 1996. Successful parenteral desensitization to paclitaxel. *J Allergy Clin Immunol,* 97**,** 42-6.

EVANS, A., ARMSTRONG, S., WHELEHAN, P., THOMSON, K., RAUCHHAUS, P., PURDIE, C., JORDAN, L., JONES, L., THOMPSON, A. & VINNICOMBE, S. 2013. Can shear-wave elastography predict response to neoadjuvant chemotherapy in women with invasive breast cancer? *Br J Cancer,* 109**,** 2798-802.

EVANS, W. E. & RELLING, M. V. 1989. Clinical pharmacokinetics-pharmacodynamics of anticancer drugs. *Clin Pharmacokinet,* 16**,** 327-36.

FALOU, O., SADEGHI-NAINI, A., PREMATILAKE, S., SOFRONI, E., PAPANICOLAU, N., IRADJI, S., JAHEDMOTLAGH, Z., LEMON-WONG, S., PIGNOL, J. P., RAKOVITCH, E., ZUBOVITS, J., SPAYNE, J., DENT, R., TRUDEAU, M., BOILEAU, J. F., WRIGHT, F. C., YAFFE, M. J. & CZARNOTA, G. J. 2013. Evaluation of neoadjuvant chemotherapy response in women with locally advanced breast cancer using ultrasound elastography. *Transl Oncol,* 6**,** 17-24.

FALOU, O., SOLIMAN, H., SADEGHI-NAINI, A., IRADJI, S., LEMON-WONG, S., ZUBOVITS, J., SPAYNE, J., DENT, R., TRUDEAU, M., BOILEAU, J. F., WRIGHT, F. C., YAFFE, M. J. & CZARNOTA, G. J. 2012. Diffuse optical spectroscopy evaluation of treatment response in women with locally advanced breast cancer receiving neoadjuvant chemotherapy. *Transl Oncol,* 5**,** 238-46.

FAN, B., WANG, X. Y., YANG, X. D., ZHONG, H., WU, C. X. & JIANG, X. X. 2011. Blood oxygen level-dependent MRI for the monitoring of neoadjuvant chemotherapy in breast carcinoma: initial experience. *Magn Reson Imaging,* 29**,** 153-9.

FANTINI, S. & SASSAROLI, A. 2012. Near-infrared optical mammography for breast cancer detection with intrinsic contrast. *Ann Biomed Eng,* 40**,** 398-407.

FELDWEG, A. M., LEE, C. W., MATULONIS, U. A. & CASTELLS, M. 2005. Rapid desensitization for hypersensitivity reactions to paclitaxel and docetaxel: a new standard protocol used in 77 successful treatments. *Gynecol Oncol,* 96**,** 824-9.

FELEPPA, E. J., LIZZI, F. L., COLEMAN, D. J. & YAREMKO, M. M. 1986. Diagnostic spectrum analysis in ophthalmology: a physical perspective. *Ultrasound Med Biol,* 12**,** 623-31.

FELEPPA, E. J., MAMOU, J., PORTER, C. R. & MACHI, J. 2011. Quantitative ultrasound in cancer imaging. *Semin Oncol,* 38**,** 136-50.

FERLAY, J., SOERJOMATARAM, I., DIKSHIT, R., ESER, S., MATHERS, C., REBELO, M., PARKIN, D. M., FORMAN, D. & BRAY, F. 2015. Cancer incidence and mortality worldwide: sources, methods and major patterns in GLOBOCAN 2012. *Int J Cancer,* 136**,** E359-86.

FISHER, B., BRYANT, J., WOLMARK, N., MAMOUNAS, E., BROWN, A., FISHER, E. R., WICKERHAM, D. L., BEGOVIC, M., DECILLIS, A., ROBIDOUX, A., MARGOLESE, R. G., CRUZ, A. B., JR., HOEHN, J. L., LEES, A. W., DIMITROV, N. V. & BEAR, H. D. 1998. Effect of preoperative chemotherapy on the outcome of women with operable breast cancer. *J Clin Oncol,* 16**,** 2672-85.

FISHER, R. A. 1936. The Use of Multiple Measurements in Taxonomic Problems. *Annals of Eugenics,* 7**,** 179-188.

FITZGIBBONS, P. L., PAGE, D. L., WEAVER, D., THOR, A. D., ALLRED, D. C., CLARK, G. M., RUBY, S. G., O'MALLEY, F., SIMPSON, J. F., CONNOLLY, J. L., HAYES, D. F., EDGE, S. B., LICHTER, A. & SCHNITT, S. J. 2000. Prognostic factors in breast cancer. College of American Pathologists Consensus Statement 1999. *Arch Pathol Lab Med,* 124**,** 966-78.

FU, D., CALVO, J. A. & SAMSON, L. D. 2012. Balancing repair and tolerance of DNA damage caused by alkylating agents. *Nat Rev Cancer,* 12**,** 104-20.

GANGEH, M. J., TADAYYON, H., SANNACHI, L., SADEGHI-NAINI, A., TRAN, W. T. & CZARNOTA, G. J. 2016. Computer Aided Theragnosis Using Quantitative Ultrasound Spectroscopy and Maximum Mean Discrepancy in Locally Advanced Breast Cancer. *IEEE Trans Med Imaging,* 35**,** 778-90.

GARATTINI, S. 2007. Pharmacokinetics in cancer chemotherapy. *Eur J Cancer,* 43**,** 271-82.

GARCIA VICENTE, A. M., CRUZ MORA, M. A., LEON MARTIN, A. A., MUNOZ SANCHEZ MDEL, M., RELEA CALATAYUD, F., VAN GOMEZ LOPEZ, O., ESPINOSA AUNION, R., GONZALEZ AGEITOS, A. & SORIANO CASTREJON, A. 2014. Glycolytic activity with 18F-FDG PET/CT predicts final neoadjuvant chemotherapy response in breast cancer. *Tumour Biol,* 35**,** 11613-20.

GAUDET, M. M., GAPSTUR, S. M., SUN, J., DIVER, W. R., HANNAN, L. M. & THUN, M. J. 2013. Active smoking and breast cancer risk: original cohort data and meta-analysis. *J Natl Cancer Inst,* 105**,** 515-25.

GIBBS, P. & TURNBULL, L. W. 2003. Textural analysis of contrast-enhanced MR images of the breast. *Magn Reson Med,* 50**,** 92-8.

GIBSON, A. P., HEBDEN, J. C. & ARRIDGE, S. R. 2005. Recent advances in diffuse optical imaging. *Phys Med Biol,* 50**,** R1-43.

GILBERT, L. A. & HEMANN, M. T. 2010. DNA damage-mediated induction of a chemoresistant niche. *Cell,* 143**,** 355-66.

GIORDANO, S. H. 2003. Update on Locally Advanced Breast Cancer. *The Oncologist,* 8**,** 521-530.

GOEL, S., DUDA, D. G., XU, L., MUNN, L. L., BOUCHER, Y., FUKUMURA, D. & JAIN, R. K. 2011. Normalization of the vasculature for treatment of cancer and other diseases. *Physiol Rev,* 91**,** 1071-121.

GOLDHIRSCH, A., WINER, E. P., COATES, A. S., GELBER, R. D., PICCART-GEBHART, M., THURLIMANN, B., SENN, H. J. & PANEL, M. 2013. Personalizing the treatment of women with early breast cancer: highlights of the St Gallen International Expert Consensus on the Primary Therapy of Early Breast Cancer 2013. *Ann Oncol,* 24**,** 2206-23.

GOLDSTEIN, N. S., DECKER, D., SEVERSON, D., SCHELL, S., VICINI, F., MARGOLIS, J. & DEKHNE, N. S. 2007. Molecular classification system identifies invasive breast carcinoma patients who are most likely and those who are least likely to achieve a complete pathologic response after neoadjuvant chemotherapy. *Cancer,* 110**,** 1687-96.

GREEN, A. R., SORIA, D., STEPHEN, J., POWE, D. G., NOLAN, C. C., KUNKLER, I., THOMAS, J., KERR, G. R., JACK, W., CAMERON, D., PIPER, T., BALL, G. R., GARIBALDI, J. M., RAKHA, E. A., BARTLETT, J. M. & ELLIS, I. O. 2016. Nottingham Prognostic Index Plus: Validation of a clinical decision making tool in breast cancer in an independent series. *J Pathol Clin Res,* 2**,** 32-40.

GUPTA, R. & UNDRILL, P. E. 1995. The use of texture analysis to delineate suspicious masses in mammography. *Phys Med Biol,* 40**,** 835-55.
HAAGENSEN, C. D. & STOUT, A. P. 1943. Carcinoma of the Breast. II-Criteria of Operability. *Ann Surg,* 118**,** 1032-51.
HALL, P. S., HAMILTON, P., HULME, C. T., MEADS, D. M., JONES, H., NEWSHAM, A., MARTI, J., SMITH, A. F., MASON, H., VELIKOVA, G., ASHLEY, L. & WRIGHT, P. 2015. Costs of cancer care for use in economic evaluation: a UK analysis of patient-level routine health system data. *Br J Cancer,* 112**,** 948-56.
HAMPER, U. M., DEJONG, M. R., CASKEY, C. I. & SHETH, S. 1997. Power Doppler imaging: clinical experience and correlation with color Doppler US and other imaging modalities. *Radiographics,* 17**,** 499-513.
HAN, J. & KAMBER, M. 2006. *Data mining : concepts and techniques,* Amsterdam ; Boston
San Francisco, CA, Elsevier ; Morgan Kaufmann.
HANAHAN, D. & WEINBERG, R. A. 2011. Hallmarks of cancer: the next generation. *Cell,* 144**,** 646-74.
HARALICK, R. M. 1979. Statistical and Structural Approaches to Texture. *Proceedings of the IEEE,* 67**,** 786 - 804.
HARALICK, R. M., SHANMUGAM, K. & DINSTEIN, I. 1973. Textural features for image classification. *IEEE Transactions on Systems, Man and Cybernetics,* 3**,** 610-621.
HARBECK, N., THOMSSEN, C. & GNANT, M. 2013. St. Gallen 2013: brief preliminary summary of the consensus discussion. *Breast Care (Basel),* 8**,** 102-9.
HARRINGTON, K. J. 2016. The biology of cancer. *Medicine,* 44**,** 1-5.
HARVEY, J. M., KLERK, N. H. D., ROBBINS, P. D. & STERRETT, G. F. 1995. Histological grading of breast cancer: a study of reproducibility of consensus grading. *The Breast,* 4**,** 297-300.
HASHIZUME, H., BALUK, P., MORIKAWA, S., MCLEAN, J. W., THURSTON, G., ROBERGE, S., JAIN, R. K. & MCDONALD, D. M. 2000. Openings between defective endothelial cells explain tumor vessel leakiness. *Am J Pathol,* 156**,** 1363-80.
HATT, M., GROHEUX, D., MARTINEAU, A., ESPIE, M., HINDIE, E., GIACCHETTI, S., DE ROQUANCOURT, A., VISVIKIS, D. & CHEZE-LE REST, C. 2013. Comparison between 18F-FDG PET image-derived indices for early prediction of response to neoadjuvant chemotherapy in breast cancer. *J Nucl Med,* 54**,** 341-9.
HAVILAND, J. S., OWEN, J. R., DEWAR, J. A., AGRAWAL, R. K., BARRETT, J., BARRETT-LEE, P. J., DOBBS, H. J., HOPWOOD, P., LAWTON, P. A., MAGEE, B. J., MILLS, J., SIMMONS, S., SYDENHAM, M. A., VENABLES, K., BLISS, J. M., YARNOLD, J. R. & GROUP, S. T. 2013. The UK Standardisation of Breast Radiotherapy (START) trials of radiotherapy hypofractionation for treatment of early breast cancer: 10-year follow-up results of two randomised controlled trials. *Lancet Oncol,* 14**,** 1086-94.
HAYASHI, M., YAMAMOTO, Y., IBUSUKI, M., FUJIWARA, S., YAMAMOTO, S., TOMITA, S., NAKANO, M., MURAKAMI, K., IYAMA, K. & IWASE, H. 2012. Evaluation of tumor stiffness by elastography is predictive for pathologic complete response to neoadjuvant chemotherapy in patients with breast cancer. *Ann Surg Oncol,* 19**,** 3042-9.

HAYBITTLE, J. L., BLAMEY, R. W., ELSTON, C. W., JOHNSON, J., DOYLE, P. J., CAMPBELL, F. C., NICHOLSON, R. I. & GRIFFITHS, K. 1982. A prognostic index in primary breast cancer. *Br J Cancer,* 45**,** 361-6.
HEIJBLOM, M., KLAASE, J. M., VAN DEN ENGH, F. M., VAN LEEUWEN, T. G., STEENBERGEN, W. & MANOHAR, S. 2011. Imaging tumor vascularization for detection and diagnosis of breast cancer. *Technol Cancer Res Treat,* 10**,** 607-23.
HEYS, S. D., HUTCHEON, A. W., SARKAR, T. K., OGSTON, K. N., MILLER, I. D., PAYNE, S., SMITH, I., WALKER, L. G., EREMIN, O. & ABERDEEN BREAST, G. 2002. Neoadjuvant docetaxel in breast cancer: 3-year survival results from the Aberdeen trial. *Clin Breast Cancer,* 3 Suppl 2**,** S69-74.
HIEKEN, T. J., BOUGHEY, J. C., JONES, K. N., SHAH, S. S. & GLAZEBROOK, K. N. 2013. Imaging response and residual metastatic axillary lymph node disease after neoadjuvant chemotherapy for primary breast cancer. *Ann Surg Oncol,* 20**,** 3199-204.
HONIG, A., RIEGER, L., SUTTERLIN, M., WALLWIENER, D., DIETL, J. & SOLOMAYER, E. F. 2005. State of the art of neoadjuvant chemotherapy in breast cancer: rationale, results and recent developments. *Ger Med Sci,* 3**,** Doc08.
HONKOOP, A. H., VAN DIEST, P. J., DE JONG, J. S., LINN, S. C., GIACCONE, G., HOEKMAN, K., WAGSTAFF, J. & PINEDO, H. M. 1998. Prognostic role of clinical, pathological and biological characteristics in patients with locally advanced breast cancer. *Br J Cancer,* 77**,** 621-6.
HORSKA, A. & BARKER, P. B. 2010. Imaging of brain tumors: MR spectroscopy and metabolic imaging. *Neuroimaging Clin N Am,* 20**,** 293-310.
HORTOBAGYI, G. N., AMES, F. C., BUZDAR, A. U., KAU, S. W., MCNEESE, M. D., PAULUS, D., HUG, V., HOLMES, F. A., ROMSDAHL, M. M., FRASCHINI, G. & ET AL. 1988. Management of stage III primary breast cancer with primary chemotherapy, surgery, and radiation therapy. *Cancer,* 62**,** 2507-16.
HOWLADER, N., ALTEKRUSE, S. F., LI, C. I., CHEN, V. W., CLARKE, C. A., RIES, L. A. & CRONIN, K. A. 2014. US incidence of breast cancer subtypes defined by joint hormone receptor and HER2 status. *J Natl Cancer Inst,* 106.
HRICAK, H. 2011. Oncologic imaging: a guiding hand of personalized cancer care. *Radiology,* 259**,** 633-40.
HU, M., YAO, J., CARROLL, D. K., WEREMOWICZ, S., CHEN, H., CARRASCO, D., RICHARDSON, A., VIOLETTE, S., NIKOLSKAYA, T., NIKOLSKY, Y., BAUERLEIN, E. L., HAHN, W. C., GELMAN, R. S., ALLRED, C., BISSELL, M. J., SCHNITT, S. & POLYAK, K. 2008. Regulation of in situ to invasive breast carcinoma transition. *Cancer Cell,* 13**,** 394-406.
HUANG, O., JIANG, M., CHEN, X. S., WU, J. Y., CHEN, W. G., LI, Y. F. & SHEN, K. W. 2015. Prognostic factors of survival in pathologic incomplete response patients with locally advanced breast cancer after neoadjuvant chemotherapy. *Cell Biochem Biophys,* 71**,** 1181-90.
HUBER, K. E., CAREY, L. A. & WAZER, D. E. 2009. Breast cancer molecular subtypes in patients with locally advanced disease: impact on prognosis, patterns of recurrence, and response to therapy. *Semin Radiat Oncol,* 19**,** 204-10.

HUBER, S., MEDL, M., HELBICH, T., TAUCHER, S., WAGNER, T., RUDAS, M., ZUNA, I. & DELORME, S. 2000. Locally advanced breast carcinoma: computer assisted semiquantitative analysis of color Doppler ultrasonography in the evaluation of tumor response to neoadjuvant chemotherapy (work in progress). *J Ultrasound Med,* 19**,** 601-7.

HUDIS, C. A. 2007. Trastuzumab--mechanism of action and use in clinical practice. *N Engl J Med,* 357**,** 39-51.

HUNT, J. W., WORTHINGTON, A. E., XUAN, A., KOLIOS, M. C., CZARNOTA, G. J. & SHERAR, M. D. 2002. A model based upon pseudo regular spacing of cells combined with the randomisation of the nuclei can explain the significant changes in high-frequency ultrasound signals during apoptosis. *Ultrasound Med Biol,* 28**,** 217-26.

HUOBER, J., VON MINCKWITZ, G., DENKERT, C., TESCH, H., WEISS, E., ZAHM, D. M., BELAU, A., KHANDAN, F., HAUSCHILD, M., THOMSSEN, C., HOGEL, B., DARB-ESFAHANI, S., MEHTA, K. & LOIBL, S. 2010. Effect of neoadjuvant anthracycline-taxane-based chemotherapy in different biological breast cancer phenotypes: overall results from the GeparTrio study. *Breast Cancer Res Treat,* 124**,** 133-40.

HYLTON, N. M. 2009. Can diffuse optical spectroscopic tomography be used to characterize breast lesions and their response to treatment? *Radiology,* 252**,** 330-1.

INIC, Z., ZEGARAC, M., INIC, M., MARKOVIC, I., KOZOMARA, Z., DJURISIC, I., INIC, I., PUPIC, G. & JANCIC, S. 2014. Difference between Luminal A and Luminal B Subtypes According to Ki-67, Tumor Size, and Progesterone Receptor Negativity Providing Prognostic Information. *Clin Med Insights Oncol,* 8**,** 107-11.

INSANA, M. F. & HALL, T. J. 1990. Parametric ultrasound imaging from backscatter coefficient measurements: image formation and interpretation. *Ultrason Imaging,* 12**,** 245-67.

INTES, X. 2005. Time-domain optical mammography SoftScan: initial results. *Acad Radiol,* 12**,** 934-47.

INTES, X., NTZIACHRISTOS, V., CULVER, J. P., YODH, A. & CHANCE, B. 2002. Projection access order in algebraic reconstruction technique for diffuse optical tomography. *Phys Med Biol,* 47**,** N1-10.

IQBAL, J., GINSBURG, O., ROCHON, P. A., SUN, P. & NAROD, S. A. 2015. Differences in breast cancer stage at diagnosis and cancer-specific survival by race and ethnicity in the United States. *JAMA,* 313**,** 165-73.

JACQUES, S. L. 2013. Optical properties of biological tissues: a review. *Phys Med Biol,* 58**,** R37-61.

JAIN, A. K., DUIN, R. P. W. & MAO, J. 2000. Statistical Pattern Recognition: A Review. *IEEE Transactions on Pattern Analysis and Machine Intelligence,* 22**,** 4-37.

JAIN, R. K. 2005. Normalization of tumor vasculature: an emerging concept in antiangiogenic therapy. *Science,* 307**,** 58-62.

JAIN, R. K. 2013. Normalizing tumor microenvironment to treat cancer: bench to bedside to biomarkers. *J Clin Oncol,* 31**,** 2205-18.

JAKUBOWSKI, D. B., CERUSSI, A. E., BEVILACQUA, F., SHAH, N., HSIANG, D., BUTLER, J. & TROMBERG, B. J. 2004. Monitoring neoadjuvant chemotherapy in breast cancer using quantitative diffuse optical spectroscopy: a case study. *J Biomed Opt,* 9**,** 230-8.

JEMAL, A., MURRAY, T., WARD, E., SAMUELS, A., TIWARI, R. C., GHAFOOR, A., FEUER, E. J. & THUN, M. J. 2005. Cancer statistics, 2005. *CA Cancer J Clin,* 55**,** 10-30.

JENSEN, J. A. 2017. *Field II Simulation Program* [Online]. Available: http://field-ii.dk [Accessed 2017 2017].

JI, B., CHEN, B., WANG, T., SONG, Y., CHEN, M., JI, T., WANG, X., GAO, S. & MA, Q. 2015. (9)(9)mTc-3PRGD(2) SPECT to monitor early response to neoadjuvant chemotherapy in stage II and III breast cancer. *Eur J Nucl Med Mol Imaging,* 42**,** 1362-70.

JIANG, L., WEATHERALL, P. T., MCCOLL, R. W., TRIPATHY, D. & MASON, R. P. 2013. Blood oxygenation level-dependent (BOLD) contrast magnetic resonance imaging (MRI) for prediction of breast cancer chemotherapy response: a pilot study. *J Magn Reson Imaging,* 37**,** 1083-92.

JIANG, S., POGUE, B. W., CARPENTER, C. M., POPLACK, S. P., WELLS, W. A., KOGEL, C. A., FORERO, J. A., MUFFLY, L. S., SCHWARTZ, G. N., PAULSEN, K. D. & KAUFMAN, P. A. 2009. Evaluation of breast tumor response to neoadjuvant chemotherapy with tomographic diffuse optical spectroscopy: case studies of tumor region-of-interest changes. *Radiology,* 252**,** 551-60.

JIANG, S., POGUE, B. W., KAUFMAN, P. A., GUI, J., JERMYN, M., FRAZEE, T. E., POPLACK, S. P., DIFLORIO-ALEXANDER, R., WELLS, W. A. & PAULSEN, K. D. 2014. Predicting breast tumor response to neoadjuvant chemotherapy with diffuse optical spectroscopic tomography prior to treatment. *Clin Cancer Res,* 20**,** 6006-15.

JUNTTILA, M. R. & DE SAUVAGE, F. J. 2013. Influence of tumour micro-environment heterogeneity on therapeutic response. *Nature,* 501**,** 346-54.

KANG, H., LEE, H. Y., LEE, K. S. & KIM, J. H. 2012. Imaging-based tumor treatment response evaluation: review of conventional, new, and emerging concepts. *Korean J Radiol,* 13**,** 371-90.

KANNARKAT, G., LASHER, E. E. & SCHIFF, D. 2007. Neurologic complications of chemotherapy agents. *Curr Opin Neurol,* 20**,** 719-25.

KEAM, B., IM, S. A., KOH, Y., HAN, S. W., OH, D. Y., CHO, N., KIM, J. H., HAN, W., KANG, K. W., MOON, W. K., KIM, T. Y., PARK, I. A., NOH, D. Y., CHUNG, J. K. & BANG, Y. J. 2011. Early metabolic response using FDG PET/CT and molecular phenotypes of breast cancer treated with neoadjuvant chemotherapy. *BMC Cancer,* 11**,** 452.

KELLAND, L. R. 2005. Overcoming the immortality of tumour cells by telomere and telomerase based cancer therapeutics--current status and future prospects. *Eur J Cancer,* 41**,** 971-9.

KENNECKE, H., YERUSHALMI, R., WOODS, R., CHEANG, M. C., VODUC, D., SPEERS, C. H., NIELSEN, T. O. & GELMON, K. 2010. Metastatic behavior of breast cancer subtypes. *J Clin Oncol,* 28**,** 3271-7.

KESSLER, L. G., BARNHART, H. X., BUCKLER, A. J., CHOUDHURY, K. R., KONDRATOVICH, M. V., TOLEDANO, A., GUIMARAES, A. R., FILICE, R., ZHANG, Z., SULLIVAN, D. C. & GROUP, Q. T. W. 2015. The emerging science of quantitative imaging biomarkers terminology and definitions for scientific studies and regulatory submissions. *Stat Methods Med Res,* 24**,** 9-26.

KIM, H. C., AL-MAHROUKI, A., GORJIZADEH, A., SADEGHI-NAINI, A., KARSHAFIAN, R. & CZARNOTA, G. J. 2014. Quantitative ultrasound

characterization of tumor cell death: ultrasound-stimulated microbubbles for radiation enhancement. *PLoS One,* 9**,** e102343.
KIM, S. I., SOHN, J., KOO, J. S., PARK, S. H., PARK, H. S. & PARK, B. W. 2010. Molecular subtypes and tumor response to neoadjuvant chemotherapy in patients with locally advanced breast cancer. *Oncology,* 79**,** 324-30.
KING, M. C., MARKS, J. H., MANDELL, J. B. & NEW YORK BREAST CANCER STUDY, G. 2003. Breast and ovarian cancer risks due to inherited mutations in BRCA1 and BRCA2. *Science,* 302**,** 643-6.
KO, E. S., HAN, B. K., KIM, R. B., KO, E. Y., SHIN, J. H., HAHN, S. Y., NAM, S. J., LEE, J. E., LEE, S. K., IM, Y. H. & PARK, Y. H. 2013. Analysis of factors that influence the accuracy of magnetic resonance imaging for predicting response after neoadjuvant chemotherapy in locally advanced breast cancer. *Ann Surg Oncol,* 20**,** 2562-8.
KOLESNIKOV-GAUTHIER, H., VANLEMMENS, L., BARANZELLI, M. C., VENNIN, P., SERVENT, V., FOURNIER, C., CARPENTIER, P. & BONNETERRE, J. 2012. Predictive value of neoadjuvant chemotherapy failure in breast cancer using FDG-PET after the first course. *Breast Cancer Res Treat,* 131**,** 517-25.
KOLIOS, M. C., CZARNOTA, G. J., LEE, M., HUNT, J. W. & SHERAR, M. D. 2002. Ultrasonic spectral parameter characterization of apoptosis. *Ultrasound Med Biol,* 28**,** 589-97.
KONG, X., MORAN, M. S., ZHANG, N., HAFFTY, B. & YANG, Q. 2011. Meta-analysis confirms achieving pathological complete response after neoadjuvant chemotherapy predicts favourable prognosis for breast cancer patients. *Eur J Cancer,* 47**,** 2084-90.
KRUMBHAAR, E. B. & KRUMBHAAR, H. D. 1919. The Blood and Bone Marrow in Yelloe Cross Gas (Mustard Gas) Poisoning: Changes produced in the Bone Marrow of Fatal Cases. *J Med Res,* 40**,** 497-508 3.
KUERER, H. M., NEWMAN, L. A., SMITH, T. L., AMES, F. C., HUNT, K. K., DHINGRA, K., THERIAULT, R. L., SINGH, G., BINKLEY, S. M., SNEIGE, N., BUCHHOLZ, T. A., ROSS, M. I., MCNEESE, M. D., BUZDAR, A. U., HORTOBAGYI, G. N. & SINGLETARY, S. E. 1999. Clinical course of breast cancer patients with complete pathologic primary tumor and axillary lymph node response to doxorubicin-based neoadjuvant chemotherapy. *J Clin Oncol,* 17**,** 460-9.
KUKRETI, S., CERUSSI, A. E., TANAMAI, W., HSIANG, D., TROMBERG, B. J. & GRATTON, E. 2010. Characterization of metabolic differences between benign and malignant tumors: high-spectral-resolution diffuse optical spectroscopy. *Radiology,* 254**,** 277-84.
LEE, J., KARSHAFIAN, R., PAPANICOLAU, N., GILES, A., KOLIOS, M. C. & CZARNOTA, G. J. 2012. Quantitative ultrasound for the monitoring of novel microbubble and ultrasound radiosensitization. *Ultrasound Med Biol,* 38**,** 1212-21.
LEE, M. C. & NEWMAN, L. A. 2007. Management of patients with locally advanced breast cancer. *Surg Clin North Am,* 87**,** 379-98, ix.
LEFF, D. R., WARREN, O. J., ENFIELD, L. C., GIBSON, A., ATHANASIOU, T., PATTEN, D. K., HEBDEN, J., YANG, G. Z. & DARZI, A. 2008. Diffuse optical imaging of the healthy and diseased breast: a systematic review. *Breast Cancer Res Treat,* 108**,** 9-22.

LEO, G. D., TRIMBOLI, R. M., SELLA, T. & SARDANELLI, F. 2017. Optical Imaging of the Breast: Basic Principles and Clinical Applications. *AJR Am J Roentgenol,* 209**,** 230-238.
LEONE, J. P., LEONE, J., ZWENGER, A. O., ITURBE, J., VALLEJO, C. T. & LEONE, B. A. 2015. Prognostic significance of tumor subtypes in male breast cancer: a population-based study. *Breast Cancer Res Treat,* 152**,** 601-9.
LERSKI, R. A., STRAUGHAN, K., SCHAD, L. R., BOYCE, D., BLUML, S. & ZUNA, I. 1993. MR image texture analysis--an approach to tissue characterization. *Magn Reson Imaging,* 11**,** 873-87.
LI, C. I., ANDERSON, B. O., DALING, J. R. & MOE, R. E. 2003. Trends in incidence rates of invasive lobular and ductal breast carcinoma. *JAMA,* 289**,** 1421-4.
LI, H., GIGER, M. L., OLOPADE, O. I., MARGOLIS, A., LAN, L. & CHINANDER, M. R. 2005. Computerized texture analysis of mammographic parenchymal patterns of digitized mammograms. *Acad Radiol,* 12**,** 863-73.
LI, S. P., MAKRIS, A., GOGBASHIAN, A., SIMCOCK, I. C., STIRLING, J. J. & GOH, V. 2012. Predicting response to neoadjuvant chemotherapy in primary breast cancer using volumetric helical perfusion computed tomography: a preliminary study. *Eur Radiol,* 22**,** 1871-80.
LICHTENSTEIN, P., HOLM, N. V., VERKASALO, P. K., ILIADOU, A., KAPRIO, J., KOSKENVUO, M., PUKKALA, E., SKYTTHE, A. & HEMMINKI, K. 2000. Environmental and heritable factors in the causation of cancer--analyses of cohorts of twins from Sweden, Denmark, and Finland. *N Engl J Med,* 343**,** 78-85.
LIEDTKE, C., MAZOUNI, C., HESS, K. R., ANDRE, F., TORDAI, A., MEJIA, J. A., SYMMANS, W. F., GONZALEZ-ANGULO, A. M., HENNESSY, B., GREEN, M., CRISTOFANILLI, M., HORTOBAGYI, G. N. & PUSZTAI, L. 2008. Response to neoadjuvant therapy and long-term survival in patients with triple-negative breast cancer. *J Clin Oncol,* 26**,** 1275-81.
LIN, S. C., HEBA, E., WOLFSON, T., ANG, B., GAMST, A., HAN, A., ERDMAN, J. W., JR., O'BRIEN, W. D., JR., ANDRE, M. P., SIRLIN, C. B. & LOOMBA, R. 2015. Noninvasive Diagnosis of Nonalcoholic Fatty Liver Disease and Quantification of Liver Fat Using a New Quantitative Ultrasound Technique. *Clin Gastroenterol Hepatol,* 13**,** 1337-1345 e6.
LIU, Q. 2011. Role of optical spectroscopy using endogenous contrasts in clinical cancer diagnosis. *World J Clin Oncol,* 2**,** 50-63.
LIZZI, F. L., ASTOR, M., FELEPPA, E. J., SHAO, M. & KALISZ, A. 1997a. Statistical framework for ultrasonic spectral parameter imaging. *Ultrasound Med Biol,* 23**,** 1371-82.
LIZZI, F. L., ASTOR, M., LIU, T., DENG, C. X., COLEMAN, D. J. & SILVERMAN, R. H. 1997b. Ultrasonic spectrum analysis for tissue assays and therapy evaluation. *International Journal of Imaging Systems and Technology,* 8**,** 3-10.
LIZZI, F. L., GREENEBAUM, M., FELEPPA, E. J., ELBAUM, M. & COLEMAN, D. J. 1983. Theoretical framework for spectrum analysis in ultrasonic tissue characterization. *J Acoust Soc Am,* 73**,** 1366-73.
LODGE, M. A., CARSON, R. E., CARRASQUILLO, J. A., WHATLEY, M., LIBUTTI, S. K. & BACHARACH, S. L. 2000. Parametric images of blood flow in oncology PET studies using [15O]water. *J Nucl Med,* 41**,** 1784-92.

LOGAN, G. J., DABBS, D. J., LUCAS, P. C., JANKOWITZ, R. C., BROWN, D. D., CLARK, B. Z., OESTERREICH, S. & MCAULIFFE, P. F. 2015. Molecular drivers of lobular carcinoma in situ. *Breast Cancer Res,* 17**,** 76.
LOWE, S. W. & LIN, A. W. 2000. Apoptosis in cancer. *Carcinogenesis,* 21**,** 485-95.
LU, Z. F., ZAGZEBSKI, J. A. & LEE, F. T. 1999. Ultrasound backscatter and attenuation in human liver with diffuse disease. *Ultrasound Med Biol,* 25**,** 1047-54.
LUO, J. & ELLEDGE, S. J. 2008. Cancer: Deconstructing oncogenesis. *Nature,* 453**,** 995-6.
MADSEN, E. L., ZAGZEBSKI, J. A., BANJAVIE, R. A. & JUTILA, R. E. 1978. Tissue mimicking materials for ultrasound phantoms. *Med Phys,* 5**,** 391-4.
MAJNO, G. & JORIS, I. 1995. Apoptosis, oncosis, and necrosis. An overview of cell death. *Am J Pathol,* 146**,** 3-15.
MAMOU, J. & OELZE, M. L. 2013. *Quantitative ultrasound in soft tissues,* Dordrecht, Springer.
MANI, S., CHEN, Y., LI, X., ARLINGHAUS, L., CHAKRAVARTHY, A. B., ABRAMSON, V., BHAVE, S. R., LEVY, M. A., XU, H. & YANKEELOV, T. E. 2013. Machine learning for predicting the response of breast cancer to neoadjuvant chemotherapy. *J Am Med Inform Assoc,* 20**,** 688-95.
MANKOFF, D. A., DUNNWALD, L. K., GRALOW, J. R., ELLIS, G. K., CHARLOP, A., LAWTON, T. J., SCHUBERT, E. K., TSENG, J. & LIVINGSTON, R. B. 2002. Blood flow and metabolism in locally advanced breast cancer: relationship to response to therapy. *J Nucl Med,* 43**,** 500-9.
MANN, H. B. & WHITNEY, D. R. 1947. On a test of whether one or 2 random variables is stochastically larger than the other. *Annals of Mathematical Statistics,* 18**,** 50-60.
MARCHIO, C. & SAPINO, A. 2011. The pathologic complete response open question in primary therapy. *J Natl Cancer Inst Monogr,* 2011**,** 86-90.
MARTINCICH, L., BERTOTTO, I., MONTEMURRO, F., PONZONE, R., CARBONARO, L. A., REGGE, D. & SARDANELLI, F. 2011. Variation of breast vascular maps on dynamic contrast-enhanced MRI after primary chemotherapy of locally advanced breast cancer. *AJR Am J Roentgenol,* 196**,** 1214-8.
MARTINOLI, C., DERCHI, L. E., RIZZATTO, G. & SOLBIATI, L. 1998. Power Doppler sonography: general principles, clinical applications, and future prospects. *Eur Radiol,* 8**,** 1224-35.
MARTONI, A. A., ZAMAGNI, C., QUERCIA, S., ROSATI, M., CACCIARI, N., BERNARDI, A., MUSTO, A., FANTI, S., SANTINI, D. & TAFFURELLI, M. 2010. Early (18)F-2-fluoro-2-deoxy-d-glucose positron emission tomography may identify a subset of patients with estrogen receptor-positive breast cancer who will not respond optimally to preoperative chemotherapy. *Cancer,* 116**,** 805-13.
MASSON, E. & ZAMBONI, W. C. 1997. Pharmacokinetic optimisation of cancer chemotherapy. Effect on outcomes. *Clin Pharmacokinet,* 32**,** 324-43.
MASUDA, N., LEE, S. J., OHTANI, S., IM, Y. H., LEE, E. S., YOKOTA, I., KUROI, K., IM, S. A., PARK, B. W., KIM, S. B., YANAGITA, Y., OHNO, S., TAKAO, S., AOGI, K., IWATA, H., JEONG, J., KIM, A., PARK, K. H., SASANO, H., OHASHI, Y. & TOI, M. 2017. Adjuvant Capecitabine for

Breast Cancer after Preoperative Chemotherapy. *N Engl J Med,* 376**,** 2147-2159.
MCCORMACK, V. A. & DOS SANTOS SILVA, I. 2006. Breast density and parenchymal patterns as markers of breast cancer risk: a meta-analysis. *Cancer Epidemiol Biomarkers Prev,* 15**,** 1159-69.
MCHUGH, M. L. 2012. Interrater reliability: the kappa statistic. *Biochem Med (Zagreb),* 22**,** 276-82.
MCPHERSON, K., STEEL, C. M. & DIXON, J. M. 2000. ABC of breast diseases. Breast cancer-epidemiology, risk factors, and genetics. *BMJ,* 321**,** 624-8.
MCSHANE, L. M., ALTMAN, D. G., SAUERBREI, W., TAUBE, S. E., GION, M., CLARK, G. M. & STATISTICS SUBCOMMITTEE OF THE, N. C. I. E. W. G. O. C. D. 2005. Reporting recommendations for tumor marker prognostic studies (REMARK). *J Natl Cancer Inst,* 97**,** 1180-4.
MECHETNER, E. B. & RONINSON, I. B. 1992. Efficient inhibition of P-glycoprotein-mediated multidrug resistance with a monoclonal antibody. *Proc Natl Acad Sci U S A,* 89**,** 5824-8.
MEINARDI, M. T., GIETEMA, J. A., VAN VELDHUISEN, D. J., VAN DER GRAAF, W. T., DE VRIES, E. G. & SLEIJFER, D. T. 2000. Long-term chemotherapy-related cardiovascular morbidity. *Cancer Treat Rev,* 26**,** 429-47.
METCALFE, K., LUBINSKI, J., LYNCH, H. T., GHADIRIAN, P., FOULKES, W. D., KIM-SING, C., NEUHAUSEN, S., TUNG, N., ROSEN, B., GRONWALD, J., AINSWORTH, P., SWEET, K., EISEN, A., SUN, P., NAROD, S. A. & HEREDITARY BREAST CANCER CLINICAL STUDY, G. 2010. Family history of cancer and cancer risks in women with BRCA1 or BRCA2 mutations. *J Natl Cancer Inst,* 102**,** 1874-8.
METCALFE, P., LINEY, G. P., HOLLOWAY, L., WALKER, A., BARTON, M., DELANEY, G. P., VINOD, S. & TOME, W. 2013. The potential for an enhanced role for MRI in radiation-therapy treatment planning. *Technol Cancer Res Treat,* 12**,** 429-46.
METZ, C. E. 2006. Receiver operating characteristic analysis: a tool for the quantitative evaluation of observer performance and imaging systems. *J Am Coll Radiol,* 3**,** 413-22.
MICHISHITA, S., KIM, S. J., SHIMAZU, K., SOTA, Y., NAOI, Y., MARUYAMA, N., KAGARA, N., SHIMODA, M., SHIMOMURA, A. & NOGUCHI, S. 2015. Prediction of pathological complete response to neoadjuvant chemotherapy by magnetic resonance imaging in breast cancer patients. *Breast,* 24**,** 159-65.
MILLER, A. B., WALL, C., BAINES, C. J., SUN, P., TO, T. & NAROD, S. A. 2014. Twenty five year follow-up for breast cancer incidence and mortality of the Canadian National Breast Screening Study: randomised screening trial. *BMJ,* 348**,** g366.
MINARIKOVA, L., BOGNER, W., PINKER, K., VALKOVIC, L., ZARIC, O., BAGO-HORVATH, Z., BARTSCH, R., HELBICH, T. H., TRATTNIG, S. & GRUBER, S. 2016. Investigating the prediction value of multiparametric magnetic resonance imaging at 3 T in response to neoadjuvant chemotherapy in breast cancer. *Eur Radiol*.
MINCHINTON, A. I. & TANNOCK, I. F. 2006. Drug penetration in solid tumours. *Nat Rev Cancer,* 6**,** 583-92.
MITTAL, B. R., SINGH, R. K., KUMARI, S., MANOHAR, K., BHATTACHARYA, A. & SINGH, G. 2012. Role of Tc99m-Sestamibi scintimammography in

assessing response to neoadjuvant chemotherapy in patients with locally advanced breast cancer. *Indian J Nucl Med,* 27**,** 221-5.
MIZUTANI, H., TADA-OIKAWA, S., HIRAKU, Y., KOJIMA, M. & KAWANISHI, S. 2005. Mechanism of apoptosis induced by doxorubicin through the generation of hydrogen peroxide. *Life Sci,* 76**,** 1439-53.
MOHER, D., LIBERATI, A., TETZLAFF, J., ALTMAN, D. G. & GROUP, P. 2009. Preferred reporting items for systematic reviews and meta-analyses: the PRISMA statement. *PLoS Med,* 6**,** e1000097.
MOURANT, J. R., CANPOLAT, M., BROCKER, C., ESPONDA-RAMOS, O., JOHNSON, T. M., MATANOCK, A., STETTER, K. & FREYER, J. P. 2000. Light scattering from cells: the contribution of the nucleus and the effects of proliferative status. *J Biomed Opt,* 5**,** 131-7.
MURRAY, N., WINSTANLEY, J., BENNETT, A., FRANCIS, K. & GUIDELINE DEVELOPMENT, G. 2009. Diagnosis and treatment of advanced breast cancer: summary of NICE guidance. *BMJ,* 338**,** b509.
MUTHUKKARUPPAN, V. R., KUBAI, L. & AUERBACH, R. 1982. Tumor-induced neovascularization in the mouse eye. *J Natl Cancer Inst,* 69**,** 699-708.
NACHAR, N. 2008. The Mann-Whityney U: A test for assessing whether two independent samples come from the same distribution. *Tutorials in Quantitative Methods for Psychology,* 4**,** 13-20.
NAROD, S. A. 2012. Tumour size predicts long-term survival among women with lymph node-positive breast cancer. *Curr Oncol,* 19**,** 249-53.
NATIONAL COMPREHENSIVE CANCER NETWORK. 2016. *Breast Cancer (Version 2.2016)* [Online]. Available: https://www.nccn.org/professionals/physician_gls/f_guidelines.asp [Accessed January 17, 2017 2017].
NATIONAL INSTITUTE FOR HEALTH AND CARE EXCELLENCE, N. 2017. *Managing advanced breast cancer* [Online]. Available: http:/pathways.nice.org.uk/pathways/advanced-breast-cancer [Accessed September 6 2017 2017].
NATIONAL INSTITUTE FOR HEALTH AND CLINICAL EXCELLENCE (NICE) 2009a. Advanced Breast Cancer: Diagnosis and Treatment. Cardiff (UK).
NATIONAL INSTITUTE FOR HEALTH AND CLINICAL EXCELLENCE (NICE) 2009b. Early and Locally Advanced Breast Cancer: Diagnosis and Treatment. Cardiff (UK): (NICE).
NATIONAL INSTITUTE FOR HEALTH AND CLINICAL EXCELLENCE (NICE) 2011. Breast Cancer. Cardiff (UK).
NATIONAL INSTITUTE FOR HEALTH AND CLINICAL EXCELLENCE (NICE) 2012. Neutropenic sepsis: prevention and management in people with cancer. Cardiff, UK.
NEWMAN, L. A. 2009. Epidemiology of locally advanced breast cancer. *Semin Radiat Oncol,* 19**,** 195-203.
NISHIDA, N., YANO, H., NISHIDA, T., KAMURA, T. & KOJIRO, M. 2006. Angiogenesis in cancer. *Vasc Health Risk Manag,* 2**,** 213-9.
O'BRIEN, W. D., JR. 2007. Ultrasound-biophysics mechanisms. *Prog Biophys Mol Biol,* 93**,** 212-55.
O'CONNOR, J. P., ABOAGYE, E. O., ADAMS, J. E., AERTS, H. J., BARRINGTON, S. F., BEER, A. J., BOELLAARD, R., BOHNDIEK, S. E., BRADY, M., BROWN, G., BUCKLEY, D. L., CHENEVERT, T. L., CLARKE, L. P., COLLETTE, S., COOK, G. J., DESOUZA, N. M., DICKSON, J. C., DIVE, C., EVELHOCH, J. L., FAIVRE-FINN, C.,

GALLAGHER, F. A., GILBERT, F. J., GILLIES, R. J., GOH, V., GRIFFITHS, J. R., GROVES, A. M., HALLIGAN, S., HARRIS, A. L., HAWKES, D. J., HOEKSTRA, O. S., HUANG, E. P., HUTTON, B. F., JACKSON, E. F., JAYSON, G. C., JONES, A., KOH, D. M., LACOMBE, D., LAMBIN, P., LASSAU, N., LEACH, M. O., LEE, T. Y., LEEN, E. L., LEWIS, J. S., LIU, Y., LYTHGOE, M. F., MANOHARAN, P., MAXWELL, R. J., MILES, K. A., MORGAN, B., MORRIS, S., NG, T., PADHANI, A. R., PARKER, G. J., PARTRIDGE, M., PATHAK, A. P., PEET, A. C., PUNWANI, S., REYNOLDS, A. R., ROBINSON, S. P., SHANKAR, L. K., SHARMA, R. A., SOLOVIEV, D., STROOBANTS, S., SULLIVAN, D. C., TAYLOR, S. A., TOFTS, P. S., TOZER, G. M., VAN HERK, M., WALKER-SAMUEL, S., WASON, J., WILLIAMS, K. J., WORKMAN, P., YANKEELOV, T. E., BRINDLE, K. M., MCSHANE, L. M., JACKSON, A. & WATERTON, J. C. 2016. Imaging biomarker roadmap for cancer studies. *Nat Rev Clin Oncol*.

O'CONNOR, J. P., JACKSON, A., ASSELIN, M. C., BUCKLEY, D. L., PARKER, G. J. & JAYSON, G. C. 2008. Quantitative imaging biomarkers in the clinical development of targeted therapeutics: current and future perspectives. *Lancet Oncol,* 9**,** 766-76.

O'CONNOR, J. P., ROSE, C. J., WATERTON, J. C., CARANO, R. A., PARKER, G. J. & JACKSON, A. 2015. Imaging intratumor heterogeneity: role in therapy response, resistance, and clinical outcome. *Clin Cancer Res,* 21**,** 249-57.

O'FLYNN, E. A. & DESOUZA, N. M. 2011. Functional magnetic resonance: biomarkers of response in breast cancer. *Breast Cancer Res,* 13**,** 204.

O'SULLIVAN, T. D., LEPROUX, A., CHEN, J. H., BAHRI, S., MATLOCK, A., ROBLYER, D., MCLAREN, C. E., CHEN, W. P., CERUSSI, A. E., SU, M. Y. & TROMBERG, B. J. 2013. Optical imaging correlates with magnetic resonance imaging breast density and reveals composition changes during neoadjuvant chemotherapy. *Breast Cancer Res,* 15**,** R14.

OELZE, M. L. & MAMOU, J. 2016. Review of Quantitative Ultrasound: Envelope Statistics and Backscatter Coefficient Imaging and Contributions to Diagnostic Ultrasound. *IEEE Trans Ultrason Ferroelectr Freq Control,* 63**,** 336-51.

OELZE, M. L., ZACHARY, J. F. & O'BRIEN, W. D., JR. 2002. Characterization of tissue microstructure using ultrasonic backscatter: theory and technique for optimization using a Gaussian form factor. *J Acoust Soc Am,* 112**,** 1202-11.

OGINO, K., NAKAJIMA, M., KAKUTA, M., HAYASHI, M., YAMAGUCHI, S., TSUCHIOKA, T., KUBOTA, K., SAKAMOTO, S. & KATO, H. 2014. Utility of FDG-PET/CT in the evaluation of the response of locally advanced breast cancer to neoadjuvant chemotherapy. *Int Surg,* 99**,** 309-18.

OGSTON, K. N., MILLER, I. D., PAYNE, S., HUTCHEON, A. W., SARKAR, T. K., SMITH, I., SCHOFIELD, A. & HEYS, S. D. 2003. A new histological grading system to assess response of breast cancers to primary chemotherapy: prognostic significance and survival. *Breast,* 12**,** 320-7.

OKADA, H. & MAK, T. W. 2004. Pathways of apoptotic and non-apoptotic death in tumour cells. *Nat Rev Cancer,* 4**,** 592-603.

PADHANI, A. R. 2002. Functional MRI for anticancer therapy assessment. *Eur J Cancer,* 38**,** 2116-27.

PAIK, S., SHAK, S., TANG, G., KIM, C., BAKER, J., CRONIN, M., BAEHNER, F. L., WALKER, M. G., WATSON, D., PARK, T., HILLER, W., FISHER,

E. R., WICKERHAM, D. L., BRYANT, J. & WOLMARK, N. 2004. A multigene assay to predict recurrence of tamoxifen-treated, node-negative breast cancer. *N Engl J Med,* 351**,** 2817-26.
PAIK, S., TANG, G., SHAK, S., KIM, C., BAKER, J., KIM, W., CRONIN, M., BAEHNER, F. L., WATSON, D., BRYANT, J., COSTANTINO, J. P., GEYER, C. E., JR., WICKERHAM, D. L. & WOLMARK, N. 2006. Gene expression and benefit of chemotherapy in women with node-negative, estrogen receptor-positive breast cancer. *J Clin Oncol,* 24**,** 3726-34.
PAKALNISKIS, M. G., WELLS, W. A., SCHWAB, M. C., FROEHLICH, H. M., JIANG, S., LI, Z., TOSTESON, T. D., POPLACK, S. P., KAUFMAN, P. A., POGUE, B. W. & PAULSEN, K. D. 2011. Tumor angiogenesis change estimated by using diffuse optical spectroscopic tomography: demonstrated correlation in women undergoing neoadjuvant chemotherapy for invasive breast cancer? *Radiology,* 259**,** 365-74.
PARK, J. O., LEE, S. I., SONG, S. Y., KIM, K., KIM, W. S., JUNG, C. W., PARK, Y. S., IM, Y. H., KANG, W. K., LEE, M. H., LEE, K. S. & PARK, K. 2003. Measuring response in solid tumors: comparison of RECIST and WHO response criteria. *Jpn J Clin Oncol,* 33**,** 533-7.
PARK, J. S., MOON, W. K., LYOU, C. Y., CHO, N., KANG, K. W. & CHUNG, J. K. 2011. The assessment of breast cancer response to neoadjuvant chemotherapy: comparison of magnetic resonance imaging and 18F-fluorodeoxyglucose positron emission tomography. *Acta Radiol,* 52**,** 21-8.
PARKER, W. B. 2009. Enzymology of purine and pyrimidine antimetabolites used in the treatment of cancer. *Chem Rev,* 109**,** 2880-93.
PARKIN, D. M. 2011a. 3. Cancers attributable to consumption of alcohol in the UK in 2010. *Br J Cancer,* 105 Suppl 2**,** S14-8.
PARKIN, D. M. 2011b. 10. Cancers attributable to exposure to hormones in the UK in 2010. *Br J Cancer,* 105 Suppl 2**,** S42-8.
PATTERSON, M. S., CHANCE, B. & WILSON, B. C. 1989. Time resolved reflectance and transmittance for the non-invasive measurement of tissue optical properties. *Appl Opt,* 28**,** 2331-6.
PEROU, C. M., SORLIE, T., EISEN, M. B., VAN DE RIJN, M., JEFFREY, S. S., REES, C. A., POLLACK, J. R., ROSS, D. T., JOHNSEN, H., AKSLEN, L. A., FLUGE, O., PERGAMENSCHIKOV, A., WILLIAMS, C., ZHU, S. X., LONNING, P. E., BORRESEN-DALE, A. L., BROWN, P. O. & BOTSTEIN, D. 2000. Molecular portraits of human breast tumours. *Nature,* 406**,** 747-52.
PETTY, G. W. 2006. *A first course in atmospheric radiation,* Madison, Wis., Sundog Pub.
PICKLES, M. D., LOWRY, M., MANTON, D. J., GIBBS, P. & TURNBULL, L. W. 2005. Role of dynamic contrast enhanced MRI in monitoring early response of locally advanced breast cancer to neoadjuvant chemotherapy. *Breast Cancer Res Treat,* 91**,** 1-10.
PIEN, H. H., FISCHMAN, A. J., THRALL, J. H. & SORENSEN, A. G. 2005. Using imaging biomarkers to accelerate drug development and clinical trials. *Drug Discov Today,* 10**,** 259-66.
PIETRAS, K. & OSTMAN, A. 2010. Hallmarks of cancer: interactions with the tumor stroma. *Exp Cell Res,* 316**,** 1324-31.
POGUE, B. W., POPLACK, S. P., MCBRIDE, T. O., WELLS, W. A., OSTERMAN, K. S., OSTERBERG, U. L. & PAULSEN, K. D. 2001. Quantitative hemoglobin tomography with diffuse near-infrared spectroscopy: pilot results in the breast. *Radiology,* 218**,** 261-6.

POLYAK, K. 2011. Heterogeneity in breast cancer. *J Clin Invest,* 121**,** 3786-8.
POWLES, T. J., HICKISH, T. F., MAKRIS, A., ASHLEY, S. E., O'BRIEN, M. E., TIDY, V. A., CASEY, S., NASH, A. G., SACKS, N., COSGROVE, D. & ET AL. 1995. Randomized trial of chemoendocrine therapy started before or after surgery for treatment of primary breast cancer. *J Clin Oncol,* 13**,** 547-52.
PRITT, B. & WEAVER, D. L. 2005. Accurate determination of breast cancer size: The role of histopathology and imaging. *Current Diagnostic Pathology,* 11**,** 435-442.
RAHIB, L., SMITH, B. D., AIZENBERG, R., ROSENZWEIG, A. B., FLESHMAN, J. M. & MATRISIAN, L. M. 2014. Projecting cancer incidence and deaths to 2030: the unexpected burden of thyroid, liver, and pancreas cancers in the United States. *Cancer Res,* 74**,** 2913-21.
RAK, J., MITSUHASHI, Y., BAYKO, L., FILMUS, J., SHIRASAWA, S., SASAZUKI, T. & KERBEL, R. S. 1995. Mutant ras Oncogenes Upregulate VEGF/VPF Expression: Implications for Induction and Inhibition of Tumor Angiogenesis. *Cancer Research,* 55**,** 4575-4580.
RAKHA, E. A., SORIA, D., GREEN, A. R., LEMETRE, C., POWE, D. G., NOLAN, C. C., GARIBALDI, J. M., BALL, G. & ELLIS, I. O. 2014. Nottingham Prognostic Index Plus (NPI+): a modern clinical decision making tool in breast cancer. *Br J Cancer,* 110**,** 1688-97.
RICHARDS-KORTUM, R. & SEVICK-MURACA, E. 1996. Quantitative optical spectroscopy for tissue diagnosis. *Annu Rev Phys Chem,* 47**,** 555-606.
ROBLYER, D., UEDA, S., CERUSSI, A., TANAMAI, W., DURKIN, A., MEHTA, R., HSIANG, D., BUTLER, J. A., MCLAREN, C., CHEN, W. P. & TROMBERG, B. 2011. Optical imaging of breast cancer oxyhemoglobin flare correlates with neoadjuvant chemotherapy response one day after starting treatment. *Proc Natl Acad Sci U S A,* 108**,** 14626-31.
ROFSTAD, E. K., GALAPPATHI, K. & MATHIESEN, B. S. 2014. Tumor interstitial fluid pressure-a link between tumor hypoxia, microvascular density, and lymph node metastasis. *Neoplasia,* 16**,** 586-94.
ROUZIER, R., PEROU, C. M., SYMMANS, W. F., IBRAHIM, N., CRISTOFANILLI, M., ANDERSON, K., HESS, K. R., STEC, J., AYERS, M., WAGNER, P., MORANDI, P., FAN, C., RABIUL, I., ROSS, J. S., HORTOBAGYI, G. N. & PUSZTAI, L. 2005. Breast cancer molecular subtypes respond differently to preoperative chemotherapy. *Clin Cancer Res,* 11**,** 5678-85.
RUCKER, G., SCHIMEK-JASCH, T. & NESTLE, U. 2012. Measuring inter-observer agreement in contour delineation of medical imaging in a dummy run using Fleiss' kappa. *Methods Inf Med,* 51**,** 489-94.
RUDIN, M. & WEISSLEDER, R. 2003. Molecular imaging in drug discovery and development. *Nat Rev Drug Discov,* 2**,** 123-31.
SACHELARIE, I., GROSSBARD, M. L., CHADHA, M., FELDMAN, S., GHESANI, M. & BLUM, R. H. 2006. Primary systemic therapy of breast cancer. *Oncologist,* 11**,** 574-89.
SADEGHI-NAINI, A., FALOU, O., TADAYYON, H., AL-MAHROUKI, A., TRAN, W., PAPANICOLAU, N., KOLIOS, M. C. & CZARNOTA, G. J. 2013a. Conventional frequency ultrasonic biomarkers of cancer treatment response in vivo. *Transl Oncol,* 6**,** 234-43.
SADEGHI-NAINI, A., PAPANICOLAU, N., FALOU, O., ZUBOVITS, J., DENT, R., VERMA, S., TRUDEAU, M., BOILEAU, J. F., SPAYNE, J., IRADJI, S., SOFRONI, E., LEE, J., LEMON-WONG, S., YAFFE, M., KOLIOS, M.

C. & CZARNOTA, G. J. 2013b. Quantitative ultrasound evaluation of tumor cell death response in locally advanced breast cancer patients receiving chemotherapy. *Clin Cancer Res,* 19**,** 2163-74.
SADEGHI-NAINI, A., SANNACHI, L., PRITCHARD, K., TRUDEAU, M., GANDHI, S., WRIGHT, F. C., ZUBOVITS, J., YAFFE, M. J., KOLIOS, M. C. & CZARNOTA, G. J. 2014. Early prediction of therapy responses and outcomes in breast cancer patients using quantitative ultrasound spectral texture. *Oncotarget,* 5**,** 3497-511.
SADEGHI-NAINI, A., VORAUER, E., CHIN, L., FALOU, O., TRAN, W. T., WRIGHT, F. C., GANDHI, S., YAFFE, M. J. & CZARNOTA, G. J. 2015. Early detection of chemotherapy-refractory patients by monitoring textural alterations in diffuse optical spectroscopic images. *Med Phys,* 42**,** 6130-46.
SAFTLAS, A. F., HOOVER, R. N., BRINTON, L. A., SZKLO, M., OLSON, D. R., SALANE, M. & WOLFE, J. N. 1991. Mammographic densities and risk of breast cancer. *Cancer,* 67**,** 2833-8.
SANCHEZ-MUNOZ, A., GARCIA-TAPIADOR, A. M., MARTINEZ-ORTEGA, E., DUENAS-GARCIA, R., JAEN-MORAGO, A., ORTEGA-GRANADOS, A. L., FERNANDEZ-NAVARRO, M., DE LA TORRE-CABRERA, C., DUENAS, B., RUEDA, A. I., MORALES, F., RAMIREZ-TOROSA, C., MARTIN-SALVAGO, M. D. & SANCHEZ-ROVIRA, P. 2008. Tumour molecular subtyping according to hormone receptors and HER2 status defines different pathological complete response to neoadjuvant chemotherapy in patients with locally advanced breast cancer. *Clin Transl Oncol,* 10**,** 646-53.
SANNACHI, L., TADAYYON, H., SADEGHI-NAINI, A., TRAN, W., GANDHI, S., WRIGHT, F., OELZE, M. & CZARNOTA, G. 2015. Non-invasive evaluation of breast cancer response to chemotherapy using quantitative ultrasonic backscatter parameters. *Med Image Anal,* 20**,** 224-36.
SANTAGATA, S., THAKKAR, A., ERGONUL, A., WANG, B., WOO, T., HU, R., HARRELL, J. C., MCNAMARA, G., SCHWEDE, M., CULHANE, A. C., KINDELBERGER, D., RODIG, S., RICHARDSON, A., SCHNITT, S. J., TAMIMI, R. M. & INCE, T. A. 2014. Taxonomy of breast cancer based on normal cell phenotype predicts outcome. *J Clin Invest,* 124**,** 859-70.
SANTAGO, P. & GAGE, H. D. 1995. Statistical models of partial volume effect. *IEEE Trans Image Process,* 4**,** 1531-40.
SARACCO, A., SZABO, B. K., TANCZOS, E., BERGH, J. & HATSCHEK, T. 2017. Contrast-enhanced ultrasound (CEUS) in assessing early response among patients with invasive breast cancer undergoing neoadjuvant chemotherapy. *Acta Radiol,* 58**,** 394-402.
SASLOW, D., BOETES, C., BURKE, W., HARMS, S., LEACH, M. O., LEHMAN, C. D., MORRIS, E., PISANO, E., SCHNALL, M., SENER, S., SMITH, R. A., WARNER, E., YAFFE, M., ANDREWS, K. S., RUSSELL, C. A. & AMERICAN CANCER SOCIETY BREAST CANCER ADVISORY, G. 2007. American Cancer Society guidelines for breast screening with MRI as an adjunct to mammography. *CA Cancer J Clin,* 57**,** 75-89.
SATALOFF, D. M., MASON, B. A., PRESTIPINO, A. J., SEINIGE, U. L., LIEBER, C. P. & BALOCH, Z. 1995. Pathologic response to induction chemotherapy in locally advanced carcinoma of the breast: a determinant of outcome. *J Am Coll Surg,* 180**,** 297-306.
SATO, C., SHIMADA, M., TANIKAWA, Y. & HOSHI, Y. 2013. Estimating the absorption coefficient of the bottom layer in four-layered turbid mediums

based on the time-domain depth sensitivity of near-infrared light reflectance. *J Biomed Opt,* 18**,** 097005.
SCHAAFSMA, B. E., VAN DE GIESSEN, M., CHAREHBILI, A., SMIT, V. T., KROEP, J. R., LELIEVELDT, B. P., LIEFERS, G. J., CHAN, A., LOWIK, C. W., DIJKSTRA, J., VAN DE VELDE, C. J., WASSER, M. N. & VAHRMEIJER, A. L. 2015. Optical mammography using diffuse optical spectroscopy for monitoring tumor response to neoadjuvant chemotherapy in women with locally advanced breast cancer. *Clin Cancer Res,* 21**,** 577-84.
SCHEGERIN, M., TOSTESON, A. N., KAUFMAN, P. A., PAULSEN, K. D. & POGUE, B. W. 2009. Prognostic imaging in neoadjuvant chemotherapy of locally-advanced breast cancer should be cost-effective. *Breast Cancer Res Treat,* 114**,** 537-47.
SCHRADER, J., GORDON-WALKER, T. T., AUCOTT, R. L., VAN DEEMTER, M., QUAAS, A., WALSH, S., BENTEN, D., FORBES, S. J., WELLS, R. G. & IREDALE, J. P. 2011. Matrix stiffness modulates proliferation, chemotherapeutic response, and dormancy in hepatocellular carcinoma cells. *Hepatology,* 53**,** 1192-205.
SCHWARTZ, L. H., LITIERE, S., DE VRIES, E., FORD, R., GWYTHER, S., MANDREKAR, S., SHANKAR, L., BOGAERTS, J., CHEN, A., DANCEY, J., HAYES, W., HODI, F. S., HOEKSTRA, O. S., HUANG, E. P., LIN, N., LIU, Y., THERASSE, P., WOLCHOK, J. D. & SEYMOUR, L. 2016. RECIST 1.1-Update and clarification: From the RECIST committee. *Eur J Cancer,* 62**,** 132-7.
SEHGAL, C. M., WEINSTEIN, S. P., ARGER, P. H. & CONANT, E. F. 2006. A review of breast ultrasound. *J Mammary Gland Biol Neoplasia,* 11**,** 113-23.
SEVICK-MURACA, E. M., HOUSTON, J. P. & GURFINKEL, M. 2002. Fluorescence-enhanced, near infrared diagnostic imaging with contrast agents. *Curr Opin Chem Biol,* 6**,** 642-50.
SHIA, W. C., CHEN, D. R., HUANG, Y. L., WU, H. K. & KUO, S. J. 2015. Effectiveness of evaluating tumor vascularization using 3D power Doppler ultrasound with high-definition flow technology in the prediction of the response to neoadjuvant chemotherapy for T2 breast cancer: a preliminary report. *Phys Med Biol,* 60**,** 7763-78.
SHUNG, K. K. & THIEME, G. A. 1993. *Ultrasonic scattering in biological tissues,* Boca Raton, CRC Press.
SIEGEL, R., MA, J., ZOU, Z. & JEMAL, A. 2014. Cancer statistics, 2014. *CA Cancer J Clin,* 64**,** 9-29.
SIEGEL, R. L., MILLER, K. D. & JEMAL, A. 2015. Cancer statistics, 2015. *CA Cancer J Clin,* 65**,** 5-29.
SIEGEL, S. & CASTELLAN, N. J. 1988. *Nonparametric statistics for the behavioral sciences,* New York, McGraw-Hill.
SIMS, A. H., HOWELL, A., HOWELL, S. J. & CLARKE, R. B. 2007. Origins of breast cancer subtypes and therapeutic implications. *Nat Clin Pract Oncol,* 4**,** 516-25.
SIMSTEIN, R., BUROW, M., PARKER, A., WELDON, C. & BECKMAN, B. 2003. Apoptosis, chemoresistance, and breast cancer: insights from the MCF-7 cell model system. *Exp Biol Med (Maywood),* 228**,** 995-1003.
SINGH, S., PRADHAN, S., SHUKLA, R. C., ANSARI, M. A. & KUMAR, A. 2005. Color Doppler ultrasound as an objective assessment tool for

chemotherapeutic response in advanced breast cancer. *Breast Cancer,* 12**,** 45-51.
SLAMON, D. J., LEYLAND-JONES, B., SHAK, S., FUCHS, H., PATON, V., BAJAMONDE, A., FLEMING, T., EIERMANN, W., WOLTER, J., PEGRAM, M., BASELGA, J. & NORTON, L. 2001. Use of chemotherapy plus a monoclonal antibody against HER2 for metastatic breast cancer that overexpresses HER2. *N Engl J Med,* 344**,** 783-92.
SMID, M., WANG, Y., ZHANG, Y., SIEUWERTS, A. M., YU, J., KLIJN, J. G., FOEKENS, J. A. & MARTENS, J. W. 2008. Subtypes of breast cancer show preferential site of relapse. *Cancer Res,* 68**,** 3108-14.
SOLIMAN, H., GUNASEKARA, A., RYCROFT, M., ZUBOVITS, J., DENT, R., SPAYNE, J., YAFFE, M. J. & CZARNOTA, G. J. 2010. Functional imaging using diffuse optical spectroscopy of neoadjuvant chemotherapy response in women with locally advanced breast cancer. *Clin Cancer Res,* 16**,** 2605-14.
SORET, M., BACHARACH, S. L. & BUVAT, I. 2007. Partial-volume effect in PET tumor imaging. *J Nucl Med,* 48**,** 932-45.
SPANU, A., FARRIS, A., CHESSA, F., SANNA, D., PITTALIS, M., MANCA, A. & MADEDDU, G. 2008. Planar scintimammography and SPECT in neoadjuvant chemo or hormonotherapy response evaluation in locally advanced primary breast cancer. *Int J Oncol,* 32**,** 1275-83.
SPARANO, J. A., GRAY, R. J., MAKOWER, D. F., PRITCHARD, K. I., ALBAIN, K. S., HAYES, D. F., GEYER, C. E., JR., DEES, E. C., PEREZ, E. A., OLSON, J. A., JR., ZUJEWSKI, J., LIVELY, T., BADVE, S. S., SAPHNER, T. J., WAGNER, L. I., WHELAN, T. J., ELLIS, M. J., PAIK, S., WOOD, W. C., RAVDIN, P., KEANE, M. M., GOMEZ MORENO, H. L., REDDY, P. S., GOGGINS, T. F., MAYER, I. A., BRUFSKY, A. M., TOPPMEYER, D. L., KAKLAMANI, V. G., ATKINS, J. N., BERENBERG, J. L. & SLEDGE, G. W. 2015. Prospective Validation of a 21-Gene Expression Assay in Breast Cancer. *N Engl J Med,* 373**,** 2005-14.
SPAYNE, M. C., GARD, C. C., SKELLY, J., MIGLIORETTI, D. L., VACEK, P. M. & GELLER, B. M. 2012. Reproducibility of BI-RADS breast density measures among community radiologists: a prospective cohort study. *Breast J,* 18**,** 326-33.
SRINIVASAN, S., POGUE, B. W., JIANG, S., DEHGHANI, H., KOGEL, C., SOHO, S., GIBSON, J. J., TOSTESON, T. D., POPLACK, S. P. & PAULSEN, K. D. 2003. Interpreting hemoglobin and water concentration, oxygen saturation, and scattering measured in vivo by near-infrared breast tomography. *Proc Natl Acad Sci U S A,* 100**,** 12349-54.
SRINIVASAN, S., POGUE, B. W., JIANG, S., DEHGHANI, H., KOGEL, C., SOHO, S., GIBSON, J. J., TOSTESON, T. D., POPLACK, S. P. & PAULSEN, K. D. 2006. In vivo hemoglobin and water concentrations, oxygen saturation, and scattering estimates from near-infrared breast tomography using spectral reconstruction. *Acad Radiol,* 13**,** 195-202.
STEWART, V. R. & SIDHU, P. S. 2006. New directions in ultrasound: microbubble contrast. *Br J Radiol,* 79**,** 188-94.
STRAVER, M. E., GLAS, A. M., HANNEMANN, J., WESSELING, J., VAN DE VIJVER, M. J., RUTGERS, E. J., VRANCKEN PEETERS, M. J., VAN TINTEREN, H., VAN'T VEER, L. J. & RODENHUIS, S. 2010. The 70-gene signature as a response predictor for neoadjuvant chemotherapy in breast cancer. *Breast Cancer Res Treat,* 119**,** 551-8.

SWANTON, C. 2012. Intratumor heterogeneity: evolution through space and time. *Cancer Res,* 72**,** 4875-82.
SYMMANS, W. F., PEINTINGER, F., HATZIS, C., RAJAN, R., KUERER, H., VALERO, V., ASSAD, L., PONIECKA, A., HENNESSY, B., GREEN, M., BUZDAR, A. U., SINGLETARY, S. E., HORTOBAGYI, G. N. & PUSZTAI, L. 2007. Measurement of residual breast cancer burden to predict survival after neoadjuvant chemotherapy. *J Clin Oncol,* 25**,** 4414-22.
SYMMANS, W. F., VOLM, M. D., SHAPIRO, R. L., PERKINS, A. B., KIM, A. Y., DEMARIA, S., YEE, H. T., MCMULLEN, H., ORATZ, R., KLEIN, P., FORMENTI, S. C. & MUGGIA, F. 2000. Paclitaxel-induced apoptosis and mitotic arrest assessed by serial fine-needle aspiration: implications for early prediction of breast cancer response to neoadjuvant treatment. *Clin Cancer Res,* 6**,** 4610-7.
TADAYYON, H., SADEGHI-NAINI, A., WIRTZFELD, L., WRIGHT, F. C. & CZARNOTA, G. 2014. Quantitative ultrasound characterization of locally advanced breast cancer by estimation of its scatterer properties. *Med Phys,* 41**,** 012903.
TADAYYON, H., SANNACHI, L., GANGEH, M., SADEGHI-NAINI, A., TRAN, W., TRUDEAU, M. E., PRITCHARD, K., GHANDI, S., VERMA, S. & CZARNOTA, G. J. 2016. Quantitative ultrasound assessment of breast tumor response to chemotherapy using a multi-parameter approach. *Oncotarget,* 7**,** 45094-45111.
TADAYYON, H., SANNACHI, L., GANGEH, M. J., KIM, C., GHANDI, S., TRUDEAU, M., PRITCHARD, K., TRAN, W. T., SLODKOWSKA, E., SADEGHI-NAINI, A. & CZARNOTA, G. J. 2017. A priori Prediction of Neoadjuvant Chemotherapy Response and Survival in Breast Cancer Patients using Quantitative Ultrasound. *Scientific Reports,* 7**,** 45733.
TADAYYON, H., SANNACHI, L., SADEGHI-NAINI, A., AL-MAHROUKI, A., TRAN, W. T., KOLIOS, M. C. & CZARNOTA, G. J. 2015. Quantification of Ultrasonic Scattering Properties of In Vivo Tumor Cell Death in Mouse Models of Breast Cancer. *Transl Oncol,* 8**,** 463-73.
TAKAMURA, Y., MIYOSHI, Y., TAGUCHI, T. & NOGUCHI, S. 2001. Prediction of chemotherapeutic response by Technetium 99m--MIBI scintigraphy in breast carcinoma patients. *Cancer,* 92**,** 232-9.
TANENBAUM, L. N. 2006. Clinical 3T MR imaging: mastering the challenges. *Magn Reson Imaging Clin N Am,* 14**,** 1-15.
TERUEL, J. R., HELDAHL, M. G., GOA, P. E., PICKLES, M., LUNDGREN, S., BATHEN, T. F. & GIBBS, P. 2014. Dynamic contrast-enhanced MRI texture analysis for pretreatment prediction of clinical and pathological response to neoadjuvant chemotherapy in patients with locally advanced breast cancer. *NMR Biomed,* 27**,** 887-96.
THERASSE, P., ARBUCK, S. G., EISENHAUER, E. A., WANDERS, J., KAPLAN, R. S., RUBINSTEIN, L., VERWEIJ, J., VAN GLABBEKE, M., VAN OOSTEROM, A. T., CHRISTIAN, M. C. & GWYTHER, S. G. 2000. New guidelines to evaluate the response to treatment in solid tumors. European Organization for Research and Treatment of Cancer, National Cancer Institute of the United States, National Cancer Institute of Canada. *J Natl Cancer Inst,* 92**,** 205-16.
THOMAS, D. B., GAO, D. L., RAY, R. M., WANG, W. W., ALLISON, C. J., CHEN, F. L., PORTER, P., HU, Y. W., ZHAO, G. L., PAN, L. D., LI, W., WU, C., CORIATY, Z., EVANS, I., LIN, M. G., STALSBERG, H. & SELF,

S. G. 2002. Randomized trial of breast self-examination in Shanghai: final results. *J Natl Cancer Inst,* 94**,** 1445-57.
THORN, C. F., OSHIRO, C., MARSH, S., HERNANDEZ-BOUSSARD, T., MCLEOD, H., KLEIN, T. E. & ALTMAN, R. B. 2011. Doxorubicin pathways: pharmacodynamics and adverse effects. *Pharmacogenet Genomics,* 21**,** 440-6.
TIRKES, T., HOLLAR, M. A., TANN, M., KOHLI, M. D., AKISIK, F. & SANDRASEGARAN, K. 2013. Response criteria in oncologic imaging: review of traditional and new criteria. *Radiographics,* 33**,** 1323-41.
TORRE, L. A., BRAY, F., SIEGEL, R. L., FERLAY, J., LORTET-TIEULENT, J. & JEMAL, A. 2015. Global cancer statistics, 2012. *CA Cancer J Clin,* 65**,** 87-108.
TOZAKI, M., SAKAMOTO, M., OYAMA, Y., MARUYAMA, K. & FUKUMA, E. 2010. Predicting pathological response to neoadjuvant chemotherapy in breast cancer with quantitative 1H MR spectroscopy using the external standard method. *J Magn Reson Imaging,* 31**,** 895-902.
TRAN, W. T., GANGEH, M. J., SANNACHI, L., CHIN, L., WATKINS, E., BRUNI, S. G., RASTEGAR, R. F., CURPEN, B., TRUDEAU, M., GANDHI, S., YAFFE, M., SLODKOWSKA, E., CHILDS, C., SADEGHI-NAINI, A. & CZARNOTA, G. J. 2017. Predicting breast cancer response to neoadjuvant chemotherapy using pretreatment diffuse optical spectroscopic texture analysis. *Br J Cancer,* 116**,** 1329-1339.
TRAN, W. T., SANNACHI, L., PAPANICOLAU, N., TADAYYON, H., AL MAHROUKI, A., EL KAFFAS, A., GORJIZADEH, A., LEE, J. & CZARNOTA, G. J. 2016. Quantitative ultrasound imaging of therapy response in bladder cancer in vivo. *Oncoscience,* 3**,** 122-33.
TRAVAINI, L. L., BAIO, S. M., CREMONESI, M., DE CICCO, C., FERRARI, M., TRIFIRO, G., PRISCO, G., VIALE, G., COLLEONI, M. A., RADICE, D., SIVOLAPENKO, G. B. & PAGANELLI, G. 2007. Neoadjuvant therapy in locally advanced breast cancer: 99mTc-MIBI mammoscintigraphy is not a reliable technique to predict therapy response. *Breast,* 16**,** 262-70.
TROMBERG, B. J., CERUSSI, A., SHAH, N., COMPTON, M., DURKIN, A., HSIANG, D., BUTLER, J. & MEHTA, R. 2005. Imaging in breast cancer: diffuse optics in breast cancer: detecting tumors in pre-menopausal women and monitoring neoadjuvant chemotherapy. *Breast Cancer Res,* 7**,** 279-85.
TROMBERG, B. J., POGUE, B. W., PAULSEN, K. D., YODH, A. G., BOAS, D. A. & CERUSSI, A. E. 2008. Assessing the future of diffuse optical imaging technologies for breast cancer management. *Med Phys,* 35**,** 2443-51.
TROMBERG, B. J., ZHANG, Z., LEPROUX, A., O'SULLIVAN, T. D., CERUSSI, A. E., CARPENTER, P. M., MEHTA, R. S., ROBLYER, D., YANG, W., PAULSEN, K. D., POGUE, B. W., JIANG, S., KAUFMAN, P. A., YODH, A. G., CHUNG, S. H., SCHNALL, M., SNYDER, B. S., HYLTON, N., BOAS, D. A., CARP, S. A., ISAKOFF, S. J., MANKOFF, D. & INVESTIGATORS, A. 2016. Predicting Responses to Neoadjuvant Chemotherapy in Breast Cancer: ACRIN 6691 Trial of Diffuse Optical Spectroscopic Imaging. *Cancer Res,* 76**,** 5933-5944.
TRUEB, R. M. 2009. Chemotherapy-induced alopecia. *Semin Cutan Med Surg,* 28**,** 11-4.

TRYFONIDIS, K., SENKUS, E., CARDOSO, M. J. & CARDOSO, F. 2015. Management of locally advanced breast cancer-perspectives and future directions. *Nat Rev Clin Oncol,* 12**,** 147-62.

TURNBULL, C. & RAHMAN, N. 2008. Genetic predisposition to breast cancer: past, present, and future. *Annu Rev Genomics Hum Genet,* 9**,** 321-45.

UEDA, S., ROBLYER, D., CERUSSI, A., DURKIN, A., LEPROUX, A., SANTORO, Y., XU, S., O'SULLIVAN, T. D., HSIANG, D., MEHTA, R., BUTLER, J. & TROMBERG, B. J. 2012. Baseline tumor oxygen saturation correlates with a pathologic complete response in breast cancer patients undergoing neoadjuvant chemotherapy. *Cancer Res,* 72**,** 4318-28.

UEDA, S., YOSHIZAWA, N., SHIGEKAWA, T., TAKEUCHI, H., OGURA, H., OSAKI, A., SAEKI, T., UEDA, Y., YAMANE, T., KUJI, I. & SAKAHARA, H. 2016. Near-Infrared Diffuse Optical Imaging for Early Prediction of Breast Cancer Response to Neoadjuvant Chemotherapy: A Comparative Study Using 18F-FDG PET/CT. *J Nucl Med,* 57**,** 1189-95.

UNDEVIA, S. D., GOMEZ-ABUIN, G. & RATAIN, M. J. 2005. Pharmacokinetic variability of anticancer agents. *Nat Rev Cancer,* 5**,** 447-58.

UNTCH, M., REZAI, M., LOIBL, S., FASCHING, P. A., HUOBER, J., TESCH, H., BAUERFEIND, I., HILFRICH, J., EIDTMANN, H., GERBER, B., HANUSCH, C., KUHN, T., DU BOIS, A., BLOHMER, J. U., THOMSSEN, C., DAN COSTA, S., JACKISCH, C., KAUFMANN, M., MEHTA, K. & VON MINCKWITZ, G. 2010. Neoadjuvant treatment with trastuzumab in HER2-positive breast cancer: results from the GeparQuattro study. *J Clin Oncol,* 28**,** 2024-31.

UPPULURI, A. 2008. *GLCM texture features* [Online]. Available: https://www.mathworks.com/matlabcentral/fileexchange/22187-glcm-texture-features [Accessed 2016 2016].

VALERO, V. V., BUZDAR, A. U. & HORTOBAGYI, G. N. 1996. Locally Advanced Breast Cancer. *Oncologist,* 1**,** 8-17.

VLAD, R. M., KOLIOS, M. C. & CZARNOTA, G. J. 2011. Ultrasound imaging of apoptosis: spectroscopic detection of DNA-damage effects at high and low frequencies. *Methods Mol Biol,* 682**,** 165-87.

VON MINCKWITZ, G., BLOHMER, J. U., COSTA, S. D., DENKERT, C., EIDTMANN, H., EIERMANN, W., GERBER, B., HANUSCH, C., HILFRICH, J., HUOBER, J., JACKISCH, C., KAUFMANN, M., KUMMEL, S., PAEPKE, S., SCHNEEWEISS, A., UNTCH, M., ZAHM, D. M., MEHTA, K. & LOIBL, S. 2013. Response-guided neoadjuvant chemotherapy for breast cancer. *J Clin Oncol,* 31**,** 3623-30.

VON MINCKWITZ, G., UNTCH, M., BLOHMER, J. U., COSTA, S. D., EIDTMANN, H., FASCHING, P. A., GERBER, B., EIERMANN, W., HILFRICH, J., HUOBER, J., JACKISCH, C., KAUFMANN, M., KONECNY, G. E., DENKERT, C., NEKLJUDOVA, V., MEHTA, K. & LOIBL, S. 2012. Definition and impact of pathologic complete response on prognosis after neoadjuvant chemotherapy in various intrinsic breast cancer subtypes. *J Clin Oncol,* 30**,** 1796-804.

WALKER, L. G., HEYS, S. D., WALKER, M. B., OGSTON, K., MILLER, I. D., HUTCHEON, A. W., SARKAR, T. K., AH-SEE, A. K. & EREMIN, O. 1999. Psychological factors can predict the response to primary chemotherapy in patients with locally advanced breast cancer. *Eur J Cancer,* 35**,** 1783-8.

WANG, L., MCLEOD, H. L. & WEINSHILBOUM, R. M. 2011. Genomics and drug response. *N Engl J Med,* 364**,** 1144-53.
WANG, S. & SUMMERS, R. M. 2012. Machine learning and radiology. *Med Image Anal,* 16**,** 933-51.
WARD, C., LANGDON, S. P., MULLEN, P., HARRIS, A. L., HARRISON, D. J., SUPURAN, C. T. & KUNKLER, I. H. 2013. New strategies for targeting the hypoxic tumour microenvironment in breast cancer. *Cancer Treat Rev,* 39**,** 171-9.
WEIGELT, B. & REIS-FILHO, J. S. 2009. Histological and molecular types of breast cancer: is there a unifying taxonomy? *Nat Rev Clin Oncol,* 6**,** 718-30.
WELCH, A. J. & GEMERT, M. J. C. V. 2010. *Optical-thermal response of laser-irradiated tissue,* New York, Plenum Press.
WELLS, P. N. & LIANG, H. D. 2011. Medical ultrasound: imaging of soft tissue strain and elasticity. *J R Soc Interface,* 8**,** 1521-49.
WHITING, P. F., RUTJES, A. W., WESTWOOD, M. E., MALLETT, S., DEEKS, J. J., REITSMA, J. B., LEEFLANG, M. M., STERNE, J. A., BOSSUYT, P. M. & GROUP, Q.-. 2011. QUADAS-2: a revised tool for the quality assessment of diagnostic accuracy studies. *Ann Intern Med,* 155**,** 529-36.
WHITMAN, G. J. & STROM, E. A. 2009. Workup and staging of locally advanced breast cancer. *Semin Radiat Oncol,* 19**,** 211-21.
WILCZEK, B., VON SCHOULTZ, E., BERGH, J., ERIKSSON, E., LARSSON, S. A. & JACOBSSON, H. 2003. Early assessment of neoadjuvant chemotherapy by FEC-courses of locally advanced breast cancer using 99mTc-MIBI. *Acta Radiol,* 44**,** 284-7.
WILL, B. P., BERTHELOT, J. M., LE PETIT, C., TOMIAK, E. M., VERMA, S. & EVANS, W. K. 2000. Estimates of the lifetime costs of breast cancer treatment in Canada. *Eur J Cancer,* 36**,** 724-35.
WILLMANN, J. K., VAN BRUGGEN, N., DINKELBORG, L. M. & GAMBHIR, S. S. 2008. Molecular imaging in drug development. *Nat Rev Drug Discov,* 7**,** 591-607.
WOLF, S., BARTON, D., KOTTSCHADE, L., GROTHEY, A. & LOPRINZI, C. 2008. Chemotherapy-induced peripheral neuropathy: prevention and treatment strategies. *Eur J Cancer,* 44**,** 1507-15.
WOLFE, J. N. 1976. Risk for breast cancer development determined by mammographic parenchymal pattern. *Cancer,* 37**,** 2486-92.
WOLMARK, N., WANG, J., MAMOUNAS, E., BRYANT, J. & FISHER, B. 2001. Preoperative chemotherapy in patients with operable breast cancer: nine-year results from National Surgical Adjuvant Breast and Bowel Project B-18. *J Natl Cancer Inst Monogr***,** 96-102.
WU, J., GONG, G., CUI, Y. & LI, R. 2016. Intratumor partitioning and texture analysis of dynamic contrast-enhanced (DCE)-MRI identifies relevant tumor subregions to predict pathological response of breast cancer to neoadjuvant chemotherapy. *J Magn Reson Imaging,* 44**,** 1107-1115.
XU, C., VAVADI, H., MERKULOV, A., LI, H., ERFANZADEH, M., MOSTAFA, A., GONG, Y., SALEHI, H., TANNENBAUM, S. & ZHU, Q. 2015. Ultrasound-Guided Diffuse Optical Tomography for Predicting and Monitoring Neoadjuvant Chemotherapy of Breast Cancers: Recent Progress. *Ultrason Imaging*.
XU, R. X. & POVOSKI, S. P. 2007. Diffuse optical imaging and spectroscopy for cancer. *Expert Rev Med Devices,* 4**,** 83-95.

YAGER, J. D. & DAVIDSON, N. E. 2006. Estrogen carcinogenesis in breast cancer. *N Engl J Med,* 354**,** 270-82.
YANG, X., TRIDANDAPANI, S., BEITLER, J. J., YU, D. S., YOSHIDA, E. J., CURRAN, W. J. & LIU, T. 2012. Ultrasound GLCM texture analysis of radiation-induced parotid-gland injury in head-and-neck cancer radiotherapy: an in vivo study of late toxicity. *Med Phys,* 39**,** 5732-9.
YEH, E. T. & BICKFORD, C. L. 2009. Cardiovascular complications of cancer therapy: incidence, pathogenesis, diagnosis, and management. *J Am Coll Cardiol,* 53**,** 2231-47.
YU, Y., JIANG, Q., MIAO, Y., LI, J., BAO, S., WANG, H., WU, C., WANG, X., ZHU, J., ZHONG, Y., HAACKE, E. M. & HU, J. 2010. Quantitative analysis of clinical dynamic contrast-enhanced MR imaging for evaluating treatment response in human breast cancer. *Radiology,* 257**,** 47-55.
ZAMAN, M. U., NASIR, Z., RAZA, T., HASHMI, H., HASHMI, A. & FATIMA, N. 2009. Dual phase qualitative and quantitative 99mTc-MIBI scintimammography for predicting response to neoadjuvant chemotherapy in breast cancer. *J Coll Physicians Surg Pak,* 19**,** 173-8.
ZHU, Q., DEFUSCO, P. A., RICCI, A., JR., CRONIN, E. B., HEGDE, P. U., KANE, M., TAVAKOLI, B., XU, Y., HART, J. & TANNENBAUM, S. H. 2013. Breast cancer: assessing response to neoadjuvant chemotherapy by using US-guided near-infrared tomography. *Radiology,* 266**,** 433-42.
ZHU, Q., TANNENBAUM, S., HEGDE, P., KANE, M., XU, C. & KURTZMAN, S. H. 2008. Noninvasive monitoring of breast cancer during neoadjuvant chemotherapy using optical tomography with ultrasound localization. *Neoplasia,* 10**,** 1028-40.
ZHU, Q., WANG, L., TANNENBAUM, S., RICCI, A., JR., DEFUSCO, P. & HEGDE, P. 2014. Pathologic response prediction to neoadjuvant chemotherapy utilizing pretreatment near-infrared imaging parameters and tumor pathologic criteria. *Breast Cancer Res,* 16**,** 456.
ZOLLER, B., LI, X., SUNDQUIST, J. & SUNDQUIST, K. 2014. Familial transmission of prostate, breast and colorectal cancer in adoptees is related to cancer in biological but not in adoptive parents: a nationwide family study. *Eur J Cancer,* 50**,** 2319-27.
ZWEIG, M. H. & CAMPBELL, G. 1993. Receiver-operating characteristic (ROC) plots: a fundamental evaluation tool in clinical medicine. *Clin Chem,* 39**,** 561-77.